Modeling and Sliding-Mode Control of Flexible-Link Robotic Structures for Vibration Suppression

Doctoral Thesis
(Dissertation)

to be awarded the degree
Doktor-Ingenieur
(Dr.-Ing.)
the German equivalent of a Ph.D. in engineering

submitted by

Franklyn Gerardo Duarte Vera
from San Cristóbal, Venezuela.

Approved by the Faculty of Mathematics/Computer Science
and Mechanical Engineering,
Clausthal University of Technology,

Date of oral examination
18.08.2016

Chairperson of the Board of Examiners
Prof. Dr.-Ing. Armin Lohrengel

Chief Reviewer
Prof. Dr.-Ing. Christian Bohn

Reviewer
Profin. Dr.-Ing. Stefanie Retka

Abstract

In many applications, the use of slender and light flexible structures has increased due to the requirement of more energetically efficient structures. This kind of structures is easily prone to vibrate due to external forces or due to forces generated in the inner structure during the movement. One objective of this work is to generate models of flexible-link structures: cantilever beam, one flexible-link robot and two flexible-link robot; which include rotational actuators, piezoelectric actuators, and different kinds of sensors (acceleration and deformation). The models are obtained under a classical mechanics approach of Lagrange Euler energy balance; the assumed mode method is used to approximate the flexibility of the elastic components. In the model formulation, new rotation angles are introduced in the distal joints and the joint inertia is separated according to this new kinematic consideration. Some parts of the resulting model involving integral terms are calculated using symbolic programming software; whereas other parts are implemented and calculated dynamically during simulation. The resulting models are programmed in Matlab/Simulink subjected to a novel verification methodology and then validated experimentally in a platform constructed for the implementation. The second objective is to develop, from simplified models of the flexible-link structures, robust controllers for joint tracking and active vibration suppression. Therefore, robust control is used with two basic purposes: to face the model uncertainties due to the discrepancies between the models and real systems and to suppress the vibration of the flexible-link structures. Three control strategies are proposed: Dual loop control approach, decentralized and centralized Lyapunov model-based sliding mode control approach. The values required for the implementation of the controller are obtained from the formulated models. The controllers were implemented in a dSPACE rapid prototyping control card and the experimental results show the effectiveness of the proposed control strategies in terms of joint tracking and vibration suppression.

To God, Virgen de La Consolación and Divino Niño Jesús.

To my Marlenita, woman that I admire and love. I want to thank you for your support, comprehension and love.

To Amelie, my beloved Daughter.

To my Mother María Irma Vera de Duarte, to my Father Antonio María Duarte. To my Siblings Deysi, Yamile and José Antonio and to my Aunt Juanita.

Contents

List of Abbreviations

AVC	Active vibration control
DOF	Degree of freedom
FFT	Fast Fourier transform
FEM	Finite element method
LPF	Low-pass filter
LPM	Lumped parameter method
LQR	Linear quadratic regulator
MIMO	Multiple-input multiple-output
SMC	Sliding mode control
SISO	Single-input single-output
P	Proportional
PD	Proportional-derivative
PID	Proportional-integral-derivative
PZT	Piezoelectric material (lead zirconate titanate)
SPA	Singular perturbation approach
VSS	Variable structure system

List of Variables

A	Transversal area
$\overline{A}$	Boundary of nonlinear uncertainty
A_i	Amplitude of point i
$\boldsymbol{A}_i$	Rotation matrix of frame i
$\boldsymbol{A}_\mathrm{p}$	System dynamic matrix
$\boldsymbol{B}_\mathrm{p}$	Input matrix
$\boldsymbol{B}_\mathrm{pi}$	Input matrix with piezoelectric actuator
$\boldsymbol{B}_\mathrm{l}(t)$	Boundary layer
$\overline{c}$	Piezolectric moment constant
$\boldsymbol{c}$	Coriolis and centripetal effects
$\boldsymbol{C}_\mathrm{p}$	Output matrix
$\overline{C}$	Boundary of time derivative of nonlinear uncertainty
$\boldsymbol{D}_\mathrm{p}$	Direct transfer matrix
e	Error
$c_{i,j}$	Constant of the mode shape
$\boldsymbol{D}$	Damping matrix
E	Elasticity modulus

$\boldsymbol{E}_i$	Deformation rotation matrix of link
$\boldsymbol{f}(\boldsymbol{x})$	Nonlinear dynamic
$\boldsymbol{f}$	Generalized force
f_i	Generalized force
f_{chirp}	Frequency of the chirp signal
$\boldsymbol{g}(\boldsymbol{x}_1)$	Nonlinear complement sliding surface
H_∞	H-infinity norm
I	Second moment of area
$\mathbf{I}$	Identity matrix
$J_{\text{D}}, J_{\text{D}_i}$	Distal inertia
$J_{\text{h}}, J_{\text{h}_i}$	Inertia of hub
$J_{\text{h}_{i\text{A}}}$	Inertia of hub (fixed part)
$J_{\text{h}_{i\text{B}}}$	Inertia of hub (movil part)
$J_{\text{GB}i}$	Inertia of gear box
$J_{h_i\,\text{BC}}$	Equivalent inertia
J_{p}	Inertia of tipload
$\boldsymbol{K}$	Stiffness matrix
$\bar{\boldsymbol{K}}$	Feedback gain matrix
k_{D}	Derivative gain
k_{I}	Integral gain
k_{P}	Proportional gain
k_{V}	Velocity feedback gain
L	Lagrangian
l, l_i	Length of the link
$\boldsymbol{M}$	Mass matrix
$M(x), M(x,t)$	Bending moment
$m_{\text{D}}, m_{\text{D}_i}$	Distal inertia
$m_{\text{l}}, m_{\text{l}_i}$	Mass of the link
$m_{\text{h}}, m_{\text{h}_i}$	Mass of the hub
$m_{\text{l}}, m_{\text{l}_i}$	Mass of the link
m_{p}	Mass of Tipload
n	Total number of DOF
n_{R}	Number of rigid DOF
$n_{\text{F}}, n_{\text{F}_i}$	Number of flexible DOF
$\overline{\text{O}_i\tilde{\text{O}}_i}$	Clamp offset
$p_{A_{\text{p}}}$	Eigenvalues of $\boldsymbol{A}_{\text{p}}$
$\boldsymbol{p}_i(x,t)$	Absolute position of point i along the link
${}^i\boldsymbol{p}_i(x_i)$	Relative position of point i along the link with respect to frame i
${}^i\boldsymbol{r}_j(t)$	Relative position of frame j with respect to frame i

$\boldsymbol{r}_{\mathrm{C}}, \boldsymbol{r}_{\mathrm{C}_i}$	Absolute clamp position
${}^{i}\boldsymbol{r}_{\mathrm{C}}, {}^{i}\boldsymbol{r}_{\mathrm{C}_i}$	Relative clamp position
$\boldsymbol{q}$	Generalized coordinates
q_i	Generalized modal coordinate
$q_z(x), q_z(x,t)$	Distributed load
$q_{\mathrm{f}i}(t), q_{\mathrm{f}ij}(t)$	Flexible modal variable
$\boldsymbol{S}$	Coefficient matrix of a linear sliding manifold
T	Total kinetic energy
t_i	Link thickness
t_r	Reaching time
$T_{\mathrm{h}}, T_{\mathrm{h}_i}$	Kinetic energy of hub
$T_{\mathrm{l}}, T_{\mathrm{l}_i}$	Kinetic energy of the link
T_{p}	Kinetic energy of tipload
U	Total potential energy
$U_{\mathrm{l}}, U_{\mathrm{l}_i}$	Potential energy of the link
$\boldsymbol{u}$	Input of the system
$u(x)$	Field of axial displacements
$\boldsymbol{u}_{\mathrm{c}}$	Corrective control input
$\boldsymbol{u}_{\mathrm{eq}}(t)$	Equivalent control input
$V(x), V(x,t)$	Shear force
$V(\boldsymbol{x},t)$	Lyapunov candidate function
v	Auxiliar control input
v_{pi}	Piezoelectric voltage
$\tilde{\boldsymbol{W}}$	Auxiliar matrix
$\boldsymbol{W}_i$	Cumulative transformation until frame i
$w(x), w(x,t)$	Transversal displacement
$w_{\mathrm{e}}(t), w_{\mathrm{e}_i}(t)$	Transversal displacement at the tip of the link
$\boldsymbol{x}$	Plant states
$\dot{\boldsymbol{x}}_{\mathrm{e}}$	Equoivalent trajectory of the states
x_{pi_i}	Location of extreme I of piezoelectric actuator
x_{s_i}	Location of sensor i
$\boldsymbol{y}$	Output
z	Distance from neutral axis
$\overline{z}$	Auxiliar sliding variable
$\alpha_i(t)$	Absolute angular position of frame i
$\hat{\alpha}_i(t)$	Absolute angular position of frame $\hat{i}$
δ	Logarithmic decrement
δ_{ij}	Delta Kronecker symbol
$\varepsilon(x), \varepsilon_i$	Axial strain

Φ_i	Thickness of the boundary layer
$\theta(x)$	Angular distortion
$\hat{\lambda}_i$	Convex coeeficients of Filippov
λ_i	Convergence rate of the induced dynamics
$\boldsymbol{\xi}$	Damping coefficients vector
ρ_l, ρ_{l_i}	Linear mass density
ρ_i	Sliding mode gain
$\sigma_{xx}(x)$	Normal stress
$\sigma_i(\boldsymbol{x})$	Sliding manifold
$\boldsymbol{\sigma}(\boldsymbol{x})$	Sliding surface
$\tau_{\mathrm{fr}}(t), \tau_{\mathrm{fr}_i}(t)$	Friction torque
$\tau_{\mathrm{m}}(t), \tau_{\mathrm{m}_i}(t)$	Motor torque
$\phi_i(x), \phi_{ij}(x)$	Mode shape
$\varphi(x_1, x_2)$	Nonlinear uncertainty
$\omega, \omega_i, \omega_{ij}$	Natural frequency
ω_{d}	Damped frequency
$\boldsymbol{\psi}$	Deformation transformation matrix

1 Introduction

Robots are built to help in different kinds of tasks which could be repetitive for human beings or require considerable force with dexterity. These tasks can also take place in hazardous environments. Normally the manipulators, industrial robots, are heavy and stiff in order to provide enough force and to meet the accuracy requirements at the tip of the robot. These robots move at speeds much lower than the fundamental natural frequency of the structure. An alternative is the use of lightweight flexible-link manipulators because they have many advantages such as lower energy consumption; requirement of smaller actuators. Likewise they are more maneuverable and transportable, they have less overall cost and higher payload to robot weight ratio. Normally these structures have to be made up of slender members in order to reach a bigger workspace then the robot becomes more flexible. High operational speeds induce relatively high inertial forces that deform the flexible link and makes the structure prone to vibrate; also the position control or the actuators can be an internal source of excitation. Moreover, external sources of vibration are machinery operating nearby or collisions of the structure.

In addition, the dynamics of flexible-link robots is much more complicated than the corresponding rigid-link manipulators. A higher number of degrees of freedom (DOF) is required to model its behavior. Further complications arise due to highly nonlinear nature of the system. The system has a distributed flexibility along the links which result in partial differential governing equations. Not only the distributed flexibility nature of the dynamics is a complication, but also the moving boundary conditions at the tip of the flexible links connected to the next link are major difficulties.

Indeed, unwanted vibrations and the difficulties that arise in modeling must be overcome, and then flexible-link robots will gain more space in industrial environments. The modeling issues have been treated with different discretization techniques in order to truncate the order of the model. With the discretization the partial differential equation are turned into ordinary differential equations which makes the problem bearable. The models developed can be used for simulation purposes and for controller calculation to attenuate unwanted vibrations.

From the control point of view feedforward and feedback techniques have been applied in this kind of structures. Feedback control techniques require knowing accurately the dynamic properties of the robot and the trajectory has to be known in advance; it introduces limitations due to the uncertainties present in the model and a possible influent change in the boundary condition related to the configuration. On the other hand, feedback control techniques have been applied in a centralized and decentralized fashion, but when the control strategies is noncollocated the closed loop system has an unstable zero dynamics. Hence, elastic vibrations of light weight links must be considered in the design and control of the manipulators with link flexibility. It is interesting to develop control strategies that were able to deal with the aforementioned aspects.

1.1 Motivation

Flexible-link robots have low stiffness which causes structural vibrations simultaneously with robot movements, complicating the overall motion. The structural dynamics of lightweight flexible structures is strongly affected by the addition of masses (actuators, sensors, etc.). For

the majority of experimental studies the rotational actuator under feedback techniques is not capable to reduce significantly the unwanted vibrations.

Active vibration control (AVC) technique is a feasible countermeasure to attenuate the vibration produced during the motion and when the final kinematic configuration is reached. There are many possible electroactive materials to be used for AVC purposes such as piezoceramics, shape memory alloys, electrorheological fluids, polymer biomaterials and magnetorestrictive materials, this list will increase with the development in materials science. Piezoelectric ceramics are effective distributed strain actuators as well as sensors due to their high stiffness, good linearity, ease of integration, low temperature sensitivity, and relatively low noise. For this reason, piezoelectric materials are commonly used as actuators in smart structures. These materials can be easily incorporated into the flexible-link robot structure either embedded or bonded; these materials are light and do not change the (uncontrolled) dynamics of the system significantly.

Flexible-link structures are involved in fields such as space robotics, overhead cranes, long arm manipulation and flexible object handling; anywhere the stiffness of the structure is limited. A potential application of very light flexible-link robots is the interaction with human beings, because they with appropriate sensors and very low inertia could be inoffensive for the user. Flexible link-robots will gain more participation in certain applications in the near future as an alternative to industrial robots and parallel robots. The former are heavy and bulky with all the related consequences. The latter they could be light, but their workspace is reduced.

The mathematical models obtained for robotics structures are always approximations; the development of a model for a flexible-link robot introduces uncertainties because the models must be truncated. This truncation avoid modelling high-order dynamics. Then the controllers, to be designed considering the previous model, need to be robust with respect to the neglected dynamics and possible variation in parameters.

This work aims developing models for different flexible-link structures, where the AVC controllers for these structures are model based. The proposed controllers use, on the flexible links, piezoelectric actuators and piezoresistive sensors. In order to face high-order dynamics and uncertainties a model-based robust complement is proposed.

1.2 Objectives

Considering the potential of flexible-link robot the present work propose the development of models and robust control strategies that provide position tracking and active vibration control in flexible-link serial structures. The structures object of this study are: cantilever beam, one flexible-link robot and two flexible-link robot. All the structures are provided with patch piezoelectric actuators bonded on their surfaces and the robotic structures are provided with rotational actuators.

In order to reach the main objective, the development of analytical dynamical models is performed using a recursive kinematic formulation following the Lagrangian formalism to obtain the equation of motion. The obtained models are verified with a novel systematic proposal. The models are validated in a suitable and versatile experimental platform that was built to test the structures under study. Different model-based robust control strategies are formulated, implemented and its performance is evaluated experimentally.

1.3 State of the Art

The modeling and control of flexible robotic structures has been done since the middle of the 70s, the pioneer is Prof. Wayne Book of Georgia Tech Institute, where he proposed the first model approach for this kind of structures. Dynamic modelling of flexible-link robotic structures has been the focus of many researchers [1]. Unlike conventional rigid robots, the elastic behavior of flexible robots makes more difficult their model formulation. One of the most important characteristic of the flexible manipulator models is the bigger influence of low vibration modes than the higher ones on the system dynamics. Nevertheless, this high order dynamics, which is not considered directly in the controller designed, may give rise to the appearance of bad system behaviors. The flexibility of the links leads to oscillatory behavior at the tip of the link, it makes the regulation problem or tracking trajectory a difficult task that requires complex closed-loop control. Two main problems complicate the control design for flexible manipulators: the high order of the system (theoretically infinite) and the nonminimum phase dynamics that exists between the tip position and the input (torque applied at the joints and output the position of the tip robot).

1.3.1 Robot Modeling

In the model formulation of rigid robots, the equations of motion can be described by ordinary differential equations; these equations of motion can be implemented directly for simulation or control purposes. Otherwise for flexible-link robots, during the modeling process due to the continuous nature of the link and their distributed mass and flexibility arise partial differential equations involving spatial and time dependency. For implementation, simulation and control purposes this kind of equation are commonly avoided. Then spatial discretization techniques are applied with the objective of separate the spatial-time dependent variables in a combination of spatial dependent variables and time dependent variables. In the literature basically three approaches can be found: assumed mode method (AMM), finite element method (FEM) and lumped parameter method (LPM).

In AMM approach the flexible element is considered to take predefined forms (shapes of vibration or eigen functions) which are related to each mode of vibration of the structure. The final deformation results as the sum of the modes multiplied by their correspondent amplitude. Here a separation between the time-dependent variables (amplitude or modal variable) and space dependent variables (mode of vibration or space variable) is performed. This method was proposed by [2]. In the AMM formulation, the link flexibility is represented by the truncated finite modal series, in terms of spatial mode eigen functions and time-varying mode amplitudes.

This method has been used in flexible robots modeling [3-6,8-10]. The way boundary conditions and trial functions are chosen play an important role in model for simulation. For instance, if clamped free boundary conditions are chosen it results in an identity block in the input matrix for the input torques and joint variable direct measurable [3,5,6]. Pinned-pinned boundary conditions lead to ease in specifying the arm tip and have been used in trajectory control, it introduces a small change in the lower block of the input matrix [11-13]. In [4,6,7,9,10,14-20] have been reported that if the inertia of the joint is much bigger than the inertia of the link, if there is a control loop closed in the joint or if there is a gearbox between the actuator and joint, the clamped condition yields better results compared to pinned boundary condition. They also reported experimental verifications. An interesting equivalence of these two cases is reported by [13]. In [15], also stated that when pinned boundary

conditions are assumed, this boundary condition tends asymptotically to the clamped boundary condition.

The FEM has not been often employed for use in the design of controllers for flexible-link robot manipulators [1,3,8,21]. Nevertheless, it is an useful tool for the design of mechanical structures, especially in the design of robotic system itself [22]. In the FEM, the boundary conditions and changes in geometry and physical properties can be accounted in a straightforward way. This advantage has been used to derive closed-form equations of motion and for the analysis of controllers [22-30]. This method has been also mainly used for the dynamic simulation of flexible robotic structures with complex geometry [31-34]. Here the model of each link with distributed flexibility is discretized in smaller elements, the behaviors of the variables under study are assumed to have certain local distribution in each element (shape function). In this method, each flexible link is considered an assemblage of a finite number of elements, where every element is a part of a continuous member of the robot. The displacements are compatible and the internal forces are in balance at certain points called nodes, the entire link is compelled to act as one entity. The displacement at any point of the continuous element is expressed in terms of finite number of displacements at the nodal points multiplied by polynomial interpolation functions. The equations of motion for the overall robotic system are then derived by first deriving the equations of motion for a typical element and then suitably assembling the individual elements' equations of motion.

Finally, LPM has been seldom used in modeling of flexible-link robotic structures. Here the system is considered to have discrete components with their mass and inertia located in points along the flexible element. In the case of the beam the mass is assumed to be concentrated and there are virtual springs at virtual joints to emulate the flexibility of the whole element. This modeling technique assumes as many fictitious joints as necessary to appropriately describe the deflection of a flexible link. Each nonactuated fictitious joint is also accompanied by a linear spring to restrict the joint motion and represent the flexibility. If the vibrations of a link in different orthogonal planes are considered separately (two laterals and one longitudinal vibration) and each is represented by a pseudoprismatic joint, then it can be said that this method models the first mode of vibration in each direction. Furthermore, three pseudorevolute joints may be added to represent the effect of rotational vibrations. An end-effector deflection prediction scheme in terms of the geometry-dependent "influence coefficients" was developed by [35]. In [36] this model was used for identification of inaccessible oscillations in n-link flexible robotic systems. In [37] the model of a single flexible-link was developed where a separation of the dynamic model terms that depend on the geometry of the link from the terms that depend on the lumped masses of the link was performed. The lumped parameter model is the simplest one, but the manipulator is modelled as spring-mass system, it often does not yield sufficiently accurate results.

Several works have been developed in the control of flexible-link robotic structures, a brief review of some of them is presented. There are multiple possibilities of criteria for classification, for example: modeling technique, separation according the speed of the system, kind of control strategy, kinematic configuration, etc. Here the research is classified according the kinematic configuration of the flexible-link robot i.e. one flexible-link robot and two flexible-link robot.

1.3.2 Control of Flexible-link Robots

The different approach employed in control of flexible-link robots are presented according to their kinematic configuration. Here it is restricted to robots with rotational joint with one and two flexible links.

One Flexible-link Robot

The case of one flexible-link robot has the advantage that it can be approximated to a linear system under certain assumptions. For instance if Coriolis and centripetal effects are neglected a linear representation can be obtained and linear control techniques applied.

Under the AMM, different control strategies have been proposed. In [38] feedforward input shaping techniques are proposed where a feedforward term that convolves in real time the desired reference input with a sequence of impulses to produce a vibration-free output. The delay times of the prefilters are adapted to match the system's natural frequency. Experimental results for a single flexible link are presented to verify the technique. Also in [39] a controller design is proposed, it is based on the use of a conventional rigid body robot controller and the use of a closed loop shaped-input filter to reduce the nonlinear vibrations of the flexible link. The controller is proposed for different kinematic configurations and it is tested experimentally.

In [40] an approach of vibration damping qualified for application to any kind of flexible robot even without an analytic model is presented. It uses a passive design for decentralized actuator control. The actuators of the robot are controlled to act like virtual passive mechanical spring-damper elements and the damping of the eigen modes is increased by pole placement technique.

Robots with link flexibility and joint flexibility were addressed in [41], feedforward model-based control law is shown, also it is suggested that with a complementary feedback standard proportional-derivative (PD) controller the performance of the system can be improved. Simulation results using the software FLEXARM were shown for a two-link robot.

In [42] a modified Lyapunov-based proportional-integral-derivative (PID) controller was implemented. For joint positioning the PD part was used and for the flexibility an integral element was used having as input the deflection of the tip of the link, the control strategy was validated experimentally.

Singular perturbation approach (SPA) proposed by [43] was used in [44,45] to separate the dynamic model of the flexible robot in slow dynamics (joint dynamics) and fast dynamics (flexible dynamics), joint tracking is achieved through a linear sliding mode controller (SMC) and the link is damped with a linear quadratic regulator (LQR) controller then the control law is the sum of both control signals; it was experimentally validated without considering any payload.

In [46] a flexible-link robot with an additional translational DOF is presented; a nonlinear control scheme based on partial feedback linearization was implemented experimentally, which incorporates a lead zirconate titanate (PZT) actuator as a secondary input to the system. PZTs were also used for AVC in [47] where SMC was used for joint tracking and for AVC of perturbation induced by a fast movement was used positive position feedback due to its spillover insensitivy; in this work for the attenuation of chattering effect a dead-band in the switching control is used. Results were given only in simulation.

Computed torque is a method commonly used in rigid robots, [48] proposed it to be used in flexible-link robots, one torque for the rigid part and one for the flexible part and a relation between these torques was established using sliding mode technique, also an adaptive version is proposed to face parameter uncertainties. Simulation results were shown.

A modified PID is utilized in [49] to solve the problem of achieving an accurate tip position of a flexible-link manipulator, the controller is made up of a PD for the joint and an integral term including the vibration of the tip, the error signal is reformulated in terms of the tip

position related to the joint variable. Tip position is estimated through shape of vibration and strain gage measurement. Experimental results were shown.

In [50] a controller based on the nonlinear state dependent Riccati equation is proposed. Here is also stated that it can not be calculated online, then a gain-scheduling LQR according to the states is proposed for the rejection of vibration assuming that the Lyapunov function is an explicit function of the states. The effectiveness of the proposed control strategy is proved experimentally.

In [9] a decentralized controller was proposed for a one flexible-link robot provided with piezoelectric actuators. Joint tracking is performed via a model-free PID controller tuned with the Ziegler-Nichols method. For the AVC a dual loop with a second order SMC for the flexible link is proposed and implemented. The experimental results showed the effectiveness of this approach.

Under the FEM, to the best knowledge of the author, not much research can be found. This is due to the fact that the controller calculated from FEM models tend to be rather complex and can not be implemented online. In [27] a simulation algorithm characterizing the dynamic behavior of one flexible-link manipulator is developed using finite difference methods. A graphic environment in Matlab/Simulink is presented where several open-loop and closed-loop control strategies such as PD and PID can be incorporated in the simulations.

A model for dynamic simulation purposes is presented in [30], the model include the possibility to apply two bending moments to emulate a piezoelectric actuator. Three controllers are available: active force, P and PD. The robot model with the control strategies is validated experimentally.

In [51] a SMC for tip trajectory tracking is proposed. Here a modification in the sliding variable is introduced by adding a corrective term to the desired angular trajectory, this term takes into account the angular deviation of the tip by changing the sliding variable and introducing a PID complement in order to accelerate the convergence. The governing partial differential equations of the links are solved via finite difference method. Simulation results are shown.

Under the LPM different control strategies have been proposed. In [52] an AVC is proposed using an actuator bonded along a flexible pointing system (similar to a one flexible-link robot). Two methods for the generation of trajectory based on the model of the structure are presented. The resulting trajectories are supposed not to excite the modes of vibration of the flexible structure and the continuous piezoelectric actuator is used to increase the damping.

Backstepping control strategy is utilized in [53] to obtain tip point tracking of position and velocity. The authors took advantage under certain assumptions of the LPM which results in a model in strict feedback form. According to the control design the controllers require joint acceleration and tip point acceleration. Three backstepping controllers, two robust controllers and adaptive were developed and tested in simulation.

In [37] a control scheme is proposed that minimizes the effects of the friction in the joints. The control scheme is composed of two feedback nested loops, a PD inner loop to control the motor position and an outer loop to control the tip position. The controller for the tip position loop is composed of feedforward and feedback terms. A limitation of this method is the necessity of achieving a motor response faster than the vibrational modes considered in the model of the link. Experimental results are shown.

An approach for the use of PZT actuators in a flexible robot was presented by [54,55]. The combined control scheme is composed of a PD controller for the position of the joint and a

command voltage applied to the PZT actuators for vibration damping. The command voltage employees linear tip velocity feedback, which makes the scheme easy to implement. The system is modeled using AMM but the stability is proven with a LPM. [54] presents only simulation and [55] makes a complement evaluating the influence of the PZT location and presenting experimental evaluation.

A hybrid controller with a dual loop is presented in [19], in this work a combination of continuous-time controller with discrete-time controller is used. Joint tracking is performed using a PID controller with feedforward gains and tuned with the Ziegler-Nichols method. The flexible-link model is obtained from a black-box identification process considering it as a cantilever beam then a H_∞ was calculated for the AVC loop. The controller was tested experimentally.

Two Flexible-link Robot

Once the flexible robot has at least one distal link its model turns into high nonlinear formulation. The influence of distributed flexibility on modelling and controller design has to be well understood to attain the design objectives. In the two flexible-link robots the influence of Coriolis and centripetal effects is more important in the dynamic behavior of the robot in control design than for the one flexible-link robot. The review is also organized according to the modeling technique.

Also for two flexible-link robots the modeling approach most widely used is AMM. There have been some attempts of linearizing models of multilink flexible robots, this can be done in the case of low speeds and very small deformations [17,18]. In [17] the dynamics is linearized for the whole robot workspace assuming very low joint speeds, an observer-based state-feedback is proposed. This strategy is proposed as a complement to the positioning controller. The proposed controller was tested experimentally. In [18] is proposed the use of a PD controller for the called “fine motion” with the model linearized in an operating point assuming all the time derivatives equal to zero. As long as for the “gross motion” an adaptive model following algorithm which is a Luenberger observer and a combination of state feedback and PD controller with time-varying gains. Simulation results are shown.

Input shaping techniques have been also applied to this kind of structures. In [56] the advantages and disadvantages of this control strategy for a two flexible-link robot are discussed, the most important aspect is the low robustness to model uncertainties and its low performance for big movements. Then decentralized PD controllers are suggested to overcome the drawbacks. Susequently in [57] good experimental results for the previous control strategy are shown.

Feedback linearization was utilized in [58]; the flexible-link robot was considered as a rigid robot for the model formulation and subsequent feedback linearization, then the control signals from augmented nonlinear PD controller are convolved with input shaping prefilters to avoid the excitation of the resonance frequencies of the structure. The proposed controller is capable to attenuate some of the nonlinearities due to Coriolis and centripetal effects. Experimental results for this proposal are shown. An extension of this work is presented in [59] where an adaptive complement is added to account payload changes then the nonlinear joint controller is adjusted and the frequencies of the prefilters as well.

Inversion-based nonlinear control is presented in [12] for accurate trajectory tracking. Here it is stressed that the adoption of clamped boundary conditions at the actuation side of the flexible links, allows considerable simplification with respect to the case of pinned boundary

conditions. The proposed control strategy is a nonlinear state feedback compensation term and of a linear feedback stabilization term. The proposed controller is tested in simulation.

SPA was used by [60] to divide the dynamics of the flexible system and calculate a composite PID controller. For the slow sub-controller, a PD controller with disturbance observer is used and for the fast sub-controller, modal feedback PID control is utilized. An analysis of the influence of parameter was conducted, some guidelines were established for the tuning process. Experimental results are shown.

In [61] the dynamics of the system is split using SPA, then a dual loop is proposed. The slow dynamic is treated as it were a rigid-link robot, an additional robust decomposition is performed and the changes in mass matrix, Coriolis, stiffness, damping, gravity and/or friction then compensators are calculated for each model uncertainty (assumed to be bounded and partially due to link flexibility). The fast dynamics is taken from the SPA formulation and approximated to be linear and a standard H_∞ controller is calculated for each link. The control strategy is tested experimentally.

Hybrid PD PID controllers are presented in [62,63]. In [62] a hybrid collocated PD and noncollocated PID controller designed for joint tracking and vibration control, respectively. In the PID loop the feedback signal is the acceleration at the tip of each link. Then the control law for each joint is the sum of the control signal of each controller. This decentralized model-free control strategy was tested in simulations. An extension is presented in [63] where the authors propose a complement to the previous controller to enhance its performance. Simulation results show better performance index including this modified P-type learning algorithm.

A decentralized approach has been utilized in [64], where augmented SMC have been calculated for a two flexible-link robot. The robot is subdivided in one flexible-link subsystems; this has the advantage that they require just local measurements and a possible extension to the multilink case is straightforward. The parameters of the controllers are calculated to minimize a functional in terms of the joint errors and modal variables. The controller was tested in simulations.

AVC techniques are applied in [65] where a two flexible-link is provided with PZT along the links for acting and sensing purposes. The joints are regulated via an augmented nonlinear PD controller and the links are approximated as linear elements and a frequency varying LQR with frequency-dependent weightings is used in the AVC loop. Preliminary experimental results are shown.

In [66] an AVC is proposed with the use of continuous PZT bonded along the links. The system dynamics is decoupled using SPA, the slow dynamics is linearized via computed torque method; fast dynamics is influenced by the PZT and the control law uses joint error as feedback signal. The authors suggest that as long as the applied voltage can vary along the link, therefore virtually “all” the modes of vibration of the structure can be damped out. The controller was tested in simulations.

An AVC model-free controller is proposed by [67]. The developed controllers are based on the basic energy-work relationship, in order to avoid the problems of model-based methods such as truncation and spillover. Two kind of PD-based controllers for the rotational actuators and PZT are proposed: decentralized and centralized. Nevertheless, a model is formulated under Lagrangian formalism and AMM to simulate the robot and test the proposed controllers.

A decentralized controller was proposed in [10] for a two flexible-link robot provided with piezoelectric actuators. Joint tracking is performed via model-free PID controllers tuned with the Ziegler-Nichols method. For the AVC a dual loop with a second order SMC for each flexible link is proposed and implemented. The experimental results showed the effectiveness of this approach.

FEM is not the common choice for designing controllers is flexible-link robots, nevertheless some works can be found in the literature. In [25] a direct dynamic model for the flexible-link robot was developed, after discretization the DOF are joint variables and elastic DOF of the links resulting from the discretization of their elastic transformation rotation matrices. For controller calculation the rigid dynamics is linearized then computer torque method is used. Active damping is achieved through an LQR with full stated feedback. The closed loop system is tested experimentally.

In [68] a flexible-link robot is modeled using FEM. A PD based fuzzy logic control strategy is also developed to reduce the end-point vibration, the control strategy is collocated and decentralized. A genetic algorithm is used to optimize the rule base of the fuzzy logic controller. A coupled fuzzy control strategy is proposed to improve the performance of the system. Results are shown in simulations.

Also neural networks have been applied to flexible-link manipulators as in [69]. The FEM model is formulated assigning one element pro link. A nonlinear control law is calculated for the rigid dynamics whose stability is verified. Then an additional joint controller based in neural networks is employed to bear with the effects of link flexibility (uncertainties). The control strategy was tested in simulation.

Other similar kinematic configuration has been also subject of study, two-link flexible robotic structures with the first link *rigid* and the second link *flexible* [70-74], the robots are modeled under lagragian formalism and flexibility with AMM. In [70] small angular displacements are considered of the joints. A decentralized approach is proposed for each link, then a set of local subsystem to be controlled is formulated using only local measurements and the influence (coupling) with the previous link is considered an uncertainty. The control proposed for each link is a PD with feedforward velocity. The control strategy was experimentally validated. A similar system was utilized by [71], here a two stage control strategy is proposed. The inner loop is based on a nonlinear feedback law derived from the asymptotic expansions which results in a PD controller with joint acceleration feedforward. The outer loop is a frequency weighed LQG to compensate the nonmodeled dynamics. The controller was validated experimentally. Stable model inversion control has been proposed in [72], control strategies are proposed to avoid the instabilities caused by the zero dynamics when the tip trajectory tracking is formulated. As countermeasure three stable model inversion controllers using numerical methods based on approximate nonlinear regulation, frequency domain learning and time domain learning are proposed. The effectiveness of the control strategies was tested experimentally. In [73,74] an optimal trajectory based on the flexible dynamic subsystem is calculated, this optimization can reduce the excitation of the mode of vibration and the effect of the uncertain vibration. A SMC is proposed for the slow subsystem and implemented to overcome the influence of error modeling in the optimization process. The trajectories resulting from the optimization showed a high overshoot for the second joint. The controllers were validated experimentally.

Regarding LPM for two flexible-link robots, the mass matrix of such models is supposed to be diagonal or semi-diagonal, which is advantageous for calculations such as a matrix inversion. However, assigning spring constants for the pseudo-joints is not straightforward, and therefore, such models are rarely used for dynamic analysis of flexible manipulators [75].

1.4 Contribution of this Research

Considering the state of the art this work presents some interesting contributions. In this work are presented dynamic models of the structures under study which are modular and its formulation and implementation differs from previous approaches in the sense how the model is stated. In this work, the model after performing the energy balance is separated into integral terms and algebraical terms. The integral terms are calculated via symbolic software which are subsequently integrated as embedded function in Matlab/Simulink where the algebraic terms are also implemented. It makes possible to monitor or follow the single contribution of all the element of the robot and verify its influence in the whole structure. The models obtained here are *direct dynamic models*. In the model formulation are included the actuators and sensors available in the experimental setup.

Another important point in the model formulation of flexible-link robots is the inclusion of an offset due to the link support at the joint, it is commonly neglected. Here it is included to obtain a better approximation to the reality and the whole models are formulated including these additional transformation matrices. For the two flexible-link robot in the model formulation the inertia of the second joint (distal joint) is divided into two parts, the inertia of the relative fix joint and the inertia of the relative rotating joint. In the distal joints angular position and velocities of each part is considered separately. The existing models do not make any distinction about this aspect.

A novel methodology for the robot model validation is proposed to verify if the model is correctly implemented. The vector of Coriolis and centripetal effects is calculated through two different ways and then is compared, also two independent mass matrices are also compared. Some model structure properties are also considered to verify the correctness of the resulting models.

Here different control architectures are presented, ranging from decentralized controllers to a totally centralized controller. Dual loop controllers have certain similarity with the singular perturbation approach, but the controllers are much easier to implement. As long as the presented Lyapunov model-based controller consider a reduced-order model of the whole flexible structure, then the truncation and uncertainties are compensated with the sliding mode complement, it reduces the robot settling time by increasing the links damping and joint tracking.

1.5 Outline of the Dissertation

Three control strategies with sliding mode complement are presented in this work: dual loop approach and centralized and decentralized Lyapunov model-based approaches for joint trajectory tracking and AVC of the flexible-link robots. Additionally a control strategy is proposed for a cantilever flexible beam

This work is organized as follows. In Chapter 2, the models of the flexible beam, one flexible-link robot and two flexible-link robot are developed applying the Lagrangian formalism and AMM to discretize the flexibility of the links. The models including actuators and sensors are subjected to verification and experimental validation. These models are used for the controller calculation of the next Chapter. In Chapter 3, a short theoretical background of SMC is presented then the three previous mentioned control strategies are developed and details of their architecture are given. The controllers obtained in Chapter 3 are validated with experimental results in Chapter 4. The conclusions are given in Chapter 5.

2 Modelling of Vibrating Structures with Flexible Links

In this section three structures are going to be addressed, the complexity is increasing progresively. First a flexible cantilever beam, second a single flexible-link robot and finally a two flexible-link robot. The robots studied here are provided only with rotational holonomic joints. The verification and validation of the models is done following the approach proposed by [76]. Each model to be obtained is a conceptual or theoretical model, this model is implemented and subjected to verification (assumption, approaches and implementation) and finally the model is validated.

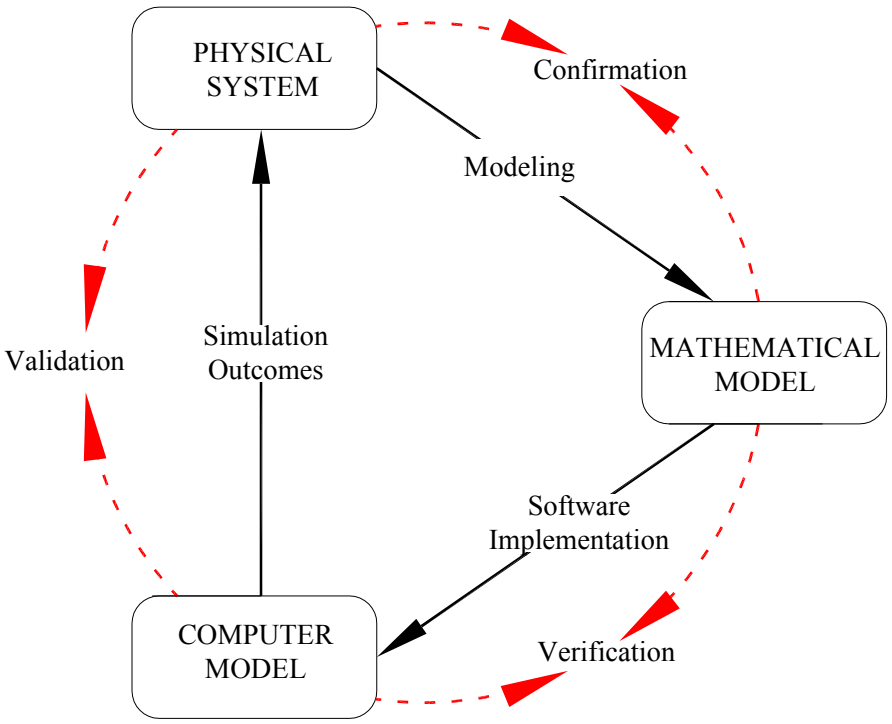

Figure 2.1: Model verification and validation process [76].

The verification process begins with the exhaustive revision of the model obtained analytically, taking into account the algebraic properties of the resulting model (symmetry, anti-symmetry, diagonally). Then the model is implemented using informatic tools as Maple for symbolic calculations and Matlab for simulations. The model should be explicit to provide a clear understanding of dynamic interaction and coupling effects, to be useful for control design, and to guide reduction and/or simplification based on terms relevance. The model should be complete that it is simple enough (e.g., finite- versus infinite-dimensional) while inheriting the most relevant properties [6]. Finally, the implemented model is subjected to validation contrasting the results of the simulations with the measurement of the real system, being both of them tested under the same conditions.

2.1 Cantilever Beam

The first element to be studied in this work is a cantilever beam bending in the horizontal plane, because until the final complex system the beam model is involved. Deflection in beams has been widely studied, in this work the model for the beam proposed is based on the Euler assumptions for pure bending. Development of the beam modeling is briefly reviewed here. Beams can be composed in an infinite number of small elements, a local equilibrium is established and the equations of motion for the differential element are integrated along the continuum. For the sake of completeness, first the static case is addressed and then the dynamic case. As starting point, the following Euler-Bernoulli assumptions are taken into account [77]:

- Cross-sections are plane and normal to the neutral axis remain plane and normal to it after deformation.
- Shear deformations are neglected.
- Beam deflections are small.
- The material is linear elastic according to Hooke's law

This continuum domain is modelled using partial differential equation due to the dependency on location and time. The beam under consideration is shown in Fig. 2.2, it extends from $x = 0$ to $x = l$ and it has a flexural rigidity EI which could be a function of x. For convenience the first part of the modeling is performed with a Newtonian approach and the second part with Lagrangian approach.

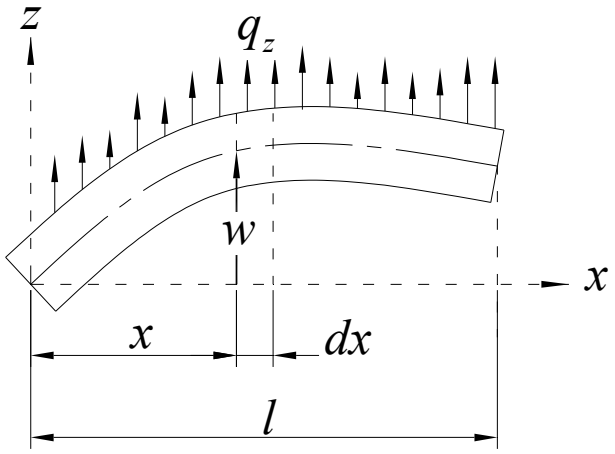

Figure 2.2: Bending beam.

2.1.1 Beam under Static Conditions

The equilibrium equation can be obtained extracting a small element with a differential thickness dx (see Fig. 2.3). All the acting forces and moments are illustrated, i.e. shearing force V, bending moment M, distributed load q_z.

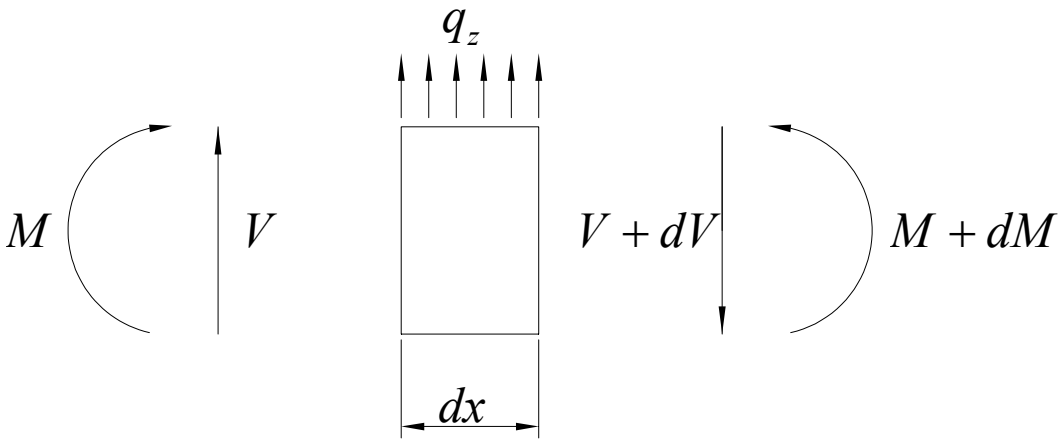

Figure 2.3: Body free diagram for an infinitesimal beam element.

The balance of vertical forces provides

$$V(x) + q_z(x)dx - V(x) + dV(x) = 0\,, \tag{2.1}$$

from this the distributed load can be stated as

$$q_z(x) = \frac{dV(x)}{dx}\,. \tag{2.2}$$

The balance of moment with respect to a point located in the right side of the element

$$-\frac{q_z(x)dx^2}{2} - M(x) - V(x)dx + M(x) + dM(x) = 0\,, \tag{2.3}$$

neglecting dx^2 term, the shearing force can be stated as

$$V(x) = \frac{dM(x)}{dx}\,. \tag{2.4}$$

The normal stress distribution in pure bending is assumed to be linear, taking the value of 0 in the neutral axis and maximal in the extreme fibers as it is shown in Fig. 2.4.

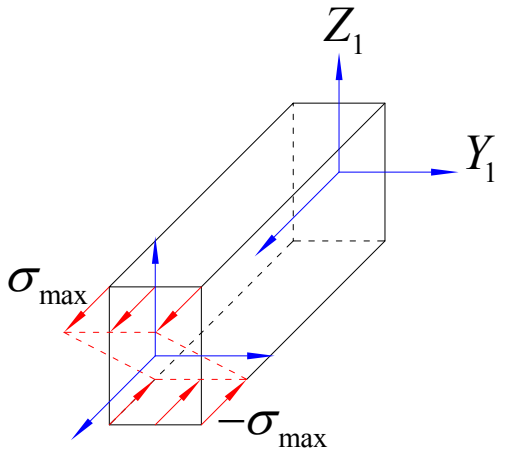

Figure 2.4: Distribution of normal stress in the plane yz.

The bending moment is calculated integrating axial stresses across the transversal area

$$M(x) = -\int_A \sigma_{xx}(x)\, z\, dA\,. \tag{2.5}$$

Under the assumption of pure bending, Hooke's law can be expressed as

$$\sigma_{xx}(x) = E\varepsilon(x)\,. \tag{2.6}$$

The axial strain can be expressed in terms of the axial displacement field

$$\varepsilon(x) = \frac{du(x)}{dx}\ . \tag{2.7}$$

Under the assumption of Navier for bending, the infinitesimal axial displacement is related to the infinitesimal rotation of the differential element

$$du(x) = -z\ d\theta(x)\ . \tag{2.8}$$

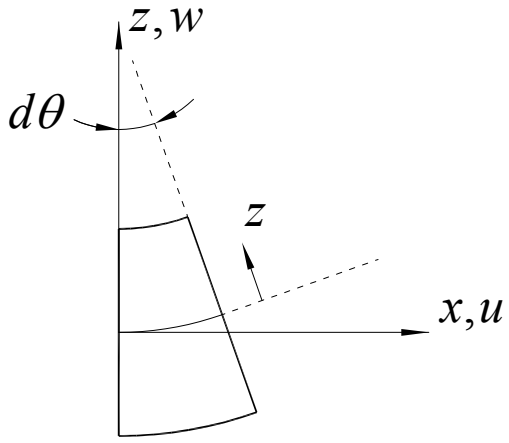

Figure 2.5: Navier assumption.

For small transversal displacements, the rotation of the element is related to the transversal displacement (see Fig. 2.6). Then the following approximation is done

$$\tan(\theta(x)) = \frac{dw(x)}{dx} \approx \theta(x)\,. \tag{2.9}$$

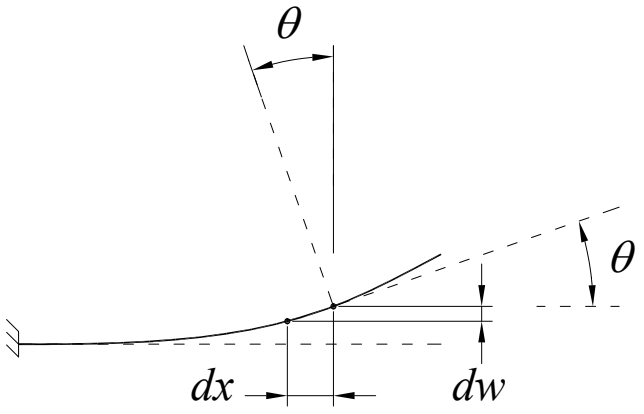

Figure 2.6: Rotation of an element of the beam.

The kinematic relation between the axial strain and transversal displacement is obtained

$$\varepsilon(x) = \frac{du(x)}{dx} = -\frac{d\theta(x)}{dx}\,z = -\frac{d^2w(x)}{dx^2}\,z\,. \tag{2.10}$$

Bending moment and shear force can be expressed in terms of the transversal displacement $w(x)$

$$M(x) = -\int_A E\varepsilon(x)\ z\ dA\,, \tag{2.11}$$

$$M(x) = \int_A E \frac{d^2 w(x)}{dx^2} z^2 \, dA, \tag{2.12}$$

$$M(x) = E \frac{d^2 w(x)}{dx^2} \int_A z^2 \, dA, \tag{2.13}$$

$$I = \int_A z^2 \, dA, \tag{2.14}$$

$$M(x) = EI \frac{d^2 w(x)}{dx^2}, \tag{2.15}$$

$$V(x) = EI \frac{d^3 w(x)}{dx^3}, \tag{2.16}$$

where E is uniform across A i.e. the beam considered in this research is made up of one isotropic material.

2.1.2 Beam under Dynamic Conditions

In the previous analysis an expression for the inner bending moment and shear force are obtained for the static case. For the case of vibrating beams all the variables depend also on time, then the ordinary differentiation turns into a partial differentiation

$$M(x,t) = EI \frac{\partial^2 w(x,t)}{\partial x^2}, \tag{2.17}$$

$$V(x,t) = EI \frac{\partial^3 w(x,t)}{\partial x^3}. \tag{2.18}$$

Then the force due to the inertia of the elements

$$\rho_l \, dx \frac{\partial^2 w(x,t)}{\partial t^2}. \tag{2.19}$$

In the Fig. 2.3 force due to the element inertia has to be included, then the vertical force balance

$$V(x,t) + q_z(x,t)dx - V(x,t) - dV(x,t) = \rho_l \, dx \frac{\partial^2 w(x,t)}{\partial t^2}, \tag{2.20}$$

$$-\frac{q_z(x,t)dx^2}{2} - M(x,t) - V(x,t)dx + M(x,t) + dM(x,t) = 0. \tag{2.21}$$

Inner shear force and bending moment can be written as

$$dV(x,t) = \frac{\partial V(x,t)}{\partial x} dx, \tag{2.22}$$

$$dM(x,t) = \frac{\partial M(x,t)}{\partial x} dx, \tag{2.23}$$

then

$$-\frac{\partial V(x,t)}{\partial x} dx + q_z(x,t)dx = \rho_l \, dx \frac{\partial^2 w(x,t)}{\partial t^2}, \tag{2.24}$$

$$V(x,t) = \frac{\partial M(x,t)}{\partial x}. \tag{2.25}$$

Substituting (2.25) in (2.24)

$$-\frac{\partial^2 M(x,t)}{\partial x^2}+q_z(x,t)=\rho_l\,\frac{\partial^2 w(x,t)}{\partial t^2}\,. \tag{2.26}$$

Then the relation between moment and transversal displacement (2.17) is substituted in (2.24) to obtain the equation of motion in forced vibration

$$\rho_l\,\frac{\partial^2 w(x,t)}{\partial t^2}+EI\,\frac{\partial^4 w(x,t)}{\partial x^4}=q_z(x,t)\,. \tag{2.27}$$

For the case of free vibration $q_z(x,t)=0$ therefore (2.24) turn into

$$\rho_l\,\frac{\partial^2 w(x,t)}{\partial t^2}+EI\,\frac{\partial^4 w(x,t)}{\partial x^4}=0\,, \tag{2.28}$$

$$\frac{\partial^2 w(x,t)}{\partial t^2}+c^2\,\frac{\partial^4 w(x,t)}{\partial x^4}=0\,, \tag{2.29}$$

where

$$c=\sqrt{\frac{EI}{\rho_l}}\,. \tag{2.30}$$

With the modelling approach used along this work, the links i.e. beams are assumed to be subjected only to free vibrations. Additionally, they are considered to be clamped at one end, the reason of this is explained in section 2.2.1. Then including a tip load, the geometric boundary conditions are given by

$$w(x,t)\big|_{x=0}=0\,, \tag{2.31}$$

$$\left.\frac{\partial w(x,t)}{\partial x}\right|_{x=0}=0\,, \tag{2.32}$$

and the natural boundary conditions by

$$EI\left.\frac{\partial^2 w(x,t)}{\partial x^2}\right|_{x=l}=-J_{\mathrm{p}}\,\frac{d^2}{dt^2}\left(\left.\frac{\partial w(x,t)}{\partial x}\right|_{x=l}\right), \tag{2.33}$$

$$EI\left.\frac{\partial^3 w(x,t)}{\partial x^3}\right|_{x=l}=m_{\mathrm{p}}\left.\frac{d^2 w(x,t)}{dt^2}\right|_{x=l}\,. \tag{2.34}$$

In order to approximate the transversal displacement the AMM proposed by Meirovicht [2], where the time dependency and special dependency of the transversal displacement of the beam can be separated in order to transform the partial differential equation into an ordinary differential equation to obtain an n-dimensional model i.e. n flexible modes are taken into account

$$w(x,t)=\sum_{i=1}^{n}\phi_i(x)\,q_{\mathrm{fi}}(t)\,, \tag{2.35}$$

where $q_{\mathrm{fi}}(t)$ the time-varying variable related to the spatial assumed mode shape $\phi_i(x)$. The procedure is done considering one DOF, but at the end it could be extended for more degrees of freedom. With this separation of variables (2.35) then (2.29) can be solved as follows

$$\frac{c^2}{\phi_i(x)}\,\frac{d^4\phi_i(x)}{dx^4}=-\frac{1}{q_{\mathrm{fi}}(t)}\,\frac{d^2 q_{\mathrm{fi}}(t)}{dt^2}=a=\omega^2\,, \tag{2.36}$$

where $a=\omega^2$ is a positive constant, then (2.36) can be separated in two equations

$$\frac{d^2 q_{\mathrm{fi}}(t)}{dt^2}+\omega^2 q_{\mathrm{fi}}(t)=0\,, \tag{2.37}$$

$$\frac{d^4\phi_i(x)}{dx^4} - \beta^4\phi_i(x) = 0\,, \tag{2.38}$$

where

$$\beta_i^4 = \frac{\omega_i^2}{c^2} = \frac{\rho_1\omega_i^2}{EI}\,. \tag{2.39}$$

The solution of (2.37) is a function of the form

$$q_{fi}(t) = e^{j\omega_i^2 t}\,. \tag{2.40}$$

Meanwhile the solution of (2.38) is a function of the form

$$\phi_i(x) = Ce^{sx}\,, \tag{2.41}$$

where C and s are constants. To derive the auxiliary equation

$$s^4 - \beta^4 = 0\,, \tag{2.42}$$

with roots in $s_{1,2} = \pm\beta$ and $s_{3,4} = \pm j\beta$, then the solution of (2.38) is

$$\phi_i(x) = c_{1,i}e^{\beta_i x} + c_{2,i}e^{-\beta_i x} + c_{3,i}e^{j\beta_i x} + c_{4,i}e^{-j\beta_i x} \tag{2.43}$$

where $c_{1,i}$, $c_{2,i}$, $c_{3,i}$ and $c_{4,i}$ which are calculated from the boundary conditions. Therefore (2.43) can be expressed as

$$\phi_i(x) = c_{1,i}\sin(\beta_i x) + c_{2,i}\cos(\beta_i x) + c_{3,i}\sinh(\beta_i x) + c_{4,i}\cosh(\beta_i x)\,. \tag{2.44}$$

The natural frequencies of the beam can be calculated from (2.39)

$$\omega_i = \sqrt{\frac{\beta_i^4 EI}{\rho_1}}\,. \tag{2.45}$$

In order to calculate β_i, the boundary conditions are modified according to the AMM

$$q_{fi}(t)\phi_i(x)\big|_{x=0} = 0 \Rightarrow \phi_i(x)\big|_{x=0} = 0\,, \tag{2.46}$$

$$q_{fi}(t)\frac{\partial\phi_i(x)}{\partial x}\bigg|_{x=0} = 0 \Rightarrow \phi_i'(x)\big|_{x=0} = 0\,. \tag{2.47}$$

On the other hand the first natural boundary condition turns into

$$EI\phi_i''(x)\big|_{x=l}\, q_{fi}(t) = -J_p\,\phi_i'(x)\big|_{x=l}\,\ddot{q}_{fi}(t)\,, \tag{2.48}$$

considering that

$$\frac{\ddot{q}_{fi}(t)}{q_{fi}(t)} = \frac{\beta_i^4 EI}{\rho_1}\,, \tag{2.49}$$

therefore (2.48) can be expressed as

$$\phi_i''(x)\big|_{x=l} - \beta_i^4\frac{J_p}{\rho_1}\phi_i'(x)\big|_{x=l} = 0\,. \tag{2.50}$$

The second natural boundary condition turns into

$$EI\phi_i'''(x)\big|_{x=l}\, q_{fi}(t) = m_p\,\phi_i(x)\big|_{x=l}\,\ddot{q}_{fi}(t)\,, \tag{2.51}$$

then considering (2.49), (2.51) turns into

$$\phi_i'''(x)\big|_{x=l} + \beta_i^4\frac{m_p}{\rho_1}\phi_i(x)\big|_{x=l} = 0\,. \tag{2.52}$$

With each boundary condition substituted in (2.44) can be stated; for the first boundary condition (2.46)

$$c_{2,i} + c_{4,i} = 0\,, \tag{2.53}$$

for the second boundary condition (2.47)

$$c_{1,i} + c_{3,i} = 0\,, \tag{2.54}$$

for the third boundary condition (2.50)

$$\begin{aligned} &-c_{1,i}\rho_1 \sin(\beta_i l) - c_{2,i}\rho_1 \cos(\beta_i l) + c_{3,i}\rho_1 \sinh(\beta_i l) + c_{4,i}\rho_1 \cosh(\beta_i l) \\ &-\beta_i^3 J_\mathrm{p} c_{1,i} \cos(\beta_i l) + \beta_i^3 J_\mathrm{p} c_{2,i} \sin(\beta_i l) - \beta_i^3 J_\mathrm{p} c_{3,i} \cosh(\beta_i l) \\ &-\beta_i^3 J_\mathrm{p} c_{4,i} \sinh \beta_i l) = 0 \end{aligned}\,, \tag{2.55}$$

for the fourth boundary condition (2.52)

$$\begin{aligned} &-c_{1,i}\rho_1 \cos(\beta_i l) + c_{2,i}\rho_1 \sin(\beta_i l) + c_{3,i}\rho_1 \cosh(\beta_i l) + c_{4,i}\rho_1 \sinh(\beta_i l) \\ &+\beta_i m_\mathrm{p} c_{1,i} \sin(\beta_i l) + \beta_i m_\mathrm{p} c_{2,i} \cos(\beta_i l) + \beta_i m_\mathrm{p} c_{3,i} \sinh(\beta_i l) \\ &+\beta_i m_\mathrm{p} c_{4,i} \cosh \beta_i l) = 0 \end{aligned}\,. \tag{2.56}$$

Then a linear system of equations is formulated from (2.53), (2.54), (2.55) and (2.56)

$$\tilde{\boldsymbol{W}} \begin{bmatrix} c_{1,i} \\ c_{2,i} \\ c_{3,i} \\ c_{4,i} \end{bmatrix} = \begin{bmatrix} 0 \\ 0 \\ 0 \\ 0 \end{bmatrix}, \tag{2.57}$$

where

$$\tilde{w}_{1,1} = \tilde{w}_{1,3} = \tilde{w}_{2,2} = \tilde{w}_{2,4} = 1\,, \tag{2.58}$$

$$\tilde{w}_{1,2} = \tilde{w}_{1,4} = \tilde{w}_{2,1} = \tilde{w}_{2,3} = 0\,, \tag{2.59}$$

$$\tilde{w}_{3,1} = \rho_1 \cos(\beta_i l) + m_\mathrm{p}\beta_i \sin(\beta_i l)\,, \tag{2.60}$$

$$\tilde{w}_{3,2} = \rho_1 \sin(\beta_i l) + m_\mathrm{p}\beta_i \cos(\beta_i l)\,, \tag{2.61}$$

$$\tilde{w}_{3,3} = \rho_1 \cosh(\beta_i l) + m_\mathrm{p}\beta_i \sinh(\beta_i l)\,, \tag{2.62}$$

$$\tilde{w}_{3,4} = \rho_1 \sinh(\beta_i l) + m_\mathrm{p}\beta_i \cosh(\beta_i l)\,, \tag{2.63}$$

$$\tilde{w}_{4,1} = -\rho_1 \sinh(\beta_i l) - \beta_i^3 J_\mathrm{p} \cos(\beta_i l)\,, \tag{2.64}$$

$$\tilde{w}_{4,2} = -\rho_1 \cos(\beta_i l) + \beta_i^3 J_\mathrm{p} \sin(\beta_i l)\,, \tag{2.65}$$

$$\tilde{w}_{4,3} = \rho_1 \sinh(\beta_i l) - \beta_i^3 J_\mathrm{p} \cosh(\beta_i l)\,, \tag{2.66}$$

$$\tilde{w}_{4,4} = \rho_1 \cosh(\beta_i l) - \beta_i^3 J_\mathrm{p} \sinh(\beta_i l)\,. \tag{2.67}$$

The parameter β_i for each mode of vibration arises from the nontrivial solution of (2.57) i.e. $\det(\tilde{\boldsymbol{W}}) = 0$, therefore the following transcendental equation is obtained

$$\begin{aligned} &m_\mathrm{p} J_\mathrm{p} \beta_i^4 + \rho_1^2 \cos(\beta_i l) \cosh(\beta_i l) - \rho_1 \beta_i^3 J_p \sin(\beta_i l) \cosh(\beta_i l) \\ &+m_\mathrm{p}\rho_1 \beta_i \cos(\beta_i l) \sinh(\beta_i l) - m_\mathrm{p} J_\mathrm{p} \beta_i^4 \cos(\beta_i l) \cosh(\beta_i l) \\ &+\rho_1 \beta_i^3 J_\mathrm{p} \cos(\beta_i l) \sinh(\beta_i l) - m_\mathrm{p}\rho_1 \beta_i \sin(\beta_i l) \cosh(\beta_i l) + \rho_1^2 = 0 \end{aligned}\,. \tag{2.68}$$

The solutions of (2.68) can be obtained numerically and with $\boldsymbol{\beta} = \begin{bmatrix} \beta_1 & \dots & \beta_n \end{bmatrix}^\mathrm{T}$ the natural frequencies ω_i of the beam are obtained using (2.39). To calculate the constants

$c_{j,i}\ i = 1..4\ \hat{}\ j = 1..n$ the components of $\boldsymbol{\beta}$ are substituted for each mode of vibration. Nevertheless, the third and fourth linear equations are linearly related. Then an additional condition is required, it is related to the orthogonality of the modes of vibration

$$\int_0^l \rho_l\, \phi_i(x)\, \phi_j(x)\, dx + m_p\, \phi_i(l)\, \phi_j(l) + J_p\, \phi_i'(l)\, \phi_j'(l) = m_l \delta_{ij} \tag{2.69}$$

where δ_{ij} is the Kronecker delta symbol. At this point all the c_{ji} can be calculated.

As next step for the deduction of the beam equation of motion some kinematic relations are defined

$$\boldsymbol{p}_1(x,t) = \left[x \;\; w(x,t)\right]^T, \tag{2.70}$$

$$\dot{\boldsymbol{p}}_1(x,t) = \left[0 \;\; \dot{w}(x,t)\right]^T, \tag{2.71}$$

$${}^1\boldsymbol{r}_2(t) = \left[l \;\; w_e(t)\right]^T, \tag{2.72}$$

$${}^1\dot{\boldsymbol{r}}_2(t) = \left[0 \;\; \dot{w}_e(t)\right]^T, \tag{2.73}$$

where the sub index $_e$ indicates that the term is evaluated at the endpoint of the link i.e. $x = l$ (see Fig. 2.7). Here the position of any point along the deformed beam $\boldsymbol{p}_1(x,t)$ and the position of the tip of the beam ${}^1\boldsymbol{r}_2(t)$ are defined to calculate the Lagrangian, which is defined as the difference between the kinetic energy and potential energy of the system

$$L = T - U\,. \tag{2.74}$$

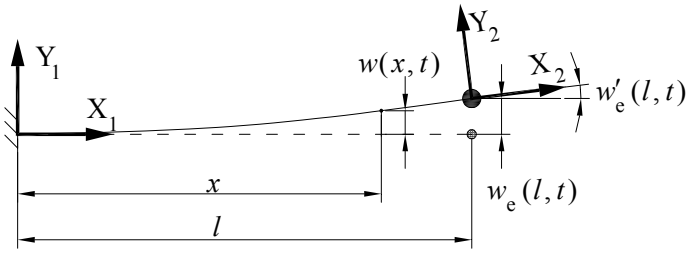

Figure 2.7: Kinematic relations for cantilever beam.

The kinetic energy is made up of the contribution of the link and payload

$$T = T_l + T_p, \tag{2.75}$$

$$T_l = \frac{1}{2}\rho_l \int_0^l \dot{\boldsymbol{p}}_1(x,t)^T\, \dot{\boldsymbol{p}}_1(x,t) dx\,, \tag{2.76}$$

$$T_p = \frac{1}{2} m_p\, {}^1\dot{\boldsymbol{r}}_2^{\,T}\, {}^1\dot{\boldsymbol{r}}_2 + \frac{1}{2} J_p \dot{w}_e'(t)\,. \tag{2.77}$$

All the systems considered in this work move in the horizontal plane i.e. there is no gravity involved in the analysis. Therefore potential energy is only due to elastic deformation

$$U = \frac{1}{2} EI \int_0^l \left(\frac{\partial^2 w(x,t)}{\partial x^2} \right)^2 dx\,. \tag{2.78}$$

Regarding potential energy, it is important to mention that the potential passive energy added to the system by including the stiffness of the piezoelectric patches can be neglected (see Appendix A.2).

The previous equations can be reformulated as

$$T_{\mathrm{l}} = \frac{1}{2}\rho_l \int_0^l \dot{w}(x,t)^2\, dx = \frac{1}{2}\rho_l \int_0^l \left(\sum_{i=1}^{n} \phi_i(x)\, \dot{q}_i(t) \right)^2 dx\,, \tag{2.79}$$

$$T_{\mathrm{p}} = \frac{1}{2} m_{\mathrm{p}} \dot{w}_{\mathrm{e}}^2(t) + \frac{1}{2} J_{\mathrm{p}} \dot{w}_{\mathrm{e}}'^2(t) = \frac{1}{2} m_{\mathrm{p}} \left(\sum_{i=1}^{n} \phi_i(l)\, \dot{q}_i(t) \right)^2 + \frac{1}{2} J_{\mathrm{p}} \left(\sum_{i=1}^{n} \phi_i'(l)\, \dot{q}_i(t) \right)^2, \tag{2.80}$$

$$U = \frac{1}{2} EI \int_0^l \left(\sum_{i=1}^{n} \phi_i''(x)\, q_i(t) \right)^2 dx\ . \tag{2.81}$$

Then the n Lagrange equations to be satisfied are

$$\frac{d}{dt}\frac{\partial L}{\partial \dot{q}_i} - \frac{\partial L}{\partial q_i} = f_i, \quad i = 1..n\,. \tag{2.82}$$

Because the potential energy has no dependency on the modal velocities the first term of the Lagrangian is reduced to

$$\frac{d}{dt}\frac{\partial L}{\partial \dot{q}_i} = \frac{d}{dt}\frac{\partial T_{\mathrm{l}}}{\partial \dot{q}_i} + \frac{d}{dt}\frac{\partial T_{\mathrm{p}}}{\partial \dot{q}_i}\,. \tag{2.83}$$

The potential energy does not depend on the position. The second term of the Lagrangian is reduced to

$$\frac{\partial L}{\partial q_i} = -\frac{\partial U}{\partial q_i}\ . \tag{2.84}$$

Substituting (2.79) – (2.81) in (2.83) and (2.84)

$$\frac{d}{dt}\frac{\partial T_{\mathrm{l}}}{\partial \dot{q}_i} = \int_0^l \phi_i(x) \sum_{i=1}^{n} \phi_j(x)\, \ddot{q}_{\mathrm{j}}(t)\, dx\,, \tag{2.85}$$

$$\frac{d}{dt}\frac{\partial T_{\mathrm{p}}}{\partial \dot{q}_i} = m_{\mathrm{p}} \phi_{\mathrm{e}i} \sum_{i=1}^{n} \phi_{\mathrm{e}j}\, \ddot{q}_{\mathrm{j}}(t) + J_{\mathrm{p}} \phi_{\mathrm{e}i}' \sum_{i=1}^{n} \phi_{\mathrm{e}j}'\, \ddot{q}_{\mathrm{j}}(t)\,, \tag{2.86}$$

$$\frac{\partial U}{\partial q_i} = EI \int_0^l \phi_i''(x) \sum_{j=1}^{n} \phi_j''(x)\, q_j(t)\, dx\,. \tag{2.87}$$

The first modes of vibration have the bigger amplitude; therefore the model is truncated in the second mode of vibration i.e. $n = 2$. Then the equations take the following form

$$\frac{d}{dt}\frac{\partial T_{\mathrm{l}}}{\partial \dot{q}_1} = \rho_l \int_0^l \phi_1^2(x) dx\, \ddot{q}_1(t) + \rho_l \int_0^l \phi_1(x)\phi_2(x) dx\, \ddot{q}_2(t)\,, \tag{2.88}$$

$$\frac{d}{dt}\frac{\partial T_{\mathrm{l}}}{\partial \dot{q}_2} = \rho_l \int_0^l \phi_1(x)\phi_2(x) dx\, \ddot{q}_1(t) + \rho_l \int_0^l \phi_2^2(x) dx\, \ddot{q}_2(t)\,, \tag{2.89}$$

$$\frac{d}{dt}\frac{\partial T_{\mathrm{p}}}{\partial \dot{q}_1} = \left(m_{\mathrm{p}} \phi_{\mathrm{e}1}^2 + J_{\mathrm{p}} \phi_{\mathrm{e}1}'^2 \right) \ddot{q}_1(t) + \left(m_{\mathrm{p}} \phi_{\mathrm{e}1} \phi_{\mathrm{e}2} + J_{\mathrm{p}} \phi_{\mathrm{e}1}' \phi_{\mathrm{e}2}' \right) \ddot{q}_2(t)\,, \tag{2.90}$$

$$\frac{d}{dt}\frac{\partial T_{\mathrm{p}}}{\partial \dot{q}_2} = \left(m_{\mathrm{p}} \phi_{\mathrm{e}1} \phi_{\mathrm{e}2} + J_{\mathrm{p}} \phi_{\mathrm{e}1}' \phi_{\mathrm{e}2}' \right) \ddot{q}_1(t) + \left(m_{\mathrm{p}} \phi_{\mathrm{e}2}^2 + J_{\mathrm{p}} \phi_{\mathrm{e}2}'^2 \right) \ddot{q}_2(t)\,, \tag{2.91}$$

$$\frac{\partial U}{\partial q_1} = \left(EI \int_0^l \phi_1''^2(x) dx \right) q_1(t) + \left(EI \int_0^l \phi_1''(x)\phi_2''(x) dx \right) q_2(t)\ , \tag{2.92}$$

$$\frac{\partial U}{\partial q_2} = \left(EI \int_0^l \phi_1''(x)\phi_2''(x) dx \right) q_1(t) + \left(EI \int_0^l \phi_2''^2(x) dx \right) q_2(t)\ , \tag{2.93}$$

$$\frac{d}{dt}\frac{\partial L}{\partial \dot{q}_i}-\frac{\partial L}{\partial q_i}=f_i,\quad i=1,2\ , \tag{2.94}$$

$$\begin{bmatrix} \frac{d}{dt}\frac{\partial T_1}{\partial \dot{q}_1}+\frac{d}{dt}\frac{\partial T_p}{\partial \dot{q}_1}+\frac{\partial U}{\partial q_1} \\ \frac{d}{dt}\frac{\partial T_1}{\partial \dot{q}_2}+\frac{d}{dt}\frac{\partial T_p}{\partial \dot{q}_2}+\frac{\partial U}{\partial q_2} \end{bmatrix}=\begin{bmatrix} f_1 \\ f_2 \end{bmatrix}. \tag{2.95}$$

After some simplifications the equation of motion in standard form can be stated

$$\boldsymbol{M}\,\ddot{\boldsymbol{q}}+\boldsymbol{K}\boldsymbol{q}=\boldsymbol{f}\ , \tag{2.96}$$

where

$$m_{1,1}=\rho_l\int_0^l\phi_1^2(x)dx+m_p\phi_{e1}^2+J_p\phi_{e1}'^2=m_{_1}\,, \tag{2.97}$$

$$m_{1,2}=\rho_l\int_0^l\phi_1(x)\phi_2(x)dx+m_p\phi_{e1}\phi_{e2}+J_p\phi_{e1}'\phi_{e2}'=0\,, \tag{2.98}$$

$$m_{2,1}=\rho_l\int_0^l\phi_1(x)\phi_2(x)dx+m_p\phi_{e1}\phi_{e2}+J_p\phi_{e1}'\phi_{e2}'=0\,, \tag{2.99}$$

$$m_{2,2}=\rho_l\int_0^l\phi_2^2(x)dx+m_p\phi_{e2}^2+J_p\phi_{e2}'^2=m_{_1}\,, \tag{2.100}$$

$$k_{1,1}=EI\int_0^l\phi_1''^2(x)dx=m_{_1}\omega_1^2\ , \tag{2.101}$$

$$k_{1,2}=EI\int_0^l\phi_1''(x)\phi_2''(x)dx\approx 0\ , \tag{2.102}$$

$$k_{2,1}=EI\int_0^l\phi_1''(x)\phi_2''(x)dx\approx 0 \tag{2.103}$$

$$k_{2,2}=EI\int_0^l\phi_2''^2(x)dx=m_{_1}\omega_2^2\ . \tag{2.104}$$

The stiffness matrix $\boldsymbol{K}$ is diagonal due to the orthogonality of the modes of vibrations [78]. Continuous structures show a structural damping due to friction in its microstructural particles, and then there is an energy lost from kinetic energy to thermal energy. The passive structural system damping can be assumed to be proportional [77,79,80]

$$\boldsymbol{M}\,\ddot{\boldsymbol{q}}+\boldsymbol{K}\boldsymbol{q}+\boldsymbol{D}\dot{\boldsymbol{q}}=\boldsymbol{f}\ , \tag{2.105}$$

$$\boldsymbol{D}=2\boldsymbol{\xi}\left(\boldsymbol{K}\boldsymbol{M}\right)^{\frac{1}{2}}. \tag{2.106}$$

It can be stated in this manner, considering that

$$\boldsymbol{M}=\mathrm{diag}\left(m_1\right)\ , \tag{2.107}$$

$$\begin{bmatrix}\dot{\boldsymbol{q}}\\ \ddot{\boldsymbol{q}}\end{bmatrix}=\begin{bmatrix}\mathbf{0} & \mathbf{I}\\ -\boldsymbol{M}^{-1}\boldsymbol{K} & -\boldsymbol{M}^{-1}\boldsymbol{D}\end{bmatrix}\begin{bmatrix}\boldsymbol{q}\\ \dot{\boldsymbol{q}}\end{bmatrix}+\begin{bmatrix}\mathbf{0}\\ \boldsymbol{M}^{-1}\end{bmatrix}\begin{bmatrix}\mathbf{0}\\ \boldsymbol{f}\end{bmatrix}. \tag{2.108}$$

The physical system is of the type M-K-D, but the solutions to the eigenvalue problem are obtained during the calculation of the resonance frequencies (M-K system). According to [81] this can be done as long as the following equality is fulfilled

$$\left(\boldsymbol{M}^{-1}\boldsymbol{K}\right)\left(\boldsymbol{M}^{-1}\boldsymbol{D}\right)=\left(\boldsymbol{M}^{-1}\boldsymbol{D}\right)\left(\boldsymbol{M}^{-1}\boldsymbol{K}\right). \tag{2.109}$$

In the case of a cantilever beam the resulting system is linear, then it is possible to transform (2.108) into a continuous-time state-space representation

$$\begin{aligned}\dot{\boldsymbol{x}}&=\boldsymbol{A}_p\boldsymbol{x}+\boldsymbol{B}_p\boldsymbol{u}\\ \boldsymbol{y}&=\boldsymbol{C}_p\boldsymbol{x}+\boldsymbol{D}_p\boldsymbol{u}\end{aligned} \tag{2.110}$$

where $\boldsymbol{x} \in \mathbb{R}^{2n}$, $\boldsymbol{u} \in \mathbb{R}^{m}$, $\boldsymbol{y} \in \mathbb{R}^{p}$, $\boldsymbol{A}_{\mathrm{p}} \in \mathbb{R}^{2n \times 2n}$, $\boldsymbol{B}_{\mathrm{p}} \in \mathbb{R}^{2n \times m}$, $\boldsymbol{C}_{\mathrm{p}} \in \mathbb{R}^{p \times 2n}$, $\boldsymbol{D}_{\mathrm{p}} \in \mathbb{R}^{p \times m}$

$$\boldsymbol{x} = \begin{bmatrix} \boldsymbol{q} \\ \dot{\boldsymbol{q}} \end{bmatrix}, \tag{2.111}$$

$$\boldsymbol{A}_{\mathrm{p}} = \begin{bmatrix} \mathbf{0} & \mathbf{I} \\ -\boldsymbol{M}^{-1}\boldsymbol{K} & -\boldsymbol{M}^{-1}\boldsymbol{D} \end{bmatrix}, \tag{2.112}$$

$$\boldsymbol{B}_{\mathrm{p}} = \begin{bmatrix} \mathbf{0} \\ \boldsymbol{M}^{-1} \end{bmatrix}, \tag{2.113}$$

$$\boldsymbol{u} = \begin{bmatrix} \mathbf{0} \\ \boldsymbol{f} \end{bmatrix}, \tag{2.114}$$

$$\boldsymbol{f} = \boldsymbol{B}_{\mathrm{pi}} v_{\mathrm{pi}}, \tag{2.115}$$

and

$$\boldsymbol{C}_{\mathrm{p}} = \mathbf{I}, \ \boldsymbol{D}_{\mathrm{p}} = \mathbf{0}. \tag{2.116}$$

The matrix $\boldsymbol{B}_{\mathrm{pi}} \in \mathbb{R}^{n \times m}$ performs the conversion in the piezoelectric actuators from voltage v_{pi} to applied bending moment as it was shown in Appendix A.1.

$$\boldsymbol{B}_{\mathrm{pi}} = \left[\bar{c} \left(\phi_1'(x_{\mathrm{pi}_2}) - \phi_1'(x_{\mathrm{pi}_1}) \right) \ \bar{c} \left(\phi_2'(x_{\mathrm{pi}_2}) - \phi_2'(x_{\mathrm{pi}_1}) \right) \right]^{\mathrm{T}}. \tag{2.117}$$

For implementation purposes the flexible variables are defined in term of deformations as follows

$$\begin{bmatrix} q_1 \\ q_2 \end{bmatrix} = \boldsymbol{\psi}^{-1} \begin{bmatrix} \varepsilon_1 \\ \varepsilon_2 \end{bmatrix}. \tag{2.118}$$

Assuming $\boldsymbol{\psi}$ is a constant non-singular matrix and it is defined by

$$\boldsymbol{\psi} = t_1 \begin{bmatrix} \phi_1''(x)\big|_{x=x_{s_1}} & \phi_2''(x)\big|_{x=x_{s_1}} \\ \phi_1''(x)\big|_{x=x_{s_2}} & \phi_2''(x)\big|_{x=x_{s_2}} \end{bmatrix}, \tag{2.119}$$

where x_{s_1} and x_{s_2} define the location of the deformation sensors (strain gages) along the beam (see Fig. 2.8)

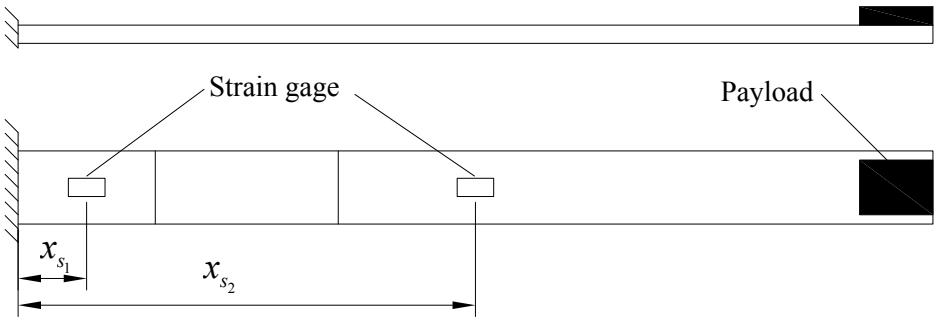

Figure 2.8: Location of the sensors along the beam.

The beam under study has the dimensions given in Tab. 2.1 and their first two modes of vibration and their spatial derivatives are shown in Figs. 2.9 and 2.10. The sensors are located away from the nodes of deformation ($\phi'' = 0$) in order to get information of the two considered modes of vibration.

Table 2.1 Physical parameters of the cantilever beam

Parameter	Value	Complementary information
Material	Aluminum	DIN $AlMg_3$ F22
l	0.31	m
m_l	0.059	kg
EI	1.6333	Nm^2
t_l	0.002	m
m_p	0.060	kg
J_p	$1.84x10^{-5}$	kg m^2
x_{s1}	0.015	m
x_{s2}	0.175	m
ρ_l	0.1876	kg m^{-1}
$\phi_1''(x_{s1})$	27.6856	m^{-1}
$\phi_1''(x_{s2})$	11.6153	m^{-1}
$\phi_2''(x_{s1})$	245.7602	m^{-1}
$\phi_2''(x_{s2})$	-207.5059	m^{-1}

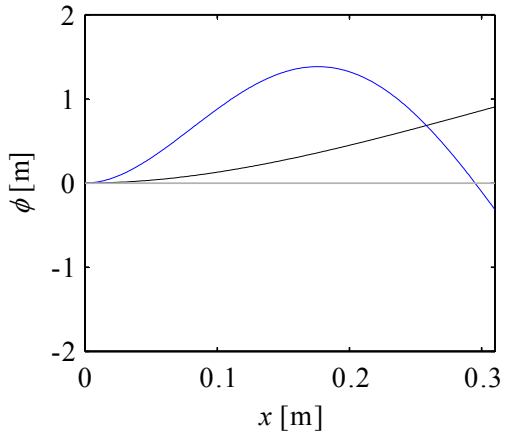

Figure 2.9: Modes of vibration of the beam.
First mode (black), second mode (blue) and undeformed beam (gray).

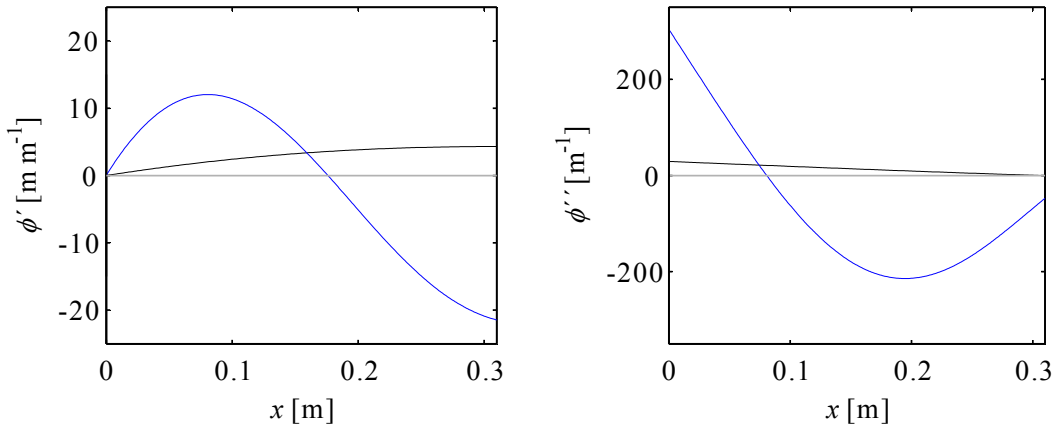

Figure 2.10: Spatial derivatives of the modes of vibration of the beam. Left: first derivative, right: second derivative. First mode (black), second mode (blue) and undeformed beam (gray).

In order to observe the influence of the inertial parameter in the resonance frequencies of the beam a parametric sensitivity analysis [82] was done, where the mass and inertia of the tipload vary from the values given in Tab. 2.1. The dimensions of the beam are considered taking into account the dimensions of the complete robotic arm i.e. its dimensions correspond to the first flexible link. In Figs. 2.11, 2.12, 2.13 and 2.14 results of this analysis are shown.

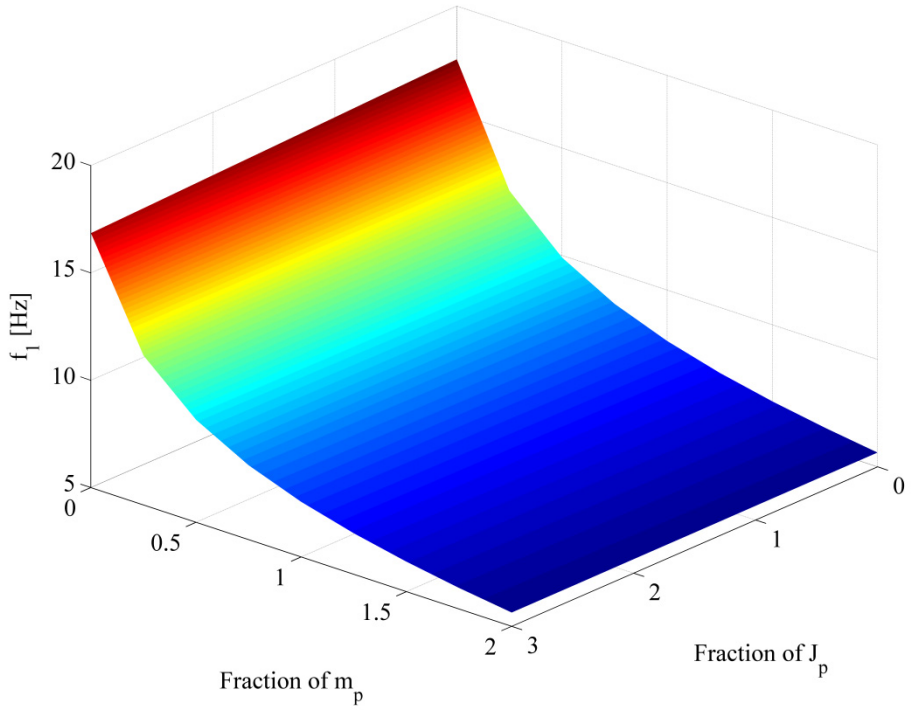

Figure 2.11: First resonance frequency of the beam under different tipload values.

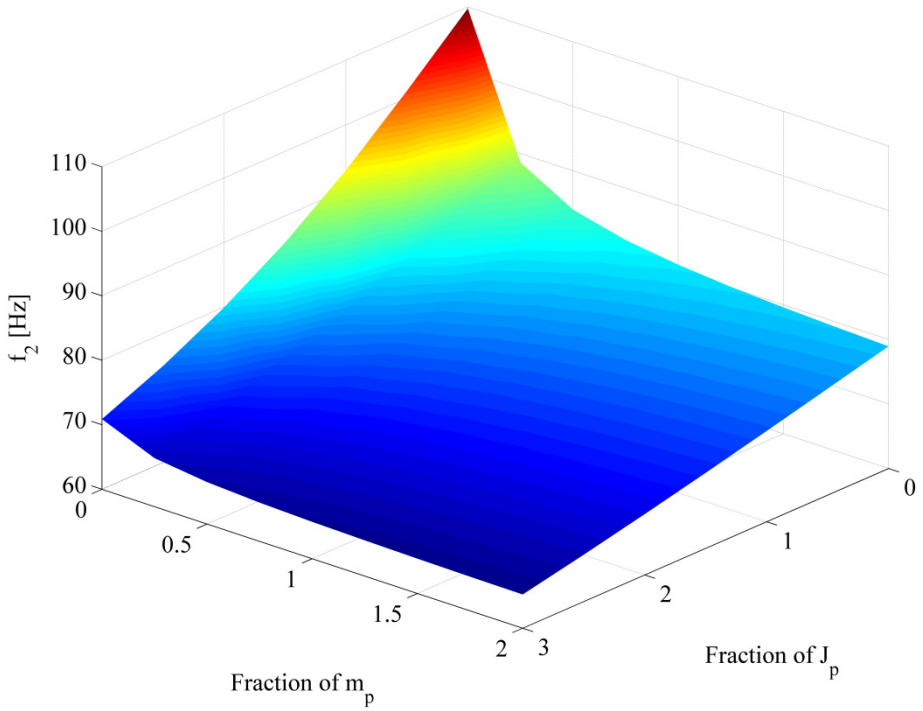

Figure 2.12: Second resonance frequency of the beam under different tipload values.

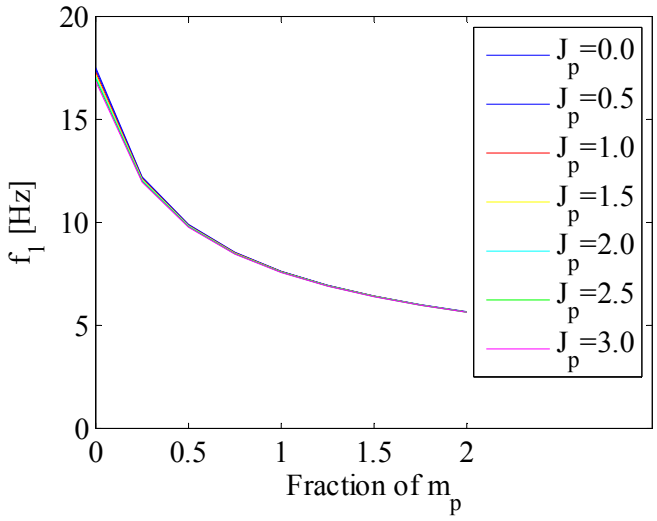

Figure 2.13: First resonance frequency of the beam under different natural boundary conditions.

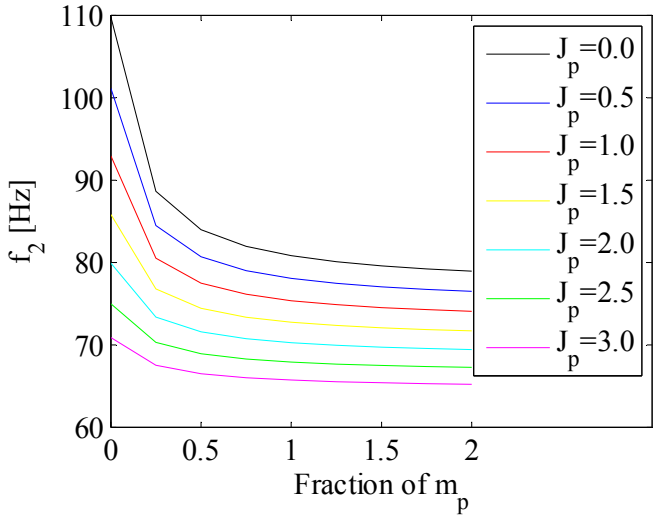

Figure 2.14: Second resonance frequency of the beam under different natural boundary conditions.

From this results can be seen that for the first resonance frequency the beam is dominated exclusively by m_p, where J_p has practically no influence. It is due to the slenderness of the beam, where $\rho_l \int_0^l \phi_l^2(x)dx + m_p \phi_{e1}^2 \gg J_p \phi_{e1}'^2$. On the other hand the second resonance frequency is slightly influenced by J_p because the slope of the second mode of vibration at the tip of the beam (ϕ_{e2}') is not as small as for the first mode.

2.1.3 Model Verification

According to Schlesinger [76], the implemented model must represent the conceptual or theoretical model as close as possible. From the implementation of orthogonality condition for the modes of vibration, a modal representation for the flexible coordinates is obtained. Therefore the mass, damping and stiffness matrices are diagonal (see (2.97-2.107)), after the implementation it is fulfilled. Also the elements of the stiffness satisfy the condition $k_{i,i} = m_l \omega_i^2$. It is shown with a numerical example using the default values given in Tab. 2.1. The matrices of the equation of motion considering a modal damping of $\xi_1 = 0.0035$ ^ $\xi_2 = 0.045$ for the aluminum are given by

$$\boldsymbol{M} = \begin{bmatrix} m_1 & 0 \\ 0 & m_1 \end{bmatrix} = \begin{bmatrix} 0.059 & 0 \\ 0 & 0.059 \end{bmatrix}, \tag{2.120}$$

$$\boldsymbol{K} = \begin{bmatrix} m_1\omega_1^2 & 0 \\ 0 & m_1\omega_2^2 \end{bmatrix} = \begin{bmatrix} 135 & 0 \\ 0 & 13229 \end{bmatrix}, \tag{2.121}$$

$$\boldsymbol{D} = \begin{bmatrix} 2\xi_1\left(k_{1,1}m_1\right)^{0.5} & 0 \\ 0 & 2\xi_2\left(k_{2,2}m_1\right)^{0.5} \end{bmatrix} = \begin{bmatrix} 0.0197 & 0 \\ 0 & 2.5144 \end{bmatrix}, \tag{2.122}$$

$$\boldsymbol{\psi} = \begin{bmatrix} \phi_1''(x)\big|_{x=x_{s1}} & \phi_2''(x)\big|_{x=x_{s1}} \\ \phi_1''(x)\big|_{x=x_{s2}} & \phi_2''(x)\big|_{x=x_{s2}} \end{bmatrix} = \begin{bmatrix} 27.6856 & 245.7602 \\ 11.6153 & -207.5059 \end{bmatrix}. \tag{2.123}$$

The correspondence of dynamic behavior between the implemented model and the conceptual is illustrated in the Fig. 2.15.

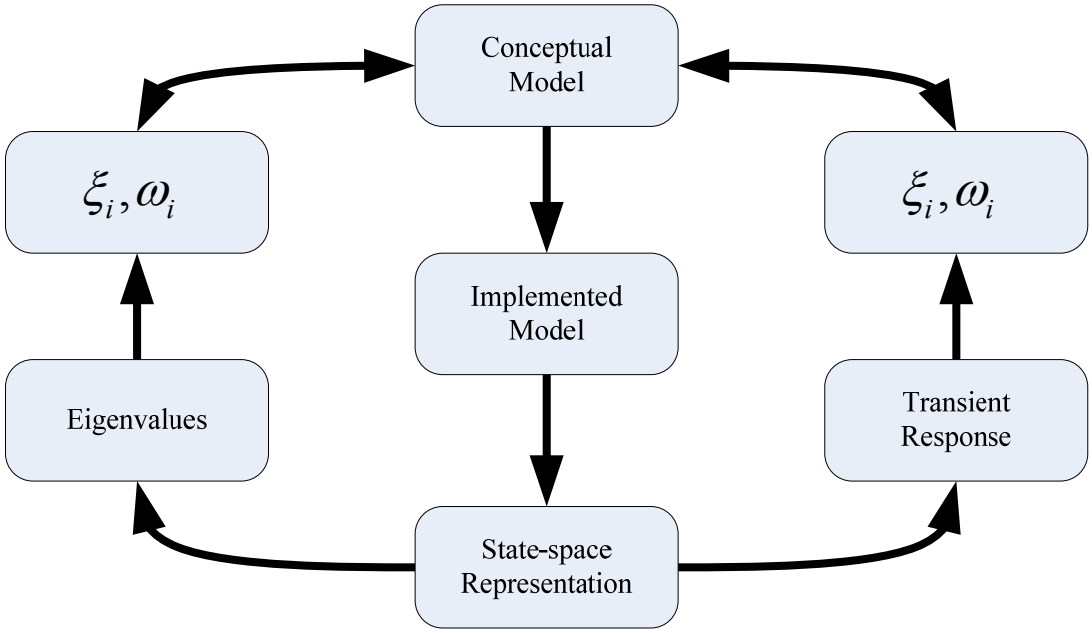

Figure 2.15: Suggested verification sequence for the beam model.

The model can be verified establishing a state-space representation, calculating the eigenvalues of the dynamic matrix and finally calculating the damping and natural frequencies. On the other hand, the implemented model can be simulated and from its transient response the natural frequencies and damping are obtained. The state-space representation matrices are

$$\boldsymbol{A}_{\mathrm{p}} = \begin{bmatrix} 0 & 0 & 1 & 0 \\ 0 & 0 & 0 & 1 \\ 2286.2 & 0 & -0.3347 & 0 \\ 0 & 224220 & 0 & -42.6167 \end{bmatrix}, \tag{2.124}$$

$$\boldsymbol{B}_{\mathrm{p}} = \begin{bmatrix} 0 \\ 0 \\ 0.0218 \\ 0.0709 \end{bmatrix}, \tag{2.125}$$

$$\boldsymbol{C}_{\mathrm{p}} = \begin{bmatrix} 1 & 0 & 0 & 0 \\ 0 & 1 & 0 & 0 \end{bmatrix}, \tag{2.126}$$

and

$$\boldsymbol{D}_{\mathrm{p}} = \begin{bmatrix} 0 \\ 0 \end{bmatrix}. \tag{2.127}$$

The eigenvalues of A_{p} define the dynamic behavior of the system and are given by

$$p_{A_{\mathrm{p}}} = \begin{bmatrix} -0.1673 + 47.8136i \\ -0.1673 - 47.8136i \\ -21.3080 + 473.04i \\ -21.3080 - 473.04i \end{bmatrix}. \tag{2.128}$$

From $s_{\mathrm{p}} = -\omega_i \xi_i \pm i\omega_i \sqrt{1-\xi_i^2}$, the natural frequency and damping for each mode can be calculated. Values are shown in Tab. 2.1. The next step in the verification of the model is the simulation of the free response of the beam and from the time evolution of the modal variables the damping factors and natural frequencies can be calculated for a final triangulation. Damping factors (ξ) are calculated from the logarithmic decrement (δ)

$$\delta = \frac{1}{n_c} \ln\left(\frac{x_{A1}}{x_{A2}}\right), \tag{2.129}$$

$$\xi = \frac{1}{\sqrt{1+\left(\frac{2\pi}{\delta}\right)^2}}. \tag{2.130}$$

According to the low values of damping factor for aluminum, which are $\xi << 1$, can the damped frequencies assumed to be practically equal to the resonance frequencies, i.e.

$$\omega_d = \omega_i \sqrt{1-\xi_i^2} \approx \omega_i. \tag{2.131}$$

In Fig. 2.16 is shown the time evolution of the modal coordinates when are subjected to the initial conditions $\boldsymbol{x}(0) = \left[8.42 \cdot 10^{-4} \;\; 2.12 \cdot 10^{-6} \;\; 0 \;\; 0\right]^{\mathrm{T}}$.

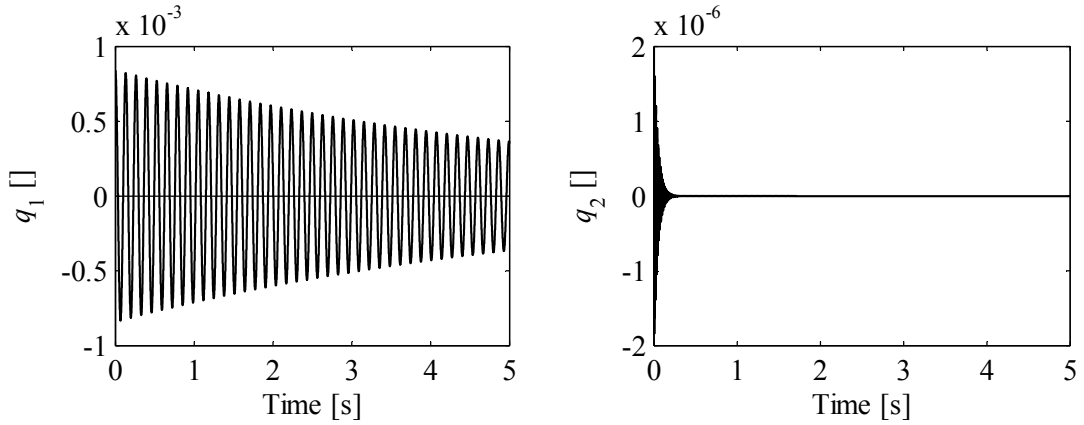

Figure 2.16: Free response to initial conditions for the beam (simulation).

Taking into account eight cycles ($n_c = 8$), the logarithmic decrement for the first and second mode in transient response are $\delta_1 = 0.022$ and $\delta_2 = 0.283$, respectively. Damping factors and natural frequencies are given in Tab. 2.2.

Table 2.2 Summary of model beam verification

Parameter	Theoretical- value	State-space	Transient response
$\omega_1\,[\mathrm{rad/s}]$	47.81	47.80	47.18
$\omega_2\,[\mathrm{rad/s}]$	473.52	474.00	473.31
ξ_1	0.0035	0.0035	0.0035
ξ_2	0.0450	0.0450	0.0449

Tab. 2.2 shows similar values for the parameters are obtained through different procedures. From this can be concluded that the model is correctly implemented because there is correspondence between the theoretical model and its implementation.

2.1.4 Model Validation

In order to verify the quality of the proposed model, the behavior of the beam is studied when it is subjected to some initial condition different from zero and when the beam is subjected to harmonic signal through the piezoelectric actuator. It is important to mention that the initial conditions are the same of the simulations, then simulation model and physical system can be compared.

The beam is described in Fig. 2.8, in a first experience the beam is subjected to a static force at its free end, it generates deformation on the beam the values of $q_1(0)$ and $q_2(0)$ are different from zero. The force has a magnitude of $0.225\,N$, which generates as initial condition $\boldsymbol{x}(0) = \left[\,8.42\cdot10^{-4}\;\; 2.12\cdot10^{-6}\;\; 0\;\; 0\,\right]^{\mathrm{T}}$. This force is removed, and then the free vibration occurs. The numerical description of the implemented model is given in the previous section. The implemented model is also subjected to this initial condition. In Figs. 2.17 and 2.18 the time evolution of the flexible variables of the beam is shown.

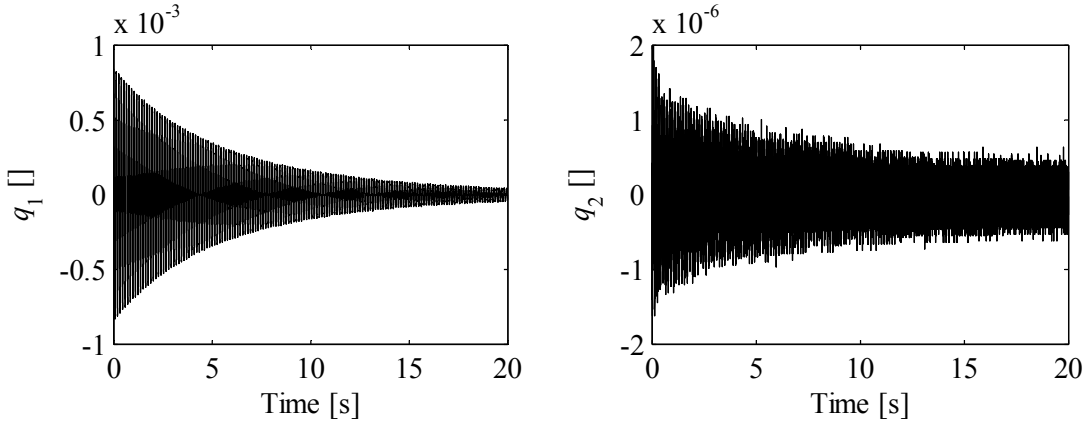

Figure 2.17: Free response to initial conditions for the beam.

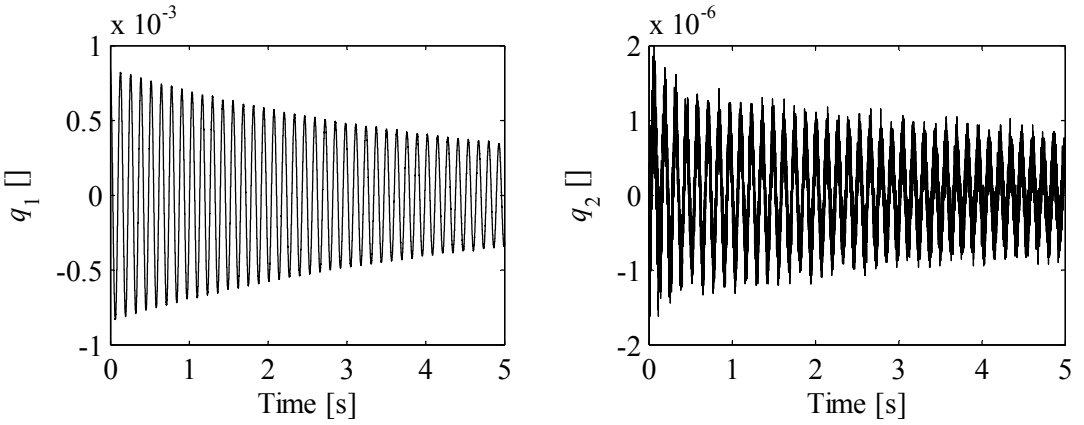

Figure 2.18: Free response to initial conditions for the beam (zoomed).

The damping factor 0.0035 for the first mode is obtained applying (2.129) and (2.130) to $q_1(t)$. The first natural frequency is obtained plotting the energy density spectrum of the signals generated from the strain gages, it has a value of $\omega_1 = 7.70\,\text{Hz}\,(48.38\,\text{rad/s})$ this value is read from Fig. 2.19.

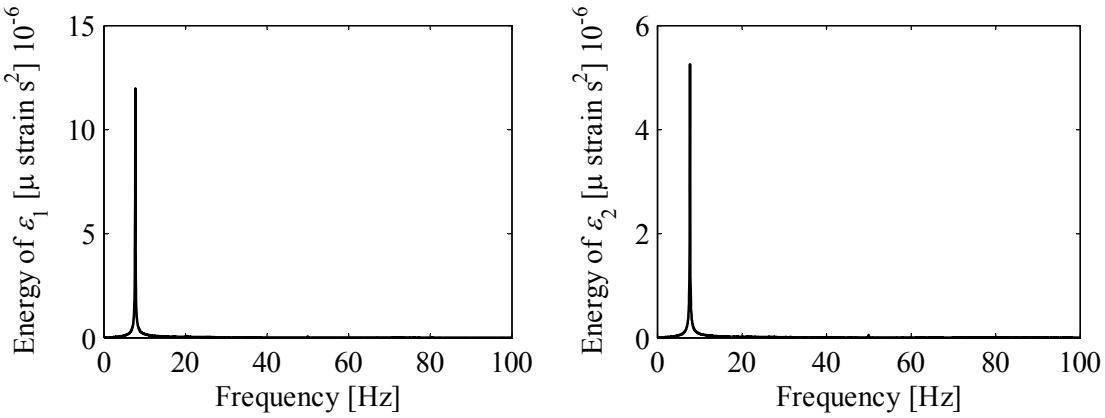

Figure 2.19: Energy density spectrum of the signals from strain gages. Sampling time 1 ms.

The amplitude of the second mode, as well as the amplitude of the second flexible mode, is in this case very small i.e. the influence (amplitude) in the transient response is very small. In order to show the second mode vibration ε_1 and acceleration at the tip are plotted using logarithmic scale for the vertical axes (see Fig. 2.20).

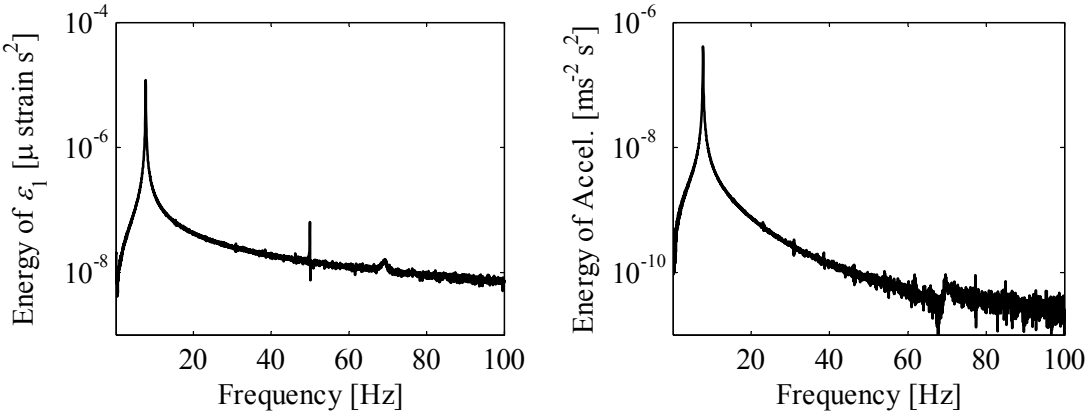

Figure 2.20: Energy density spectrum of the signals from strain gage and accelerometer. Sampling time 1 ms.

A small peak appears in the left figure, but it its due to the frequency response of the signal processing filters. The free response is also compared, the damping factor is read from the

free response of the beam as well as from an experimentally identified model and then the damping factor of the implemented model is calibrated accordingly. In Fig. 2.21 can be seen as result of this both free responses show similar behavior.

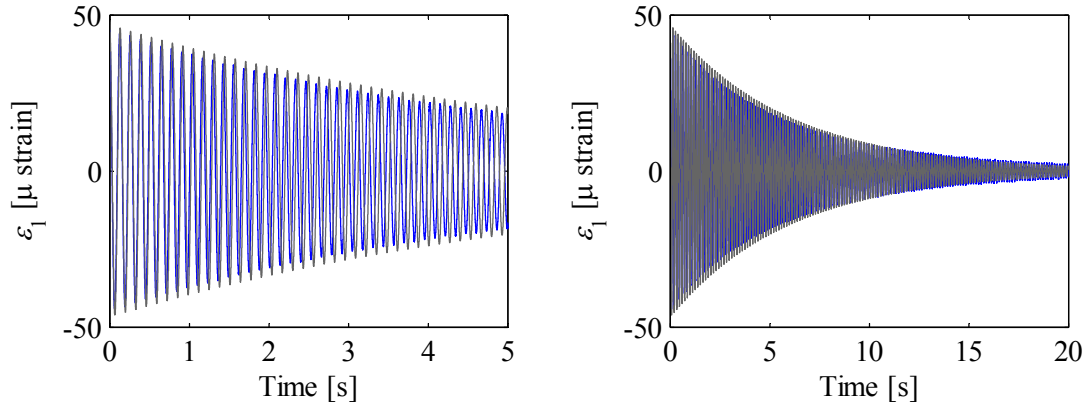

Figure 2.21: Free response ε_1 of model (gray) and beam (blue).

Nevertheless, the second mode of the beam as well as the second mode of the implemented model can be excited by means of one chirp signal sent through the piezoelectric actuators. The chirp signal used has amplitude of $0.2\,\text{Nm}$ and covers a range of frequencies from $0.001\,\text{Hz}$ until $100\,\text{Hz}$. In Fig. 2.22 the behavior of the chirp frequency and the response in deformation of the beam (black) and model (gray) to the same chirp input signal.

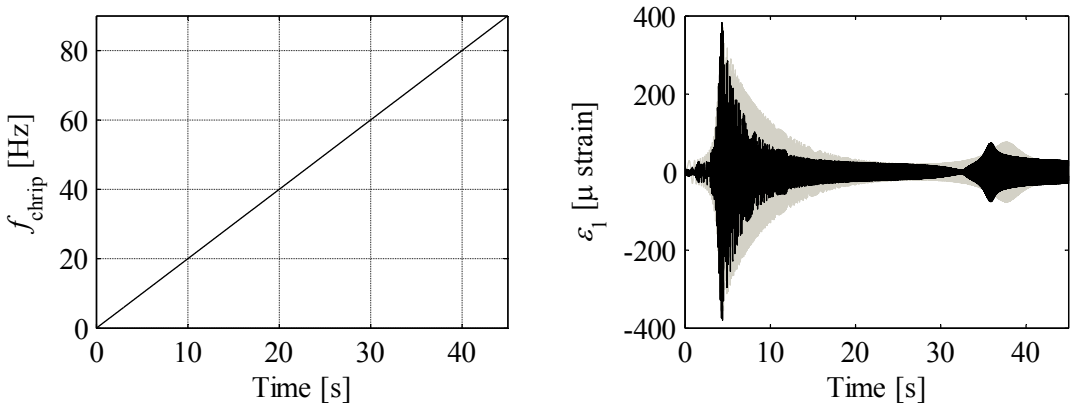

Figure 2.22: Linear frequency evolution (left) and deformation response strain gage 1 (right).

Regarding the second resonance frequency, which is measured in the response to the chirp input signal, the beam shows a frequency of $\omega_2 = 71.74\,\text{Hz}\,(450.76\,\text{rad/s})$ on the other hand the model shows $\omega_2 = 75.38\,\text{Hz}\,(473.62\,\text{rad/s})$.

In Tab. 2.3 the frequency values are compared, there is a small discrepancy of 1.19% for the first mode and 5.71% for the second mode. It can be a result of the additional mass and inertia included by the accelerometer cable or inaccuracies in the estimation of tip load inertia. On the other hand, the bigger discrepancy appears in the second mode of vibration, but it has a very small influence in the transient response which means that this discrepancy introduces a negligible error.

Table 2.3 Comparison between natural frequencies of model and beam.

Parameter	Theoretical value	Measured value	Error (%)
$\omega_1\,[\text{rad/s}]$	47.80	48.38	1.19
$\omega_2\,[\text{rad/s}]$	473.52	450.76	5.05

2.2 One Flexible-link Robot

As next step, a robot with a rotational DOF provided with one rotational actuator and one flexible link is considered. The model is based on the beam formulation presented is the last subsection; substantial changes in the Lagrangian are introduced due to the rotation of the system in the horizontal plane and some additional assumptions are taken into account.

2.2.1 Equation of Motion

The modeling process is performed by dividing the robot arm in four parts: link, piezoelectric actuators, deformation sensors and the rotational actuator. Again, some assumptions are considered for the modeling of the single flexible-link robot, i.e. there is no change in the link's length, absence of longitudinal stiffening, the predominant and only considered deformation is pure bending, uniform density and flexural rigidity along the link and there is no presence of gravity due to the shape of the robot workspace.

As first step to obtain the model is to establish the kinematic relationship between the different frames of the robot. The frames located as proposed by [3,6] where the link starts at the point of rotation (see Fig. 2.23). A rotation matrix $\boldsymbol{A}_1$ is defined for the change of orientation from frame $\hat{\mathrm{O}}_0\hat{\mathrm{X}}_0\hat{\mathrm{Y}}_0$ to $\mathrm{O}_1\mathrm{X}_1\mathrm{Y}_1$

$$\boldsymbol{A}_1 = \begin{bmatrix} \cos(q_1) & -\sin(q_1) \\ \sin(q_1) & \cos(q_1) \end{bmatrix}. \tag{2.132}$$

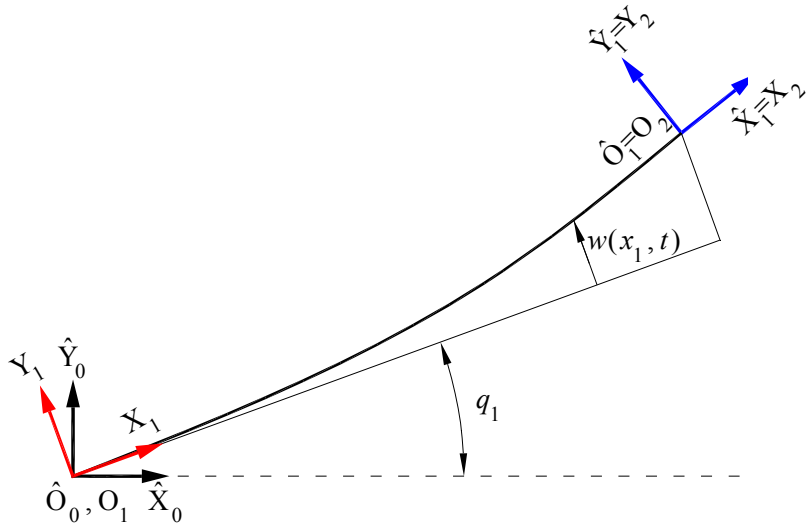

Figure 2.23: Frames for the flexible-link robot without shoulder.

The robot arm considered in this work is provided with a shoulder to fix the flexible link to the joint shaft (see Fig. 2.24), therefore a vector ${}^1\boldsymbol{r}_C$, referred to $\mathrm{O}_1\mathrm{X}_1\mathrm{Y}_1$, is defined from O_1 to the end of the shoulder where the flexible link begins and a new frame $\tilde{\mathrm{O}}_1\tilde{\mathrm{X}}_1\tilde{\mathrm{Y}}_1$ is located. The position of an arbitrary point along the deformed link is given by

$$\boldsymbol{p}_1(x_1) = \boldsymbol{r}_C + \boldsymbol{A}_1\, {}^1\tilde{\boldsymbol{p}}_1(\tilde{x}_1), \tag{2.133}$$

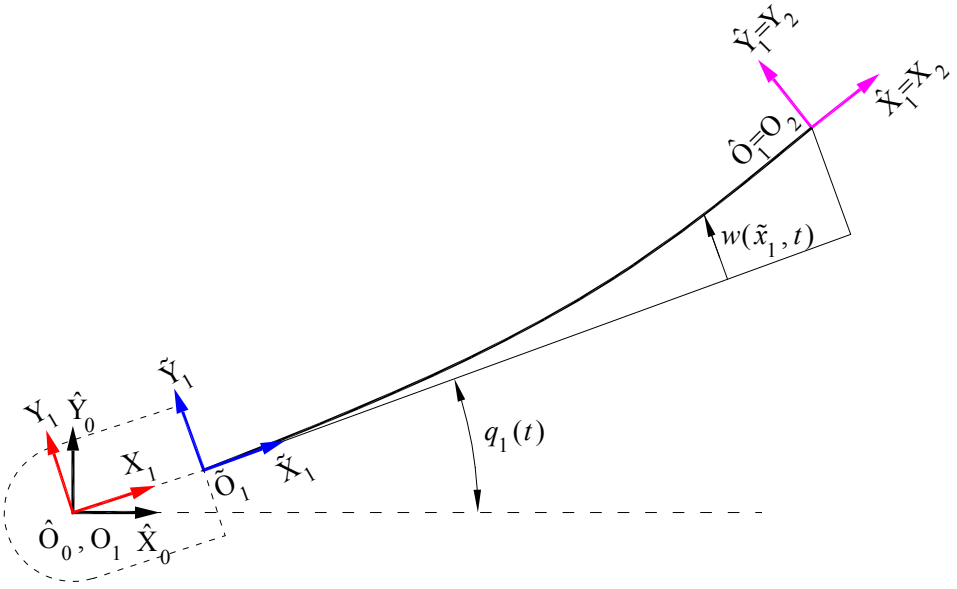

Figure 2.24: Frames for the flexible-link robot with shoulder.

where ${}^{\tilde{1}}\boldsymbol{p}_1(\tilde{x}_1)$ is the position of an arbitrary point along the link referred to the frame $\tilde{O}_1\tilde{X}_1\tilde{Y}_1$. It could be done because the axes of both frames are parallel. Therefore the absolute position $\boldsymbol{p}_1(x_1)$ and velocity $\dot{\boldsymbol{p}}_1(x_1)$ are defined as

$$\boldsymbol{r}_C = \boldsymbol{A}_1\, {}^1\boldsymbol{r}_C, \tag{2.134}$$

$$\boldsymbol{p}_1(x_1) = \boldsymbol{A}_1\left({}^1\boldsymbol{r}_C + {}^1\tilde{\boldsymbol{p}}_1(\tilde{x}_1)\right) = \boldsymbol{A}_1\, {}^1\boldsymbol{p}_1(\tilde{x}_1), \tag{2.135}$$

$$\dot{\boldsymbol{p}}_1(x_1) = \dot{\boldsymbol{A}}_1\, {}^1\boldsymbol{p}_1(\tilde{x}_1) + \boldsymbol{A}_1\, {}^1\dot{\boldsymbol{p}}_1(\tilde{x}_1). \tag{2.136}$$

Details about the calculation of these vectors are given in Appendix B.1. The point and apostrophe denotes time and spatial differentiation, respectively. The deflection of the link $w(\tilde{x}_1,t)$ is defined with respect to the called "shadow link" or not deformed link. The transversal displacement at the free end of the link is defined by

$$w_e(t) = w(\tilde{x}_1,t)\big|_{\tilde{x}_1=l}. \tag{2.137}$$

The vectors required for the energy analysis are given by

$${}^1\boldsymbol{r}_C = \left[\overline{O_1\tilde{O}_1}\;\; 0\right]^T, \tag{2.138}$$

$${}^1\tilde{\boldsymbol{p}}_1(\tilde{x}_1) = \left[\tilde{x}_1\;\; w(\tilde{x}_1,t)\right]^T, \tag{2.139}$$

$$\boldsymbol{r}_2 = \boldsymbol{A}_1\left({}^1\boldsymbol{r}_C + {}^1\tilde{\boldsymbol{r}}_2\right), \tag{2.140}$$

$${}^1\boldsymbol{r}_2 = {}^1\boldsymbol{r}_C + {}^1\tilde{\boldsymbol{r}}_2, \tag{2.141}$$

and

$${}^1\tilde{\boldsymbol{r}}_2 = \left[l\;\; w_e(t)\right]^T. \tag{2.142}$$

The absolute angular velocities of frames $O_1X_1Y_1$ and $\hat{O}_1\hat{X}_1\hat{Y}_1$ are given by

$$\dot{\alpha}_1(t) = \dot{q}_1(t), \tag{2.143}$$

$$\dot{\alpha}_2(t) = \dot{q}_1(t) + \dot{w}_e'(t). \tag{2.144}$$

The one flexible- link robot is modeled following the Lagrangian dynamic formalism. The Lagrange function

$$L = T - U\,, \tag{2.74}$$

which is calculated from the kinetic and potential energy for each component of the system. The total kinetic energy (T) of the structure is the sum of the kinetic energy of the hub, the link and the payload, it is given by

$$T = T_{\mathrm{h}} + T_{\mathrm{l}} + T_{\mathrm{p}}\,, \tag{2.145}$$

where

$$T_{\mathrm{h}} = \frac{1}{2} J_{\mathrm{h}}\, \dot{q}_1^{\,2}\,, \tag{2.146}$$

$$T_{\mathrm{l}} = \frac{1}{2} \rho_{\mathrm{l}} \int_0^l \dot{\boldsymbol{p}}_1^{\mathrm{T}}(\tilde{x}_1)\; \dot{\boldsymbol{p}}_1(\tilde{x}_1)\, d\tilde{x}_1\,, \tag{2.147}$$

$$T_{\mathrm{p}} = \frac{1}{2} m_{\mathrm{p}} \dot{\boldsymbol{r}}_2^{\mathrm{T}} \dot{\boldsymbol{r}}_2 + \frac{1}{2} J_{\mathrm{p}} \left(\dot{q}_1 + \dot{w}_e'\right)^2. \tag{2.148}$$

The robot has its workspace in a horizontal plane; hence gravitational force has no influence on the energy balance. The potential energy is due to the flexibility of the link and it is related to the profile of transversal displacements by

$$U = \frac{1}{2} EI \int_0^l \left(\frac{\partial^2 w(\tilde{x}_1, t)}{\partial\, x_1^2} \right)^2 d\tilde{x}_1\,. \tag{2.149}$$

The energy associated to the deformation of the piezoelectric actuator is considered negligible with respect to the link. Rigid-link robots are modeled with a set of ordinary differential equation (ODE) while flexible-link robots with a set of partial differential equations (PDE) due to its distributed flexibility. For simulation and control design purposes, an approximation to obtain ordinary differential equations must be done. The link is considered as a beam, whose movement is governed by

$$\rho_{\mathrm{l}} \frac{\partial^2 w(x,t)}{\partial t^2} + EI \frac{\partial^4 w(x,t)}{\partial x^4} = 0\,, \tag{2.28}$$

and the boundary conditions for the solution of the partial differential equation are assumed to be of the fully constrained type (cantilever beam). This assumption is made in modeling of flexible links, where clamped-free boundary conditions are used to determine a mathematical model of the link (beam) as long as either the joint has a large inertia compared with the link or there is a gear reduction with a high reduction ratio [15] or a feedback position control loop with a large gain is closed around the joint [6,16]. In this direction [18] states also that the mode shapes of the links quickly converge to the mode shapes of clamped beam under joint variable feedback control for even low values of feedback gains of interest. The boundary conditions are defined in the same manner as for the cantilever beam, taking into account the new coordinate frames

$$w(\tilde{x}_1, t)\big|_{\tilde{x}_1 = 0} = 0\,, \tag{2.150}$$

$$\left.\frac{\partial w(\tilde{x}_1, t)}{\partial \tilde{x}_1}\right|_{\tilde{x}_1 = 0} = 0\,, \tag{2.151}$$

$$\left(EI\right) \left.\frac{\partial^2 w(\tilde{x}_1, t)}{\partial \tilde{x}_1^2}\right|_{\tilde{x}_1 = l} = -J_{\mathrm{p}} \frac{d^2}{dt^2} \left(\left.\frac{\partial w(\tilde{x}_1, t)}{\partial \tilde{x}_1}\right|_{\tilde{x}_1 = l} \right), \tag{2.152}$$

$$(EI)\frac{\partial^3 w(\tilde{x}_1,t)}{\partial \tilde{x}_1^3}\bigg|_{\tilde{x}_1=l} = m_{\mathrm{p}}\frac{d^2}{dt^2}\left(w(\tilde{x}_1,t)\big|_{\tilde{x}_1=l}\right). \tag{2.153}$$

It is important to remark that the structure of the equations of motion and the assumed modes depend on the boundary conditions used, which is a critical choice for these models. Assumed mode models are further described in [4,6,7]. To obtain the aforementioned ODEs from the PDEs an approximation is made, performing a separation between the spatial-dependent and time-dependent variables, which has been already presented as AMM [2]

$$w(\tilde{x}_1,t) = \sum_{i=1}^{n}\phi_i(\tilde{x}_1)\, q_{\mathrm{fi}}(t), \tag{2.154}$$

where ϕ_i are the assumed mode shape functions and q_{fi} are the flexible modal coordinates. Theoretically there are infinite numbers of DOF, but for practical considerations, such as boundedness of actuating energy and limitation of the actuators and the sensors working frequency range, it is more reasonable to truncate this number at a finite one n [83-85]. Therefore the model is truncated in the second mode, additionally in experimental studies [86,87,88] where system identification for cantilevered beams was performed, just the first two modes of vibration have considerable amplitude. The mode shape functions are assumed to have the form

$$\phi_i(\tilde{x}_1) = c_{1,i}\sin(\beta_i\tilde{x}_1) + c_{2,i}\cos(\beta_i\tilde{x}_1) + c_{3,i}\sinh(\beta_i\tilde{x}_1) + c_{4,i}\cosh(\beta_i\tilde{x}_1). \tag{2.155}$$

The conversion of the boundary conditions in terms of shape functions and the calculation of resonance frequencies for a similar case is explained is section 2.1.2 from equation (2.44) to (2.68). The resonance frequencies for the link are given from the solution of

$$\begin{aligned} &m_{\mathrm{p}}J_{\mathrm{p}}\beta_i^4 + \rho_{\mathrm{l}}^2\cos(\beta_i l)\cosh(\beta_i l) - \rho_{\mathrm{l}}\beta_i^3 J_p\sin(\beta_i l)\cosh(\beta_i l) \\ &+m_{\mathrm{p}}\rho_{\mathrm{l}}\beta_i\cos(\beta_i l)\sinh(\beta_i l) - m_{\mathrm{p}}J_{\mathrm{p}}\beta_i^4\cos(\beta_i l)\cosh(\beta_i l) \\ &+\rho_{\mathrm{l}}\beta_i^3 J_{\mathrm{p}}\cos(\beta_i l)\sinh(\beta_i l) - m_{\mathrm{p}}\rho_{\mathrm{l}}\beta_i\sin(\beta_i l)\cosh(\beta_i l) + \rho_{\mathrm{l}}^2 = 0 \end{aligned} \tag{2.156}$$

The orthonormalization condition

$$\int_0^l \rho_{\mathrm{l}}\,\phi_i(\tilde{x}_1)\,\phi_j(\tilde{x}_1)\,d\tilde{x}_1 + m_{\mathrm{p}}\,\phi_i(l)\,\phi_j(l) + J_{\mathrm{p}}\,\phi_i'(l)\,\phi_j'(l) = m_l\delta_{ij}, \tag{2.157}$$

is formulated as the same condition as for the cantilever beam to obtain the $c_{i,j}$ constants of the mode shape function. With the expression for each mode shape the Lagrange function can be calculated. Additionally, the following change of variables is introduced

$$q_{\mathrm{f1}}(t) = q_2(t), \tag{2.158}$$

$$q_{\mathrm{f2}}(t) = q_3(t). \tag{2.159}$$

Then finally the equations of motion are determined using the Euler-Lagrange equation

$$\frac{d}{dt}\frac{\partial L}{\partial \dot{q}_i} - \frac{\partial L}{\partial q_i} = f_i, \quad i = 1..n. \tag{2.82}$$

For this robot one rotational DOF and two flexible degrees of freedom are considered, therefore

$$n = n_R + n_F = 1 + 2 = 3. \tag{2.160}$$

According to the dependency on each generalized coordinate, (2.82) can be reformulated as follows

$$\begin{bmatrix} \dfrac{d}{dt}\dfrac{\partial T_{\mathrm{h}}}{\partial \dot{q}_1}+\dfrac{d}{dt}\dfrac{\partial T_{\mathrm{l}}}{\partial \dot{q}_1}+\dfrac{d}{dt}\dfrac{\partial T_{\mathrm{p}}}{\partial \dot{q}_1} \\ \dfrac{d}{dt}\dfrac{\partial T_{\mathrm{l}}}{\partial \dot{q}_2}+\dfrac{d}{dt}\dfrac{\partial T_{\mathrm{p}}}{\partial \dot{q}_2}-\dfrac{\partial T_{\mathrm{l}}}{\partial q_2}-\dfrac{\partial T_{\mathrm{p}}}{\partial q_2}+\dfrac{\partial U}{\partial q_2} \\ \dfrac{d}{dt}\dfrac{\partial T_{\mathrm{l}}}{\partial \dot{q}_3}+\dfrac{d}{dt}\dfrac{\partial T_{\mathrm{p}}}{\partial \dot{q}_3}-\dfrac{\partial T_{\mathrm{l}}}{\partial q_3}-\dfrac{\partial T_{\mathrm{p}}}{\partial q_3}+\dfrac{\partial U}{\partial q_3} \end{bmatrix} = \begin{bmatrix} f_1 \\ f_2 \\ f_3 \end{bmatrix}, \tag{2.161}$$

here f_1, f_2 and f_3 are the generalized forces, which are: motor torque and the bending moments provided by the piezoelectric actuators, respectively. The relationship between the components of (2.161), kinetic relationships and physical parameter is shown in Appendix C.1, this equation can be written in a standard form

$$\boldsymbol{M}(\boldsymbol{q})\,\ddot{\boldsymbol{q}} + \boldsymbol{c}(\boldsymbol{q},\dot{\boldsymbol{q}}) + \boldsymbol{K}\boldsymbol{q} = \boldsymbol{f}\,, \tag{2.162}$$

where $\boldsymbol{M}(\boldsymbol{q})$ is the mass matrix, $\boldsymbol{c}(\boldsymbol{q},\dot{\boldsymbol{q}})$ is the vector of Coriolis and centripetal effects and $\boldsymbol{K}$ is the rigidity modal matrix. Also proportional structural damping for the link is included, adding a damping modal matrix $\boldsymbol{D}$. Then this equation is transformed to obtain the direct dynamic model of this robot

$$\ddot{\boldsymbol{q}} = \boldsymbol{M}(\boldsymbol{q})^{-1}\left(\boldsymbol{f} - \boldsymbol{c}(\boldsymbol{q},\dot{\boldsymbol{q}}) - \boldsymbol{K}\boldsymbol{q} - \boldsymbol{D}\dot{\boldsymbol{q}}\right), \tag{2.163}$$

where the component of the symmetric mass matrix are

$$m_{1,1} = J_{\mathrm{h}} + J_{\mathrm{p}} + m_{\mathrm{p}}\,{}^{1}\boldsymbol{r}_2^{\mathrm{T}\,1}\boldsymbol{r}_2 + \rho_{\mathrm{l}}\int_0^{l}{}^{1}\boldsymbol{p}_1^{\mathrm{T}\,1}\boldsymbol{p}_1\,d\tilde{x}_1\,, \tag{2.164}$$

$$m_{1,2} = \left(l + \overline{\mathrm{O}_1\tilde{\mathrm{O}}_1}\right)m_{\mathrm{p}}\phi_{\mathrm{e}1} + J_{\mathrm{p}}\phi'_{\mathrm{e}1} + \rho_{\mathrm{l}}\int_0^{l}\tilde{x}_1\phi_1(\tilde{x}_1)d\tilde{x}_1\,, \tag{2.165}$$

$$m_{1,3} = \left(l + \overline{\mathrm{O}_1\tilde{\mathrm{O}}_1}\right)m_{\mathrm{p}}\phi_{\mathrm{e}2} + J_{\mathrm{p}}\phi'_{\mathrm{e}2} + \rho_{\mathrm{l}}\int_0^{l}\tilde{x}_1\phi_2(\tilde{x}_1)d\tilde{x}_1\,, \tag{2.166}$$

$$m_{2,2} = m_{\mathrm{p}}\phi_{\mathrm{e}1}^2 + J_{\mathrm{p}}\phi'^2_{\mathrm{e}1} + \rho_{\mathrm{l}}\int_0^{l}\phi_1(\tilde{x}_1)^2 d\tilde{x}_1 = m_{\mathrm{l}}\,, \tag{2.167}$$

$$m_{2,3} = m_{\mathrm{p}}\phi_{\mathrm{e}1}\phi_{\mathrm{e}2} + J_{\mathrm{p}}\phi'_{\mathrm{e}1}\phi'_{\mathrm{e}2} + \rho_{\mathrm{l}}\int_0^{l}\phi_1(\tilde{x}_1)\phi_2(\tilde{x}_1)d\tilde{x}_1 \approx 0\,, \tag{2.168}$$

$$m_{3,3} = m_{\mathrm{p}}\phi_{\mathrm{e}2}^2 + J_{\mathrm{p}}\phi'^2_{\mathrm{e}2} + \rho_{\mathrm{l}}\int_0^{l}\phi_2(\tilde{x}_1)^2 d\tilde{x}_1 = m_{\mathrm{l}}\,. \tag{2.169}$$

Also the component of the vector of Coriolis and centrifugal effects

$$c_1 = \left(2m_{\mathrm{p}}\,{}^{1}\boldsymbol{r}_2^{\mathrm{T}\,1}\dot{\boldsymbol{r}}_2 + 2\rho_{\mathrm{l}}\int_0^{l}{}^{1}\boldsymbol{p}_1^{\mathrm{T}\,1}\dot{\boldsymbol{p}}_1\,d\tilde{x}_1\right)\dot{q}_1\,, \tag{2.170}$$

$$\begin{aligned} c_2 = -(&m_{\mathrm{p}}\left(\phi_{\mathrm{e}1}^2 q_2 + \phi_{\mathrm{e}1}\phi_{\mathrm{e}2}q_3\right) + q_2\rho_{\mathrm{l}}\int_0^{l}\phi_1(\tilde{x}_1)^2 d\tilde{x}_1 + \cdots \\ &q_3\rho_{\mathrm{l}}\int_0^{l}\phi_1(\tilde{x}_1)\phi_2(\tilde{x}_1)d\tilde{x}_1)\dot{q}_1^2 \end{aligned}\,, \tag{2.171}$$

$$\begin{aligned} c_3 = -(&m_p\left(\phi_{\mathrm{e}1}\phi_{\mathrm{e}2}q_2 + \phi_{\mathrm{e}2}^2 q_3\right) + q_2\rho_{\mathrm{l}}\int_0^{l}\phi_1(\tilde{x}_1)\phi_2(\tilde{x}_1)d\tilde{x}_1 + \cdots \\ &q_3\rho_{\mathrm{l}}\int_0^{l}\phi_2(\tilde{x}_1)^2 d\tilde{x}_1)\dot{q}_1^2 \end{aligned}\,. \tag{2.172}$$

The stiffness matrix is calculated via

$$\boldsymbol{K} = EI\left(\operatorname{diag}\left(\int_0^{l}\left(\frac{\partial^2\phi_{i-1}(\tilde{x}_1)}{\partial\tilde{x}_1^2}\right)^2 d\tilde{x}_1\right)\right)\quad i = 1..3\,, \tag{2.173}$$

where $\phi_0(\tilde{x}_1) = 0$ and as result of the orthonormality condition this matrix turn into

$$\boldsymbol{K} = \begin{bmatrix} 0 & 0 & 0 \\ 0 & m_1\omega_1^2 & 0 \\ 0 & 0 & m_1\omega_2^2 \end{bmatrix}. \tag{2.174}$$

Furthermore, the passive proportional structural damping for the link can be introduced [77,79,80]

$$\boldsymbol{D} = 2\xi \left(\text{diag}\left(\left(k_{i,i} m_1 \right)^{\frac{1}{2}} \right) \right) \; i = 1..3\,, \tag{2.175}$$

then the damping matrix can be written as

$$\boldsymbol{D} = \begin{bmatrix} 0 & 0 & 0 \\ 0 & 2\xi_1 \left(k_{2,2} m_1 \right)^{\frac{1}{2}} & 0 \\ 0 & 0 & 2\xi_2 \left(k_{3,3} m_1 \right)^{\frac{1}{2}} \end{bmatrix}. \tag{2.176}$$

The vector of generalized coordinates includes in its first component the moment resulting from the difference of the motor moment and the friction moment.

The model for the piezoelectric patch has the same form as long as it only depends on the mode shapes, piezoelectric and mechanical properties and substrate, perfect bonding is again assumed. Then second and third components of $\boldsymbol{f}$ are provided by the piezoelectric actuators whose model is calculated in Appendix A.1. Therefore the vector of generalized coordinates is given by

$$\boldsymbol{f} = \boldsymbol{B}_{\text{pi}} \begin{bmatrix} \tau_{\text{m}}(t) - \tau_{\text{fr}}(\dot{q}_1(t)) \\ v_{\text{pi}}(t) \end{bmatrix}, \tag{2.177}$$

where the input matrix is

$$\boldsymbol{B}_{\text{pi}} = \begin{bmatrix} 1 & 0 \\ 0 & \overline{c}\left(\phi_1'(\tilde{x}_{\text{pi}_2}) - \phi_1'(\tilde{x}_{\text{pi}_1}) \right) \\ 0 & \overline{c}\left(\phi_2'(\tilde{x}_{\text{pi}_2}) - \phi_2'(\tilde{x}_{\text{pi}_1}) \right) \end{bmatrix}. \tag{2.178}$$

Due to the assumption that the link can be considered as a cantilever beam [6-16], the analysis performed in the cantilever beam of the section 2.1.2 is the same for the link of this robot and the modes of vibration as well. The dimensions of the link considered here have the same dimensions and payload of the beam previously studied (see Tab. 2.1). Then the results of the analysis of the influence of mass tipload and its inertia are in consequence the same (see Figs. 2.11-2.14).

2.2.2 Model Verification

This proposed process is performed in order to know if the robot model in correctly implemented, and to know if the physical assumption approximate to the reality. This process can also be used for the two flexible-link robot.

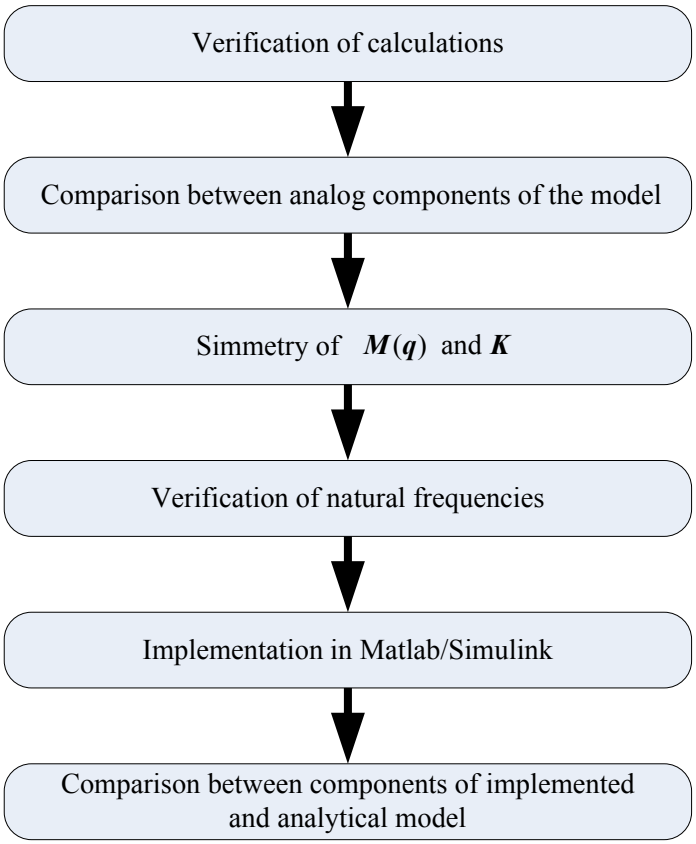

Figure 2.25: Proposed verification process for the flexible-link robots.

Verification of Calculations

In this stage the whole energy balance and the Lagrange-Euler approach was exhaustively reviewed. Unfortunately, here due to the non-commutativity of matrix multiplications the calculation could not be performed using symbolic software directly (i.e. Maple). For this reason the models were developed manually to take advantage of the orthonormality of the rotation matrices for simplifying some terms. Additionally, if the models are formulated until this point manually, then later the number of flexible modes to be considered can be introduced using the AMM approximation. The symbolic software was used to calculate the entire integral elements related to the distributed flexibility.

Comparison between analog components of the model

There exist similarities between the elements of the equation of motion (2.161) and they can be used to verify the model. These Lagrangian elements are related to the kinetic energy of the flexible-link and to the mass or body located at the extreme of the link. The first one considers kinetic relations of successively elements along the link, while the second one considers kinetic relations of concentrated masses at the tip of the link. This can be expressed as

$$\frac{d}{dt}\frac{\partial T_{\mathrm{l}}}{\partial \dot{q}_i} \sim \frac{d}{dt}\frac{\partial T_{\mathrm{p}}}{\partial \dot{q}_i}, \tag{2.179}$$

and

$$\frac{\partial T_{\mathrm{l}}}{\partial q_i} \sim \frac{\partial T_{\mathrm{p}}}{\partial q_i}. \tag{2.180}$$

As a demonstration of this a pair of analog terms are showed

$$\frac{d}{dt}\frac{\partial T_1}{\partial \dot{q}_1} = \ddot{q}_1\rho_l\int_0^{l\,1}\boldsymbol{p}_1(\tilde{x}_1)^{\mathrm{T}\,1}\boldsymbol{p}_1(\tilde{x}_1)d\tilde{x}_1 + \ddot{q}_2\rho_l\int_0^l \tilde{x}_1\phi_1(\tilde{x}_1)d\tilde{x}_1 + \ldots \\ \ddot{q}_3\rho_l\int_0^l \tilde{x}_1\phi_2(\tilde{x}_1)d\tilde{x}_1 + 2\dot{q}_1\rho_l\int_0^{l\,1}\boldsymbol{p}_1(\tilde{x}_1)^{\mathrm{T}\,1}\dot{\boldsymbol{p}}_1(\tilde{x}_1)d\tilde{x}_1 \quad , \tag{2.181}$$

$$\frac{d}{dt}\frac{\partial T_{\mathrm{p}}}{\partial \dot{q}_1} = \left[m_{\mathrm{p}}\,{}^1\boldsymbol{r}_2^{\mathrm{T}\,1}\boldsymbol{r}_2 + J_{\mathrm{p}}\right]\ddot{q}_1 + \left[\left(l + \overline{\mathrm{O}_1\tilde{\mathrm{O}}_1}\right)m_{\mathrm{p}}\phi_{\mathrm{e}1} + J_{\mathrm{p}}\phi'_{\mathrm{e}1}\right]\ddot{q}_2 + \ldots \\ \left[\left(l + \overline{\mathrm{O}_1\tilde{\mathrm{O}}_1}\right)m_{\mathrm{p}}\phi_{\mathrm{e}2} + J_{\mathrm{p}}\phi'_{\mathrm{e}2}\right]\ddot{q}_3 + 2m_{\mathrm{p}}\,{}^1\boldsymbol{r}_2^{\mathrm{T}\,1}\dot{\boldsymbol{r}}_2\,\dot{q}_1 \quad . \tag{2.182}$$

The similarities are

$${}^1\boldsymbol{p}_1(\tilde{x}_1) \sim {}^1\boldsymbol{r}_2\,, \tag{2.183}$$

$$\tilde{x}_1 \sim l + \overline{\mathrm{O}_1\tilde{\mathrm{O}}_1}\,, \tag{2.184}$$

$$\phi_1(\tilde{x}_1) \sim \phi_{\mathrm{e}1}\,, \tag{2.185}$$

$$\phi_2(\tilde{x}_1) \sim \phi_{\mathrm{e}2}\,, \tag{2.186}$$

and

$$m_{\mathrm{p}} \sim \rho_l\int_0^l f(\tilde{x}_1)d\tilde{x}_1\,. \tag{2.187}$$

In (2.181) does not appear any similar term of inertia, but this is due to the Euler assumption of neglecting the rotational inertia of the elements of the beam (flexible link). Besides inertia terms, the similarity is fulfilled between (2.181) and (2.182). Nevertheless, it can be completely verified in Appendix C.1.

Symmetry of Mass Matrix and Stiffness Matrix

Considering that the mass matrix must always be symmetric positive definite i.e. $\boldsymbol{M}(\boldsymbol{q}) = \boldsymbol{M}^{\mathrm{T}}(\boldsymbol{q})$ and $\boldsymbol{M}(\boldsymbol{q}) > 0$, consequently the matrix is nonsingular and its inverse exist. From the Lagrange formulation the mass matrix is obtained, here a verification or debugging can be done by comparing each element of the triangular upper part with its counterpart in the lower part as follows

$$m_{1,2} = m_{2,1} = \left(l + \overline{\mathrm{O}_1\tilde{\mathrm{O}}_1}\right)m_{\mathrm{p}}\phi_{\mathrm{e}1} + J_{\mathrm{p}}\phi'_{\mathrm{e}1} + \rho_l\int_0^l \tilde{x}_1\phi_1(\tilde{x}_1)d\tilde{x}_1\,, \tag{2.188}$$

$$m_{1,3} = m_{3,1} = \left(l + \overline{\mathrm{O}_1\tilde{\mathrm{O}}_1}\right)m_{\mathrm{p}}\phi_{\mathrm{e}2} + J_{\mathrm{p}}\phi'_{\mathrm{e}2} + \rho_l\int_0^l \tilde{x}_1\phi_2(\tilde{x}_1)d\tilde{x}_1\,, \tag{2.189}$$

and

$$m_{2,3} = m_{3,2} \approx 0\,, \tag{2.190}$$

the last elements are zero due to the orthogonality conditions. Here also can be verified that the last two elements of the diagonal are given by

$$m_{2,2} = m_{3,3} = m_{\mathrm{l}}\,, \tag{2.191}$$

this is also due to the employed orthogonality conditions. Considering the links as linear elastic solids, the stiffness matrix is symmetric; $\boldsymbol{K} = \boldsymbol{K}^{\mathrm{T}}$ then $k_{ij} = k_{ji}$. This is the Maxwell's Reciprocity Theorem. In this research no elasticity at the joints is considered, therefore for the first variable q_1 no flexibility is defined. Then the stiffness matrix can be calculated through two different ways

$$\boldsymbol{K} = \begin{bmatrix} 0 & 0 & 0 \\ 0 & EI\int_0^l \phi_1''^2(\tilde{x}_1)d\tilde{x}_1 & EI\int_0^l \phi_1''(\tilde{x}_1)\phi_2''(\tilde{x}_1)d\tilde{x}_1 \\ 0 & EI\int_0^l \phi_1''(\tilde{x}_1)\phi_2''(\tilde{x}_1)d\tilde{x}_1 & EI\int_0^l \phi_2''^2(\tilde{x}_1)d\tilde{x}_1 \end{bmatrix} = \begin{bmatrix} 0 & 0 & 0 \\ 0 & m_1\omega_1^2 & 0 \\ 0 & 0 & m_1\omega_2^2 \end{bmatrix}. \quad (2.192)$$

It can be also verified numerically using the physical parameter given in Tab. 2.4.

Table 2.4 Physical parameters of the one flexible-link robot

Parameter	Value	Complementary information
Material	Aluminum	DIN $AlMg_3$ F22
l	0.31	m
m_1	0.059	kg
EI	1.6333	Nm^2
t_1	0.002	m
m_p	0.060	kg
J_p	$1.84x10^{-5}$	$kg\ m^2$
x_{s1}	0.015	m
J_h	$1.458x10^{-2}$	$kg\ m^2$
ρ_1	0.1876	$kg\ m^{-1}$
$\overline{O_1\tilde{O}_1}$	0.050	m
$\phi_1''(x_{s1})$	27.6856	m^{-1}
$\phi_1''(x_{s2})$	11.6153	m^{-1}
$\phi_2''(x_{s1})$	245.7602	m^{-1}
$\phi_2''(x_{s2})$	-207.5059	m^{-1}

The mass matrix depends on the vector of generalized coordinates, therefore for verification a vector of generalized coordinates must be assumed $\boldsymbol{q} = [1\ \ 0.1\ \ 0.05]^T$. Then substituting it in the mass matrix (2.164) – (2.169), where the obtained matrix is

$$\boldsymbol{M}(\boldsymbol{q}) = \begin{bmatrix} 0.0252857 & 0.0237674 & 0.0013723 \\ 0.0237674 & 0.059 & 0 \\ 0.0013723 & 0 & 0.059 \end{bmatrix}. \quad (2.193)$$

As expected the symmetric characteristic of the mass matrix is verified, also the orthogonality conditions in elements (2,2), (2,3), (3,2) and (3,3) are satisfied. Regarding the stiffness matrix, it does not depend on generalized coordinate vector. Considering the assumed modes and physical parameter of the robot the matrix is given by

$$\boldsymbol{K} = \begin{bmatrix} 0 & 0 & 0 \\ 0 & 135 & 0 \\ 0 & 0 & 13229 \end{bmatrix}. \quad (2.194)$$

Here also due to the orthogonality conditions and due to the modal formulation for the link the stiffness matrix is diagonal.

Verification of Natural Frequencies

Natural frequencies of the link can be calculated independently in different steps of the model formulation. From the physical parameter and from the solution of the eigenvalue problem (2.156), the natural frequencies of the considered modes can be calculated. Using these values, boundary conditions, AMM and the Lagrange formalism; then equation of motion containing the stiffness matrix is obtained from the terms related to energy of elastic deformation. Therefore, the natural frequencies can be calculated from this stiffness matrix. From (2.192) can be formulated the natural frequencies

$$\omega_1 = \left(\frac{EI \int_0^l \phi_1''^2(\tilde{x}_1) d\tilde{x}_1}{m_1} \right)^{0.5}, \tag{2.195}$$

and

$$\omega_2 = \left(\frac{EI \int_0^l \phi_2''^2(\tilde{x}_1) d\tilde{x}_1}{m_1} \right)^{0.5}. \tag{2.196}$$

In Tab. 2.5 are shown the values of natural frequencies obtained independently from the model formulation.

Table 2.5 Comparison of natural frequencies of the one flexible-link robot

Parameter	Value from (2.156)	Value from (2.192)
ω_1 [rad/s]	47.81	47.83
ω_2 [rad/s]	473.52	473.51

The values of the frequencies match; it means the model with its assumption has been, at least in this part, correctly formulated.

Implementation in Matlab/Simulink

For simulation the model was implemented in Matlab/Simulink to solve the equation of motion of the robot. The model was divided in two parts, kinematic relationships and dynamic relationships. The first one contains relations between position and velocities of the components of the robot (continuous and discrete). The latter embraces mainly the relations coming from the Lagrange-Euler equation; it also subdivided into two parts: relations for discrete components (rigid parts) and relations for continuous components (flexible links). All the terms related to the flexible links result in integral forms, which are calculated using symbolic software and then implemented in Matlab/Simulink as embedded functions. The implementation of this dynamic direct model is illustrated in Fig. 2.26.

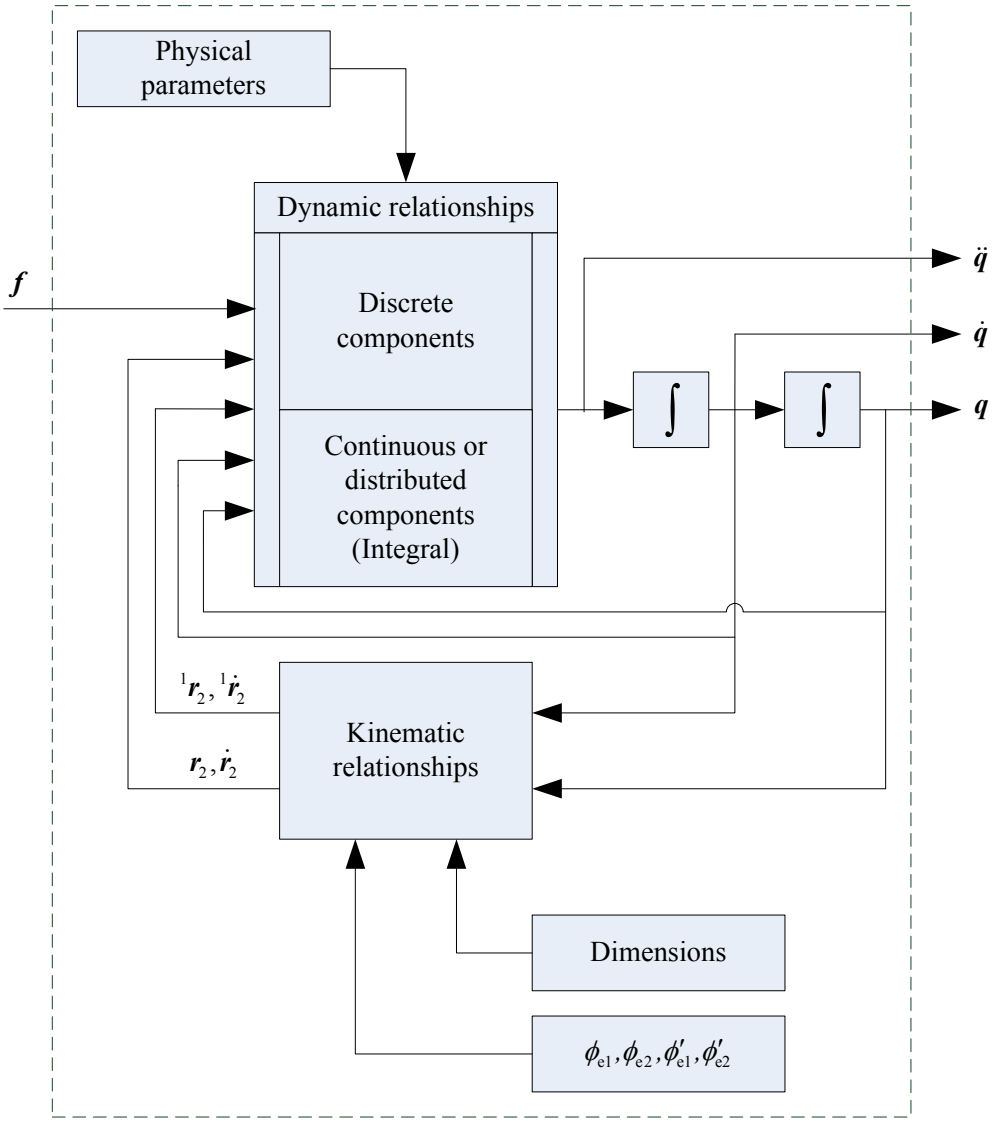

Figure 2.26: Scheme for the implementation of the model for the one flexible-link robot.

Using this implementation, other strategies can be used to perform additional verification of the robot model. It is important to mention that also this Matlab/Simulink model and its symbolically calculated elements were subjected to an exhaustive debugging process.

Comparison between components of implemented and analytical model

Another performed test is to compare the response of some parts of the implemented model with their counterparts completely analytically calculated; this is another way to verify the correctness of the implemented robot model. For this purpose, the implemented model is controlled at joint level with a PID controller to follow a joint trajectory (see Fig. 2.27). The variation of the mass matrix according to the flexible variables is very small, for this reason the determinant of the mass matrix of the implemented model and from the analytical model are compared (see Fig. 2.28). It can be seen that both curves match, therefore the mass matrix does.

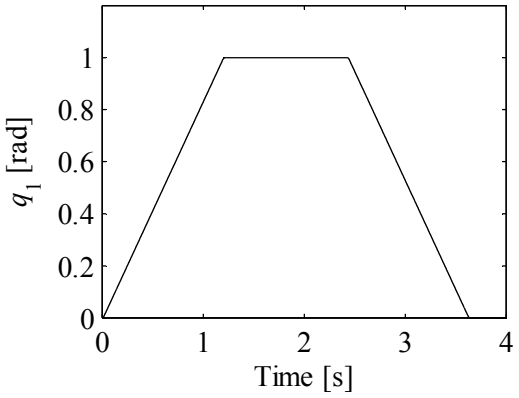

Figure 2.27: Joint trajectory.

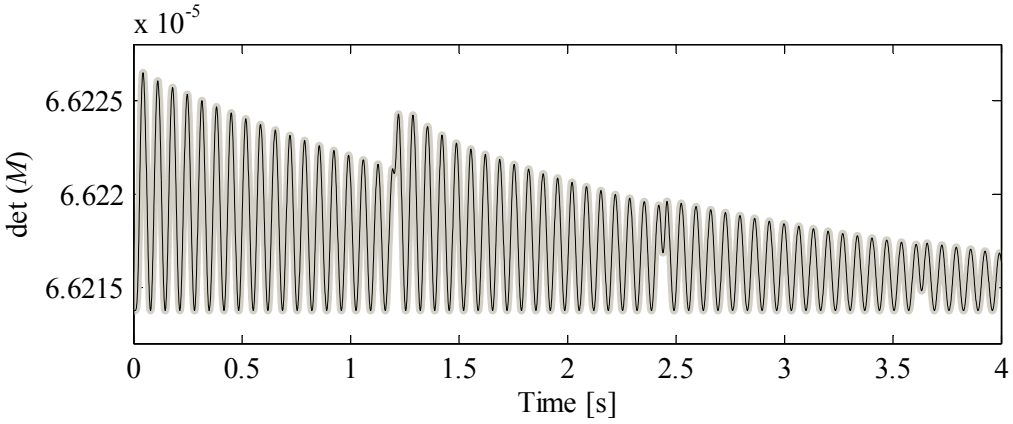

Figure 2.28: Determinant of mass matrix. Black: numerical, gray: analytical.

Also the components of the vector of Coriolis and centripetal effects for the implemented model are calculated evaluating (2.170)-(2.172) or can be analytically calculated from the mass matrix using the Christofel coefficients [6]

$$c_i = \sum_{j=1}^{n}\sum_{k=1}^{n}\left(\frac{\partial m_{ij}}{\partial q_k} - \frac{1}{2}\frac{\partial m_{jk}}{\partial q_i}\right)\dot{q}_k\dot{q}_j \,. \tag{2.197}$$

For the same joint trajectory the time evolution of the components of vector of Coriolis and centripetal effects is shown in Fig. 2.29. The components of the vector were calculated independent and the two vectors match.

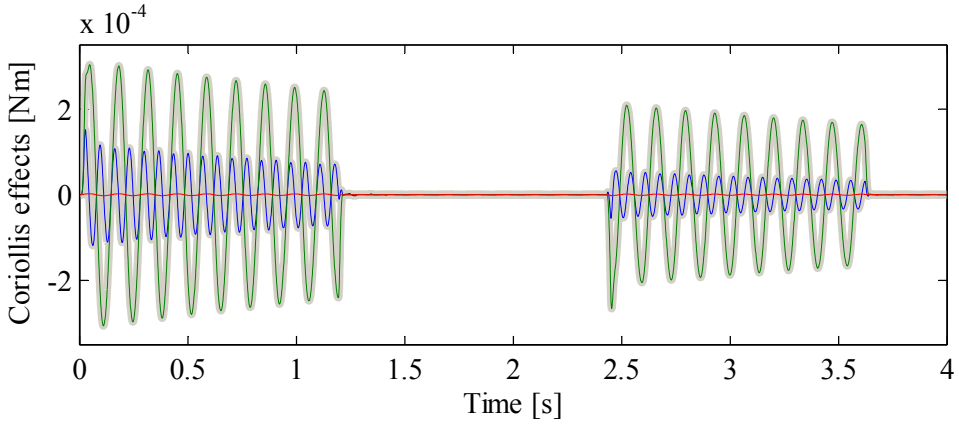

Figure 2.29: Components of vector of Coriolis and centripetal effects. Thinn lines: numerical, thick lines: analytical.

With the test performed it can be stated that the model is correctly implemented and that the implemented model correspond to the proposed conceptual model.

2.2.3 Model Validation

In order to shown how accurate the implemented model emulating the behavior of the real system some experiments have been done. The robot and the model were subjected to different inputs i.e. a bang-bang signal at joint level and to a chirp signal in the piezoelectric actuators. This procedure is also applied for the two flexible-link robot.

The transient response is compared by sending as control signal a bang-bang torque signal, of the form shown in Fig. 2.30. The maximum and minimum values are chosen to be greater than the maximum and minimum values of the friction model experimentally determined in section Appendix D. With this input signal a transient behavior is induced in the one flexible-link robot.

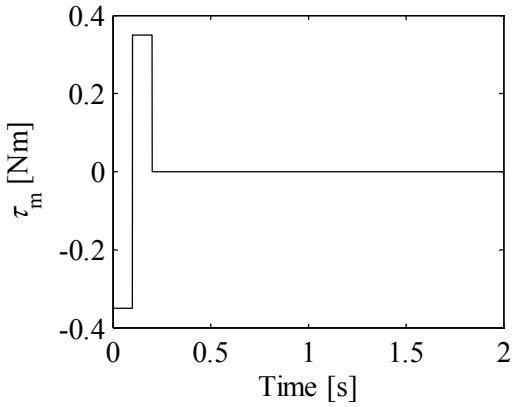

Figure 2.30: Bang-bang input signal for the servomotor.

This torque signal induces a joint movement which is mainly influenced by the joint friction (see Fig.2.31), after the static friction is defeated the joint moves. The final position differs from the initial because this friction model is a nonlinear discontinuity affected by the direction of movement.

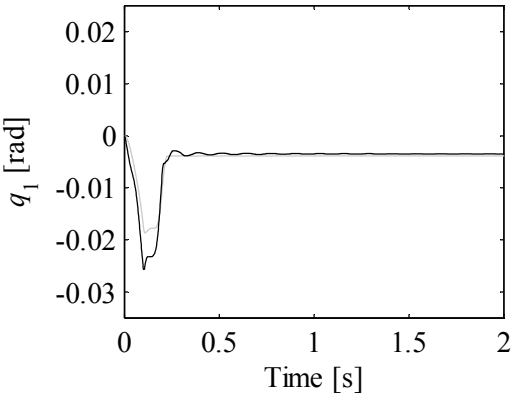

Figure 2.31: Joint displacement for bang-bang input signal in the servomotor.

The response of the robot to this joint input is shown in Fig. 2.32 in terms of deformation near the clamped end of the link. The damping factors used for the two considered modes were taken from experimental system identification performed on a clamped beam with the same boundary conditions as is suggested in [47].

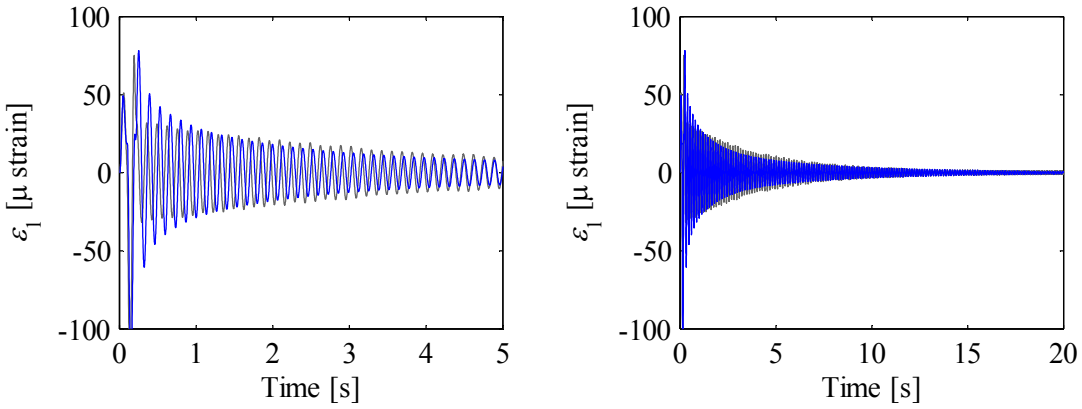

Figure 2.32: Deformation at the base of the link for bang-bang input signal in the servomotor. Gray: model. Blue: real system.

In Fig. 2.33 are shown the energy density spectra of the measured deformation, the main frequency components for the model and the real system are 47.16 rad/s (7.50 Hz) and 47.93 rad/s (7.62 Hz), respectively.

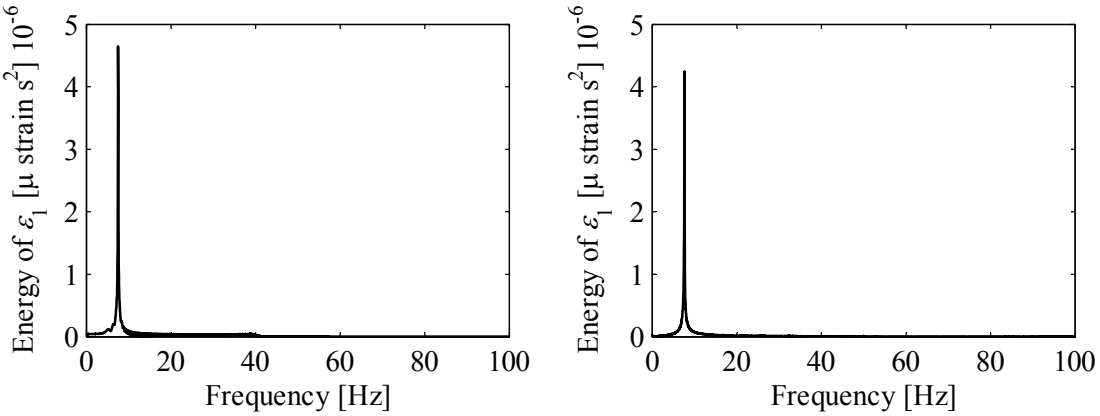

Figure 2.33: Energy density spectrum for deformation at the base of the link for bang-bang input signal in the servomotor. Sampling time 1 ms. Left: model. Right: real system.

The robot and its model are also subjected to a linear chirp signal, their responses are compared. With this not just the first mode also the second mode of the link as well as the second mode of the implemented model can be excited by this chirp signal. The signal used has amplitude of 0.1 Nm and covers a range of frequencies from 0.001 Hz until 100 Hz. In Fig. 2.34 the behavior of the chirp frequency and the response in deformation of the link (black) and model (gray) to the same input signal are shown.

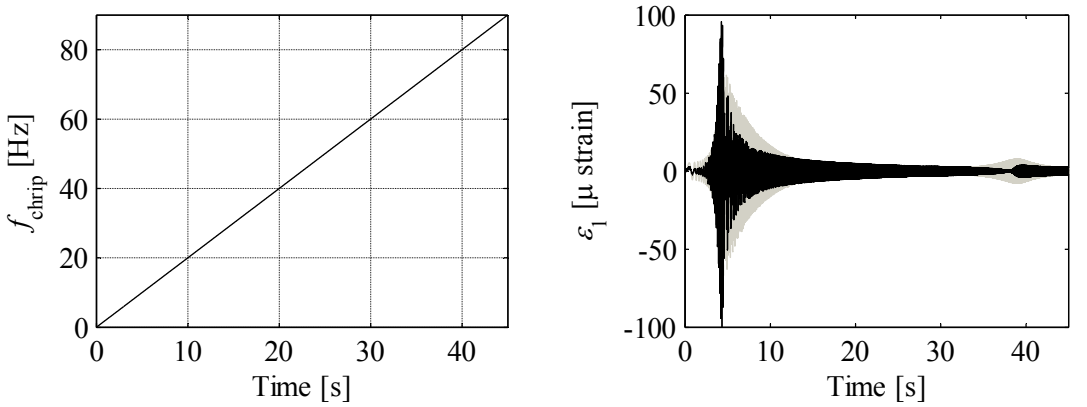

Figure 2.34: Linear frequency evolution (left) and deformation response strain gage 1 (right).

The responses are similar, nevertheless the discrepancy in due to neglect some component whose inertia is difficult to evaluate (basically cables). But this model uncertainty can be overcome with a robust control strategy which is one objective of this work.

2.3 Two Flexible-link Robot

The development of the model is similar to the previous robot and has as important support the beam model. Some equations are to be taken directly from the one flexible-link robot. In this section the modification to the formulation of [3,6], it was previously presented but here is generalized for n links and then particularized for the case under study.

2.3.1 Equation of Motion

Direct kinematic modeling of robots with a workspace restricted to a plane can be formulated in terms of displacements (vectors) and rotations (matrices). On the other hand, for robot with a three dimensional workspace [3, 13,113] propose the use of homogeneous transformation matrices. In the classical modeling approach for robots there is an inertial frame and frames located at each joint and at the tip of the robot or end effector, see Fig. 2.35.

Normally in the literature links are assumed to begin at the axis of rotation of the joints link [3,6,16,89-91], when a physical prototype is built it is not always true. For instance, clamps are required in distal links for fixing purposes and they introduce displacement from the rotation axis that need to be taken into account. The frame assignment is done following a methodology similar to the one proposed by Denavit and Hartenberg [93]. The frame assignment for an *n*-flexible-link robot is shown in Fig. 2.36.

Additional frames are located at points where the rigid clamps end and flexible links begin, they are identified with the symbol ~. Therefore, four frames are defined at link *i*. The transformation between frames $(\mathrm{X}_i, \mathrm{Y}_i)$ and $(\tilde{\mathrm{X}}_i, \tilde{\mathrm{Y}}_i)$ is a translation, then an additional vector referred to frame $(\mathrm{X}_i, \mathrm{Y}_i)$ is also defined

$$ {}^{i}\boldsymbol{r}_{\mathrm{C}i} = \left[\overline{\mathrm{O}_i\tilde{\mathrm{O}}_i} \;\; 0 \right]^{\mathrm{T}} . \tag{2.198} $$

The absolute position of one point along the link and at the endpoint are given by

$$ \boldsymbol{p}_i = \boldsymbol{r}_i + \boldsymbol{W}_i \, {}^{i}\boldsymbol{p}_i , \tag{2.199} $$

$$ \boldsymbol{r}_{i+1} = \boldsymbol{r}_i + \boldsymbol{W}_i \, {}^{i}\boldsymbol{r}_{i+1} , \tag{2.200} $$

respectively. ${}^{i}\boldsymbol{p}_i$ and ${}^{i}\boldsymbol{r}_{i+1}$ are the position of the afore mentioned point but referred to frame $(\mathrm{X}_i, \mathrm{Y}_i)$ are stated as

$$ {}^{i}\boldsymbol{p}_i = {}^{i}\boldsymbol{r}_{\mathrm{C}i} + {}^{i}\tilde{\boldsymbol{p}}_i = \left[\overline{\mathrm{O}_i\tilde{\mathrm{O}}_i} + \tilde{x}_i \;\; w_i(\tilde{x}_i, t) \right]^{\mathrm{T}} , \tag{2.201} $$

$$ {}^{i}\boldsymbol{r}_{i+1} = {}^{i}\boldsymbol{r}_{\mathrm{C}i} + {}^{i}\tilde{\boldsymbol{r}}_{i+1} = \left[\overline{\mathrm{O}_i\tilde{\mathrm{O}}_i} + l_i \;\; w_{\mathrm{e}i} \right]^{\mathrm{T}} . \tag{2.202} $$

Here $\boldsymbol{W}_i$ is the cumulative transformation from inertial frame to frame $(\mathrm{X}_i, \mathrm{Y}_i)$, which is defined recursively as

$$ \boldsymbol{W}_i = \boldsymbol{W}_{i-1}\boldsymbol{E}_{i-1}\boldsymbol{A}_i . \tag{2.203} $$

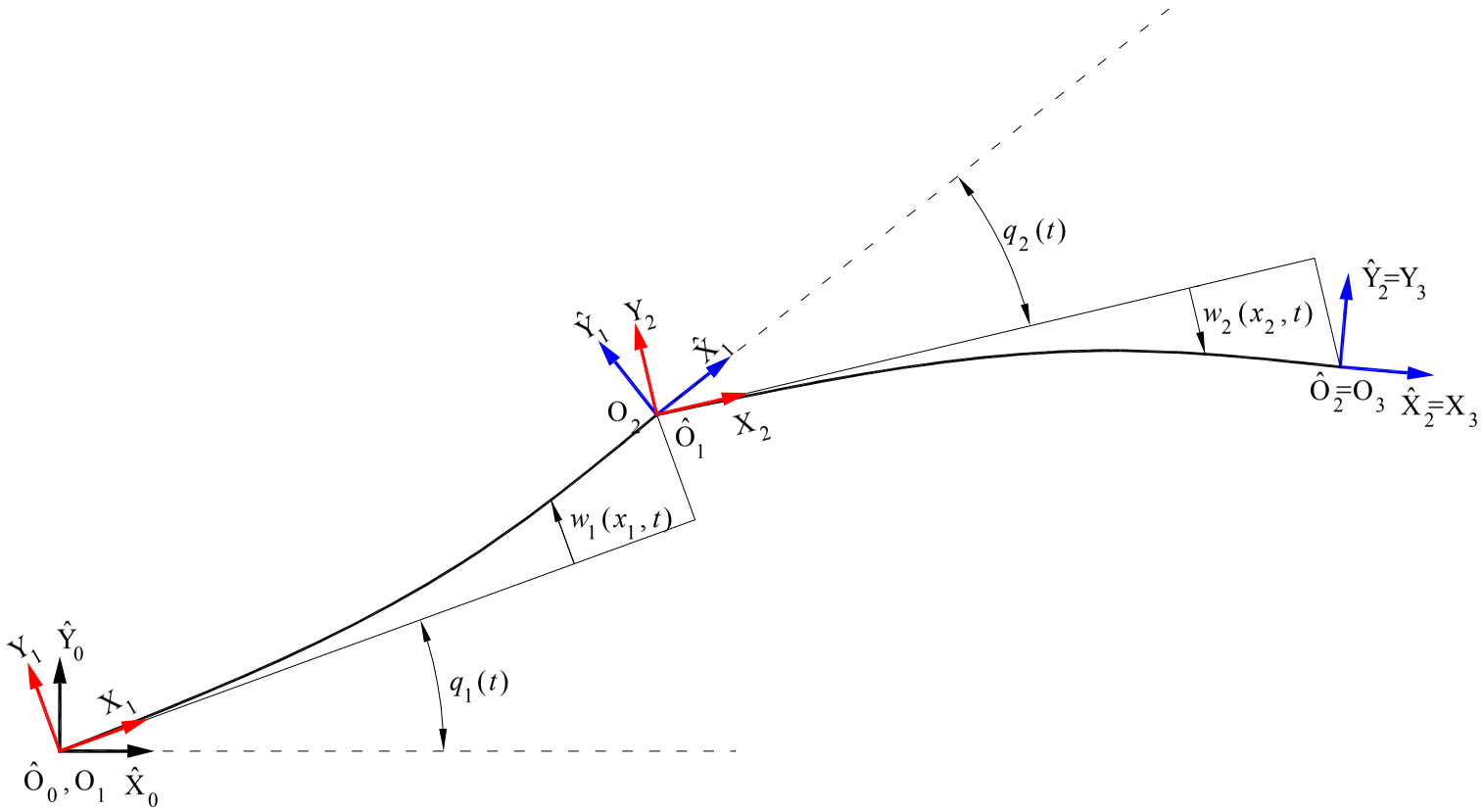

Figure 2.35: Frames for the two-flexible-link robot without shoulder.

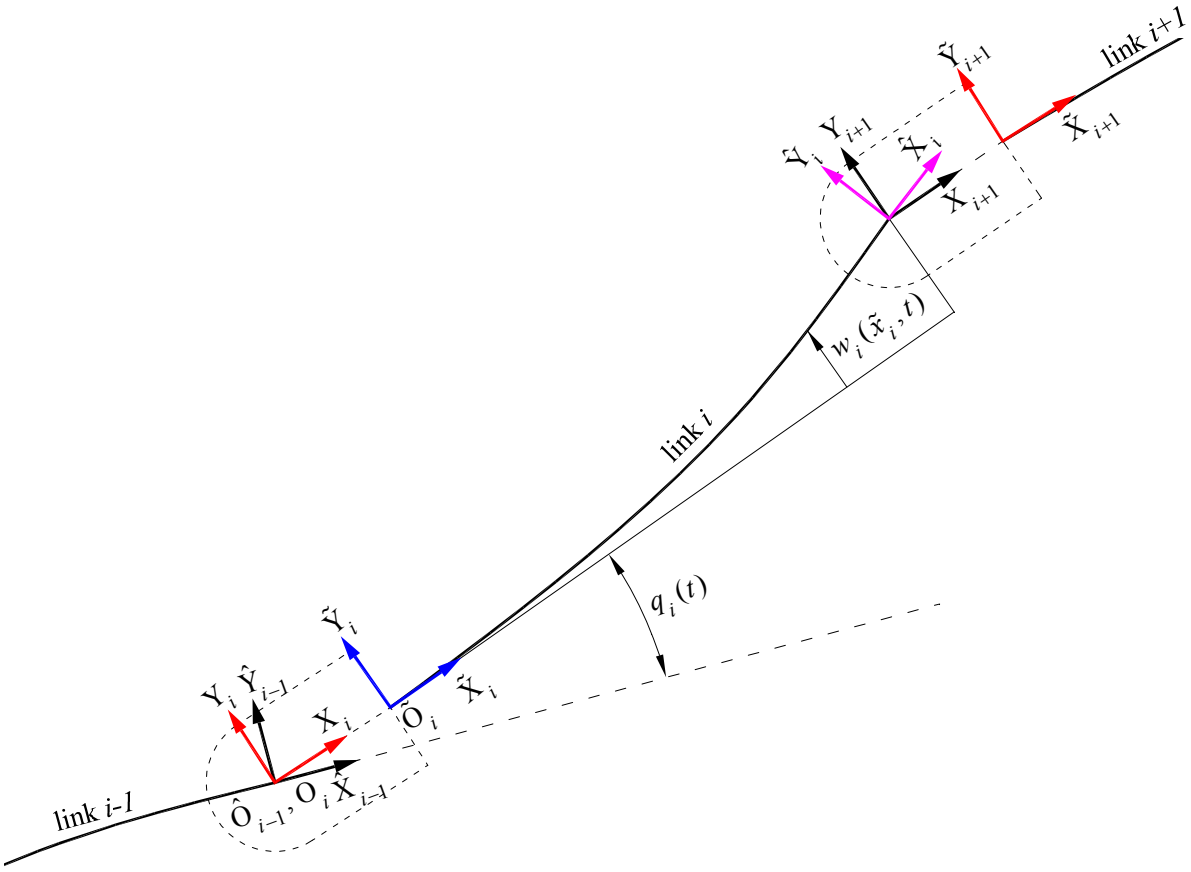

Figure 2.36: Frames for *n*-flexible-link robot with shoulder.

$\boldsymbol{A}_i$ represents the change in orientation due to the rotational joint located in Z_i

$$\boldsymbol{A}_i = \begin{bmatrix} \cos(q_i) & -\sin(q_i) \\ \sin(q_i) & \cos(q_i) \end{bmatrix}. \tag{2.204}$$

The matrix $\boldsymbol{E}_{i-1}$ represents the influence of the elastic deformation of the previous link *i-1* in the orientation of link *i* as follows

$$\boldsymbol{E}_i = \begin{bmatrix} 1 & -\left.\dfrac{\partial w_i(\tilde{x}_i,t)}{\partial \tilde{x}_i}\right|_{\tilde{x}_i=l_i} \\ \left.\dfrac{\partial w_i(\tilde{x}_i,t)}{\partial \tilde{x}_i}\right|_{\tilde{x}_i=l_i} & 1 \end{bmatrix} = \begin{bmatrix} 1 & -w'_{\mathrm{e}i} \\ w'_{\mathrm{e}i} & 1 \end{bmatrix}. \tag{2.205}$$

And the last required kinematic relation is the orientation of the defined frames $(\mathrm{X}_i, \mathrm{Y}_i)$ along the link

$$\alpha_i = \sum_{j=1}^{i} q_j + \sum_{k=1}^{i-1} w'_{\mathrm{e}k} \quad i \le n_{\mathrm{R}} + 1. \tag{2.206}$$

In the case of intermediate joints a new angle has to be defined $\hat{\alpha}_i$, this angle represents the absolute rotation of frame $(\hat{\mathrm{X}}_i, \hat{\mathrm{Y}}_i)$

$$\hat{\alpha}_i = \sum_{j=1}^{i-1} q_j + \sum_{k=1}^{i-1} w'_{\mathrm{e}k} \quad 1 < i \le n_{\mathrm{R}}, \tag{2.207}$$

this distinction is required later for the energy balance, because the joints have a relative fixed (attached to the end of the previous link) and a rotational inertia which includes the inertia of motor gear. Details for the calculation of these elements and its time derivatives are given in Appendix B.2. Applying the previous approach the frame assignment is shown in Fig. 2.37

After explaining in general terms some kinematic relations the particularization for a robot with two flexible links follows. First, the vectors associated to the first link are the same from (2.133) to (2.143). As mentioned in the intermediate joint appear two angles and two angular velocities instead of one i.e. $\hat{\alpha}_2$, $\dot{\hat{\alpha}}_2$, α_2 and $\dot{\alpha}_2$

$$\hat{\alpha}_2 = q_1 + w'_{e1}, \tag{2.208}$$

$$\dot{\hat{\alpha}}_2 = \dot{q}_1 + \dot{w}'_{e1}, \tag{2.209}$$

$$\alpha_2 = q_1 + q_2 + w'_{e1}, \tag{2.210}$$

$$\dot{\alpha}_2 = \dot{q}_1 + \dot{q}_2 + \dot{w}'_{e1}. \tag{2.211}$$

The absolute position and velocity of any point along the second link are given by

$$\boldsymbol{p}_2 = \boldsymbol{A}_1 \left({}^1\boldsymbol{r}_2 + \boldsymbol{E}_1 \boldsymbol{A}_2 {}^2\boldsymbol{p}_2 \right) = \boldsymbol{A}_1 {}^1\boldsymbol{r}_2 + \boldsymbol{A}_1 \boldsymbol{E}_1 \boldsymbol{A}_2 {}^2\boldsymbol{p}_2 . \tag{2.212}$$

$$\begin{aligned} \dot{\boldsymbol{p}}_2 \; = \; & \boldsymbol{S}\boldsymbol{A}_1 {}^1\boldsymbol{r}_2 \dot{q}_1 + \boldsymbol{A}_1 {}^1\dot{\boldsymbol{r}}_2 + \boldsymbol{S}\boldsymbol{A}_1 \boldsymbol{E}_1 \boldsymbol{A}_2 {}^2\boldsymbol{p}_2 \dot{q}_1 + \ldots \\ & \boldsymbol{A}_1 \dot{\boldsymbol{E}}_1 \boldsymbol{A}_2 {}^2\boldsymbol{p}_2 + \boldsymbol{A}_1 \boldsymbol{E}_1 \boldsymbol{S}\boldsymbol{A}_2 {}^2\boldsymbol{p}_2 \dot{q}_2 + \boldsymbol{A}_1 \boldsymbol{E}_1 \boldsymbol{A}_2 {}^2\dot{\boldsymbol{p}}_2 \end{aligned}, \tag{2.213}$$

where

$${}^2\boldsymbol{r}_{C2} = \left[\overline{\mathrm{O}_2\tilde{\mathrm{O}}_2} \;\; 0 \right]^{\mathrm{T}}, \tag{2.214}$$

$${}^2\tilde{\boldsymbol{p}}_2 = \left[\tilde{x}_2 \;\; w_2(\tilde{x}_2, t) \right]^{\mathrm{T}}, \tag{2.215}$$

$${}^2\boldsymbol{p}_2 = \left[\tilde{x}_2 + \overline{\mathrm{O}_2\tilde{\mathrm{O}}_2} \;\; w_2(\tilde{x}_2, t) \right]^{\mathrm{T}}, \tag{2.216}$$

$${}^2\dot{\boldsymbol{p}}_2 = \left[0 \;\; \dot{w}_2(\tilde{x}_2, t) \right]^{\mathrm{T}}, \tag{2.217}$$

$$\boldsymbol{E}_1 = \begin{bmatrix} 1 & -w'_{e1} \\ w'_{e1} & 1 \end{bmatrix}, \tag{2.218}$$

$$\dot{\boldsymbol{E}}_1 = \begin{bmatrix} 1 & -\dot{w}'_{e1} \\ \dot{w}'_{e1} & 1 \end{bmatrix}, \tag{2.219}$$

and

$$\boldsymbol{A}_2 = \begin{bmatrix} \cos(q_2) & -\sin(q_2) \\ \sin(q_2) & \cos(q_2) \end{bmatrix}. \tag{2.220}$$

In similar way the expression for the tip robot absolute position and velocity are calculated

$$\boldsymbol{r}_3 = \boldsymbol{A}_1 {}^1\boldsymbol{r}_2 + \boldsymbol{A}_1 \boldsymbol{E}_1 \boldsymbol{A}_2 {}^2\boldsymbol{r}_3 \tag{2.221}$$

$$\begin{aligned} \dot{\boldsymbol{r}}_3 \; = \; & \boldsymbol{S}\boldsymbol{A}_1 {}^1\boldsymbol{r}_2 \dot{q}_1 + \boldsymbol{A}_1 {}^1\dot{\boldsymbol{r}}_2 + \boldsymbol{S}\boldsymbol{A}_1 \boldsymbol{E}_1 \boldsymbol{A}_2 {}^2\boldsymbol{r}_3 \dot{q}_1 + \cdots \\ & \cdots + \boldsymbol{A}_1 \dot{\boldsymbol{E}}_1 \boldsymbol{A}_2 {}^2\boldsymbol{r}_3 + \boldsymbol{A}_1 \boldsymbol{E}_1 \boldsymbol{S}\boldsymbol{A}_2 {}^2\boldsymbol{r}_3 \dot{q}_2 + \boldsymbol{A}_1 \boldsymbol{E}_1 \boldsymbol{A}_2 {}^2\dot{\boldsymbol{r}}_3 \end{aligned} \tag{2.222}$$

Finally the absolute angle and absolute angular velocity of the tip of the robot

$$\alpha_3 = q_1 + q_2 + w'_{e1} + w'_{e2}, \tag{2.223}$$

$$\dot{\alpha}_3 = \dot{q}_1 + \dot{q}_2 + \dot{w}'_{e1} + \dot{w}'_{e2}. \tag{2.224}$$

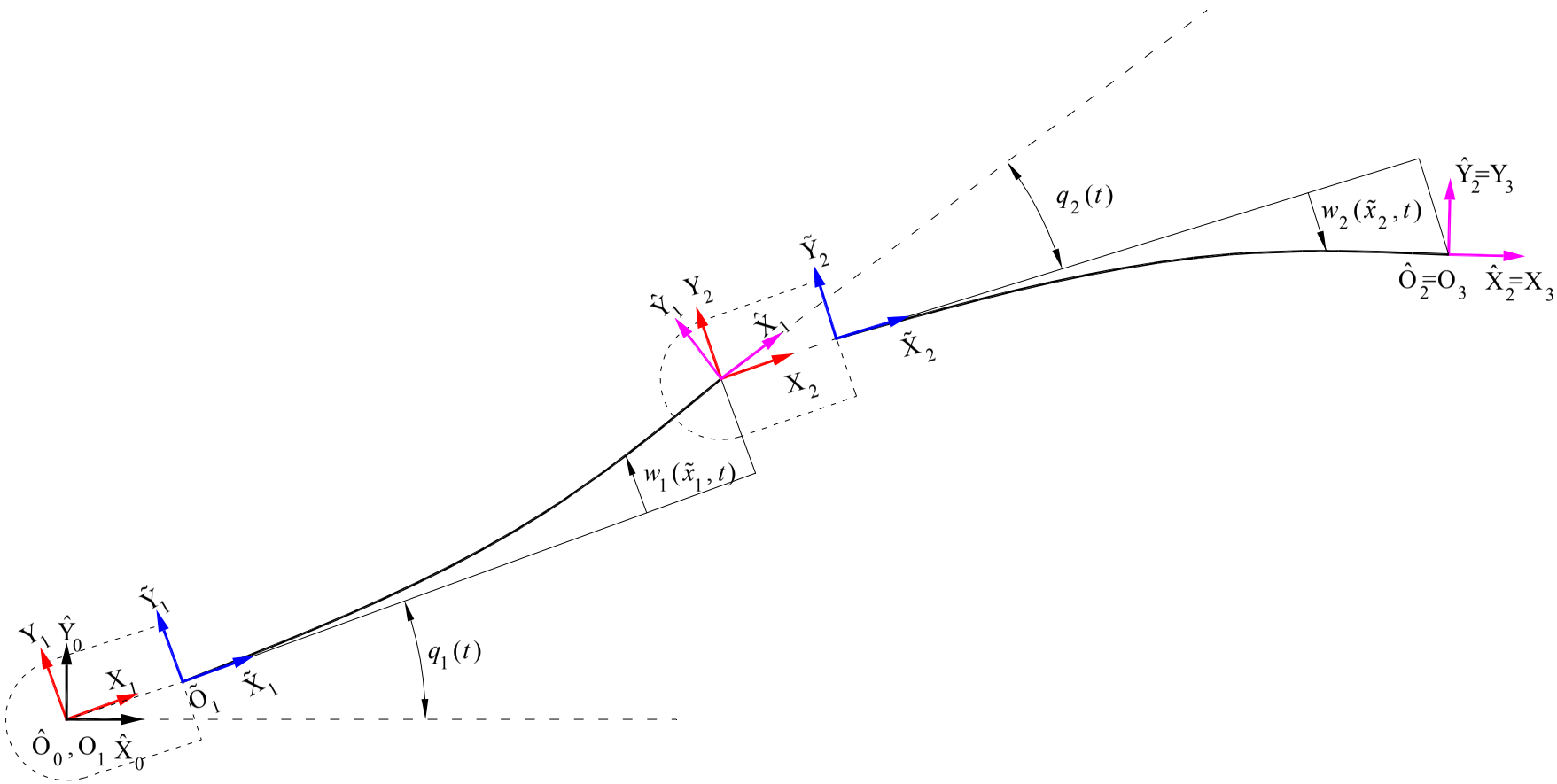

Figure 2.37: Frames for the two flexible-link robot with shoulder.

The two flexible-link robot is also modeled following the Lagrangian dynamic formalism. The Lagrange function

$$L = T - U\,, \tag{2.74}$$

is calculated from the kinetic and potential energy for each component of the system. The total kinetic energy (T) of the structure is the sum of the kinetic energy of the hubs, the links and the payload, it is given by

$$T = \sum_{i=1}^{n_{\mathrm{R}}} T_{\mathrm{h}\,i} + \sum_{i=1}^{n_{\mathrm{R}}} T_{\mathrm{l}\,i} + T_{\mathrm{p}}\,, \tag{2.225}$$

where

$$T_{\mathrm{h1}} = \frac{1}{2} J_{\mathrm{h1}}\, \dot{q}_1^{\,2}\,, \tag{2.226}$$

$$T_{\mathrm{h2}} = \frac{1}{2} m_{\mathrm{h2}} \dot{\boldsymbol{r}}_2^{\mathrm{T}} \dot{\boldsymbol{r}}_2 + \frac{1}{2} J_{\mathrm{h2A}} \dot{\hat{\alpha}}_2^2 + \frac{1}{2} J_{\mathrm{h2B}} \dot{\alpha}_2^2\,, \tag{2.227}$$

$$T_{\mathrm{l1}} = \frac{1}{2} \rho_{\mathrm{l}} \int_0^l \dot{\boldsymbol{p}}_1^{\mathrm{T}}(\tilde{x}_1)\; \dot{\boldsymbol{p}}_1(\tilde{x}_1)\, d\tilde{x}_1\,, \tag{2.228}$$

$$T_{\mathrm{l2}} = \frac{1}{2} \rho_{\mathrm{l}} \int_0^l \dot{\boldsymbol{p}}_2^{\mathrm{T}}(\tilde{x}_2)\; \dot{\boldsymbol{p}}_2(\tilde{x}_2)\, d\tilde{x}_2\,, \tag{2.229}$$

and

$$T_{\mathrm{p}} = \frac{1}{2} m_{\mathrm{p}} \dot{\boldsymbol{r}}_3^{\mathrm{T}} \dot{\boldsymbol{r}}_3 + \frac{1}{2} J_{\mathrm{p}} \dot{\alpha}_3^2\,. \tag{2.230}$$

In (2.227) the separation of rotational inertias is due to the fact that the joint is made up of two different bodies. One (J_{h2A}) is fixed to the end of link 1 and the other part (J_{h2B}) is impulsed by the rotational actuator, it means that they rotate with different angular velocities therefore their kinetic energies must be calculated separately. This robot has its workspace in a horizontal plane; hence gravitational force has no influence on the energy balance. The potential energy of the robot is due to the flexibility of its links and it is related to the profiles of transversal displacements by

$$U = \sum_{i=1}^{n_{\mathrm{R}}} U_{\mathrm{l}_i}\,, \tag{2.231}$$

$$U_{\mathrm{l}_1} = \frac{1}{2} \left(EI\right)_1 \int_0^l \left(\frac{\partial^2 w(\tilde{x}_1, t)}{\partial\, x_1^2} \right)^2 d\tilde{x}_1\,. \tag{2.232}$$

$$U_{\mathrm{l}_2} = \frac{1}{2} \left(EI\right)_2 \int_0^l \left(\frac{\partial^2 w(\tilde{x}_2, t)}{\partial\, x_2^2} \right)^2 d\tilde{x}_2\,. \tag{2.233}$$

Here also the energy associated to the deformation of the piezoelectric actuator is assumed to be negligible with respect to the links. Flexible-link robots are modeled with partial differential equations (PDE) due to its distributed flexibility. Links are assumed to be uniform and are considered as beams, whose movements are governed by

$$\rho_{\mathrm{l}_i} \frac{\partial^2 w_i(\tilde{x}_i, t)}{\partial t^2} + \left(EI\right)_i \frac{\partial^4 w(\tilde{x}_i, t)}{\partial \tilde{x}_i^4} = 0\,, \tag{2.28}$$

and the boundary conditions for the solution of the partial differential equation are assumed to be of the fully constrained type (cantilever beam). As for the one flexible-link case, this assumption is suitable as long as either the joint has a large inertia compared with the link or

there is a gear reduction with a high reduction ratio [15] or a feedback position control loop with a large gain is closed around the joint [6,16]. The boundary conditions for each are defined in the same manner as for the cantilever beam and one flexible-link robot, taking into account the new coordinate frames. For the first link the boundary conditions are stated as

$$w_1(\tilde{x}_1,t)\big|_{\tilde{x}_1=0}=0\,, \tag{2.234}$$

$$\left.\frac{\partial w_1(\tilde{x}_1,t)}{\partial \tilde{x}_1}\right|_{\tilde{x}_1=0}=0\,, \tag{2.235}$$

$$(EI)_1\left.\frac{\partial^2 w_1(\tilde{x}_1,t)}{\partial \tilde{x}_1^2}\right|_{\tilde{x}_1=l_1}=-J_{\mathrm{D}}\frac{d^2}{dt^2}\left(\left.\frac{\partial w_1(\tilde{x}_1,t)}{\partial \tilde{x}_1}\right|_{\tilde{x}_1=l_1}\right), \tag{2.236}$$

$$(EI)_1\left.\frac{\partial^3 w_1(\tilde{x}_1,t)}{\partial \tilde{x}_1^3}\right|_{\tilde{x}_1=l_1}=m_{\mathrm{D}}\frac{d^2}{dt^2}\left(w_1(\tilde{x}_1,t)\big|_{\tilde{x}_1=l_1}\right). \tag{2.237}$$

Here for the natural boundary conditions (2.236) and (2.237) J_{D} and m_{D} account for the effect of the mass and inertia of the second link including the joint, respectively. For the equivalent inertia applying Steiner theorem

$$J_{\mathrm{D}}=J_{\mathrm{h}_2}+J_{\mathrm{l}_2}+m_{\mathrm{l}_2}\left(\overline{\mathrm{O}_2\tilde{\mathrm{O}}_2}+\frac{l_2}{2}\right)^2+J_{\mathrm{p}}+m_{\mathrm{p}}\left(\overline{\mathrm{O}_2\tilde{\mathrm{O}}_2}+l_2\right)^2\,, \tag{2.238}$$

and for the equivalent mass

$$m_{\mathrm{D}}=m_{\mathrm{h}_2}+m_{\mathrm{l}_2}+m_{\mathrm{p}}\,. \tag{2.239}$$

The boundary conditions for the second link are

$$w_2(\tilde{x}_2,t)\big|_{\tilde{x}_2=0}=0\,, \tag{2.240}$$

$$\left.\frac{\partial w_2(\tilde{x}_2,t)}{\partial \tilde{x}_2}\right|_{\tilde{x}_2=0}=0\,, \tag{2.241}$$

$$(EI)_2\left.\frac{\partial^2 w_2(\tilde{x}_2,t)}{\partial \tilde{x}_2^2}\right|_{\tilde{x}_2=l_2}=-J_{\mathrm{p}}\frac{d^2}{dt^2}\left(\left.\frac{\partial w_2(\tilde{x}_2,t)}{\partial \tilde{x}_2}\right|_{\tilde{x}_2=l_2}\right), \tag{2.242}$$

$$(EI)_2\left.\frac{\partial^3 w_2(\tilde{x}_2,t)}{\partial \tilde{x}_2^3}\right|_{\tilde{x}_2=l_2}=m_{\mathrm{p}}\frac{d^2}{dt^2}\left(w_2(\tilde{x}_2,t)\big|_{\tilde{x}_2=l_2}\right). \tag{2.243}$$

For simulation and control design purposes an approximation to obtain ordinary differential equations must be done. Here the AMM proposed by Meirovitch [2] is again used to approximate the transversal displacements of the links by separating the spatial depending variables (mode shapes) from the time depending variables (modal variables) introducing a new sub index to differentiate between the links

$$w_i(\tilde{x}_i,t)=\sum_{j=1}^{n_{\mathrm{Fi}}}\phi_{ij}(\tilde{x}_i)\,q_{\mathrm{f}ij}(t)\,. \tag{2.244}$$

The mode shape functions are assumed to have the form

$$\phi_{ij}(\tilde{x}_i)=c_{1ij}\sin(\beta_{ij}\tilde{x}_i)+c_{2ij}\cos(\beta_{ij}\tilde{x}_i)+c_{3ij}\sinh(\beta_{ij}\tilde{x}_i)+c_{4ij}\cosh(\beta_{ij}\tilde{x}_i)\,. \tag{2.245}$$

The conversion of the boundary conditions in terms of shape functions and the calculation of resonance frequencies for a similar case is explained is section 2.1.2 from equation (2.44) to (2.68). The resonance frequencies for the first link are given from the solution of

$$
\begin{aligned}
&m_{\mathrm{D}} J_{\mathrm{D}} \beta_{1j}{}^4 + \rho_{\mathrm{l}_1}^2 \cos(\beta_{1j} l_1) \cosh(\beta_{1j} l_1) - \rho_{\mathrm{l}_1} \beta_{1j}{}^3 J_{\mathrm{D}} \sin(\beta_{1j} l_1) \cosh(\beta_{1j} l_1) \\
&+ m_{\mathrm{D}} \rho_{\mathrm{l}_1} \beta_{1j} \cos(\beta_{1j} l_1) \sinh(\beta_{1j} l_1) - m_{\mathrm{D}} J_{\mathrm{D}} \beta_{1j}{}^4 \cos(\beta_{1j} l_1) \cosh(\beta_{1j} l_1) \\
&+ \rho_{\mathrm{l}_1} \beta_{1j}{}^3 J_{\mathrm{D}} \cos(\beta_{1j} l_1) \sinh(\beta_{1j} l_1) - m_{\mathrm{D}} \rho_{\mathrm{l}_1} \beta_{1j} \sin(\beta_{1j} l_1) \cosh(\beta_{1j} l_1) + \rho_{\mathrm{l}_1}^2 = 0
\end{aligned} \quad . \qquad (2.246)
$$

The resonance frequencies for the second link are given from the solution of

$$
\begin{aligned}
&m_{\mathrm{p}} J_{\mathrm{p}} \beta_{2j}{}^4 + \rho_{\mathrm{l}_2}^2 \cos(\beta_{2j} l_2) \cosh(\beta_{2j} l_2) - \rho_{\mathrm{l}_2} \beta_{2j}{}^3 J_p \sin(\beta_{2j} l_2) \cosh(\beta_{2j} l_2) \\
&+ m_{\mathrm{p}} \rho_{\mathrm{l}_2} \beta_{2j} \cos(\beta_{2j} l_2) \sinh(\beta_{2j} l_2) - m_{\mathrm{p}} J_{\mathrm{p}} \beta_{2j}{}^4 \cos(\beta_{2j} l_2) \cosh(\beta_{2j} l_2) \\
&+ \rho_{\mathrm{l}_2} \beta_{2j}{}^3 J_{\mathrm{p}} \cos(\beta_{2j} l_2) \sinh(\beta_{2j} l_2) - m_{\mathrm{p}} \rho_{\mathrm{l}_2} \beta_{2j} \sin(\beta_{2j} l_2) \cosh(\beta_{2j} l_2) + \rho_{\mathrm{l}_2}^2 = 0
\end{aligned} \quad . \qquad (2.247)
$$

The orthonormalization for the first link and second link are given by

$$
\int_0^{l_1} \rho_{\mathrm{l}_1} \, \phi_{1j}(\tilde{x}_1) \, \phi_{1k}(\tilde{x}_1) \, d\tilde{x}_1 + m_{\mathrm{D}} \, \phi_{1j}(l_1) \, \phi_{1k}(l_1) + J_{\mathrm{D}} \, \phi_{1j}'(l_1) \, \phi_{1k}'(l_1) = m_{l_1} \delta_{jk} \,, \qquad (2.248)
$$

and

$$
\int_0^{l_2} \rho_{\mathrm{l}_2} \, \phi_{2j}(\tilde{x}_2) \, \phi_{2k}(\tilde{x}_2) \, d\tilde{x}_2 + m_{\mathrm{p}} \, \phi_{2j}(l_2) \, \phi_{2k}(l_2) + J_{\mathrm{p}} \, \phi_{2j}'(l_2) \, \phi_{2k}'(l_2) = m_{l_2} \delta_{jk} \,, \qquad (2.249)
$$

respectively. These orthogonality conditions are introduced to calculate the c_{kij} constants of the mode shape functions for each link and each considered mode. With the expression for each mode shape the Lagrange function can be calculated. Additionally, the following change of variables is introduced

$$
q_{\mathrm{f}11}(t) = q_3(t) \,, q_{\mathrm{f}12}(t) = q_4(t) \,, \qquad (2.250)
$$

$$
q_{\mathrm{f}21}(t) = q_5(t) \,, q_{\mathrm{f}22}(t) = q_6(t) \qquad (2.251)
$$

Then finally the equations of motion are determined using the Euler-Lagrange equation

$$
\frac{d}{dt} \frac{\partial L}{\partial \dot{q}_i} - \frac{\partial L}{\partial q_i} = f_i, \quad i = 1 \,..\, n \,, \qquad (2.82)
$$

for this robot two rotational degrees of freedom and two flexible DOF pro link are considered, therefore

$$
n = n_R + n_{F1} + n_{F2} = 2 + 2 + 2 = 6 \,. \qquad (2.252)
$$

According to the dependency on each generalized coordinate, (2.82) can be stated as follows

$$
\begin{bmatrix}
\frac{d}{dt}\frac{\partial T_{\mathrm{h}_1}}{\partial \dot{q}_1} + \frac{d}{dt}\frac{\partial T_{\mathrm{h}_2}}{\partial \dot{q}_1} + \frac{d}{dt}\frac{\partial T_{\mathrm{l}_1}}{\partial \dot{q}_1} + \frac{d}{dt}\frac{\partial T_{\mathrm{l}_2}}{\partial \dot{q}_1} + \frac{d}{dt}\frac{\partial T_{\mathrm{p}}}{\partial \dot{q}_1} - \frac{\partial T_{\mathrm{l}_2}}{\partial q_1} - \frac{\partial T_{\mathrm{p}}}{\partial q_1} \\
\frac{d}{dt}\frac{\partial T_{\mathrm{h}_2}}{\partial \dot{q}_2} + \frac{d}{dt}\frac{\partial T_{\mathrm{l}_2}}{\partial \dot{q}_2} + \frac{d}{dt}\frac{\partial T_{\mathrm{p}}}{\partial \dot{q}_2} - \frac{\partial T_{\mathrm{l}_2}}{\partial q_2} - \frac{\partial T_{\mathrm{p}}}{\partial q_2} \\
\frac{d}{dt}\frac{\partial T_{\mathrm{h}_2}}{\partial \dot{q}_3} + \frac{d}{dt}\frac{\partial T_{\mathrm{l}_1}}{\partial \dot{q}_3} + \frac{d}{dt}\frac{\partial T_{\mathrm{l}_2}}{\partial \dot{q}_3} + \frac{d}{dt}\frac{\partial T_{\mathrm{p}}}{\partial \dot{q}_3} - \frac{\partial T_{\mathrm{h}_2}}{\partial q_3} - \frac{\partial T_{\mathrm{l}_1}}{\partial q_3} - \frac{\partial T_{\mathrm{l}_2}}{\partial q_3} - \frac{\partial T_{\mathrm{p}}}{\partial q_3} + \frac{\partial U_{\mathrm{l}_1}}{\partial q_3} \\
\frac{d}{dt}\frac{\partial T_{\mathrm{h}_2}}{\partial \dot{q}_4} + \frac{d}{dt}\frac{\partial T_{\mathrm{l}_1}}{\partial \dot{q}_4} + \frac{d}{dt}\frac{\partial T_{\mathrm{l}_2}}{\partial \dot{q}_4} + \frac{d}{dt}\frac{\partial T_{\mathrm{p}}}{\partial \dot{q}_4} - \frac{\partial T_{\mathrm{h}_2}}{\partial q_4} - \frac{\partial T_{\mathrm{l}_1}}{\partial q_4} - \frac{\partial T_{\mathrm{l}_2}}{\partial q_4} - \frac{\partial T_{\mathrm{p}}}{\partial q_4} + \frac{\partial U_{\mathrm{l}_1}}{\partial q_4} \\
\frac{d}{dt}\frac{\partial T_{\mathrm{l}_2}}{\partial \dot{q}_5} + \frac{d}{dt}\frac{\partial T_{\mathrm{p}}}{\partial \dot{q}_5} - \frac{\partial T_{\mathrm{l}_2}}{\partial q_5} - \frac{\partial T_{\mathrm{p}}}{\partial q_5} + \frac{\partial U_{\mathrm{l}_2}}{\partial q_5} \\
\frac{d}{dt}\frac{\partial T_{\mathrm{l}_2}}{\partial \dot{q}_6} + \frac{d}{dt}\frac{\partial T_{\mathrm{p}}}{\partial \dot{q}_6} - \frac{\partial T_{\mathrm{l}_2}}{\partial q_6} - \frac{\partial T_{\mathrm{p}}}{\partial q_6} + \frac{\partial U_{\mathrm{l}_2}}{\partial q_6}
\end{bmatrix}
=
\begin{bmatrix} f_1 \\ f_2 \\ f_3 \\ f_4 \\ f_5 \\ f_6 \end{bmatrix} \qquad (2.253)
$$

here $\left[f_1 \ \cdots \ f_6\right]^{\mathrm{T}}$ are the generalized forces, which are: motor torques and the bending moments provided by the piezoelectric actuators, respectively. The relationship between the components of (2.253), kinetic relationships and physical parameter is shown in Appendix C.2, this equation can be written in a standard form

$$\boldsymbol{M}(\boldsymbol{q})\,\ddot{\boldsymbol{q}} + \boldsymbol{c}(\boldsymbol{q},\dot{\boldsymbol{q}}) + \boldsymbol{K}\boldsymbol{q} = \boldsymbol{f}\ , \tag{2.254}$$

where $\boldsymbol{M}(\boldsymbol{q})$ is the mass matrix, $\boldsymbol{c}(\boldsymbol{q},\dot{\boldsymbol{q}})$ is the vector of Coriolis and centripetal effects and $\boldsymbol{K}$ is the rigidity modal matrix. Proportional structural damping for the links is also included, adding a damping modal matrix $\boldsymbol{D}$. Then this equation is transformed to obtain the direct dynamic model of this robot

$$\ddot{\boldsymbol{q}} = \boldsymbol{M}(\boldsymbol{q})^{-1}\left(\boldsymbol{f} - \boldsymbol{c}(\boldsymbol{q},\dot{\boldsymbol{q}}) - \boldsymbol{K}\boldsymbol{q} - \boldsymbol{D}\dot{\boldsymbol{q}}\right), \tag{2.255}$$

where the component of the mass matrix are

$$\begin{aligned} m_{11} = {} & J_{\mathrm{h}_1} + J_{\mathrm{h}_2} + m_{\mathrm{h}_2}\,{}^1\boldsymbol{r}_2^{\mathrm{T}}\,{}^1\boldsymbol{r}_2 + \rho_{\mathrm{l}_1}\int_0^{l_1}{}^1\boldsymbol{p}_1^{\mathrm{T}}\,{}^1\boldsymbol{p}_1 d\tilde{x}_1 + \cdots \\ & \rho_{\mathrm{l}_2}\int_0^{l_2}\left({}^1\boldsymbol{r}_2^{\mathrm{T}}\,{}^1\boldsymbol{r}_2 + 2\,{}^2\boldsymbol{p}_2^{\mathrm{T}}\boldsymbol{A}_2^{\mathrm{T}}\boldsymbol{E}_1^{\mathrm{T}}\,{}^1\boldsymbol{r}_2 + {}^2\boldsymbol{p}_2^{\mathrm{T}}\,{}^2\boldsymbol{p}_2\right)d\tilde{x}_2 + \cdots, \\ & m_{\mathrm{p}}\left({}^1\boldsymbol{r}_2^{\mathrm{T}}\,{}^1\boldsymbol{r}_2 + 2\,{}^1\boldsymbol{r}_2^{\mathrm{T}}E_1A_2\,{}^2\boldsymbol{r}_3 + {}^2\boldsymbol{r}_3^{\mathrm{T}}\,{}^2\boldsymbol{r}_3\right) + J_{\mathrm{p}} \end{aligned} \tag{2.256}$$

$$\begin{aligned} m_{12} = {} & J_{\mathrm{h}_2} + \rho_{\mathrm{l}_2}\int_0^{l_2}\left({}^2\boldsymbol{p}_2^{\mathrm{T}}\boldsymbol{A}_2^{\mathrm{T}}\boldsymbol{E}_1^{\mathrm{T}}\,{}^1\boldsymbol{r}_2 + {}^2\boldsymbol{p}_2^{\mathrm{T}}\,{}^2\boldsymbol{p}_2\right)d\tilde{x}_2 + \cdots \\ & m_{\mathrm{p}}\left({}^2\boldsymbol{r}_3^{\mathrm{T}}\boldsymbol{A}_2^{\mathrm{T}}\boldsymbol{E}_1^{\mathrm{T}}\,{}^1\boldsymbol{r}_2 + {}^2\boldsymbol{r}_3^{\mathrm{T}}\,{}^2\boldsymbol{r}_3\right) + J_{\mathrm{p}} \end{aligned}, \tag{2.257}$$

$$\begin{aligned} m_{13} = {} & m_{\mathrm{h}_2}\left(l_1 + \overline{\mathrm{O}_1\tilde{\mathrm{O}}_1}\right)\phi_{\mathrm{e}11} + J_{\mathrm{h}_2}\phi'_{\mathrm{e}11} + \rho_{\mathrm{l}_1}\int_0^{l_1}\tilde{x}_1\phi_{11}(\tilde{x}_1)d\tilde{x}_1 + \cdots \\ & \rho_{\mathrm{l}_2}\int_0^{l_2}\left({}^2\boldsymbol{p}_2^{\mathrm{T}}\boldsymbol{A}_2^{\mathrm{T}}\,{}^1\boldsymbol{r}_2 + {}^2\boldsymbol{p}_2^{\mathrm{T}}\boldsymbol{E}_1\,{}^2\boldsymbol{p}_2\right)\phi'_{\mathrm{e}11}d\tilde{x}_2 + \cdots \\ & \rho_{\mathrm{l}_2}\int_0^{l_2}\left[0\ \ \phi_{\mathrm{e}11}\right]\left(\boldsymbol{S}\boldsymbol{E}_1\boldsymbol{A}_2\,{}^2\boldsymbol{p}_2 + \boldsymbol{S}\,{}^1\boldsymbol{r}_2\right)d\tilde{x}_2 + \cdots \\ & m_{\mathrm{p}}\left[0\ \ \phi_{\mathrm{e}11}\right]\left(\boldsymbol{S}\boldsymbol{E}_1\boldsymbol{A}_2\,{}^2\boldsymbol{r}_3 + \boldsymbol{S}\,{}^1\boldsymbol{r}_2\right) + \cdots \\ & m_{\mathrm{p}}\left({}^2\boldsymbol{r}_3^{\mathrm{T}}\boldsymbol{A}_2^{\mathrm{T}}\,{}^1\boldsymbol{r}_2 + {}^2\boldsymbol{r}_3^{\mathrm{T}}\boldsymbol{E}_1\,{}^2\boldsymbol{r}_3\right)\phi'_{\mathrm{e}11} + J_{\mathrm{p}}\phi'_{\mathrm{e}11} \end{aligned} \tag{2.258}$$

$$\begin{aligned} m_{14} = {} & m_{\mathrm{h}_2}\left(l_1 + \overline{\mathrm{O}_1\tilde{\mathrm{O}}_1}\right)\phi_{\mathrm{e}12} + J_{\mathrm{h}_2}\phi'_{\mathrm{e}12} + \rho_{\mathrm{l}_1}\int_0^{l_1}\tilde{x}_1\phi_{12}(\tilde{x}_1)d\tilde{x}_1 + \cdots \\ & \rho_{\mathrm{l}_2}\int_0^{l_2}\left({}^2\boldsymbol{p}_2^{\mathrm{T}}\boldsymbol{A}_2^{\mathrm{T}}\,{}^1\boldsymbol{r}_2 + {}^2\boldsymbol{p}_2^{\mathrm{T}}\boldsymbol{E}_1\,{}^2\boldsymbol{p}_2\right)\phi'_{\mathrm{e}12}d\tilde{x}_2 + \cdots \\ & \rho_{\mathrm{l}_2}\int_0^{l_2}\left[0\ \ \phi_{\mathrm{e}12}\right]\left(\boldsymbol{S}\boldsymbol{E}_1\boldsymbol{A}_2\,{}^2\boldsymbol{p}_2 + \boldsymbol{S}\,{}^1\boldsymbol{r}_2\right)d\tilde{x}_2 + \cdots \\ & m_{\mathrm{p}}\left[0\ \ \phi_{\mathrm{e}12}\right]\left(\boldsymbol{S}\boldsymbol{E}_1\boldsymbol{A}_2\,{}^2\boldsymbol{r}_3 + \boldsymbol{S}\,{}^1\boldsymbol{r}_2\right) + \cdots \\ & m_{\mathrm{p}}\left({}^2\boldsymbol{r}_3^{\mathrm{T}}\boldsymbol{A}_2^{\mathrm{T}}\,{}^1\boldsymbol{r}_2 + {}^2\boldsymbol{r}_3^{\mathrm{T}}\boldsymbol{E}_1\,{}^2\boldsymbol{r}_3\right)\phi'_{\mathrm{e}12} + J_{\mathrm{p}}\phi'_{\mathrm{e}12} \end{aligned} \tag{2.259}$$

$$\begin{aligned} m_{15} = {} & \rho_{\mathrm{l}_2}\int_0^{l_2}\left[0\ \ \phi_{21}(\tilde{x}_2)\right]\left(\boldsymbol{A}_2^{\mathrm{T}}\boldsymbol{E}_1^{\mathrm{T}}\boldsymbol{S}\,{}^1\boldsymbol{r}_2 + \boldsymbol{S}\,{}^2\boldsymbol{p}_2\right)d\tilde{x}_2 + \cdots \\ & m_{\mathrm{p}}\left[0\ \ \phi_{\mathrm{e}21}\right]\left(\boldsymbol{A}_2^{\mathrm{T}}\boldsymbol{E}_1^{\mathrm{T}}\boldsymbol{S}\,{}^1\boldsymbol{r}_2 + \boldsymbol{S}\,{}^2\boldsymbol{r}_3\right) + J_{\mathrm{p}}\phi'_{\mathrm{e}21} \end{aligned}, \tag{2.260}$$

$$\begin{aligned} m_{16} = {} & \rho_{\mathrm{l}_2}\int_0^{l_2}\left[0\ \ \phi_{22}(\tilde{x}_2)\right]\left(\boldsymbol{A}_2^{\mathrm{T}}\boldsymbol{E}_1^{\mathrm{T}}\boldsymbol{S}\,{}^1\boldsymbol{r}_2 + \boldsymbol{S}\,{}^2\boldsymbol{p}_2\right)d\tilde{x}_2 + \cdots \\ & m_{\mathrm{p}}\left[0\ \ \phi_{\mathrm{e}22}\right]\left(\boldsymbol{A}_2^{\mathrm{T}}\boldsymbol{E}_1^{\mathrm{T}}\boldsymbol{S}\,{}^1\boldsymbol{r}_2 + \boldsymbol{S}\,{}^2\boldsymbol{r}_3\right) + J_{\mathrm{p}}\phi'_{\mathrm{e}22} \end{aligned}, \tag{2.261}$$

$$m_{22} = J_{h_{2BC}} + \rho_{l_2}\int_0^{l_2} {}^2\boldsymbol{p}_2^{\mathrm{T}}\,{}^2\boldsymbol{p}_2\, d\tilde{x}_2 + + m_{\mathrm{p}}\,{}^2\boldsymbol{r}_3^{\mathrm{T}}\,{}^2\boldsymbol{r}_3 + J_{\mathrm{p}}\,, \tag{2.262}$$

$$J_{h_{2BC}} = J_{h_{2B}} + J_{GB2} \tag{2.263}$$

$$\begin{aligned} m_{23} = {} & J_{\mathrm{h}_2}\phi'_{\mathrm{e}11} + \rho_{l_2}\int_0^{l_2}\left(\begin{bmatrix}0 & \phi_{\mathrm{e}11}\end{bmatrix}\boldsymbol{E}_1\boldsymbol{S}\boldsymbol{A}_2\,{}^2\boldsymbol{p}_2 + {}^2\boldsymbol{p}_2^{\mathrm{T}}\boldsymbol{E}_1^{\mathrm{T}}\,{}^2\boldsymbol{p}_2\phi'_{\mathrm{e}11}\right)d\tilde{x}_2 + \cdots \\ & m_{\mathrm{p}}\left(\begin{bmatrix}0 & \phi_{\mathrm{e}11}\end{bmatrix}\boldsymbol{E}_1\boldsymbol{S}\boldsymbol{A}_2\,{}^2\boldsymbol{r}_3 + {}^2\boldsymbol{r}_3^{\mathrm{T}}\boldsymbol{E}_1^{\mathrm{T}}\,{}^2\boldsymbol{r}_3\phi'_{\mathrm{e}11}\right) + J_{\mathrm{p}}\phi'_{\mathrm{e}11} \end{aligned}, \tag{2.264}$$

$$\begin{aligned} m_{24} = {} & J_{\mathrm{h}_2}\phi'_{\mathrm{e}12} + \rho_{l_2}\int_0^{l_2}\left(\begin{bmatrix}0 & \phi_{\mathrm{e}12}\end{bmatrix}\boldsymbol{E}_1\boldsymbol{S}\boldsymbol{A}_2\,{}^2\boldsymbol{p}_2 + {}^2\boldsymbol{p}_2^{\mathrm{T}}\boldsymbol{E}_1^{\mathrm{T}}\,{}^2\boldsymbol{p}_2\phi'_{\mathrm{e}12}\right)d\tilde{x}_2 + \cdots \\ & m_{\mathrm{p}}\left(\begin{bmatrix}0 & \phi_{\mathrm{e}12}\end{bmatrix}\boldsymbol{E}_1\boldsymbol{S}\boldsymbol{A}_2\,{}^2\boldsymbol{r}_3 + {}^2\boldsymbol{r}_3^{\mathrm{T}}\boldsymbol{E}_1^{\mathrm{T}}\,{}^2\boldsymbol{r}_3\phi'_{\mathrm{e}12}\right) + J_{\mathrm{p}}\phi'_{\mathrm{e}12} \end{aligned}, \tag{2.265}$$

$$m_{25} = \rho_{l_2}\int_0^{l_2}\begin{bmatrix}0 & \phi_{\mathrm{e}21}\end{bmatrix}\boldsymbol{S}\,{}^2\boldsymbol{p}_2 d\tilde{x}_2 + m_p\begin{bmatrix}0 & \phi_{\mathrm{e}21}\end{bmatrix}\boldsymbol{S}\,{}^2\boldsymbol{r}_3 + J_{\mathrm{p}}\phi'_{\mathrm{e}21}\,, \tag{2.266}$$

$$m_{26} = \rho_{l_2}\int_0^{l_2}\begin{bmatrix}0 & \phi_{\mathrm{e}22}\end{bmatrix}\boldsymbol{S}\,{}^2\boldsymbol{p}_2 d\tilde{x}_2 + m_p\begin{bmatrix}0 & \phi_{\mathrm{e}22}\end{bmatrix}\boldsymbol{S}\,{}^2\boldsymbol{r}_3 + J_{\mathrm{p}}\phi'_{\mathrm{e}22}\,, \tag{2.267}$$

$$\begin{aligned} m_{33} = {} & m_{\mathrm{h}_2}\phi_{\mathrm{e}11}^2 + J_{\mathrm{h}_2}\phi'^2_{\mathrm{e}11} + \rho_{l_1}\int_0^{l_1}\phi_{11}(\tilde{x}_1)^2 d\tilde{x}_1 + \rho_{l_2}\int_0^{l_2}\left(\phi_{\mathrm{e}11}^2\right)d\tilde{x}_2 + \cdots \\ & \rho_{l_2}\int_0^{l_2}\left({}^2\boldsymbol{p}_2^{\mathrm{T}}\boldsymbol{A}_2^{\mathrm{T}}\boldsymbol{S}^{\mathrm{T}}\begin{bmatrix}0 & \phi_{\mathrm{e}11}\end{bmatrix}^{\mathrm{T}}\phi'_{\mathrm{e}11} + \begin{bmatrix}0 & \phi_{\mathrm{e}11}\end{bmatrix}\boldsymbol{S}\boldsymbol{A}_2\,{}^2\boldsymbol{p}_2\phi'_{\mathrm{e}11}\right)d\tilde{x}_2 + \cdots \\ & \rho_{l_2}\int_0^{l_2}\left({}^2\boldsymbol{p}_2^{\mathrm{T}}\,{}^2\boldsymbol{p}_2\phi'^2_{\mathrm{e}11}\right)d\tilde{x}_2 + m_{\mathrm{p}}\left(\phi_{\mathrm{e}11}^2 + {}^2\boldsymbol{r}_3^{\mathrm{T}}\boldsymbol{A}_2^{\mathrm{T}}\boldsymbol{S}^{\mathrm{T}}\begin{bmatrix}0 & \phi_{\mathrm{e}11}\end{bmatrix}^{\mathrm{T}}\phi'_{\mathrm{e}11}\right) + \cdots \\ & J_{\mathrm{p}}\phi'^2_{\mathrm{e}11} + m_{\mathrm{p}}\left(\begin{bmatrix}0 & \phi_{\mathrm{e}11}\end{bmatrix}\boldsymbol{S}\boldsymbol{A}_2\,{}^2\boldsymbol{r}_3\phi'_{\mathrm{e}11} + {}^2\boldsymbol{r}_3^{\mathrm{T}}\,{}^2\boldsymbol{r}_3\phi'^2_{\mathrm{e}11}\right) \end{aligned}, \tag{2.268}$$

$$\begin{aligned} m_{34} = {} & m_{\mathrm{h}_2}\phi_{\mathrm{e}11}\phi_{\mathrm{e}12} + J_{\mathrm{h}_2}\phi'_{\mathrm{e}11}\phi'_{\mathrm{e}12} + \rho_{l_1}\int_0^{l_1}\phi_{11}(\tilde{x}_1)\phi_{12}(\tilde{x}_1)d\tilde{x}_1 + \\ & \rho_{l_2}\int_0^{l_2}\left(\phi_{\mathrm{e}11}\phi_{\mathrm{e}12} + {}^2\boldsymbol{p}_2^{\mathrm{T}}\boldsymbol{A}_2^{\mathrm{T}}\boldsymbol{S}^{\mathrm{T}}\begin{bmatrix}0 & \phi_{\mathrm{e}11}\end{bmatrix}^{\mathrm{T}}\phi'_{\mathrm{e}12}\right)d\tilde{x}_2 + \cdots \\ & \rho_{l_2}\int_0^{l_2}\left(\begin{bmatrix}0 & \phi_{\mathrm{e}12}\end{bmatrix}\boldsymbol{S}\boldsymbol{A}_2\,{}^2\boldsymbol{p}_2\phi'_{\mathrm{e}11} + {}^2\boldsymbol{p}_2^{\mathrm{T}}\,{}^2\boldsymbol{p}_2\phi'_{\mathrm{e}11}\phi'_{\mathrm{e}12}\right)d\tilde{x}_2 + \cdots, \\ & m_{\mathrm{p}}\left(\phi_{\mathrm{e}11}\phi_{\mathrm{e}12} + {}^2\boldsymbol{r}_3^{\mathrm{T}}\boldsymbol{A}_2^{\mathrm{T}}\boldsymbol{S}^{\mathrm{T}}\begin{bmatrix}0 & \phi_{\mathrm{e}11}\end{bmatrix}^{\mathrm{T}}\phi'_{\mathrm{e}12}\right) + \cdots \\ & J_{\mathrm{p}}\phi'_{\mathrm{e}11}\phi'_{\mathrm{e}12} + m_{\mathrm{p}}\left(\begin{bmatrix}0 & \phi_{\mathrm{e}12}\end{bmatrix}\boldsymbol{S}\boldsymbol{A}_2\,{}^2\boldsymbol{r}_3\phi'_{\mathrm{e}11} + {}^2\boldsymbol{r}_3^{\mathrm{T}}\,{}^2\boldsymbol{r}_3\phi'_{\mathrm{e}11}\phi'_{\mathrm{e}12}\right) \end{aligned}, \tag{2.269}$$

$$\begin{aligned} m_{35} = {} & \rho_{l_2}\int_0^{l_2}\begin{bmatrix}0 & \phi_{21}(\tilde{x}_2)\end{bmatrix}\boldsymbol{A}_2^{\mathrm{T}}\boldsymbol{E}_1^{\mathrm{T}}\begin{bmatrix}0 & \phi_{\mathrm{e}11}\end{bmatrix}^{\mathrm{T}}d\tilde{x}_2 + \cdots \\ & \rho_{l_2}\int_0^{l_2}\begin{bmatrix}0 & \phi_{21}(\tilde{x}_2)\end{bmatrix}\boldsymbol{E}_1^{\mathrm{T}}\boldsymbol{S}\,{}^2\boldsymbol{p}_2\phi'_{\mathrm{e}11}d\tilde{x}_2 + \cdots \\ & m_{\mathrm{p}}\left(\begin{bmatrix}0 & \phi_{\mathrm{e}21}\end{bmatrix}\boldsymbol{A}_2^{\mathrm{T}}\boldsymbol{E}_1^{\mathrm{T}}\begin{bmatrix}0 & \phi_{\mathrm{e}11}\end{bmatrix}^{\mathrm{T}}\right) + J_{\mathrm{p}}\phi'_{\mathrm{e}11}\phi'_{\mathrm{e}21} + \cdots \\ & m_{\mathrm{p}}\left(\begin{bmatrix}0 & \phi_{\mathrm{e}21}\end{bmatrix}\boldsymbol{E}_1^{\mathrm{T}}\boldsymbol{S}\,{}^2\boldsymbol{r}_3\phi'_{\mathrm{e}11}\right) \end{aligned}, \tag{2.270}$$

$$\begin{aligned} m_{36} = {} & \rho_{l_2}\int_0^{l_2}\begin{bmatrix}0 & \phi_{22}(\tilde{x}_2)\end{bmatrix}\boldsymbol{A}_2^{\mathrm{T}}\boldsymbol{E}_1^{\mathrm{T}}\begin{bmatrix}0 & \phi_{\mathrm{e}11}\end{bmatrix}^{\mathrm{T}}d\tilde{x}_2 + \cdots \\ & \rho_{l_2}\int_0^{l_2}\begin{bmatrix}0 & \phi_{22}(\tilde{x}_2)\end{bmatrix}\boldsymbol{E}_1^{\mathrm{T}}\boldsymbol{S}\,{}^2\boldsymbol{p}_2\phi'_{\mathrm{e}11}d\tilde{x}_2 + \cdots \\ & m_{\mathrm{p}}\left(\begin{bmatrix}0 & \phi_{\mathrm{e}22}\end{bmatrix}\boldsymbol{A}_2^{\mathrm{T}}\boldsymbol{E}_1^{\mathrm{T}}\begin{bmatrix}0 & \phi_{\mathrm{e}11}\end{bmatrix}^{\mathrm{T}}\right) + J_{\mathrm{p}}\phi'_{\mathrm{e}11}\phi'_{\mathrm{e}22} + \cdots \\ & m_{\mathrm{p}}\left(\begin{bmatrix}0 & \phi_{\mathrm{e}22}\end{bmatrix}\boldsymbol{E}_1^{\mathrm{T}}\boldsymbol{S}\,{}^2\boldsymbol{r}_3\phi'_{\mathrm{e}11}\right) \end{aligned}, \tag{2.271}$$

$$
\begin{aligned}
m_{44} = {} & m_{\mathrm{h}_2}\phi_{\mathrm{e}12}^2 + J_{\mathrm{h}_2}\phi_{\mathrm{e}12}'^2 + \rho_{\mathrm{l}_1}\int_0^{l_1}\phi_{12}(\tilde{x}_1)^2 d\tilde{x}_1 + \rho_{\mathrm{l}_2}\int_0^{l_2}\left(\phi_{\mathrm{e}12}^2\right)d\tilde{x}_2 + \cdots \\
& \rho_{\mathrm{l}_2}\int_0^{l_2}\left({}^2\boldsymbol{p}_2^{\mathrm{T}}\boldsymbol{A}_2^{\mathrm{T}}\boldsymbol{S}^{\mathrm{T}}\begin{bmatrix}0 & \phi_{\mathrm{e}12}\end{bmatrix}^{\mathrm{T}}\phi_{\mathrm{e}12}' + \begin{bmatrix}0 & \phi_{\mathrm{e}12}\end{bmatrix}\boldsymbol{S}\boldsymbol{A}_2\,{}^2\boldsymbol{p}_2\phi_{\mathrm{e}12}'\right)d\tilde{x}_2 + \cdots \\
& \rho_{\mathrm{l}_2}\int_0^{l_2}\left({}^2\boldsymbol{p}_2^{\mathrm{T}}\,{}^2\boldsymbol{p}_2\phi_{\mathrm{e}12}'^2\right)d\tilde{x}_2 + m_{\mathrm{p}}\left(\phi_{\mathrm{e}12}^2 + {}^2\boldsymbol{r}_3^{\mathrm{T}}\boldsymbol{A}_2^{\mathrm{T}}\boldsymbol{S}^{\mathrm{T}}\begin{bmatrix}0 & \phi_{\mathrm{e}12}\end{bmatrix}^{\mathrm{T}}\phi_{\mathrm{e}12}'\right) + \cdots \\
& J_{\mathrm{p}}\phi_{\mathrm{e}12}'^2 + m_{\mathrm{p}}\left(\begin{bmatrix}0 & \phi_{\mathrm{e}12}\end{bmatrix}\boldsymbol{S}\boldsymbol{A}_2\,{}^2\boldsymbol{r}_3\phi_{\mathrm{e}12}' + {}^2\boldsymbol{r}_3^{\mathrm{T}}\,{}^2\boldsymbol{r}_3\phi_{\mathrm{e}12}'^2\right)
\end{aligned}, \tag{2.272}
$$

$$
\begin{aligned}
m_{45} = {} & \rho_{\mathrm{l}_2}\int_0^{l_2}\begin{bmatrix}0 & \phi_{21}(\tilde{x}_2)\end{bmatrix}\boldsymbol{A}_2^{\mathrm{T}}\boldsymbol{E}_1^{\mathrm{T}}\begin{bmatrix}0 & \phi_{\mathrm{e}12}\end{bmatrix}^{\mathrm{T}}d\tilde{x}_2 + \cdots \\
& \rho_{\mathrm{l}_2}\int_0^{l_2}\begin{bmatrix}0 & \phi_{21}(\tilde{x}_2)\end{bmatrix}\boldsymbol{E}_1^{\mathrm{T}}\boldsymbol{S}\,{}^2\boldsymbol{p}_2\phi_{\mathrm{e}12}'d\tilde{x}_2 + \cdots \\
& m_{\mathrm{p}}\left(\begin{bmatrix}0 & \phi_{\mathrm{e}21}\end{bmatrix}\boldsymbol{A}_2^{\mathrm{T}}\boldsymbol{E}_1^{\mathrm{T}}\begin{bmatrix}0 & \phi_{\mathrm{e}12}\end{bmatrix}^{\mathrm{T}}\right) + J_{\mathrm{p}}\phi_{\mathrm{e}12}'\phi_{\mathrm{e}21}' + \cdots \\
& m_{\mathrm{p}}\left(\begin{bmatrix}0 & \phi_{\mathrm{e}21}\end{bmatrix}\boldsymbol{E}_1^{\mathrm{T}}\boldsymbol{S}\,{}^2\boldsymbol{r}_3\phi_{\mathrm{e}12}'\right)
\end{aligned}, \tag{2.273}
$$

$$
\begin{aligned}
m_{46} = {} & \rho_{\mathrm{l}_2}\int_0^{l_2}\begin{bmatrix}0 & \phi_{22}(\tilde{x}_2)\end{bmatrix}\boldsymbol{A}_2^{\mathrm{T}}\boldsymbol{E}_1^{\mathrm{T}}\begin{bmatrix}0 & \phi_{\mathrm{e}12}\end{bmatrix}^{\mathrm{T}}d\tilde{x}_2 + \cdots \\
& \rho_{\mathrm{l}_2}\int_0^{l_2}\begin{bmatrix}0 & \phi_{22}(\tilde{x}_2)\end{bmatrix}\boldsymbol{E}_1^{\mathrm{T}}\boldsymbol{S}\,{}^2\boldsymbol{p}_2\phi_{\mathrm{e}12}'d\tilde{x}_2 + \cdots \\
& m_{\mathrm{p}}\left(\begin{bmatrix}0 & \phi_{\mathrm{e}22}\end{bmatrix}\boldsymbol{A}_2^{\mathrm{T}}\boldsymbol{E}_1^{\mathrm{T}}\begin{bmatrix}0 & \phi_{\mathrm{e}12}\end{bmatrix}^{\mathrm{T}}\right) + J_{\mathrm{p}}\phi_{\mathrm{e}12}'\phi_{\mathrm{e}22}' + \cdots \\
& m_{\mathrm{p}}\left(\begin{bmatrix}0 & \phi_{\mathrm{e}22}\end{bmatrix}\boldsymbol{E}_1^{\mathrm{T}}\boldsymbol{S}\,{}^2\boldsymbol{r}_3\phi_{\mathrm{e}12}'\right)
\end{aligned}, \tag{2.274}
$$

$$
m_{55} = \rho_{\mathrm{l}_2}\int_0^{l_2}\phi_{21}(\tilde{x}_2)^2 d\tilde{x}_2 + m_{\mathrm{p}}\phi_{\mathrm{e}21}^2 + J_{\mathrm{p}}\phi_{\mathrm{e}21}'^2, \tag{2.275}
$$

$$
m_{56} = \rho_{\mathrm{l}_2}\int_0^{l_2}\phi_{21}(\tilde{x}_2)\phi_{22}(\tilde{x}_2)d\tilde{x}_2 + m_{\mathrm{p}}\phi_{\mathrm{e}21}\phi_{\mathrm{e}22} + J_{\mathrm{p}}\phi_{\mathrm{e}21}'\phi_{\mathrm{e}22}', \tag{2.276}
$$

$$
m_{66} = \rho_{\mathrm{l}_2}\int_0^{l_2}\phi_{22}(\tilde{x}_2)^2 d\tilde{x}_2 + m_{\mathrm{p}}\phi_{\mathrm{e}22}^2 + J_{\mathrm{p}}\phi_{\mathrm{e}22}'^2. \tag{2.277}
$$

The vector of Coriolis and centrifugal effects is given in Appendix C.2. The stiffness matrix due to the orthonormality condition is a diagonal matrix and it is calculated via

$$
\begin{aligned}
& \text{if } 1 < i \le n_{\mathrm{R}} \text{ then } k_{ii} = 0 \\
& \text{if } n_{\mathrm{R}} < i \le n \text{ then} \\
& \quad \text{if } n_{\mathrm{R}} < i \le n_{\mathrm{R}} + n_{\mathrm{F1}} \quad \text{then } u = 1 \text{ and } v = 1..n_{\mathrm{F1}}, \\
& \quad \text{if } n_{\mathrm{R}} + n_{\mathrm{F1}} < i \le n_{\mathrm{R}} + n_{\mathrm{F1}} + n_{\mathrm{F2}} \text{ then } u = 2 \text{ and } v = 1..n_{\mathrm{F2}} \\
& \qquad k_{i,i} = (EI)_u\int_0^{l_u}\left(\frac{\partial\phi_{uv}(\tilde{x}_u)}{\partial\tilde{x}_u}\right)^2 d\tilde{x}_u
\end{aligned} \tag{2.278}
$$

$$
\boldsymbol{K} = \begin{bmatrix}
0 & 0 & 0 & 0 & 0 & 0 \\
0 & 0 & 0 & 0 & 0 & 0 \\
0 & 0 & (EI)_1\int_0^{l_1}\phi_{11}''^2(\tilde{x}_1)d\tilde{x}_1 & 0 & 0 & 0 \\
0 & 0 & 0 & (EI)_1\int_0^{l_1}\phi_{12}''^2(\tilde{x}_1)d\tilde{x}_1 & 0 & 0 \\
0 & 0 & 0 & 0 & (EI)_2\int_0^{l_1}\phi_{21}''^2(\tilde{x}_2)d\tilde{x}_2 & 0 \\
0 & 0 & 0 & 0 & 0 & (EI)_2\int_0^{l_1}\phi_{22}''^2(\tilde{x}_2)d\tilde{x}_2
\end{bmatrix}, \tag{2.279}
$$

as result of this the stiffness matrix can also be formulated as

$$\boldsymbol{K} = \begin{bmatrix} 0 & 0 & 0 & 0 & 0 & 0 \\ 0 & 0 & 0 & 0 & 0 & 0 \\ 0 & 0 & m_{l_1}\omega_{11}^2 & 0 & 0 & 0 \\ 0 & 0 & 0 & m_{l_1}\omega_{12}^2 & 0 & 0 \\ 0 & 0 & 0 & 0 & m_{l_2}\omega_{21}^2 & 0 \\ 0 & 0 & 0 & 0 & 0 & m_{l_2}\omega_{22}^2 \end{bmatrix}. \tag{2.280}$$

Furthermore, the passive proportional structural damping for the link can be introduced [77,79,80]

$$\begin{aligned} &\text{if } 1 < i \le n_{\mathrm{R}} \text{ then } d_{ii} = 0 \\ &\text{if } n_{\mathrm{R}} < i \le n \text{ then} \\ &\quad \text{if } n_{\mathrm{R}} < i \le n_{\mathrm{R}} + n_{\mathrm{F1}} \quad \text{then } u = 1 \text{ and } v = 1..n_{\mathrm{F1}}\,, \\ &\quad \text{if } n_{\mathrm{R}} + n_{\mathrm{F1}} < i \le n_{\mathrm{R}} + n_{\mathrm{F1}} + n_{\mathrm{F2}} \text{ then } u = 2 \text{ and } v = 1..n_{\mathrm{F2}} \\ &d_{i,i} = 2\left(\operatorname{diag}\left(\left(\xi_{uv} k_{i,i} m_{l_u}\right)^{\frac{1}{2}}\right)\right) \end{aligned} \tag{2.281}$$

then the damping matrix can be written as

$$\boldsymbol{D} = \begin{bmatrix} 0 & 0 & 0 & 0 & 0 & 0 \\ 0 & 0 & 0 & 0 & 0 & 0 \\ 0 & 0 & 2\xi_{11}\left(k_{33} m_{l_1}\right)^{\frac{1}{2}} & 0 & 0 & 0 \\ 0 & 0 & 0 & 2\xi_{12}\left(k_{44} m_{l_1}\right)^{\frac{1}{2}} & 0 & 0 \\ 0 & 0 & 0 & 0 & 2\xi_{21}\left(k_{55} m_{l_2}\right)^{\frac{1}{2}} & 0 \\ 0 & 0 & 0 & 0 & 0 & 2\xi_{22}\left(k_{66} m_{l_2}\right)^{\frac{1}{2}} \end{bmatrix}. \tag{2.282}$$

The vector of generalized coordinates includes in its first two components the torques resulting from the difference of the motor torques and friction torques. The model for the piezoelectric patch has the same form as long as it only depends on the mode shapes, piezoelectric and mechanical properties and substrate, perfect bending is again assumed. Then the remaining components of $\boldsymbol{f}$ are provided by the piezoelectric actuators whose model was calculated in Appendix A.1. Therefore, the vector of generalized coordinates is given by

$$\boldsymbol{f} = \boldsymbol{B}_{\mathrm{pi}} \begin{bmatrix} \tau_{\mathrm{m}_1}(t) - \tau_{\mathrm{fr}_1}(\dot{q}_1(t)) \\ \tau_{\mathrm{m}_2}(t) - \tau_{\mathrm{fr}_2}(\dot{q}_2(t)) \\ v_{\mathrm{p}_1}(t) \\ v_{\mathrm{p}_2}(t) \end{bmatrix}, \tag{2.283}$$

where the input matrix is given by

$$\boldsymbol{B}_{\mathrm{pi}} = \begin{bmatrix} 1 & 0 & 0 & 0 \\ 0 & 1 & 0 & 0 \\ 0 & 0 & \overline{c}_1\left(\phi'_{11}(x_{\mathrm{a}2}) - \phi'_{11}(x_{\mathrm{a}1})\right) & 0 \\ 0 & 0 & \overline{c}_1\left(\phi'_{12}(x_{\mathrm{a}2}) - \phi'_{12}(x_{\mathrm{a}1})\right) & 0 \\ 0 & 0 & 0 & \overline{c}_2\left(\phi'_{21}(x_{\mathrm{a}2}) - \phi'_{21}(x_{\mathrm{a}1})\right) \\ 0 & 0 & 0 & \overline{c}_2\left(\phi'_{22}(x_{\mathrm{a}2}) - \phi'_{22}(x_{\mathrm{a}1})\right) \end{bmatrix}. \tag{2.284}$$

The flexible-link robot under study has the dimensions given in the following table.

Table 2.6 Physical parameters of the two flexible-link robot

Parameter	Value	Complementary information
Material	Aluminum	DIN $AlMg_3$ F22
l_1	0.310	m
l_2	0.300	m
$\overline{\mathrm{O}_1\tilde{\mathrm{O}}_1}$	0.050	m
$\overline{\mathrm{O}_2\tilde{\mathrm{O}}_2}$	0.055	m
m_1	0.059	kg
m_2	0.047	kg
$(EI)_1$	1.633	Nm^2
$(EI)_2$	0.689	Nm^2
t_1	0.002	m
t_2	0.0015	m
ρ_{l_1}	0.1876	$\mathrm{kg\ m}^{-1}$
ρ_{l_2}	0.1407	$\mathrm{kg\ m}^{-1}$
m_{p}	0.059	kg
J_{p}	$6.6\mathrm{x}10^{-7}$	$\mathrm{kg\ m}^2$
J_{h_1}	$6.7956\mathrm{x}10^{-2}$	$\mathrm{kg\ m}^2$
$J_{\mathrm{h}_{2\mathrm{fix}}}$	$3.779\mathrm{x}10^{-5}$	$\mathrm{kg\ m}^2$
$J_{\mathrm{h}_{2\mathrm{mov}}}$	$4.576\mathrm{x}10^{-3}$	$\mathrm{kg\ m}^2$

The first two modes of vibration for each link and their first and second spatial derivative, calculated for the given dimensions, are shown in Figs. 2.38, 2.39 and 2.40.

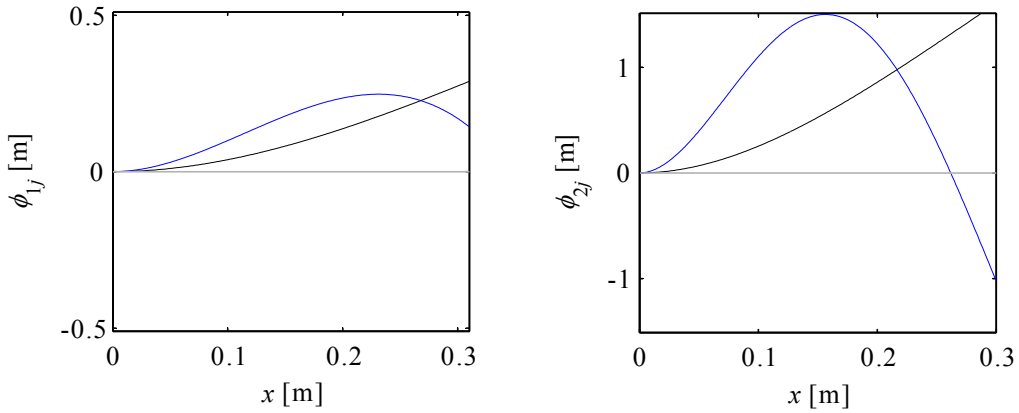

Figure 2.38: Modes of vibration of the links, first mode (black), second mode (blue) and undeformed link (gray). Left: first link, right: second link.

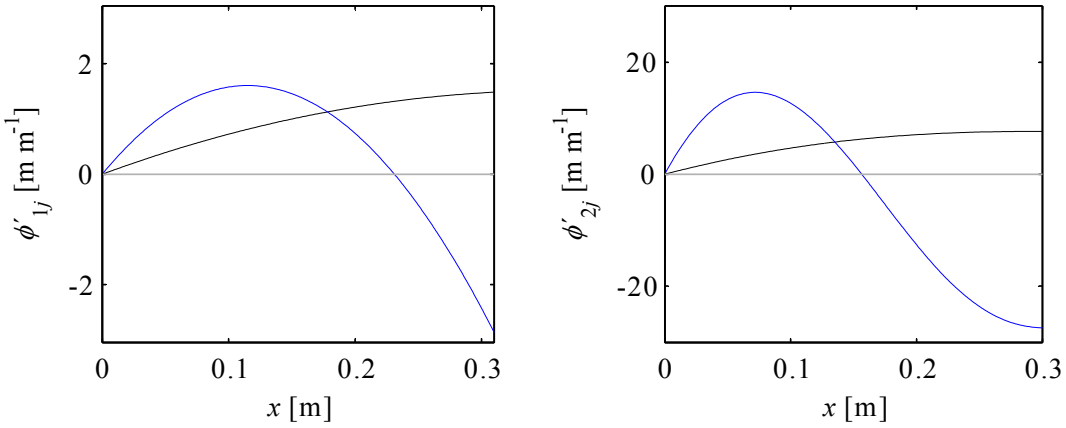

Figure 2.39: First spatial derivative of the modes of vibration of the links, first mode (black), second mode (blue) and undeformed link (gray). Left: first link, right: second link.

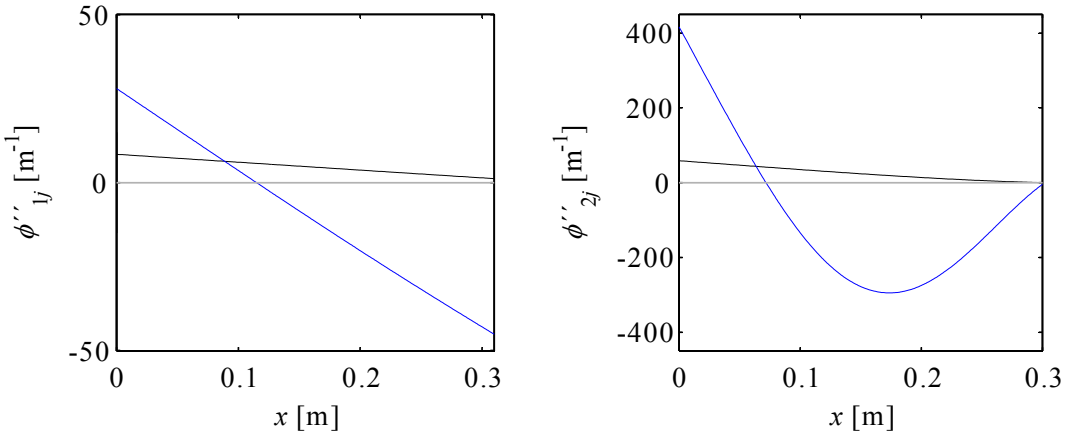

Figure 2.40: Second spatial derivative of the modes of vibration of the links, first mode (black), second mode (blue) and undeformed link (gray). Left: first link, right: second link.

2.3.2 Model Verification

This procedure follows the same structure as it was performed for the one flexible-link robot described in section 2.2.2. This is also performed in order to know if the robot model in correctly implemented, and to know if the physical assumption approximate to the reality. This procedure is shown in Fig. 2.25.

Verification of Calculations

In this stage, the whole energy balance and the Lagrange-Euler approach was also exhaustively reviewed. Here the task is much more demanding than in previous models, due to the huge amount of formulations which is a great source of possible errors. Unfortunately, here due to the non-commutativity of matrix multiplications the calculation could not be performed using symbolic software directly (i.e. Maple). For this reason, the models were developed manually to take advantage of the orthonormality of the rotation matrices and some related identities for simplifying terms. Additionally, if the models are formulated until this point manually, then later the number of flexible modes to be considered is not restricted and they can be introduced using the AMM approximation. The symbolic software was used to calculate the entire integral elements related to the distributed flexibility.

Comparison between analog components of the model

There exist similarities between the elements of the equation of motion (2.253) and they can also be used to verify the model. These similarities can be expressed as

$$\frac{d}{dt}\frac{\partial T_{\mathrm{l}_2}}{\partial \dot{q}_i} \sim \frac{d}{dt}\frac{\partial T_{\mathrm{p}}}{\partial \dot{q}_i}, \tag{2.285}$$

$$\frac{d}{dt}\frac{\partial T_{l_1}}{\partial \dot{q}_i} \sim \frac{d}{dt}\frac{\partial T_{\mathrm{h}_2}}{\partial \dot{q}_i}, \tag{2.286}$$

$$\frac{\partial T_{\mathrm{l}_2}}{\partial q_i} \sim \frac{\partial T_{\mathrm{p}}}{\partial q_i}, \tag{2.287}$$

and

$$\frac{\partial T_{\mathrm{l}_1}}{\partial q_i} \sim \frac{\partial T_{\mathrm{h}_2}}{\partial q_i}. \tag{2.288}$$

As a demonstration of this, the analog $\frac{d}{dt}\frac{\partial T_{\mathrm{l}_2}}{\partial \dot{q}_1}$ and $\frac{d}{dt}\frac{\partial T_{\mathrm{p}}}{\partial \dot{q}_1}$ terms are showed

$$\begin{aligned}\frac{d}{dt}\frac{\partial T_{\mathrm{l}_2}}{\partial \dot{q}_1} = {} & TL2q1t\_A1\ddot{q}_1 + TL2q1t\_A2\ddot{q}_2 + TL2q1t\_A3\ddot{q}_3 + \cdots \\ & TL2q1t\_A4\ddot{q}_4 + TL2q1t\_A5\ddot{q}_5 + TL2q1t\_A6\ddot{q}_6 + TL2q1t\_B\end{aligned}, \tag{2.289}$$

where

$$TL2q1t\_A1 = \rho_{\mathrm{l}_2}\int_0^{l_2}\left({}^1\boldsymbol{r}_2^{\mathrm{T}}\,{}^1\boldsymbol{r}_2 + 2\,{}^2\boldsymbol{p}_2^{\mathrm{T}}\boldsymbol{A}_2^{\mathrm{T}}\boldsymbol{E}_1^{\mathrm{T}}\,{}^1\boldsymbol{r}_2 + {}^2\boldsymbol{p}_2^{\mathrm{T}}\,{}^2\boldsymbol{p}_2\right)d\tilde{x}_2, \tag{2.290}$$

$$TL2q1t\_A2 = \rho_{\mathrm{l}_2}\int_0^{l_2}\left({}^2\boldsymbol{p}_2^{\mathrm{T}}\boldsymbol{A}_2^{\mathrm{T}}\boldsymbol{E}_1^{\mathrm{T}}\,{}^1\boldsymbol{r}_2 + {}^2\boldsymbol{p}_2^{\mathrm{T}}\,{}^2\boldsymbol{p}_2\right)d\tilde{x}_2, \tag{2.291}$$

$$TL2q1t\_A3 = \rho_{\mathrm{l}_2}\int_0^{l_2}\left(\left({}^2\boldsymbol{p}_2^{\mathrm{T}}\boldsymbol{A}_2^{\mathrm{T}}\,{}^1\boldsymbol{r}_2 + {}^2\boldsymbol{p}_2^{\mathrm{T}}\boldsymbol{E}_1\,{}^2\boldsymbol{p}_2\right)\phi'_{\mathrm{e}11} + \begin{bmatrix}0 & \phi_{\mathrm{e}11}\end{bmatrix}\left(\boldsymbol{S}\boldsymbol{E}_1\boldsymbol{A}_2\,{}^2\boldsymbol{p}_2 + \boldsymbol{S}\,{}^1\boldsymbol{r}_2\right)\right)d\tilde{x}_2, \tag{2.292}$$

$$TL2q1t\_A4 = \rho_{\mathrm{l}_2}\int_0^{l_2}\left(\left({}^2\boldsymbol{p}_2^{\mathrm{T}}\boldsymbol{A}_2^{\mathrm{T}}\,{}^1\boldsymbol{r}_2 + {}^2\boldsymbol{p}_2^{\mathrm{T}}\boldsymbol{E}_1\,{}^2\boldsymbol{p}_2\right)\phi'_{\mathrm{e}12} + \begin{bmatrix}0 & \phi_{\mathrm{e}12}\end{bmatrix}\left(\boldsymbol{S}\boldsymbol{E}_1\boldsymbol{A}_2\,{}^2\boldsymbol{p}_2 + \boldsymbol{S}\,{}^1\boldsymbol{r}_2\right)\right)d\tilde{x}_2, \tag{2.293}$$

$$TL2q1t\_A5 = \rho_{\mathrm{l}_2}\int_0^{l_2}\begin{bmatrix}0 & \phi_{21}(\tilde{x}_2)\end{bmatrix}\left(\boldsymbol{A}_2^{\mathrm{T}}\boldsymbol{E}_1^{\mathrm{T}}\boldsymbol{S}\,{}^1\boldsymbol{r}_2 + \boldsymbol{S}\,{}^2\boldsymbol{p}_2\right)d\tilde{x}_2, \tag{2.294}$$

$$TL2q1t\_A6 = \rho_{\mathrm{l}_2}\int_0^{l_2}\begin{bmatrix}0 & \phi_{22}(\tilde{x}_2)\end{bmatrix}\left(\boldsymbol{A}_2^{\mathrm{T}}\boldsymbol{E}_1^{\mathrm{T}}\boldsymbol{S}\,{}^1\boldsymbol{r}_2 + \boldsymbol{S}\,{}^2\boldsymbol{p}_2\right)d\tilde{x}_2, \tag{2.295}$$

$$TL2q1t\_B = \rho_{\mathrm{l}_2}\int_0^{l_2}\left(TL2q1t\_B1 + TL2q1t\_B2 + TL2q1t\_B3\right)d\tilde{x}_2, \tag{2.296}$$

where

$$\begin{aligned}TL2q1t\_B1 = {} & 2\,{}^1\boldsymbol{r}_2^{\mathrm{T}}\,{}^1\dot{\boldsymbol{r}}_2\dot{q}_1 + 2\,{}^2\dot{\boldsymbol{p}}_2^{\mathrm{T}}\boldsymbol{A}_2^{\mathrm{T}}\boldsymbol{E}_1^{\mathrm{T}}\,{}^1\boldsymbol{r}_2\dot{q}_1 + 2\,{}^2\boldsymbol{p}_2^{\mathrm{T}}\dot{\boldsymbol{A}}_2^{\mathrm{T}}\boldsymbol{E}_1^{\mathrm{T}}\,{}^1\boldsymbol{r}_2\dot{q}_1 + \cdots \\ & 2\,{}^2\boldsymbol{p}_2^{\mathrm{T}}\boldsymbol{A}_2^{\mathrm{T}}\dot{\boldsymbol{E}}_1^{\mathrm{T}}\,{}^1\boldsymbol{r}_2\dot{q}_1 + 2\,{}^2\boldsymbol{p}_2^{\mathrm{T}}\boldsymbol{A}_2^{\mathrm{T}}\boldsymbol{E}_1^{\mathrm{T}}\,{}^1\dot{\boldsymbol{r}}_2\dot{q}_1\end{aligned}, \tag{2.297}$$

$$TL2q1t\_B2 = 2\,{}^2\dot{\boldsymbol{p}}_2^{\mathrm{T}}\boldsymbol{A}_2^{\mathrm{T}}\dot{\boldsymbol{E}}_1^{\mathrm{T}}\boldsymbol{S}\,{}^1\boldsymbol{r}_2 + 2\,{}^2\boldsymbol{p}_2^{\mathrm{T}}\boldsymbol{A}_2^{\mathrm{T}}\dot{\boldsymbol{E}}_1^{\mathrm{T}}\,{}^1\boldsymbol{r}_2\dot{q}_2 + 2\,{}^2\dot{\boldsymbol{p}}_2^{\mathrm{T}}\boldsymbol{A}_2^{\mathrm{T}}\boldsymbol{E}_1^{\mathrm{T}}\,{}^1\boldsymbol{r}_2\dot{q}_2 + {}^2\boldsymbol{p}_2^{\mathrm{T}}\boldsymbol{A}_2^{\mathrm{T}}\boldsymbol{S}^{\mathrm{T}}\boldsymbol{E}_1^{\mathrm{T}}\,{}^1\boldsymbol{r}_2\dot{q}_2^2, \tag{2.298}$$

$$TL2q1t\_B3 = 2\,{}^2\boldsymbol{p}_2^{\mathrm{T}}\,{}^2\dot{\boldsymbol{p}}_2\dot{q}_1 + {}^2\dot{\boldsymbol{p}}_2^{\mathrm{T}}\dot{\boldsymbol{E}}_1^{\mathrm{T}}\boldsymbol{S}\boldsymbol{E}_1\,{}^2\boldsymbol{p}_2 + {}^2\boldsymbol{p}_2^{\mathrm{T}}\dot{\boldsymbol{E}}_1^{\mathrm{T}}\boldsymbol{S}\boldsymbol{E}_1\,{}^2\dot{\boldsymbol{p}}_2 + 2\,{}^2\boldsymbol{p}_2^{\mathrm{T}}\,{}^2\dot{\boldsymbol{p}}_2\dot{q}_2. \tag{2.299}$$

Then their counterpart

$$\begin{aligned}\frac{d}{dt}\frac{\partial T_{\mathrm{p}}}{\partial \dot{q}_1} = {} & TPq1t\_A1\ddot{q}_1 + TPq1t\_A2\ddot{q}_2 + TPq1t\_A3\ddot{q}_3 + \cdots \\ & TPq1t\_A4\ddot{q}_4 + TPq1t\_A5\ddot{q}_5 + TPq1t\_A6\ddot{q}_6 + TPq1t\_B\end{aligned}, \tag{2.300}$$

where

$$TPq1t\_A1 = m_{\mathrm{p}}\left({}^{1}\boldsymbol{r}_2^{\mathrm{T}}\,{}^{1}\boldsymbol{r}_2 + 2\,{}^{1}\boldsymbol{r}_2^{\mathrm{T}}E_1A_2\,{}^{2}\boldsymbol{r}_3 + {}^{2}\boldsymbol{r}_3^{\mathrm{T}}\,{}^{2}\boldsymbol{r}_3\right) + J_{\mathrm{p}}, \tag{2.301}$$

$$TPq1t\_A2 = m_{\mathrm{p}}\left({}^{2}\boldsymbol{r}_3^{\mathrm{T}}\boldsymbol{A}_2^{\mathrm{T}}\boldsymbol{E}_1^{\mathrm{T}}\,{}^{1}\boldsymbol{r}_2 + {}^{2}\boldsymbol{r}_3^{\mathrm{T}}\,{}^{2}\boldsymbol{r}_3\right) + J_{\mathrm{p}}, \tag{2.302}$$

$$TPq1t\_A3 = m_{\mathrm{p}}\begin{bmatrix}0 & \phi_{\mathrm{e}11}\end{bmatrix}\left(\boldsymbol{S}\boldsymbol{E}_1\boldsymbol{A}_2\,{}^{2}\boldsymbol{r}_3 + \boldsymbol{S}\,{}^{1}\boldsymbol{r}_2\right) + m_{\mathrm{p}}\left({}^{2}\boldsymbol{r}_3^{\mathrm{T}}\boldsymbol{A}_2^{\mathrm{T}}\,{}^{1}\boldsymbol{r}_2 + {}^{2}\boldsymbol{r}_3^{\mathrm{T}}\boldsymbol{E}_1\,{}^{2}\boldsymbol{r}_3\right)\phi'_{\mathrm{e}11} + J_{\mathrm{p}}\phi'_{\mathrm{e}11}, \tag{2.303}$$

$$TPq1t\_A4 = m_{\mathrm{p}}\begin{bmatrix}0 & \phi_{\mathrm{e}12}\end{bmatrix}\left(\boldsymbol{S}\boldsymbol{E}_1\boldsymbol{A}_2\,{}^{2}\boldsymbol{r}_3 + \boldsymbol{S}\,{}^{1}\boldsymbol{r}_2\right) + m_{\mathrm{p}}\left({}^{2}\boldsymbol{r}_3^{\mathrm{T}}\boldsymbol{A}_2^{\mathrm{T}}\,{}^{1}\boldsymbol{r}_2 + {}^{2}\boldsymbol{r}_3^{\mathrm{T}}\boldsymbol{E}_1\,{}^{2}\boldsymbol{r}_3\right)\phi'_{\mathrm{e}12} + J_{\mathrm{p}}\phi'_{\mathrm{e}12}, \tag{2.304}$$

$$TPq1t\_A5 = m_{\mathrm{p}}\begin{bmatrix}0 & \phi_{\mathrm{e}21}\end{bmatrix}\left(\boldsymbol{A}_2^{\mathrm{T}}\boldsymbol{E}_1^{\mathrm{T}}\boldsymbol{S}\,{}^{1}\boldsymbol{r}_2 + \boldsymbol{S}\,{}^{2}\boldsymbol{r}_3\right) + J_{\mathrm{p}}\phi'_{\mathrm{e}21}, \tag{2.305}$$

$$TPq1t\_A6 = m_{\mathrm{p}}\begin{bmatrix}0 & \phi_{\mathrm{e}22}\end{bmatrix}\left(\boldsymbol{A}_2^{\mathrm{T}}\boldsymbol{E}_1^{\mathrm{T}}\boldsymbol{S}\,{}^{1}\boldsymbol{r}_2 + \boldsymbol{S}\,{}^{2}\boldsymbol{r}_3\right) + J_{\mathrm{p}}\phi'_{\mathrm{e}22}, \tag{2.306}$$

and

$$TPq1t\_B = m_{\mathrm{p}}\left(TPq1t\_B1 + TPq1t\_B2 + TPq1t\_B3\right), \tag{2.307}$$

where

$$\begin{aligned} TPq1t\_B1 = {} & 2\,{}^{1}\boldsymbol{r}_2^{\mathrm{T}}\,{}^{1}\dot{\boldsymbol{r}}_2\dot{q}_1 + 2\,{}^{1}\dot{\boldsymbol{r}}_2^{\mathrm{T}}\boldsymbol{E}_1\boldsymbol{A}_2\,{}^{2}\boldsymbol{r}_3\dot{q}_1 + 2\,{}^{1}\boldsymbol{r}_2^{\mathrm{T}}\dot{\boldsymbol{E}}_1\boldsymbol{A}_2\,{}^{2}\boldsymbol{r}_3\dot{q}_1 + \cdots \\ & 2\,{}^{1}\boldsymbol{r}_2^{\mathrm{T}}\boldsymbol{E}_1\boldsymbol{S}\boldsymbol{A}_2\,{}^{2}\boldsymbol{r}_3\dot{q}_1\dot{q}_2 + 2\,{}^{1}\boldsymbol{r}_2^{\mathrm{T}}\boldsymbol{E}_1\boldsymbol{A}_2\,{}^{2}\dot{\boldsymbol{r}}_3\dot{q}_1 \end{aligned}, \tag{2.308}$$

$$TPq1t\_B2 = 2\,{}^{2}\boldsymbol{r}_3^{\mathrm{T}}\,{}^{2}\dot{\boldsymbol{r}}_3\dot{q}_1 + 2\,{}^{2}\dot{\boldsymbol{r}}_3^{\mathrm{T}}\boldsymbol{A}_2^{\mathrm{T}}\dot{\boldsymbol{E}}_1^{\mathrm{T}}\boldsymbol{S}\,{}^{1}\boldsymbol{r}_2 + 2\,{}^{2}\boldsymbol{r}_3^{\mathrm{T}}\boldsymbol{A}_2^{\mathrm{T}}\dot{\boldsymbol{E}}_1^{\mathrm{T}}\,{}^{1}\boldsymbol{r}_2\dot{q}_2 + {}^{2}\dot{\boldsymbol{r}}_3^{\mathrm{T}}\dot{\boldsymbol{E}}_1^{\mathrm{T}}\boldsymbol{S}\boldsymbol{E}_1\,{}^{2}\boldsymbol{r}_3, \tag{2.309}$$

and

$$TPq1t\_B3 = {}^{2}\boldsymbol{r}_3^{\mathrm{T}}\dot{\boldsymbol{E}}_1^{\mathrm{T}}\boldsymbol{S}\boldsymbol{E}_1\,{}^{2}\dot{\boldsymbol{r}}_3 + 2\,{}^{2}\dot{\boldsymbol{r}}_3^{\mathrm{T}}\boldsymbol{A}_2^{\mathrm{T}}\boldsymbol{E}_1^{\mathrm{T}}\,{}^{1}\boldsymbol{r}_2\dot{q}_2 + {}^{2}\boldsymbol{r}_3^{\mathrm{T}}\boldsymbol{A}_2^{\mathrm{T}}\boldsymbol{S}^{\mathrm{T}}\boldsymbol{E}_1^{\mathrm{T}}\,{}^{1}\boldsymbol{r}_2\dot{q}_2^2 + 2\,{}^{2}\boldsymbol{r}_3^{\mathrm{T}}\,{}^{2}\dot{\boldsymbol{r}}_3\dot{q}_2\,. \tag{2.310}$$

The similarities are

$${}^{1}\boldsymbol{p}_1(\tilde{x}_1) \sim {}^{1}\boldsymbol{r}_2, \tag{2.311}$$

$${}^{2}\boldsymbol{p}_2(\tilde{x}_2) \sim {}^{2}\boldsymbol{r}_3, \tag{2.312}$$

$$\phi_{11}(\tilde{x}_1) \sim \phi_{\mathrm{e}11}, \tag{2.313}$$

$$\phi_{12}(\tilde{x}_1) \sim \phi_{\mathrm{e}12}, \tag{2.314}$$

$$\phi_{21}(\tilde{x}_2) \sim \phi_{\mathrm{e}21}, \tag{2.315}$$

$$\phi_{22}(\tilde{x}_2) \sim \phi_{\mathrm{e}22}, \tag{2.316}$$

$$m_{\mathrm{h}_2} \sim \rho_{l_1}\int_0^{l_1} f(\tilde{x}_1)d\tilde{x}_1, \tag{2.317}$$

and

$$m_{\mathrm{p}} \sim \rho_{l_2}\int_0^{l_2} f(\tilde{x}_2)d\tilde{x}_2\,. \tag{2.318}$$

In (2.289), as in (2.181) for the one flexible-link case, does not appear any similar term of inertia, but this is due to the Euler assumption of neglecting the rotational inertia of the elements of the beam (flexible links). Besides inertia terms, the similarity is fulfilled between (2.289) and (2.297). Nevertheless, it can be completely verified in Appendix C.2.

Symmetry of Mass Matrix and Stiffness Matrix

Considering that the mass matrix must always be symmetric positive definite i.e. $\boldsymbol{M}(\boldsymbol{q}) = \boldsymbol{M}^{\mathrm{T}}(\boldsymbol{q})$ and $\boldsymbol{M}(\boldsymbol{q}) > 0$, consequently the matrix is nonsingular and its inverse exist. From the Lagrange formulation the mass matrix is obtained, verification or debugging can be done by comparing each element of the triangular upper part with its counterpart in the lower part. Here just some elements are compared; the remaining elements can be checked in Appendix C.2. In consideration are

$$m_{23} = m_{32} = J_{\mathrm{h}_2}\phi'_{\mathrm{e}11} + \rho_{\mathrm{l}_2}\int_0^{l_2}\left(\left[0 \;\; \phi_{\mathrm{e}11}\right]\boldsymbol{E}_1\boldsymbol{S}\boldsymbol{A}_2\,{}^2\boldsymbol{p}_2 + {}^2\boldsymbol{p}_2^{\mathrm{T}}\boldsymbol{E}_1\,{}^2\boldsymbol{p}_2\phi'_{\mathrm{e}11}\right)d\tilde{x}_2 + \cdots$$
$$m_{\mathrm{p}}\left(\left[0 \;\; \phi_{\mathrm{e}11}\right]\boldsymbol{E}_1\boldsymbol{S}\boldsymbol{A}_2\,{}^2\boldsymbol{r}_3 + {}^2\boldsymbol{r}_3^{\mathrm{T}}\boldsymbol{E}_1\,{}^2\boldsymbol{r}_3\phi'_{\mathrm{e}11}\right) + J_{\mathrm{p}}\phi'_{\mathrm{e}11} \tag{2.319}$$

and

$$\begin{aligned} m_{36} = m_{63} = {} & \rho_{\mathrm{l}_2}\int_0^{l_2}\left[0 \;\; \phi_{22}(\tilde{x}_2)\right]\boldsymbol{A}_2^{\mathrm{T}}\boldsymbol{E}_1^{\mathrm{T}}\left[0 \;\; \phi_{\mathrm{e}11}\right]^{\mathrm{T}}d\tilde{x}_2 + \cdots \\ & \rho_{\mathrm{l}_2}\int_0^{l_2}\left[0 \;\; \phi_{22}(\tilde{x}_2)\right]\boldsymbol{E}_1^{\mathrm{T}}\boldsymbol{S}^2\boldsymbol{p}_2\phi'_{\mathrm{e}11}d\tilde{x}_2 + \cdots \\ & m_{\mathrm{p}}\left(\left[0 \;\; \phi_{\mathrm{e}22}\right]\boldsymbol{A}_2^{\mathrm{T}}\boldsymbol{E}_1^{\mathrm{T}}\left[0 \;\; \phi_{\mathrm{e}11}\right]^{\mathrm{T}}\right) + J_{\mathrm{p}}\phi'_{\mathrm{e}11}\phi'_{\mathrm{e}22} + \cdots \\ & m_{\mathrm{p}}\left(\left[0 \;\; \phi_{\mathrm{e}22}\right]\boldsymbol{E}_1^{\mathrm{T}}\boldsymbol{S}^2\boldsymbol{r}_3\phi'_{\mathrm{e}11}\right) \end{aligned} . \tag{2.320}$$

The lower right block of the mass matrix is defined uniquely by the orthonormality conditions

$$m_{56} = m_{65} = \rho_{\mathrm{l}_2}\int_0^{l_2}\phi_{21}(\tilde{x}_2)\phi_{22}(\tilde{x}_2)d\tilde{x}_2 + m_{\mathrm{p}}\phi_{\mathrm{e}21}\phi_{\mathrm{e}22} + J_{\mathrm{p}}\phi'_{\mathrm{e}21}\phi'_{\mathrm{e}22} = 0\,, \tag{2.321}$$

$$m_{55} = \rho_{\mathrm{l}_2}\int_0^{l_2}\phi_{21}(\tilde{x}_2)^2d\tilde{x}_2 + m_{\mathrm{p}}\phi_{\mathrm{e}21}^2 + J_{\mathrm{p}}\phi_{\mathrm{e}21}'^2 = m_{\mathrm{l}_2}\,, \tag{2.322}$$

and

$$m_{66} = \rho_{\mathrm{l}_2}\int_0^{l_2}\phi_{22}(\tilde{x}_2)^2d\tilde{x}_2 + m_{\mathrm{p}}\phi_{\mathrm{e}22}^2 + J_{\mathrm{p}}\phi_{\mathrm{e}22}'^2 = m_{\mathrm{l}_2}\,. \tag{2.323}$$

Considering also the links as linear elastic solids, the stiffness matrix is symmetric; $\boldsymbol{K} = \boldsymbol{K}^{\mathrm{T}}$ then $k_{ij} = k_{ji}$. In this research no elasticity at the joints is considered, therefore for the first two variables q_1 and q_2 no flexibility is defined. Then the stiffness matrix can be calculated through two different ways

$$\boldsymbol{K} = \begin{bmatrix} 0 & 0 & 0 & 0 & 0 & 0 \\ 0 & 0 & 0 & 0 & 0 & 0 \\ 0 & 0 & (EI)_1\int_0^{l_1}\phi_{11}''^2d\tilde{x}_1 & (EI)_1\int_0^{l_1}\phi_{11}''\phi_{12}''d\tilde{x}_1 & 0 & 0 \\ 0 & 0 & (EI)_1\int_0^{l_1}\phi_{11}''\phi_{12}''d\tilde{x}_1 & (EI)_2\int_0^{l_1}\phi_{12}''^2d\tilde{x}_1 & 0 & 0 \\ 0 & 0 & 0 & 0 & (EI)_2\int_0^{l_1}\phi_{21}''^2d\tilde{x}_2 & (EI)_2\int_0^{l_1}\phi_{21}''\phi_{22}''d\tilde{x}_2 \\ 0 & 0 & 0 & 0 & (EI)_2\int_0^{l_1}\phi_{21}''\phi_{22}''d\tilde{x}_2 & (EI)_2\int_0^{l_1}\phi_{22}''^2d\tilde{x}_2 \end{bmatrix}, \tag{2.324}$$

and

$$\boldsymbol{K} = \begin{bmatrix} 0 & 0 & 0 & 0 & 0 & 0 \\ 0 & 0 & 0 & 0 & 0 & 0 \\ 0 & 0 & m_{\mathrm{l}_1}\omega_{11}^2 & 0 & 0 & 0 \\ 0 & 0 & 0 & m_{\mathrm{l}_1}\omega_{12}^2 & 0 & 0 \\ 0 & 0 & 0 & 0 & m_{\mathrm{l}_2}\omega_{21}^2 & 0 \\ 0 & 0 & 0 & 0 & 0 & m_{\mathrm{l}_2}\omega_{22}^2 \end{bmatrix}. \tag{2.325}$$

It can be also verified numerically using the physical parameter given in Tab. 2.6. For the mass matrix depend on the vector of generalized coordinates, therefore for verification a vector of generalized coordinates must be assumed $\boldsymbol{q} = \left[1 \;\; 0.5 \;\; 0.1 \;\; 0.05 \;\; 0.08 \;\; 0.04\right]^{\mathrm{T}}$. Then substituting it in the mass matrix (2.256) – (2.277), where the obtained matrix is

$$\boldsymbol{M}(\boldsymbol{q}) = \begin{bmatrix} 0.1438828 & 0.0112504 & 0.0676164 & -0.0112670 & 0.0263209 & 0.0100138 \\ 0.0112504 & 0.0083797 & 0.0144837 & -0.0225587 & 0.0122190 & 0.0026329 \\ 0.0676164 & 0.0144837 & 0.0650440 & -0.0254746 & 0.0299132 & 0.0097588 \\ -0.0112670 & -0.0225587 & -0.0254746 & 0.0778789 & -0.0338929 & -0.0057467 \\ 0.0263209 & 0.0122190 & 0.0299132 & -0.0338929 & 0.0470000 & 0.0000076 \\ 0.0100138 & 0.0026329 & 0.0097588 & -0.0057467 & 0.0000076 & 0.0470000 \end{bmatrix} . \quad (2.326)$$

As expected the symmetric characteristic of the mass matrix is verified, also the orthogonality is satisfied. Nevertheless, elements $m_{5,6}$ and $m_{6,5}$ are not zero, but their value represent just the 0.01% of the mass of the second link. It is considered acceptable and the source of this small discrepancy lies in neglecting of some imaginary terms encountered in the solution of some definite integral related to this crossed elements. Regarding the stiffness matrix, it does not depend on generalized coordinate vector. Considering the assumed modes and physical parameter of the robot the matrix is given by

$$\boldsymbol{K} = \begin{bmatrix} 0 & 0 & 0 & 0 & 0 & 0 \\ 0 & 0 & 0 & 0 & 0 & 0 \\ 0 & 0 & 13.86 & 0 & 0 & 0 \\ 0 & 0 & 0 & 270.84 & 0 & 0 \\ 0 & 0 & 0 & 0 & 199.09 & 0 \\ 0 & 0 & 0 & 0 & 0 & 9460.86 \end{bmatrix} . \quad (2.327)$$

Here also due to the orthogonality conditions and due to the modal formulation for each link the stiffness matrix is also diagonal.

Verification of Natural Frequencies

As in the one flexible-link case, natural frequencies for each link can be calculated independently in different steps of the model formulation. From the physical parameter and from the solutions of (2.246) and (2.247), the natural frequencies of the considered modes for each link can be calculated. Using these values, boundary conditions, AMM and the Lagrange-Euler formalism; then equation of motion containing the stiffness matrix is obtained from the terms related to the energy of elastic deformation. Therefore, the natural frequencies can be calculated from this stiffness matrix. Then (2.279) can be reformulated to obtain the natural frequencies

$$\omega_{11} = \left(\frac{(EI)_1 \int_0^{l_1} \phi_{11}''(\tilde{x}_1)^2 d\tilde{x}_1}{m_{l_1}} \right)^{0.5} , \quad (2.328)$$

$$\omega_{12} = \left(\frac{(EI)_1 \int_0^{l_1} \phi_{12}''(\tilde{x}_1)^2 d\tilde{x}_1}{m_{l_1}} \right)^{0.5} , \quad (2.329)$$

$$\omega_{21} = \left(\frac{(EI)_2 \int_0^{l_2} \phi_{21}''(\tilde{x}_2)^2 d\tilde{x}_2}{m_{l_2}} \right)^{0.5} , \quad (2.330)$$

and

$$\omega_{22} = \left(\frac{(EI)_2 \int_0^{l_2} \phi''_{22}(\tilde{x}_2)^2 d\tilde{x}_2}{m_{l_2}} \right)^{0.5} . \tag{2.331}$$

In Tab. 2.5 are shown the values of natural frequencies obtained independently in the model formulation.

Table 2.7 Comparison of natural frequencies of the two flexible-link robot

Parameter	Value from (2.156)	Value from (2.192)
ω_{11} [rad/s]	15.33	15.33
ω_{12} [rad/s]	67.75	67.75
ω_{21} [rad/s]	65.08	65.08
ω_{22} [rad/s]	448.66	448.66

The values of the frequencies match; it means the model with its assumption has been, at least in this part, correctly formulated.

Implementation in Matlab/Simulink

For simulation the model was implemented in Matlab/Simulink to solve the equation of motion of the robot. The model for the two flexible-link robot was divided in two parts: kinematic relationships and dynamic relationships, like the one flexible-link robot as well. The first one contains relations between position and velocities of the components of the robot (continuous and discrete). The latter comprises mainly the relations coming from the Lagrange-Euler equation; it also subdivided into two parts: relations for discrete components (rigid parts) and relations continuous components (flexible links). All the terms related to the flexible links result in integral forms, which are calculated using symbolic software and then implemented in Matlab/Simulink as embedded functions. The implementation of this dynamic direct model is illustrated in Fig. 2.41.Using this implementation, additional strategies can be used to perform additional verification of the robot model. It is important to mention that also this Matlab/Simulink model and its symbolically calculated elements were subjected to an exhaustive debugging process too.

Comparison between components of implemented and analytical model

Another performed test is to compare the response of some parts of the implemented model with their counterparts completely analytically calculated; this is another way to verify the correctness of the implemented robot model. For this purpose, the implemented model is controlled at joint level with two PID controllers to follow a joint trajectory (see Fig. 2.42). Similarly to the one flexible-link robot verification, the determinant of the mass matrix is taken into account because it comprises a relation between the whole elements of the mass matrix of the implemented model and from the analytical model. The time evolutions of the determinants of both mass matrices are compared (see Fig. 2.43). It can be seen that both curves match, therefore the mass matrix does.

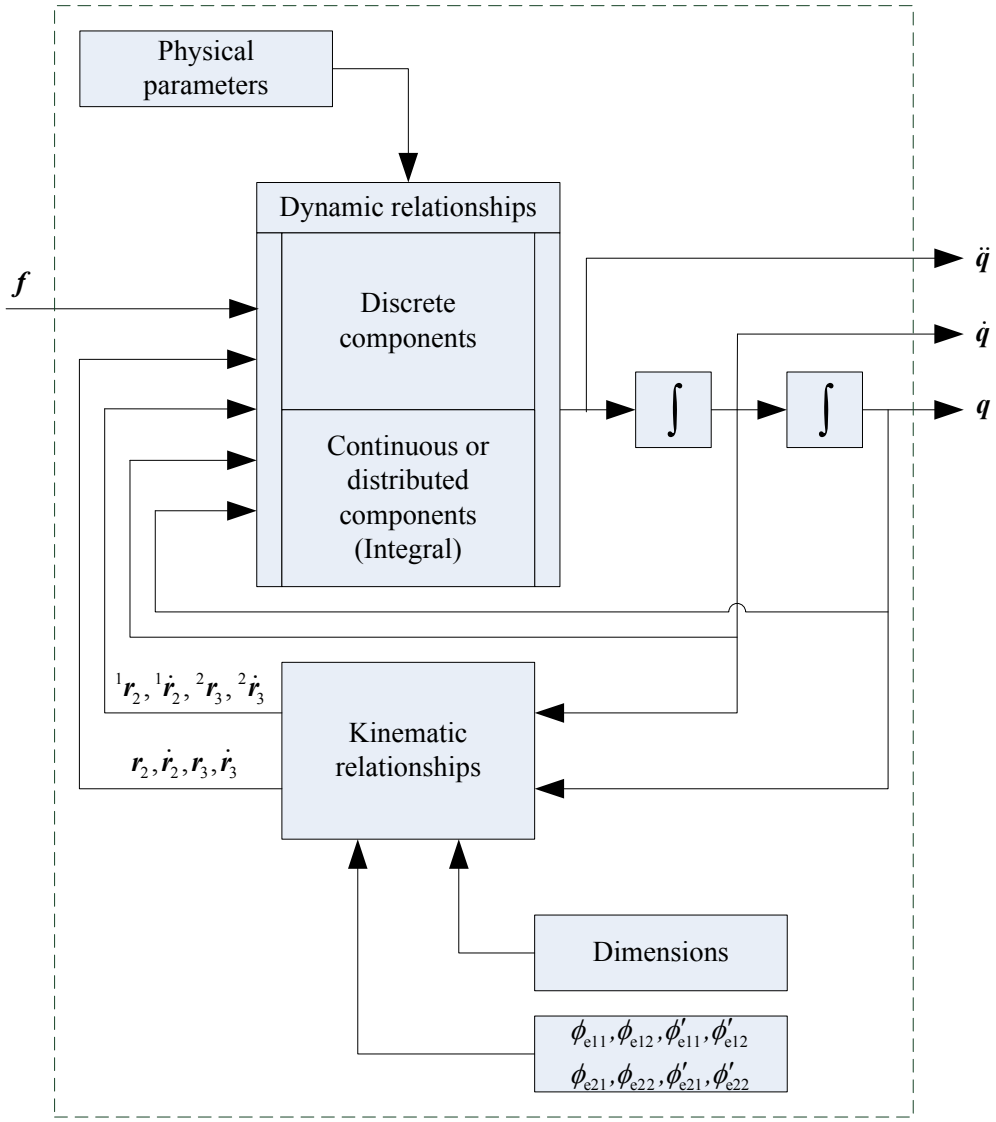

Figure 2.41: Scheme for the implementation of the model for the two flexible-link robot.

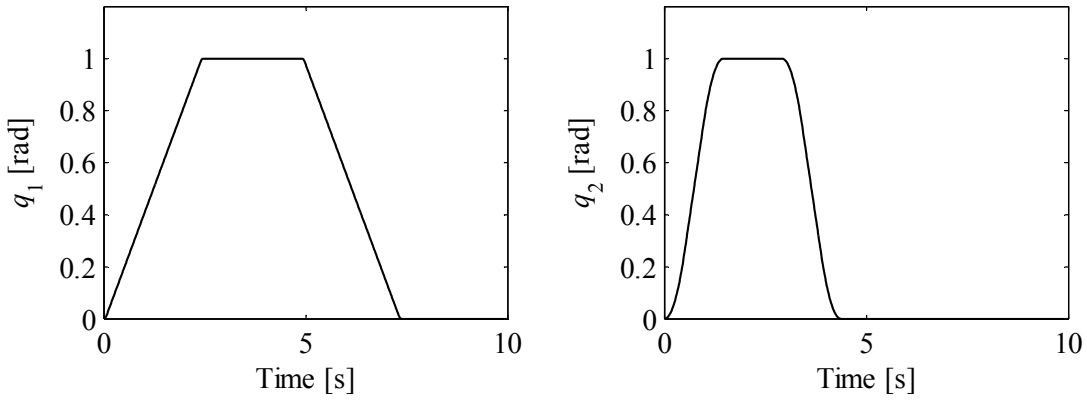

Figure 2.42: Joint trajectories.

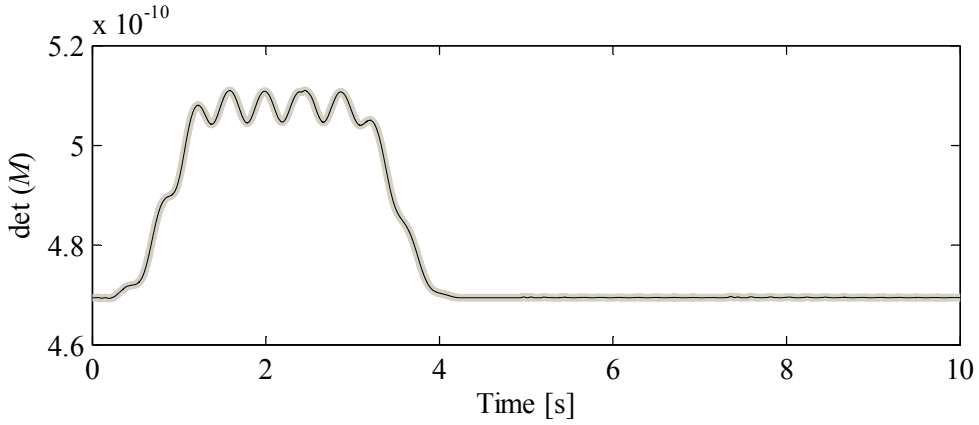

Figure 2.43: Determinant of mass matrix. Black: numerical, gray: analytical.

The configuration is similar to the one flexible-link robot, but for the two flexible-link robot the second joint variable has a strong influence in the mass matrix. For this reason the determinant fluctuates significantly more. Also the components of vector of Coriolis and centripetal effects for the implemented model are calculated evaluating (C.235) or can be analytically calculated from the mass matrix using the Christofel coefficients [6]

$$c_i = \sum_{j=1}^{n}\sum_{k=1}^{n}\left(\frac{\partial m_{ij}}{\partial q_k} - \frac{1}{2}\frac{\partial m_{jk}}{\partial q_i}\right)\dot{q}_k\dot{q}_j \,. \tag{2.332}$$

For the same joint trajectories the time evolution of the components of vector of Coriolis and centripetal effects is shown in Figs. 2.44 and 2.45 the implemented model and the analytical model, respectively. The components of the vector were calculated independently and the two vectors are very close, there is a small difference due to neglecting some imaginary terms in the integral elements, it introduces this small discrepancy which is tolerable considering that its influence in the complete model is not very significant. With the test performed it can also be stated that the model is correctly implemented and that the implemented model corresponds to the proposed conceptual model for the two flexible-link robot.

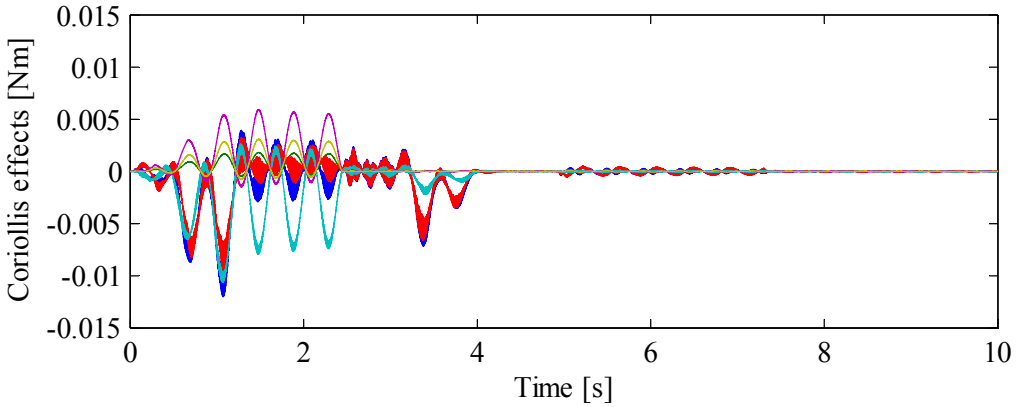

Figure 2.44: Components of Coriolis vector and centripetal effects of the implemented model.

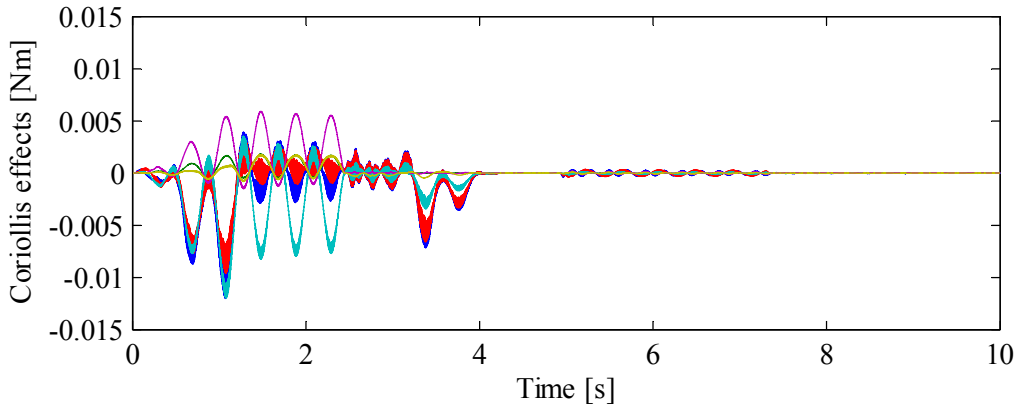

Figure 2.45: Components of Coriolis vector and centripetal effects from Christofel coefficients.

2.3.3 Model Validation

In order to compare the behavior of the implemented model with the real system some experiments have been done. The robot and the model were subjected to different inputs i.e. a bang-bang signal at joint level and to a chirp signal in the piezoelectric actuators.

The transient response is compared using as input signal a bang-bang torque. The input signal is sent to the rotational actuators in different experiences and in each experience the deformation in the links is measured. Here, as in the case for the one flexible-link robot, the maximum and minimum values are chosen to be greater than the maxima and minima values of the friction model experimentally determined in Appendix D for each joint. With this input signals (see Fig. 2.46) a transient behavior is induced in the robot.

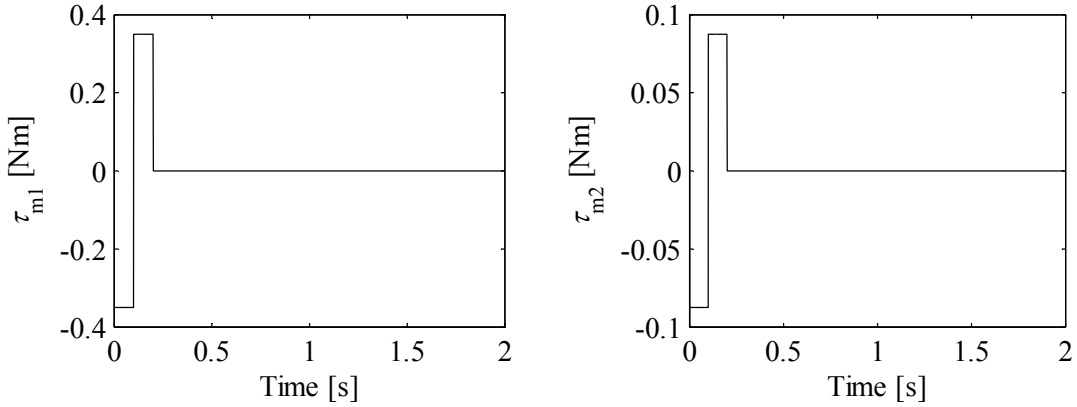

Figure 2.46: Bang-bang input signals for the joints of the robot.

This torque signal induces a joint movement which is mainly influenced by friction, after the static friction is defeated joints move. The final positions differ from the initial ones because this friction model is a nonlinear discontinuity affected by the direction of movement. First the bang-bang signal is applied in the first joint and then the response is measured by the strain gages. The response of the robot to this joint input is shown in Fig. 2.48 in terms of deformation near the clamped end of the link. The damping factors used for the two considered modes were taken from experimental system identification performed on a clamped beam with the same boundary conditions as suggested by [47].

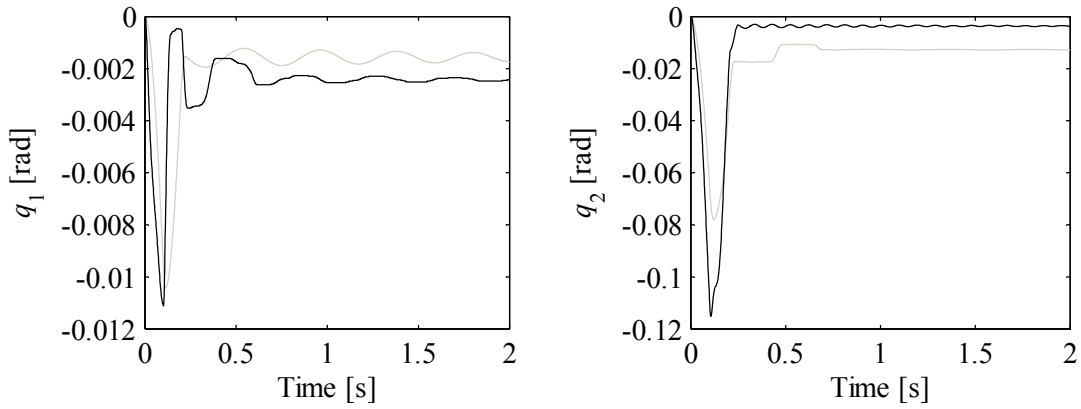

Figure 2.47: Joint displacement for bang-bang input signal in the servomotor.

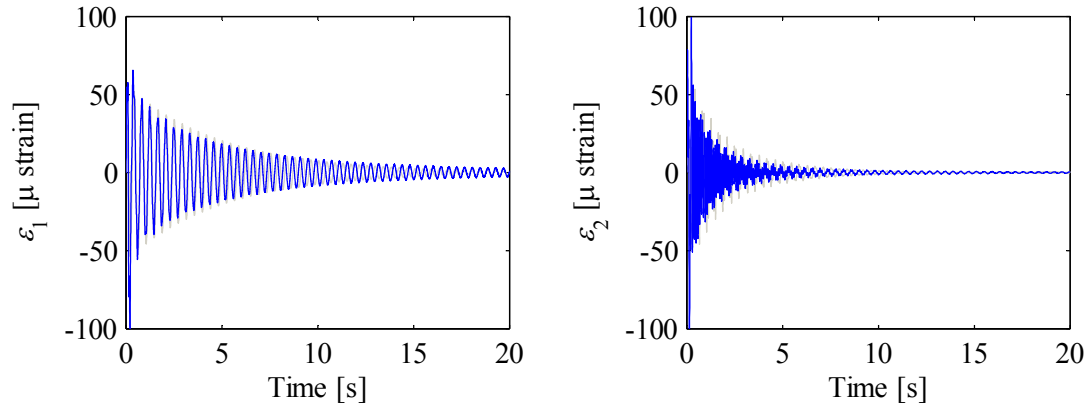

Figure 2.48: Deformation at the base of the links for bang-bang input signals.
Gray: model. Blue: real system.

In Figs. 2.49 and 2.50 are shown the energy density spectra of the measured and calculated deformation. The main frequency components for the model are for the first link 14.95 rad/s (2.38 Hz) and for the real system 15.26 rad/s (2.43 Hz). On the other hand the frequencies of the real system for the second link model are 15.39 rad/s (2.45 Hz) and 66.85 rad/s (10.64 Hz) and for the real system 15.08 rad/s (2.40 Hz) and 67.29 rad/s (10.71 Hz). The frequencies match with a small discrepancy.

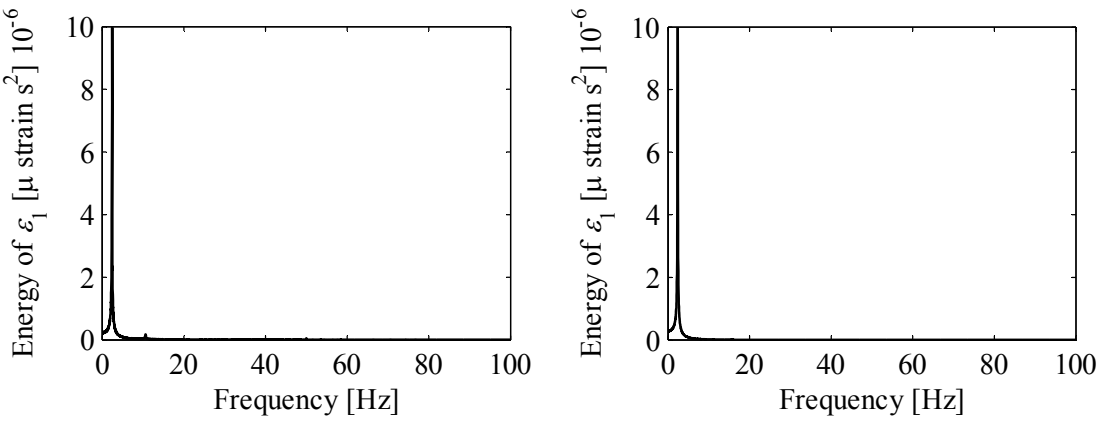

Figure 2.49: Energy density spectrum for the signals from strain gages at the base of the first link for bang-bang input signals. Sampling time 1 ms. Left: model. Right: Real system.

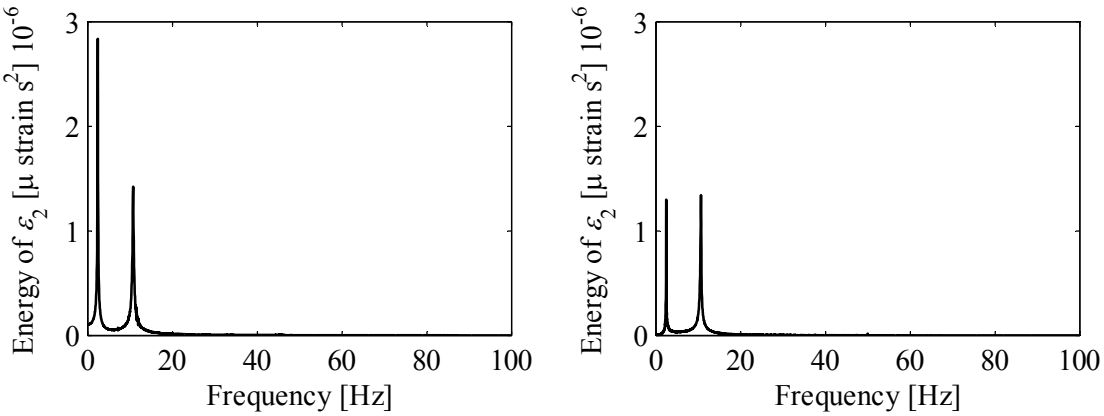

Figure 2.50: Energy density spectrum for the signals from strain gages at the base of the second link for bang-bang input signals. Sampling time 1 ms. Left: model. Right: Real system.

The robot and its model are also subjected to linear chirp signals, their responses are compared. With this signal the first and the second mode of each link of the implemented model and the robot can be excited by this chirp signal. The signals used have amplitude of 0.1 Nm and 0.15 Nm for the first and second link, respectively; these signals cover a range of frequencies from 0.001 Hz until 100 Hz. In Fig. 2.51 the behavior of the chirp frequency is shown, Fig. 2.52 shows the response in deformation of both links (black) and model (gray) to the chirp input signal applied to the piezoelectric actuators of the first link.

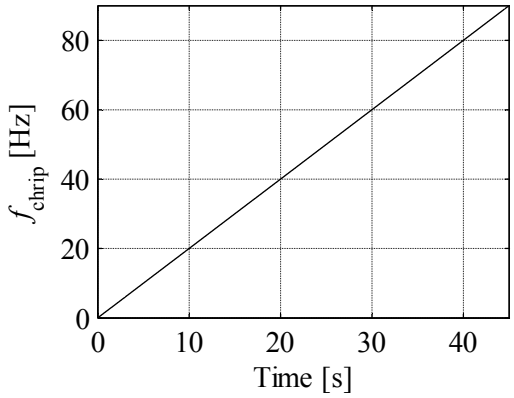

Figure 2.51: Linear frequency evolution of input signals.

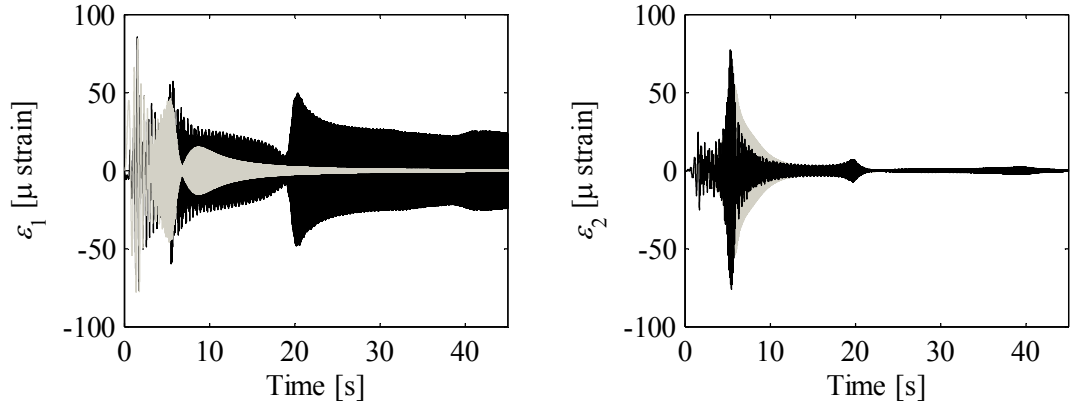

Figure 2.52: Frequency response of the links to a chirp applied in the piezoelectric actuators of the first link. Deformation measure with strain gage 1 (left) and deformation measured with strain gage 2 (right).

The chirp input signal corresponding to the piezoelectric actuators of the first link is applied and the deformation induced in both links is shown in Fig. 2.53.

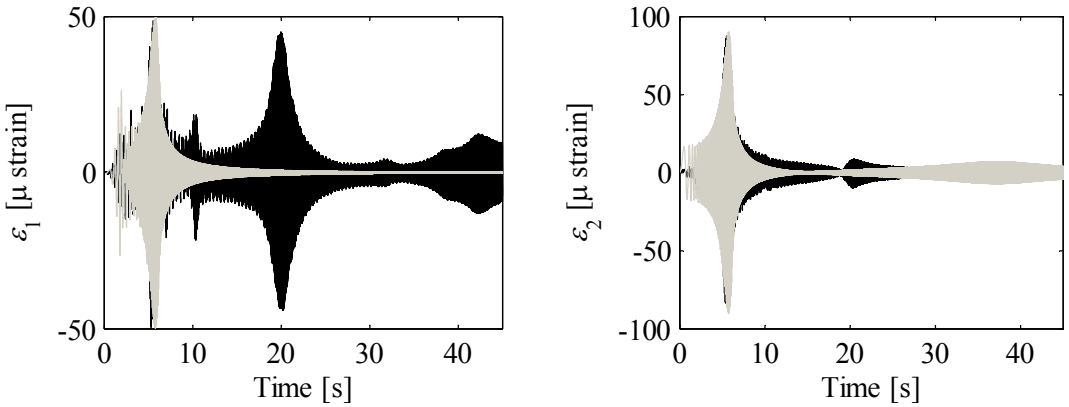

Figure 2.53: Frequency response of the links to a chirp applied in the piezoelectric actuators of the second link. Deformation measure with strain gage 1 (left) and deformation measured with strain gage 2 (right).

The responses are for both links similar, nevertheless the discrepancy is due to neglect some component whose inertia is difficult to evaluate (basically cables). In Figs. 2.56 and 2.57 are shown the spectrograms of the frequencies response of the links. The fundamental frequency of the chirp signals is represented (according to Fig. 2.51) in the spectrograms as the first inclined line with slope equal to 1. Moreover, in the ideal case (model) the pure chirp signal should only excite the resonance frequencies of the structure (see Figs. 2.55 and 2.56), which are the zones in strong red. The first resonance frequency for each element can be identified as two lower horizontal lines of Figs. 2.56 and 2.57. However,the discrepancies in the frequency responses can also be due to the generation of "overtones" of the chrirp fundamental frequency. These overtones are represented as straight lines with a slope multiple of the slope of the time evolution of the chirp frequency. The overtones excite prematurely the resonance frequencies of the robot. Furthermore, in the spectrograms appears another resonance frequency at approximately 40 Hz, this denotes the presence of an unmodeled mode i.e. a torsional model o vibration of the first link. Then it justifies the presence of high amplitude peak at approximately 20 s in Figs. 2.52 and 2.53.

It must be made clear, this discrepancy between model a physical system does not represent a failure in the modeling process. It is a consequence of assuming some parts of the model as linear and the existence of unmodeled dynamics, which introduces discrepancies between the model and real system, this model uncertainty is faced and considered under a robust control strategy which is one objective of this work.

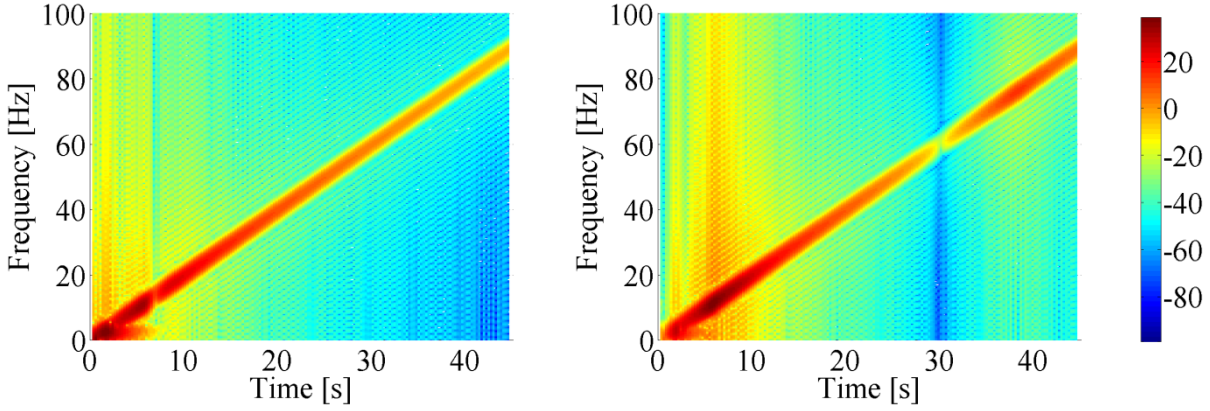

Figure 2.54: Spectrograms for the deformation simulated on the first link (left) and second link (right) for a chirp input signal applied on the piezoelectric actuators of the first link.

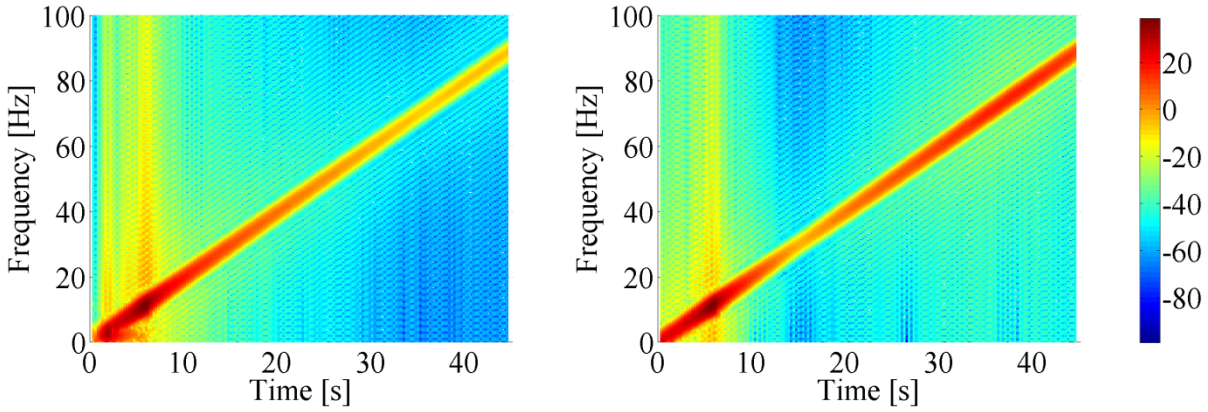

Figure 2.55: Spectrograms for the deformation simulated on the first link (left) and second link (right) for a chirp input signal applied on the piezoelectric actuators of the second link.

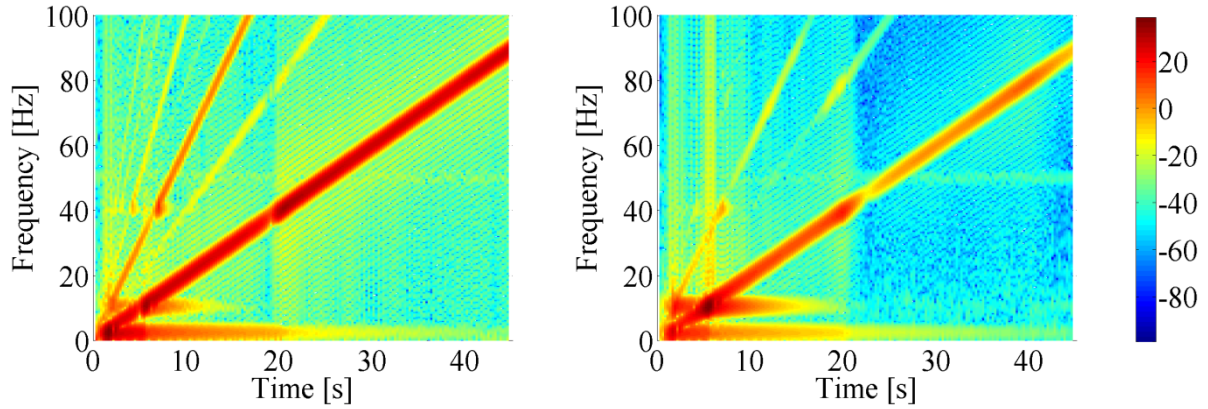

Figure 2.56: Spectrograms for the deformation measured with the strain gages on the first link (left) and second link (right) for a chirp input signal applied on the piezoelectric actuators of the first link.

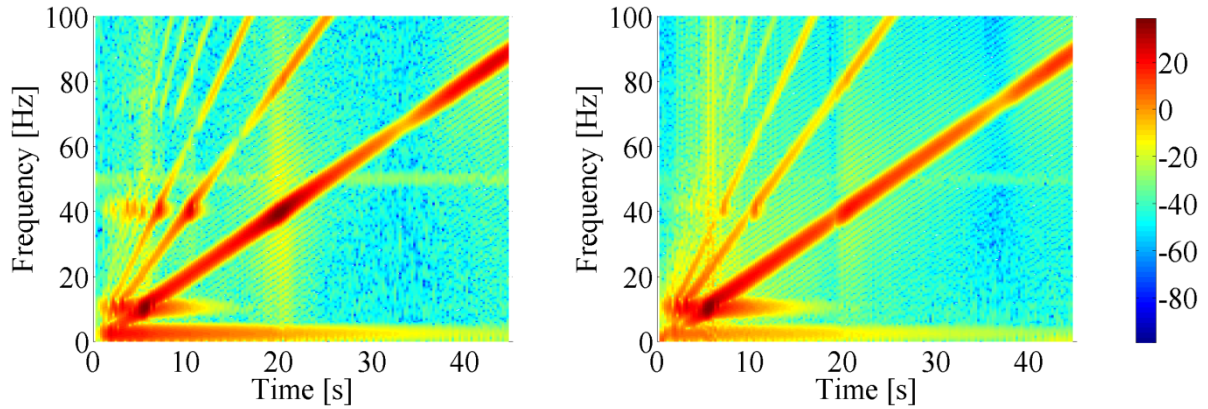

Figure 2.57: Spectrograms for the deformation measured with the strain gages on the first link (left) and second link (right) for a chirp input signal applied on the piezoelectric actuators of the second link.

3 Sliding Mode Control

In this chapter a theoretical background for SMC is given, therefore this provides the fundaments of the proposed controllers for the different flexible-link structures under study.

3.1 Introduction

In this section a brief review is done of this control strategy for linear systems and for nonlinear systems as well. It had its origin in 1960, it was first proposed and elaborated by several researchers of the former Soviet Union [92]. The basic idea of SMC is to reduce the order of the system by introducing a switching discontinuity in order to obtain a desired closed loop behavior. In the literature SMC can be found also as Variable Structure Control (VSC) and the closed loop feedback system can be also named Variable Structure System (VSS). SMC [94,95] is a viable high-speed switching state-dependent feedback control that intentionally changes the structure of the system; this is done in order to drive the plant's states trajectory onto a specified and user-chosen surface in the state space (called the sliding or switching surface or sliding manifold), and to maintain the plant's state trajectory on this surface for all subsequent time. This surface is called the switching surface because if the states trajectory of the plant is "above" the surface a control path has one gain and a different gain if the trajectory drops "below" the surface (see Fig. 3.1). The plant dynamics restricted to this surface represent the controlled system's behavior. By proper design of the sliding surface, SMC achieves the conventional goals of control such as stabilization, tracking, regulation, etc.

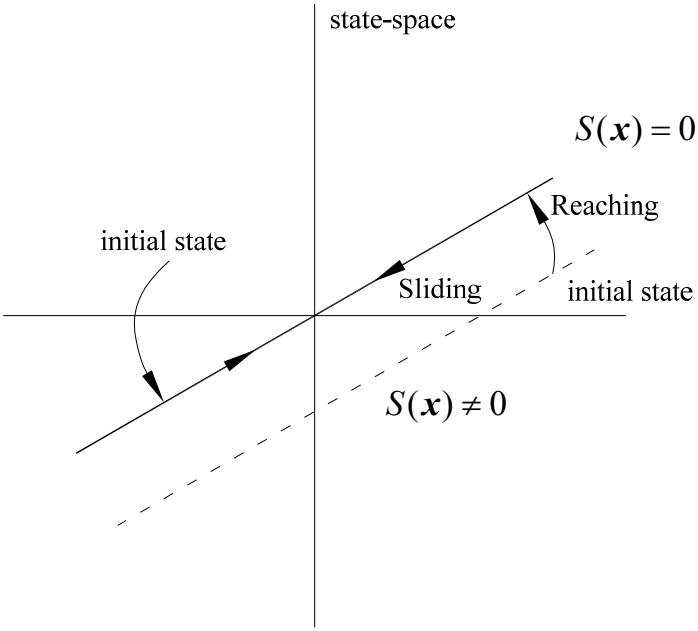

Figure 3.1: Stages of sliding mode.

3.1.1 Basic Concepts

In the formulation of control problems there is always a discrepancy between the actual plant and the model used for controller design; it can be due to different sources such as [96]: unmodeled dynamics (unstructured uncertainties), parasitic dynamics, external disturbances and plant parameters inaccuracy (structured uncertainties) among others. The SMC also

provides a robust and effective mean of controlling linear and nonlinear plants, making the closed loop system ideally insensitivity to the aforementioned sources of model discrepancy. Some definitions are required to employ this control strategy.

This work considers systems with a state model linear or nonlinear in the state vector $\boldsymbol{x}(\cdot)$ and linear in the control vector $\boldsymbol{u}(\cdot)$ of the form

$$\dot{\boldsymbol{x}} = \boldsymbol{f}(\boldsymbol{x}) + \boldsymbol{B}(\boldsymbol{x})\boldsymbol{u}(t), \tag{3.1}$$

where the state vector $\boldsymbol{x}(t) \in \mathbb{R}^{\mathrm{n}}$, the control vector $\boldsymbol{u}(t) \in \mathbb{R}^{\mathrm{m}}$, system dynamics $\boldsymbol{f}(\boldsymbol{x}) \in \mathbb{R}^{\mathrm{n}}$, and the input matrix $\boldsymbol{B}(\boldsymbol{x}) \in \mathbb{R}^{\mathrm{n\,x\,m}}$; further, each entry in $\boldsymbol{f}(\boldsymbol{x})$ and $\boldsymbol{B}(\boldsymbol{x})$ is assumed to be continuous with continuous bounded derivative with respect to $\boldsymbol{x}(t)$. Each entry $u_i(t)$ of the switching control $\boldsymbol{u}(t) \in \mathbb{R}^{\mathrm{m}}$ has the form

$$u_i(t) = \begin{cases} u_i^{+}(t) & \text{if} \quad \sigma_i(\boldsymbol{x}) > 0 \\ u_i^{-}(t) & \text{if} \quad \sigma_i(\boldsymbol{x}) < 0 \end{cases} \quad i = 1..m, \tag{3.2}$$

where $\sigma_i(\boldsymbol{x})$ is the *ith* switching surface associated with the $(n-m)-$dimensional switching surface

$$\boldsymbol{\sigma}(\boldsymbol{x}) = \left[\sigma_1(\boldsymbol{x}) \;\cdots\; \sigma_m(\boldsymbol{x})\right]^{\mathrm{T}} = \boldsymbol{0}. \tag{3.3}$$

The *sliding surface* $\boldsymbol{\sigma}(\boldsymbol{x}) = \boldsymbol{0}$ is a $(n-m)-$dimensional manifold in $\mathbb{R}^{\mathrm{n}}$ determined by the intersection of m $(n-1)-$dimensional switching surfaces $\sigma_i(\boldsymbol{x}) = 0$. The switching surfaces are designed such that the system response restricted to $\boldsymbol{\sigma}(\boldsymbol{x}) = \boldsymbol{0}$ has a desired behavior such as stability or tracking. Although general nonlinear switching surfaces (3.3) are possible, linear ones are more prevalent in design [94]. Moreover, design of linear switching surfaces can be performed using linear control techniques. A linear switching surface has the form

$$\boldsymbol{\sigma}(\boldsymbol{x}) = \boldsymbol{S}\boldsymbol{x}(t), \tag{3.4}$$

where $\boldsymbol{S}$ is a $n\ x\ m$ matrix. After switching surface design, the next important aspect of SMC is guaranteeing the existence of a *Sliding Mode*. A sliding mode exists, if in the vicinity of the switching surface, $\boldsymbol{\sigma}(\boldsymbol{x}) = \boldsymbol{0}$, the tangent or velocity vectors of the state trajectory always point toward the switching surface. Consequently, if the state trajectory intersects the sliding surface, the value of the state trajectory or "representative point" remains within a ε neighborhood of $\left\{x \middle| \boldsymbol{\sigma}(\boldsymbol{x}) = \boldsymbol{0}\right\}$. If a sliding mode exists on $\boldsymbol{\sigma}(\boldsymbol{x}) = \boldsymbol{0}$, then $\boldsymbol{\sigma}(\boldsymbol{x})$ is a sliding surface. As seen in Fig. 3.2, a sliding mode may not exist on $\sigma_i(\boldsymbol{x}) = 0$ separately, but only on the intersection.

An ideal sliding mode exists only when the state trajectory $\boldsymbol{x}(t)$ of the controlled plant satisfies $\boldsymbol{\sigma}(\boldsymbol{x}(t)) = \boldsymbol{0}$ at every $t \geq t_r$ for some t_r. This requires infinitely fast switching. In systems, all facilities responsible for the switching control function have imperfections such as delay, hysteresis, etc., which force switching to occur at a finite frequency. The system induced trajectory oscillates within a neighborhood of the switching surface. This oscillation is called chattering. If the frequency of the switching is very high compared with the dynamic response of the system, the imperfections and the finite switching frequencies are often but not always negligible.

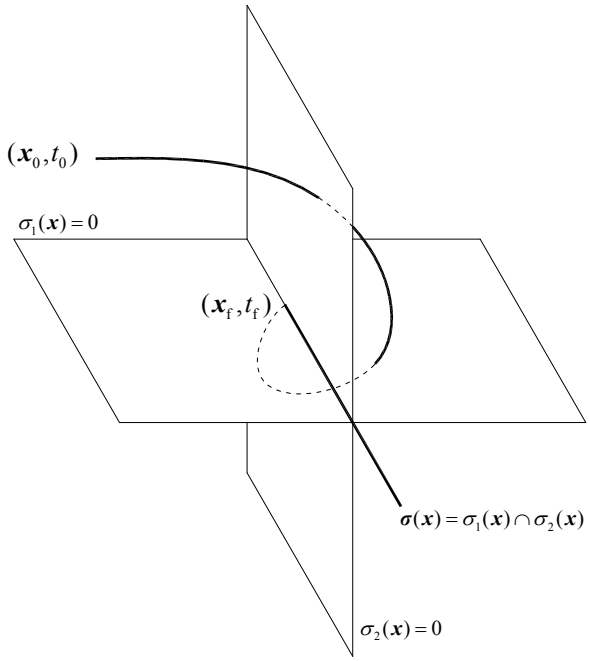

Figure 3.2: Geometric interpretation of two switching surfaces.

The presence of a sliding mode is not restricted to SMC [97], this phenomenon can appear in any dynamic system governed by differential equations with discontinuous right-hand sides, where, as stated before, the system states switch at high frequency (theoretically infinite). Once sliding mode is present, the system dynamics slide along the switching surface then an induced or equivalent dynamics is present which can be interpreted as an average dynamics, whose behavior can be estimated through the Filippov method. Let's consider a general VSS given by

$$\dot{\boldsymbol{x}}(t) = \begin{cases} \boldsymbol{f}_1 = \boldsymbol{f}(\boldsymbol{x}, \boldsymbol{u}^+) \text{ if } \sigma(\boldsymbol{x}) > 0 \\ \boldsymbol{f}_2 = \boldsymbol{f}(\boldsymbol{x}, \boldsymbol{u}^-) \text{ if } \sigma(\boldsymbol{x}) < 0 \end{cases}. \tag{3.5}$$

Then sliding mode occurs if

$$\frac{\partial \sigma(\boldsymbol{x})}{\partial \boldsymbol{x}} \boldsymbol{f}_1 < 0 \text{ and } \frac{\partial \sigma(\boldsymbol{x})}{\partial \boldsymbol{x}} \boldsymbol{f}_2 > 0, \tag{3.6}$$

or

$$L_{f_1}\sigma(\boldsymbol{x}) < 0 \text{ and } L_{f_2}\sigma(\boldsymbol{x}) > 0, \tag{3.7}$$

where $L_{f_1}\sigma(\boldsymbol{x})$ is the Lie derivative of $\sigma(\boldsymbol{x})$ in the direction $\boldsymbol{f}_1$. This derivative is the inner vectorial product of the gradient of the scalar function $\sigma(\boldsymbol{x})$ and the vector field $\boldsymbol{f}_i(\boldsymbol{x})$. From the Filippov method [98] the state trajectories of the system (3.5) on the sliding surface i.e. $\sigma(\boldsymbol{x}) = 0$ and $\dot{\sigma}(\boldsymbol{x}) = 0$ are given by the convex combination of the vector fields $\boldsymbol{f}_1$ and $\boldsymbol{f}_2$. The time derivative of the sliding surface is given by

$$\dot{\sigma}(\boldsymbol{x}) = \frac{\partial \sigma(\boldsymbol{x})}{\partial \boldsymbol{x}} \dot{\boldsymbol{x}}. \tag{3.8}$$

Then the induced dynamics of the system is introduced as a convex combination

$$\dot{\sigma}(\boldsymbol{x}) = \frac{\partial \sigma(\boldsymbol{x})}{\partial \boldsymbol{x}} \left(\lambda_1 \boldsymbol{f}_1 + \lambda_2 \boldsymbol{f}_2 \right), \tag{3.9}$$

substituting the Lie derivatives

$$\dot{\sigma}(\boldsymbol{x}) = \lambda_1 L_{f_1}\sigma(\boldsymbol{x}) + \lambda_2 L_{f_2}\sigma(\boldsymbol{x}) = 0\,, \tag{3.10}$$

then solving for λ_2

$$\lambda_2 = -\frac{L_{f_1}\sigma(\boldsymbol{x})}{L_{f_2}\sigma(\boldsymbol{x})}\,. \tag{3.11}$$

In order to respect the dynamics of the system there are some restriction for λ_1 and λ_2

$$\lambda_1, \lambda_2 \geq 0\ , \tag{3.12}$$

and

$$\lambda_1 + \lambda_2 = 1\,. \tag{3.13}$$

Finally the induced behavior of the plant in sliding mode can be defined as

$$\dot{\boldsymbol{x}}(t) = \lambda_1 \boldsymbol{f}_1 + \lambda_2 \boldsymbol{f}_2 = \boldsymbol{f}_0\,, \tag{3.14}$$

where $\boldsymbol{f}_0$ is the mean velocity of the system states under sliding mode.

3.1.2 General Controller Calculation

The general procedure for the calculation of a SMC comprises two steps: selection of a sliding surface and synthesis of a control law. These two steps are described in the following subsections.

3.1.2.1 Sliding Surface Selection

The sliding surface can be considered as the intersection of stable hyperplane(s) in the state/error space where the motion of states trajectory should be restricted to represent a desired system dynamics, which is of lower order than the given plant. In order to estimate the behavior of the system after reaching the sliding surface the *Equivalent Control Input Method* [95] can be used. Once the surface is reached ($\boldsymbol{\sigma}(\boldsymbol{x}) = \mathbf{0}$), if sliding mode exist, ideally the system remains afterwards in the surface ($\dot{\boldsymbol{\sigma}}(\boldsymbol{x}) = \mathbf{0}$). The system (3.1) is considered, whose dynamics is substituted in (3.8) as follows

$$\dot{\boldsymbol{\sigma}}(\boldsymbol{x}) = \frac{\partial \boldsymbol{\sigma}(\boldsymbol{x})}{\partial \boldsymbol{x}}\dot{\boldsymbol{x}} = \frac{\partial \boldsymbol{\sigma}(\boldsymbol{x})}{\partial \boldsymbol{x}}\Big(\boldsymbol{f}(\boldsymbol{x}) + \boldsymbol{B}(\boldsymbol{x})\boldsymbol{u}_{\text{eq}}(t)\Big) = \mathbf{0}\,. \tag{3.15}$$

Assuming the product

$$\det\left(\frac{\partial \boldsymbol{\sigma}(\boldsymbol{x})}{\partial \boldsymbol{x}}\boldsymbol{B}(\boldsymbol{x})\right) \neq 0\,, \tag{3.16}$$

invertible. Then solving (3.15) for $\boldsymbol{u}_{\text{eq}}(t)$

$$\boldsymbol{u}_{\text{eq}}(t) = -\left(\frac{\partial \boldsymbol{\sigma}(\boldsymbol{x})}{\partial \boldsymbol{x}}\boldsymbol{B}(\boldsymbol{x})\right)^{-1}\frac{\partial \boldsymbol{\sigma}(\boldsymbol{x})}{\partial \boldsymbol{x}}\boldsymbol{f}(\boldsymbol{x})\,. \tag{3.17}$$

Therefore the induced dynamics in sliding mode, given that $\boldsymbol{\sigma}(\boldsymbol{x}(t_0)) = \mathbf{0}$, is formulated as

$$\dot{\boldsymbol{x}}_{\text{e}} = \left(\mathbf{I} - \boldsymbol{B}(\boldsymbol{x})\left(\frac{\partial \boldsymbol{\sigma}(\boldsymbol{x})}{\partial \boldsymbol{x}}\boldsymbol{B}(\boldsymbol{x})\right)^{-1}\frac{\partial \boldsymbol{\sigma}(\boldsymbol{x})}{\partial \boldsymbol{x}}\right)\boldsymbol{f}(\boldsymbol{x})\,. \tag{3.18}$$

Commonly the sliding surface are of linear type (3.4) then the induced dynamics is defined by

$$\dot{\boldsymbol{x}}_{\text{e}} = \Big(\mathbf{I} - \boldsymbol{B}(\boldsymbol{x})\big(\boldsymbol{S}\boldsymbol{B}(\boldsymbol{x})\big)^{-1}\boldsymbol{S}\Big)\boldsymbol{f}(\boldsymbol{x})\,. \tag{3.19}$$

Moreover if the system is linear and time-invariant the dynamics is given in this case by

$$\dot{\boldsymbol{x}}_{\mathrm{e}} = \left(\boldsymbol{A} - \boldsymbol{B}\left(\boldsymbol{SB}\right)^{-1}\boldsymbol{SA}\right)\boldsymbol{x}\,. \tag{3.20}$$

Here result more evident that the selection of the sliding surface defines the behavior of the system during sliding motion. In the last case conventional linear techniques could be used to dimension the sliding surface. The equivalent control input can be also calculated in a different way for system formulated in *regular normal form*. Considering the following single-input single-output (SISO) system is given by

$$\begin{aligned} \dot{x}_1 &= x_2 \\ \dot{x}_2 &= f(x_1, x_2) + u \end{aligned}, \tag{3.21}$$

in which a linear surface $\sigma(x_1, x_2) = cx_1 + x_2$ is defined. If this system reach the sliding mode at $t = t_r$ then $\sigma(x_1, x_2) = 0$ and $\dot{\sigma}(x_1, x_2) = 0$ i.e.

$$\dot{\sigma}(x_1, x_2) = cx_2 + f(x_1, x_2) + u = 0\,. \tag{3.22}$$

The equivalent control input can be calculated as

$$u_{\mathrm{eq}} = -cx_2 - f(x_1, x_2)\,. \tag{3.23}$$

If there are uncertainties in the model then (3.23) cannot be implemented as long as $f(x_1, x_2)$ is not known. But if $f(x_1, x_2)$ is bounded i.e. $\left|f(x_1, x_2)\right| \le L$ with $L \ge 0$, an average of (3.23) can be calculated by low-pass filtering (LPF) a high frequency switching control input [92] $\rho\,\mathrm{sgn}(\sigma)$. Now the term with uncertainty can be substituted in (3.23) to obtain an implementable version of it as follows

$$u_{\mathrm{eq}} = -cx_2 - LPF(\rho\,\mathrm{sgn}(\sigma)) \quad \text{with} \quad \rho \ge L\,, \tag{3.24}$$

The dynamic of the sliding surface can be modified changing the value c which is related to the rate of convergence of the reduced model. In the selection of the sliding surface some properties have to be taken into account:

- Sliding surface has a lower order than the plant.
- Sliding mode does not depend on plant dynamics and is determined by parameters of the switching function only (in (3.4) depends on $\boldsymbol{S}$).
- Sliding surface does not depend on the control law.

Additionally, the *reachability condition* is defined as the condition under which the states will move toward and reach a sliding surface. The system trajectory under the reaching condition is called the reaching mode or reaching phase. Different approaches for specifying the reaching condition have been proposed [99]. Here just one reference of two of them is made. The *Direct Switching Function Approach*: the reaching condition is formulated as

$$\begin{aligned} &\dot{\sigma}_i > 0 \ \text{ if } \ \sigma_i < 0 \\ &\dot{\sigma}_i < 0 \ \text{ if } \ \sigma_i > 0 \quad i = 1...m \end{aligned}, \tag{3.25}$$

or can be also stated as

$$\sigma_i \dot{\sigma}_i < 0 \ \ i = 1...m\,. \tag{3.26}$$

This reaching condition is global but does not guarantee a finite reaching time. A similar sufficient condition that is local in nature is proposed in [95,100]

$$\lim_{\sigma_i \to -0} \dot{\sigma}_i > 0 \quad \text{and} \quad \lim_{\sigma_i \to +0} \dot{\sigma}_i < 0\ , \tag{3.27}$$

here is stated that sliding mode occurs whenever the distances σ_i to the surface and the velocity $\dot{\sigma}_i$ of its change are of opposites signs i.e. the surface is attractive.

The *Lyapunov Function Approach*: this resembles a generalized stability problem; hence the second method of Lyapunov provides a natural setting for analysis. Specifically, stability to the switching surface requires selecting a generalized Lyapunov function $V(\boldsymbol{x},t)$ which is positive definite and has a negative time derivative in the region of attraction. By choosing for example the Lyapunov function candidate

$$V(\boldsymbol{x},t)=\boldsymbol{\sigma}^{\mathrm{T}}\boldsymbol{\sigma}, \tag{3.28}$$

then a global reaching condition is given by [95,100]

$$\dot{V}(\boldsymbol{x},t)<0 \quad \text{where } \sigma\neq 0. \tag{3.29}$$

In order to guarantee a finite reaching time (3.29) is modified

$$\dot{V}(\boldsymbol{x},t)<-\bar{\varepsilon} \quad \text{where } \sigma\neq 0 \text{ and } \bar{\varepsilon}>0, \tag{3.30}$$

this approach leads to the eventual sliding mode switch scheme.

3.1.2.2 Control Law Synthesis

The control law must be synthesized to make the selected sliding surface attractive. Such that any state $\boldsymbol{x}(t)$ outside the switching surface will drive the plant state trajectory to reach the surface in finite time. On the switching surface, the sliding mode takes place, following the desired system dynamics. In this way, the overall VSS system is globally asymptotically stable. The control law in VSS is given by

$$\boldsymbol{u}=\boldsymbol{u}_{\mathrm{eq}}+\boldsymbol{u}_{\mathrm{c}}, \tag{3.31}$$

the equivalent control input has been previously calculated, then a corrective term is included $\boldsymbol{u}_{\mathrm{c}}$, this is a discontinuity term to enforce the reaching phase and to compensate uncertainties such as disturbances and model variations. This corrective control input is usually chosen as a sign function. $\boldsymbol{u}_{\mathrm{c}}$ could be implemented in at least five possible discontinuous control structures [94]:

The controller can be defined as switching functions with constant gains

$$u_{\mathrm{c}_i}=\begin{cases}\bar{\alpha}_i\,\mathrm{sgn}(\sigma_i(\boldsymbol{x})) & \sigma_i(\boldsymbol{x})\neq 0 \quad \bar{\alpha}_i<0\\ 0 & \sigma_i(\boldsymbol{x})=0\end{cases}, \tag{3.32}$$

where the sufficiency condition are met for the existence of a sliding mode since

$$\sigma_i\dot{\sigma}_i=\bar{\alpha}_i\sigma_i(\boldsymbol{x})\mathrm{sgn}(\sigma_i(\boldsymbol{x}))<0 \quad \text{if } \sigma_i(\boldsymbol{x})\neq 0. \tag{3.33}$$

A second option is the selection of switching functions with state dependent gains

$$u_{\mathrm{c}_i}=\begin{cases}\bar{\alpha}_i(\boldsymbol{x})\,\mathrm{sgn}(\sigma_i(\boldsymbol{x})) & \sigma_i(\boldsymbol{x})\neq 0 \quad \bar{\alpha}_i(\boldsymbol{x})<0\\ 0 & \sigma_i(\boldsymbol{x})=0\end{cases}, \tag{3.34}$$

similarly the sufficiency condition are met for the existence of a sliding mode if

$$\sigma_i\dot{\sigma}_i=\bar{\alpha}_i(\boldsymbol{x})\sigma_i(\boldsymbol{x})\mathrm{sgn}(\sigma_i(\boldsymbol{x}))<0 \quad \text{if } \sigma_i(\boldsymbol{x})\neq 0. \tag{3.35}$$

A third option is a linear state-feedback with switching gains

$$u_{\mathrm{c}_i}=\bar{\boldsymbol{K}}\boldsymbol{x} \quad \text{where} \quad \bar{k}_{ij}=\begin{cases}\bar{\alpha}_{ij} & \text{if } \sigma_i x_j>0\\ \bar{\beta}_{ij} & \text{if } \sigma_i x_j<0\end{cases} \tag{3.36}$$

with $\alpha_{ij} < 0$ and $\beta_{ij} > 0$ then the existence conditions are

$$\sigma_i \dot{\sigma}_i = \sigma_i \left(\bar{k}_{i1} x_1 + \bar{k}_{i2} x_2 + \cdots + \bar{k}_{in} x_n \right) < 0 . \tag{3.37}$$

A fourth option is a linear sliding-variable continuous feedback

$$u_{c_i} = \bar{k}_i \sigma_i \quad \text{where } \bar{k}_i < 0 , \tag{3.38}$$

the existence condition is given by

$$\sigma_i \dot{\sigma}_i = k_i \sigma_i^2(\boldsymbol{x}) < 0 . \tag{3.39}$$

This option can also be defined as

$$\boldsymbol{u}_c = -\bar{\boldsymbol{K}} \boldsymbol{\sigma}(\boldsymbol{x}) \quad \text{where } \bar{\boldsymbol{K}} > 0 \text{ and } \bar{\boldsymbol{K}} \in \mathbb{R}^{m \times m} , \tag{3.40}$$

and its existence condition

$$\boldsymbol{\sigma}^{\mathrm{T}}(\boldsymbol{x}) \dot{\boldsymbol{\sigma}}(\boldsymbol{x}) = \boldsymbol{\sigma}^{\mathrm{T}}(\boldsymbol{x}) \bar{\boldsymbol{K}} \boldsymbol{\sigma}(\boldsymbol{x}) < 0 \quad \boldsymbol{\sigma}(\boldsymbol{x}) \neq 0 . \tag{3.41}$$

The last option is an unitary nonlinear vector with scale factor

$$\boldsymbol{u}_c = \frac{\boldsymbol{\sigma}(\boldsymbol{x})}{\left\| \boldsymbol{\sigma}(\boldsymbol{x}) \right\|} \rho \quad \rho < 0 , \tag{3.42}$$

ρ is a scaling factor. The existence condition is defined by

$$\boldsymbol{\sigma}^{\mathrm{T}}(\boldsymbol{x}) \dot{\boldsymbol{\sigma}}(\boldsymbol{x}) = \left\| \boldsymbol{\sigma}(\boldsymbol{x}) \right\| \rho < 0 \quad \boldsymbol{\sigma}(\boldsymbol{x}) \neq 0 . \tag{3.43}$$

Some other possibilities and methods for the selection of the correcting control input can be seen in [94,95,97,98]. If the system to be controlled is in the *regular normal form* [101,102,104], it is broken down into a set of subsystems

$$\begin{aligned} \dot{\boldsymbol{x}}_1 &= \boldsymbol{f}_1(\boldsymbol{x}_1, \boldsymbol{x}_2) \\ \dot{\boldsymbol{x}}_2 &= \boldsymbol{f}_2(\boldsymbol{x}_1, \boldsymbol{x}_2) + \boldsymbol{B}(\boldsymbol{x}_1, \boldsymbol{x}_2) \boldsymbol{u} \end{aligned} , \tag{3.44}$$

where $\boldsymbol{x}_1 \in \mathbb{R}^{n-m}, \boldsymbol{x}_2 \in \mathbb{R}^m$ and $\det(B(\boldsymbol{x}_1, \boldsymbol{x}_2)) \neq 0$. A system in this form has simply computed reduced order equivalent dynamics, also referred to as the system equations of slow motion. The subsystems are of lower dimension than the complete system. This realization makes more tractable the calculation of the SMC as long as there is no need to find a diffeomorphic state-space transformation. According to the modeling technique used, the systems under study in this work the models are obtained directly in regular normal form.

Once the system reaches the sliding surface and sliding mode take place, then the dynamic of the lower subsystem of (3.44) is theoretically cancelled by the control input, it is known as partial dynamic collapse. The sliding surface can be stated as

$$\boldsymbol{\sigma}(\boldsymbol{x}_1, \boldsymbol{x}_2) = \boldsymbol{x}_2 + \boldsymbol{g}(\boldsymbol{x}_1) = \boldsymbol{0} , \tag{3.45}$$

then $\boldsymbol{x}_2$ can be expressed as

$$\boldsymbol{x}_2 = -\boldsymbol{g}(\boldsymbol{x}_1) , \tag{3.46}$$

and it assumes the role of virtual control input for the upper subsystem. Therefore, the induced dynamics of the system is given by

$$\dot{\boldsymbol{x}}_1 = \boldsymbol{f}_1(\boldsymbol{x}_1, -\boldsymbol{g}(\boldsymbol{x}_1)) , \tag{3.47}$$

which is the reduced dynamics of the system. The methods to transform a general system into this form are not included here, for further details it is suggested to consult [101-103].

3.1.2.3 Chattering Attenuation

Ideally in sliding mode the control signal must commute at infinite frequency, but it is not the case for real components which normally have switching imperfections. This is due to time delays, small time constants and hysteresis in the actuators; the discontinuity in the feedback produces a particular dynamic behavior in the vicinity of the sliding surface, it is commonly referred as chattering [100] (see Fig. 3.3).

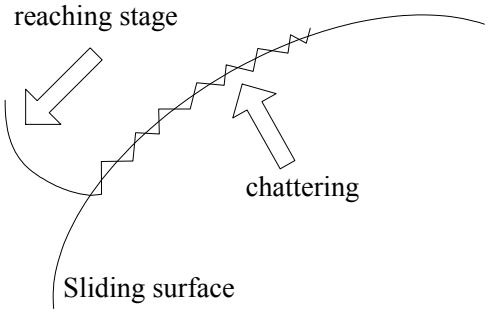

Figure 3.3: Chattering effect.

Due to the high frequency switching, chattering appears, this can be a source of excitation to the unmodeled dynamics of the system. Commonly, chattering must be eliminated for the controller to work properly. As countermeasure for this phenomenon a *boundary layer* [96] along the sliding surface can be defined in order to smooth out the discontinuity. The boundary layer is defined as

$$\boldsymbol{B}_1(t) = \left\{ \boldsymbol{x}, \left| \sigma_i(\boldsymbol{x}) \right| \le \Phi_i \right\} \quad \text{where} \quad \Phi_i > 0\,, \tag{3.48}$$

where Φ_i is the thickness of the boundary layer for the *ith* sliding surface and $\varepsilon_i = \Phi_i / \lambda_i^{n-1}$ is the boundary layer width. Assuming that an attractive sliding surface has been designed then invariant, all trajectories starting inside $\boldsymbol{B}_1(t)$ remain inside.

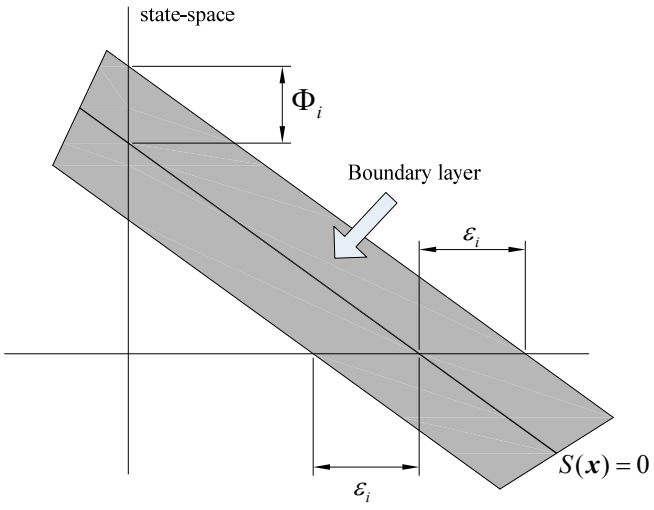

Figure 3.4: Boundary layer.

The behavior of the control law when the sliding variable is inside the boundary layer can be set to be continuous by approximating the sign function with a saturation function for the corrective control input

$$u_{c_i} = \begin{cases} -\bar{k}_i & \sigma(\boldsymbol{x}) \geq \Phi_i \\ -\bar{k}_i \dfrac{\sigma_i(\boldsymbol{x})}{\Phi_i} & -\Phi_i < \sigma_i(\boldsymbol{x}) < \Phi_i \quad \text{where} \quad k_i > 0, \\ \bar{k}_i & \sigma_i(\boldsymbol{x}) \leq -\Phi_i \end{cases} \tag{3.49}$$

or the continuous approximation can also be done with a sigmoidal function

$$u_{c_i} = -\bar{k}_i \frac{\sigma_i(\boldsymbol{x})}{|\sigma_i(\boldsymbol{x})| + a_i} \quad \text{where} \quad \bar{k}_i, a_i > 0 \ . \tag{3.50}$$

The course of (3.49) and (3.50) are shown in Fig. 3.5.

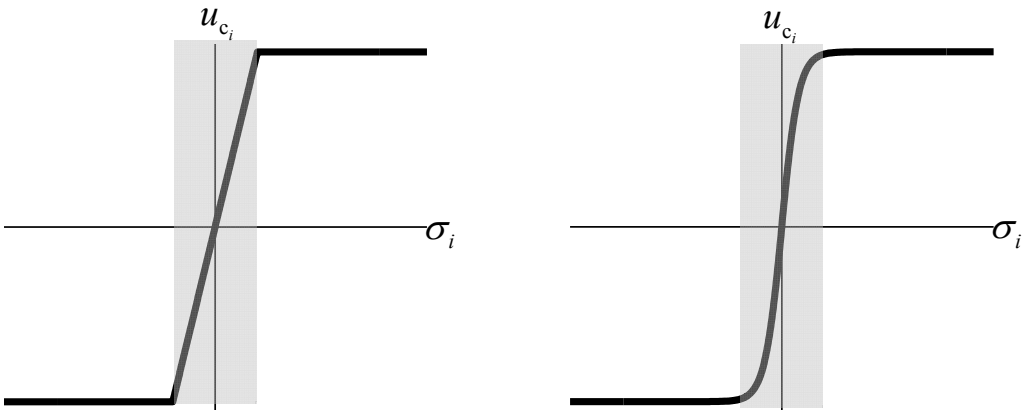

Figure 3.5: Continuous approximation for the sign function. Left: saturation function, right: sigmoidal function.

These approximations for the corrective control part induce a slight deviation in the behavior of the system in the sense that the sliding surface is not reached in finite time. Smoothing the control law influence the performance of the closed loop. Indeed, it is also called *quasi sliding mode control*, but with a right selection of the parameter for each approach the performance can be close to the pure switching control.

Other possible measure to alleviate the chattering phenomenon is the *asymptotic or high order sliding mode* [92], it considers the inclusion of a fictitious control input. The objective is to design a SMC in terms of the time-derivative of the control function, then the actual control signal is the integral of the high frequency switching function which leads to a continuous signal. Let's consider a system given in regular normal form

$$\begin{aligned} \dot{x}_1 &= x_2 \\ \dot{x}_2 &= u + f(x_1, x_2) \end{aligned}, \tag{3.51}$$

the actual control signal is formulated in terms of an additional control input

$$\dot{u} = v \, . \tag{3.52}$$

The sliding surface

$$\sigma(\boldsymbol{x}_1, \boldsymbol{x}_2) = 0 \, , \tag{3.53}$$

and the auxiliary sliding variable

$$\bar{z} = \dot{\sigma}(\boldsymbol{x}_1, \boldsymbol{x}_2) + \bar{c}\sigma(\boldsymbol{x}_1, \boldsymbol{x}_2) \, . \tag{3.54}$$

In order to obtain chattering attenuation an auxiliary sliding variable is included. The control v can be designed under the Lyapunov approach to get a finite time convergence for the auxiliary sliding variable $\bar{z} \to 0$, because the real sliding mode will occur in the auxiliary surface

$$\bar{z} = \dot{\sigma}(\boldsymbol{x}_1, \boldsymbol{x}_2) + \bar{c}\sigma(\boldsymbol{x}_1, \boldsymbol{x}_2) = 0. \tag{3.55}$$

Then $\sigma, \dot{\sigma} \to 0$ and $x_1, x_2 \to 0$ as the time increases. With this approach there is not a really sliding mode in the closed loop system but rather an asymptotic sliding mode, due to the fact that σ converges to zero asymptotically. Nevertheless the objective of attenuating chattering is obtained by trading off some performance.

There are different approaches for high order SMC, these are mainly based on asymptotic convergence, including integration of switching function to avoid chattering in the control input. For instance consider the system (3.51) with output defined as

$$y = x_1, \tag{3.56}$$

and the sliding surface

$$\sigma = e + c\dot{e}. \tag{3.57}$$

This surface is defined in terms of the error

$$e = y - y_\mathrm{d} = x_1 - x_{1\mathrm{d}}, \tag{3.58}$$

in order to perform a trajectory tracking. Then dynamics of the sliding surface is stated as

$$\dot{\sigma} = \dot{x}_{2\mathrm{d}} + c\dot{e} - f(x_1, x_2) - u = \varphi(x_1, x_2) - u, \tag{3.59}$$

where $\varphi(x_1, x_2)$ comprises the dynamics of the dynamics of the sliding surface and possible disturbances or model deviations. Nevertheless, $|\varphi(x_1, x_2)| \le \bar{A}$ and $|\dot{\varphi}(x_1, x_2)| \le \bar{C}$ are assumed to be continuous and bounded. With the following continuous control law

$$u = a|\sigma|^{1/2}\,\mathrm{sgn}(\sigma) + w \quad \text{where} \quad a > 0\ , \tag{3.60}$$

and

$$\dot{w} = b\,\mathrm{sgn}(\sigma) \quad \text{where} \quad b > 0\,, \tag{3.61}$$

defining the super twisting algorithm which is capable to reach the sliding surface and to remain in sliding mode. It means this control law is capable to reject disturbances and to bear with uncertainties in $f(x_1, x_2)$ [92]. This peculiar system characteristic is claimed to result in superb system performance which includes insensitivity to parameter variations, and complete rejection of disturbances [105].

This theoretical revision was done according to the required fundamentals for the control approaches applied to the experimental setup. Further explanation and details are given during the calculation of the controller for the different flexibles structures configuration under study. The formulated control approaches are summarized in Tab. 3.1.

Table 3.1 Proposed control approaches

Control approach	Structure	Section
Lyapunov model based SMC	Cantilever beam	3.2
Dual loop SMC	One flexible-link robot Two flexible-link robot	3.3
Centralized Laypunov model based SMC	One flexible-link robot Two flexible-link robot	3.4.2
Partially decentralized Laypunov model based SMC	Two flexible-link robot	3.4.3

3.2 SMC for Cantilever Beam

The beam modeling provides a linear time invariant system; therefore here standard SMC techniques can be applied. The model of the beam can be checked in section 2.1.2. The model used for controller calculation is reduced and it considers only the first mode of vibration. This reduction is done taking in account the results of section 2.1.3, where the response of the beam is clearly dominated by the first mode of vibration. It means that the controller is based on a simple SISO linear time-invariant model. The model of the plant is given by

$$\begin{aligned} \dot{\boldsymbol{x}} &= \boldsymbol{A}_{\mathrm{p}}\boldsymbol{x} + \boldsymbol{B}_{\mathrm{p}}u \\ y &= \boldsymbol{C}_{\mathrm{p}}\boldsymbol{x} \end{aligned}, \tag{3.62}$$

where

$$\boldsymbol{x} = \begin{bmatrix} \boldsymbol{q} \\ \dot{\boldsymbol{q}} \end{bmatrix} = \begin{bmatrix} x_1 \\ x_2 \end{bmatrix}, \tag{3.63}$$

$$\boldsymbol{A}_{\mathrm{p}} = \begin{bmatrix} 0 & 1 \\ -m_1^{-1}k & -m_1^{-1}d \end{bmatrix}, \tag{3.64}$$

$$\boldsymbol{B}_{\mathrm{p}} = \begin{bmatrix} 0 \\ m^{-1} \end{bmatrix}, \tag{3.65}$$

$$\boldsymbol{C}_{\mathrm{p}} = \mathbf{I}, \tag{3.66}$$

$$u = b_{\mathrm{pi}}v_{\mathrm{p}}, \tag{3.67}$$

and

$$b_{\mathrm{pi}} = \left[\overline{c}\left(\phi_1'(x_{\mathrm{a}2}) - \phi_1'(x_{\mathrm{a}1})\right)\right]. \tag{3.68}$$

The state-space realization is in regular normal form

$$\begin{aligned} \dot{x}_1 &= x_2 \\ \dot{x}_2 &= -m_1^{-1}k\, x_1 - m_1^{-1}d\, x_2 + m_1^{-1}b_{\mathrm{pi}}v_{\mathrm{p}} \\ y &= x_1 \end{aligned}. \tag{3.69}$$

The sliding surface is defined in terms of the states

$$\sigma = -x_2 - \lambda x_1, \tag{3.70}$$

and its time derivative

$$\dot{\sigma} = -\dot{x}_2 - \lambda\dot{x}_1 = -\dot{x}_2 - \lambda x_2. \tag{3.71}$$

The candidate Lyapunov function for the calculation of the control law

$$V = \frac{1}{2}\frac{d}{dt}\sigma^2, \tag{3.72}$$

its time derivative is

$$\dot{V} = \sigma\dot{\sigma}, \tag{3.73}$$

substituting $\dot{\sigma}$ and $\dot{x}_2$

$$\dot{V} = \sigma\left(-\lambda x_2 - \dot{x}_2\right), \tag{3.74}$$

$$\dot{V} = \sigma\left(-\lambda x_2 + m_1^{-1}k\, x_1 + m_1^{-1}d\, x_2 - u_{\mathrm{t}}\right), \tag{3.75}$$

and

$$\dot{V} = \sigma\left(\left(-\lambda + m_1^{-1}d\right)x_2 + m_1^{-1}k\, x_1 - u_{\mathrm{t}}\right). \tag{3.76}$$

The control law u_t is made up of two parts

$$u_{\mathrm{t}} = \hat{u}_{\mathrm{t}} - \rho \operatorname{sgn}(\sigma), \tag{3.77}$$

where $\hat{u}_{\mathrm{t}}$ is the continuous part and $\rho \operatorname{sgn}(\sigma)$ is a state-dependent switching function. The continuous part is calculated as if the model of the plant were perfect

$$\hat{u}_{\mathrm{t}} = \left(-\lambda + \hat{m}_1^{-1}\hat{d}\right)x_2 + \hat{m}_1^{-1}\hat{k}\, x_1, \tag{3.78}$$

but there are always discrepancies then the switching part is included to make the controller robust. Therefore the time derivative of the Lyapunov candidate function including the control law is given by

$$\dot{V} = \sigma\left(\left(-\lambda + \tilde{m}_1^{-1}\tilde{d}\ \right)x_2 + \tilde{m}_1^{-1}\tilde{k}\, x_1\right) - \rho|\sigma|, \tag{3.79}$$

where $\tilde{m}_1$, $\tilde{d}$ and $\tilde{k}$ are the difference between the actual values and the model values as follow

$$\tilde{m}_1 = m_1 - \hat{m}_1, \tag{3.80}$$

$$\tilde{d} = d - \hat{d}, \tag{3.81}$$

and

$$\tilde{k} = k - \hat{k}. \tag{3.82}$$

The stability of the closed loop in ensured as long as

$$\rho > \left|\left(\lambda - \tilde{m}_1^{-1}\tilde{d}\ \right)x_2 - \tilde{m}_1^{-1}\tilde{k}\, x_1\right| + \eta. \tag{3.83}$$

The mass of the beam can be measured with enough accuracy then $\tilde{m}_1 \approx 0$ can be assumed, and then the stability condition for the switching gain is redefined as

$$\rho > |\lambda x_2| + \eta \qquad \text{where} \qquad \eta > 0. \tag{3.84}$$

If (3.84) is satisfied the stability condition is finally stated as

$$\dot{V} = -\rho \operatorname{sgn}(\sigma) < 0. \tag{3.85}$$

The control law is finally given by

$$u_{\mathrm{t}} = \left(-\lambda + \hat{m}_1^{-1}\hat{d}\ \right)x_2 + \hat{m}_1^{-1}\hat{k}\, x_1 - \rho \operatorname{sgn}(\sigma). \tag{3.86}$$

From (3.84) the switching part of u_t can be expressed as a state dependent function with a state-dependent gain

$$u_{\mathrm{t}} = \left(-\lambda + \hat{m}_1^{-1}\hat{d}\right)x_2 + \hat{m}_1^{-1}\hat{k}\, x_1 - \left(|\lambda x_2| + \eta\right)\operatorname{sgn}(\sigma). \tag{3.87}$$

Finally the control law is expressed in voltage to be supplied to the piezo electric actuators as

$$v_{\mathrm{p}} = \frac{\left(-\lambda + \hat{m}_1^{-1}\hat{d}\right)x_2 + \hat{m}_1^{-1}\hat{k}\, x_1 - \left(|\lambda x_2| + \eta\right)\operatorname{sgn}(\sigma)}{\overline{c}\left(\phi_1'(x_{\mathrm{a}2}) - \phi_1'(x_{\mathrm{a}1})\right)}. \tag{3.88}$$

The parameter λ defines the rate of convergence of the reduced dynamics; it directly influences the damping of the system. But this parameter is limited according to [96] by the frequency of the next unmodeled mode, actuator bandwidth, actuator capability (saturation), among others.

The sensor installed in the beam measure the deformation near the clamped tip i.e. only a flexible DOF is considered and from this measurement x_1 is calculated. On the other hand, for the calculation of the sliding variable x_2, which is the time derivative of x_1, a sliding mode

observer [92] is used to estimate x_2. It is assumed that x_2 is bounded and this bound is known. The sliding mode observer is given by

$$z_1 = \hat{x}_1 - x_1 , \tag{3.89}$$

$$\bar{x}_1 = -\bar{\rho}\,\mathrm{sign}(z_1) \qquad \bar{\rho} > |x_2| + \beta , \tag{3.90}$$

$$\dot{\bar{x}}_2 \approx \frac{1}{\tau}\bar{x}_2 - \frac{\rho_f}{\tau}\mathrm{sgn}(z) , \tag{3.91}$$

where z_1 is an auxiliary sliding variable related to the estimation error for the available state. The estimated states are $\bar{x}_1$ and $\bar{x}_2$. The principle of equivalent input is used to obtain $\bar{x}_2$ by low-pass filtering the auxiliary sliding variable. The states are now available then the control law (3.88) can be fully implemented. The proposed controller is able to adjust the switching gain according to the speed of the modal variable.

3.3 Dual Loop Approach for Flexible-link Structures

In order to increase the damping of the links, a sliding mode controller for each link is designed. For the calculation in each link the control system is divided in two parts, a position control loop and an AVC loop. This has some similarities with the single perturbation approach [43] where the system model is separated into system with slow dynamics and system with fast dynamics. Here the system is considered to be completely separated and the joints are controlled using i.e. PID and the parts of the system with distributed mass and flexibility are controlled using independent SMC. The flexible part is considered to be subjected to inertial forces due to the joint prescribed trajectory. The effect of these forces is taken as bounded disturbances for the AVC loop. This separation is based on the assumption done in modeling of the flexible link, where clamped-free boundary conditions are used to determine a mathematical model of the links (beam). This can be done as long as either the joint has a large inertia compared with the link [15] or a feedback position control loop with a large gain is closed around the joint [6,16]. This approach has also been tested experimentally [19, 20]. The control strategy presented here is decentralized in the sense that each control loop uses only local measurements i.e. position control loop is fed with the measurements from encoder and AVC is fed with measurements from strain gages.

3.3.1 Position Control

The links are rigidly attached to the joints through shoulders, the joint position and trajectory are regulated using PID controllers. For the majority of industrial robotics structures PID controller are commonly used due to its capacity to satisfy design requirements without having precise knowledge of the plant model [16,96,106] and due to its simplicity for calibration. A theoretical continuous standard PID controller is defined in time domain and frequency domain as

$$u(t) = k_P e(t) + k_I \int e(t)dt + k_D \dot{e}(t) , \tag{3.92}$$

and

$$U(s) = \left(k_P + \frac{k_I}{s} + k_D s \right) E(s) , \tag{3.93}$$

respectively. The controller given by (3.92) is not commonly used; in the majority of implementations for the derivative element of the controller it is related to the output instead of the error i.e.

$$u(t) = k_{\mathrm{P}} e(t) + k_{\mathrm{I}} \int e(t)dt - k_{\mathrm{V}} \dot{q}_1(t). \tag{3.94}$$

However, here (3.92) is used as long as it is the control structure provided by the manufacturer. This involves an ideal differentiation which is not implementable because it is not causal. In reality, controllers that implement a PID algorithm carry out real differentiation; the transfer function of a real PID controller is written in the form [107]

$$U(s) = \left(k_{\mathrm{P}} + \frac{k_{\mathrm{I}}}{s} + \frac{k_{\mathrm{D}} s}{1 + \frac{k_{\mathrm{D}}}{16 k_{\mathrm{P}}} s} \right) E(s). \tag{3.95}$$

Here $k_{\mathrm{D}}/16k_{\mathrm{P}}$ is the time constant of a smoothing low pass filter, as long as this quotient tends to zero a PID controller with real differentiation is very close to an ideal one [108]. The constant factor 16 is suggested by the manufacturer of the DC motor amplifiers as suitable according to the type of sensor used for the angular position measurement.

The PID controller parameters are calibrated using the second method of Ziegler-Nichols [109]. An equivalent mass is located at the joint then k_{I} and k_{D} are set to zero, k_{P} is increased until the system has an oscillating response. Subsequently from this value the rest of the parameters are calculated as follows

$$k_{\mathrm{p}} = 0.6 k_{\mathrm{u}}, \tag{3.96}$$

$$k_{\mathrm{i}} = \frac{1.2 k_{\mathrm{p}}}{T_{\mathrm{u}}}, \tag{3.97}$$

and

$$k_{\mathrm{d}} = \frac{k_{\mathrm{p}} T_{\mathrm{u}}}{8}, \tag{3.98}$$

where k_{u} and T_{u} are the critic or ultimate gain and the critic or ultimate period, respectively. With this method a stable controller is obtained, further methods for the adjustment of the parameters can be found in [110] and references therein.

3.3.2 Active Vibration Loop

For this work AVC controllers are proposed to increase the damping of the flexible links. The nonlinear part of the model is considered to be a bounded uncertainty; from this point the active vibration sliding mode controllers are formulated. Assuming $\boldsymbol{M}(\boldsymbol{q})$ invertible and introducing a new matrix variable $\boldsymbol{H}(\boldsymbol{q}) = \boldsymbol{M}(\boldsymbol{q})^{-1}$ to formulate the nonlinear parts of the model. Nevertheless, the formulated model assumes 2 flexible degrees of freedom (DOF) per link; the controllers are designed considering the measurement of the deformation near the clamped tip i.e. only a flexible DOF as stated before. This is considered because during the transient response the amplitude of the first mode is significantly bigger than the second mode; it was verified in several simulation and measurements in the hardware also it is suggested by [65]. Therefore, the controller is formulated for the first flexible DOF, it is enough to solve to reduce the transient behavior in the point to point regulation problem. In this control design proposal the model of the robot is calculated independently for each group joint-link as it were one flexible-link robot. The model of each group is given by

$$\ddot{\boldsymbol{q}}_i = \boldsymbol{M}_i(\boldsymbol{q}_i)^{-1} \left(\boldsymbol{f}_i - \boldsymbol{c}_i(\boldsymbol{q}_i, \dot{\boldsymbol{q}}_i) - \boldsymbol{K}_i \boldsymbol{q}_i - \boldsymbol{D}_i \dot{\boldsymbol{q}}_i \right). \tag{3.99}$$

The first variable q_{1_i} is controlled by the PID controller. The flexible variable q_{2_i} for each link whose dynamics is stated as

$$\ddot{q}_{2_i} = \left(-h_{22}k_{22}q_{2_i} - h_{22}d_{22}\dot{q}_{2_i} - h_{21}c_1 - h_{22}c_2\right)_i + m_i^{-1}b_{\mathrm{pi}}v_{\mathrm{p}_i} \ . \tag{3.100}$$

Then a change of variable $[x_1 \ \ x_2]_i^{\mathrm{T}} = [q_2 \ \ \dot{q}_2]_i^{\mathrm{T}}$ to formulate the AVC loops is performed as follows

$$\begin{bmatrix} \dot{x}_1 \\ \dot{x}_2 \\ y \end{bmatrix}_i = \begin{bmatrix} 0 & 1 \\ 0 & 0 \\ 1 & 0 \end{bmatrix} \begin{bmatrix} x_1 \\ x_2 \end{bmatrix}_i + \begin{bmatrix} 0 \\ g(x_1, x_2) \\ 0 \end{bmatrix}_i + \begin{bmatrix} 0 \\ m_i^{-1}b_{\mathrm{pi}} \\ 0 \end{bmatrix}_i v_{\mathrm{p}_i}, \tag{3.101}$$

where

$$g_i(x_1, x_2) = \left(-h_{22}k_{22}x_1 - h_{22}d_{22}x_2 - h_{21}c_1 - h_{22}c_2\right)_i \ , \tag{3.102}$$

is the nonlinear part of the model. For each flexible link a linear sliding surface

$$\sigma_i = \dot{e}_i + \lambda_i e_i \, , \tag{3.103}$$

is employed, this surface can be formulated either in the state space or in the error space. In vibration control loops the desired values of the variables are zero ($e_i = x_{1,\mathrm{d}_i} - x_{1_i} = -x_{1_i}$), therefore the sliding variable and its time-derivative are redefined as

$$\sigma_i = -x_{2_i} - \lambda_i x_{1_i} \, , \tag{3.104}$$

and

$$\dot{\sigma}_i = -\dot{x}_{2_i} - \lambda_i x_{2_i} \, , \tag{3.105}$$

respectively. Substituting the dynamics of the system in the dynamics of the surface

$$\dot{\sigma}_i = \varphi_i(x_{1_i}, x_{2_i}) - u_i \, , \tag{3.106}$$

where $u_i = f_i = m_i^{-1}b_{\mathrm{pi}_i}v_{\mathrm{p}_i}$ and the cumulative uncertainty term

$$\varphi_i(x_{1_i}, x_{2_i}) = -g_i(x_{1_i}, x_{2_i}) - \lambda_i x_{2_i} \, , \tag{3.107}$$

is assumed to be continuous, smooth and bounded, as well as its time derivative

$$\left|\varphi_i(x_1, x_2)\right| \le A_i \ \text{ and } \ \left|\dot{\varphi}_i(x_1, x_2)_i\right| \le B_i \, . \tag{3.108}$$

Then σ_i must reach the value of zero to reach out the sliding surface and $\dot{\sigma}_i$ also must be zero where the system behaves like a reduced order system (in this case, first order) independent on the uncertainties [94]. It can be done choosing a control that satisfies the sliding condition [96]

$$V_i = \frac{1}{2}\frac{d}{dt}\sigma_i^{\,2} \, , \tag{3.109}$$

$$\dot{V}_i = \sigma_i\dot{\sigma}_i \le -\eta_i\left|\sigma_i\right|, \qquad \eta_i > 0 \, . \tag{3.110}$$

The control law used in this case is a super twisting SMC [92] which is given by

$$u_i = \hat{c}_i \left|\sigma_i\right|^{1/2} \mathrm{sgn}(\sigma_i) + w_i \ , \tag{3.111}$$

$$\dot{w}_i = b_i \ \mathrm{sgn}(\sigma_i) \ . \tag{3.112}$$

The values of $\hat{c}_i$ and b_i are calculated from the boundary value of $\dot{\varphi}_i(x_1, x_2)_i$

$$\hat{c}_i = 1.5\sqrt{B_i} \ \text{ and } \ b_i = 1.1B_i \, . \tag{3.113}$$

The sliding condition (3.110) ensures that all the trajectories in the phase portrait tend to the sliding surfaces, this is enforced because the auxiliary input (3.112) is intended to compensate $\varphi_i(x_{1_i}, x_{2_i})$. In the link deformation is measured near the clamped ends, and from these measurements the flexible variables x_{1_i} (i.e. q_{2_i}) are calculated. The rate of deformation x_{2_i} (i.e. $\dot{q}_{2_i}$) must be estimated, through a sliding mode observer shown in section 3.2.

The value of λ define the behavior of the system in sliding mode and also has direct influence in the active damping of the structure, but this parameter is limited by actuator saturation and more significantly by the frequency of the next not considered mode of vibration. For both robots the control architecture is similar, nevertheless it is presented in two separated section in order to make clear the difference in the required parameters for each case. This control strategy has the advantage that the controllers are relatively simple and do not require high computational capability for the final implementation. The extension to additional links is straightforward.

3.3.3 One Flexible-link Robot (SISO-PID SISO-SMC)

In this case the robot is provided only with one rotational actuator, a pair of piezo electric actuators, a pair of strain gages, incremental encoder and payload. The positioning controller is adjusted with the procedure explained in section 3.3.1. The model used for the calculation of the controller is given by

$$\ddot{\boldsymbol{q}} = \boldsymbol{M}(\boldsymbol{q})^{-1}\left(\boldsymbol{f} - \boldsymbol{c}(\boldsymbol{q},\dot{\boldsymbol{q}}) - \boldsymbol{K}\boldsymbol{q} - \boldsymbol{D}\dot{\boldsymbol{q}}\right), \tag{3.114}$$

$$\begin{bmatrix}\dot{x}_1\\ \dot{x}_2\\ y\end{bmatrix} = \begin{bmatrix}0 & 1\\ 0 & 0\\ 1 & 0\end{bmatrix}\begin{bmatrix}x_1\\ x_2\end{bmatrix} + \begin{bmatrix}0\\ g(x_1,x_2)\\ 0\end{bmatrix} + \begin{bmatrix}0\\ m^{-1}b_{\mathrm{pi}}\\ 0\end{bmatrix} v_{\mathrm{p}}, \tag{3.115}$$

where

$$g(x_1,x_2) = \left(-h_{22}k_{22}x_1 - h_{22}d_{22}x_2 - h_{21}c_1 - h_{22}c_2\right). \tag{3.116}$$

The boundary values of the cumulative uncertainty term

$$\left|\varphi(x_1,x_2)\right| \le A \text{ and } \left|\dot{\varphi}_i(x_1,x_2)\right| \le B. \tag{3.117}$$

are calculated running the extended model in Matlab/Simulink with two flexible DOF in order to take into account a possible small contribution of the second mode. With these values the SMC

$$u = \hat{c}\left|\sigma\right|^{1/2}\operatorname{sgn}(\sigma) + w, \tag{3.118}$$

$$\dot{w} = b\operatorname{sgn}(\sigma), \tag{3.119}$$

can be implemented. The proposed control architecture in this section is shown in Fig. 3.6, here the two independent loops are clearly defined. In Fig. 3.7 the structure of the AVC including the sliding model observer.

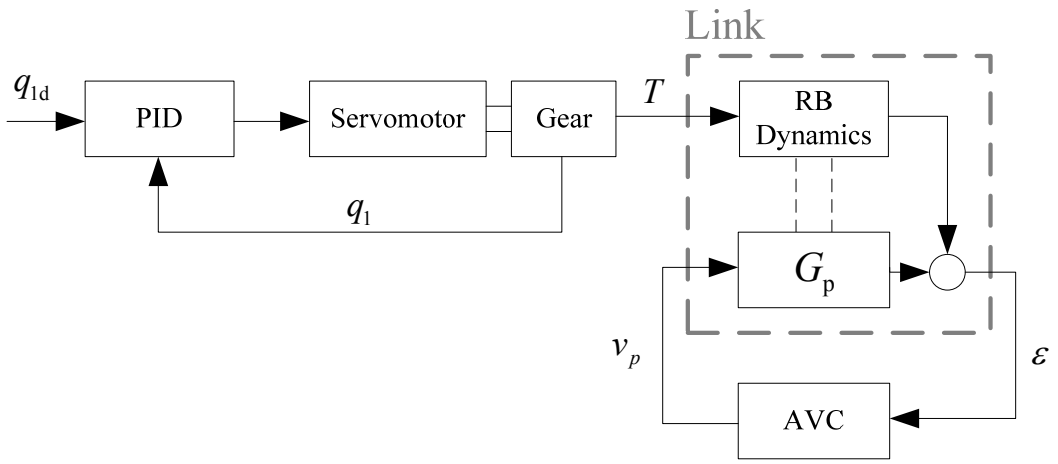

Figure 3.6: Control architecture for the one flexible-link robot (SISO-PID SISO-SMC).

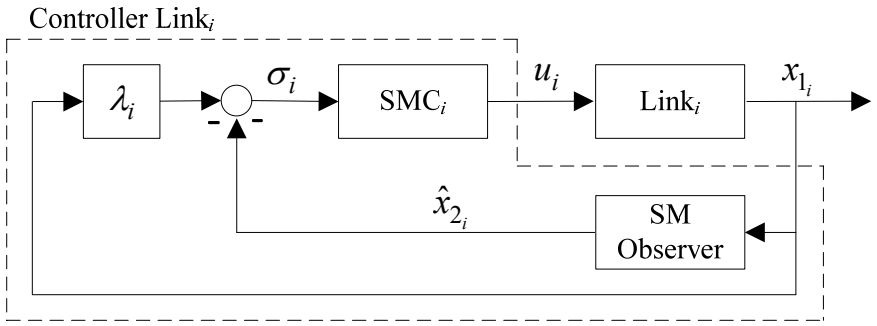

Figure 3.7: Structure of the AVC for the one flexible-link robot (SISO-PID SISO-SMC).

3.3.4 Two Flexible-link Robot (2SISO-PID 2SISO-SMC)

In this case the robot is provided with two rotational actuators, two pairs of piezo electric actuators, two pairs of strain gages, two incremental encoder and a payload. The positioning controller for each joint is adjusted with the procedure explained in section 3.3.1. This control strategy is similar to the previous section, but here the model for each joint-elastic link group is formulated as if they were one flexible-link robots. There are two important considerations to be taken into account. First for the model formulation, the natural boundary conditions at the tip of the first flexible link must include the inertial contribution of the second link. It is reflected in the inertia and mass of tip load as follows

$$J_{\mathrm{p}_1} = J_{\mathrm{h}_2} + J_{\mathrm{l}_2} + m_2\left(\frac{l_2}{2} + \left(\overline{\mathrm{O}_1\tilde{\mathrm{O}}_1}\right)_2\right)^2 + J_{\mathrm{p}_2} + m_{\mathrm{p}_2}\left(l_2 + \left(\overline{\mathrm{O}_1\tilde{\mathrm{O}}_1}\right)_2\right)^2 , \tag{3.120}$$

and

$$m_{\mathrm{p}_2} = m_{\mathrm{h}_2} + m_2 + m_{\mathrm{p}} . \tag{3.121}$$

The second consideration is related to the adjustment of the PID controllers. The first joint controller is adjusted with a rigid equivalent mass attached to the joint's shoulder, which include practically the whole robot. On the other hand, the second joint is located in a fixed support to be adjusted, also with an equivalent rigid mass to emulate the link.

The model used for the calculation of the controller is given by

$$\ddot{\boldsymbol{q}}_i = \boldsymbol{M}_i(\boldsymbol{q}_i)^{-1}\left(\boldsymbol{f}_i - \boldsymbol{c}_i(\boldsymbol{q}_i, \dot{\boldsymbol{q}}_i) - \boldsymbol{K}_i\boldsymbol{q}_i - \boldsymbol{D}_i\dot{\boldsymbol{q}}_i\right) \qquad i = 1, 2 . \tag{3.122}$$

$$\begin{bmatrix} \dot{x}_1 \\ \dot{x}_2 \\ y \end{bmatrix}_i = \begin{bmatrix} 0 & 1 \\ 0 & 0 \\ 1 & 0 \end{bmatrix} \begin{bmatrix} x_1 \\ x_2 \end{bmatrix}_i + \begin{bmatrix} 0 \\ g(x_1, x_2) \\ 0 \end{bmatrix}_i + \begin{bmatrix} 0 \\ m^{-1} b_{\mathrm{pi}} \\ 0 \end{bmatrix}_i v_{\mathrm{p}_i} \qquad i = 1,2\,, \tag{3.123}$$

where

$$g_i(x_1, x_2) = \left(-h_{22} k_{22} x_1 - h_{22} d_{22} x_2 - h_{21} c_1 - h_{22} c_2\right)_i \qquad i = 1,2\ . \tag{3.124}$$

The boundary values of the cumulative uncertainty term

$$\left|\varphi_i(x_1, x_2)\right| \le A_i \ \text{ and } \ \left|\dot{\varphi}_i(x_1, x_2)_i\right| \le B_i \qquad i = 1,2\,. \tag{3.125}$$

are calculated running the extended model for each link in Matlab/Simulink with two flexible DOF per flexible-link in order to take into account a possible small contribution of the second mode. With these values the SMC

$$u_i = \hat{c}_i \left|\sigma_i\right|^{1/2} \operatorname{sgn}(\sigma_i) + w_i \qquad i = 1,2\ , \tag{3.126}$$

$$\dot{w}_i = b_i \operatorname{sgn}(\sigma_i) \qquad i = 1,2\ , \tag{3.127}$$

can be implemented. The proposed control architecture in this section is shown in Fig. 3., here the two independent loops are clearly defined. In Fig. 3.7 the structure of the AVC including the sliding model observer is shown.

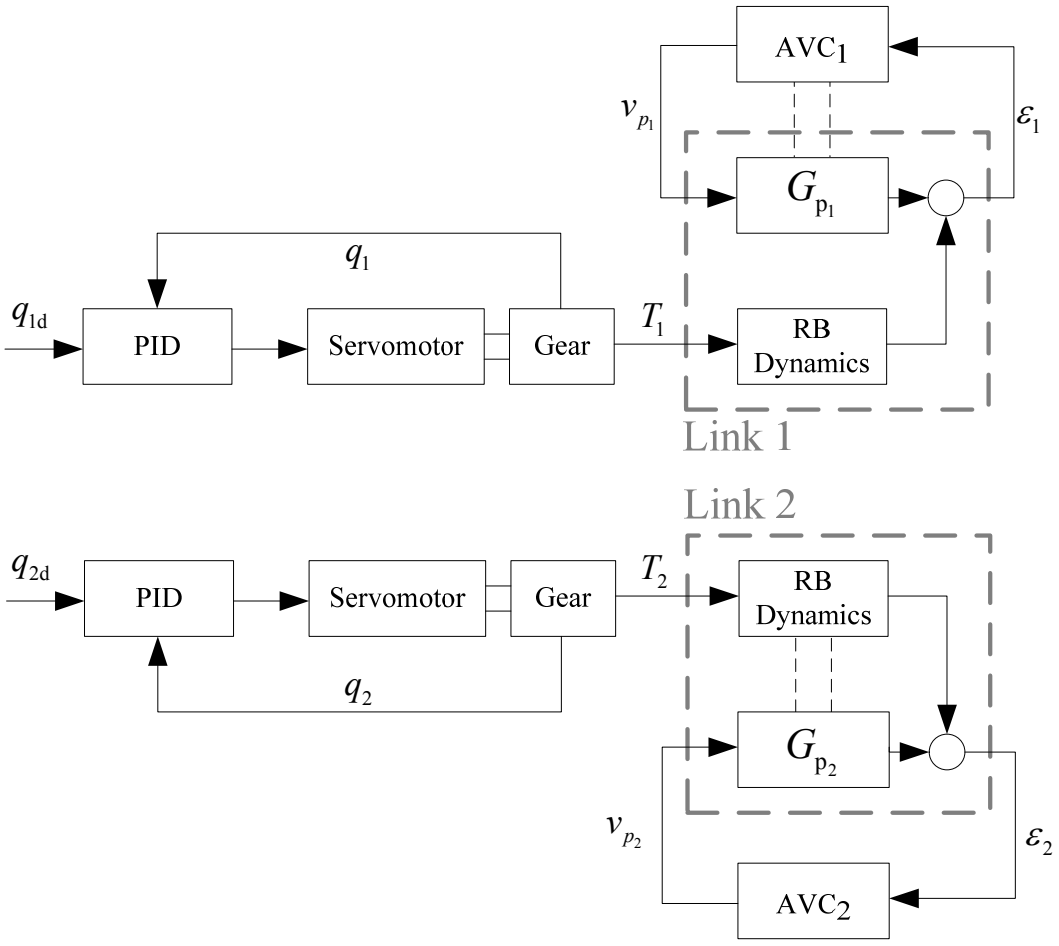

Figure 3.8: Control architecture for the two flexible-link robot (SISO-PID SISO-SMC).

3.4 Lyapunov Model-based SMC

In SMC the reachability condition of the surface or the attractiveness can be stated using the second Lyapunov method, based on this control law for the different flexible robotic structures under study is proposed. Subsequently the proposed control structure is particularized for different approaches. The uncertainties present in the model are present due to discrepancies between the model and the plant. According to the structure of the models, regular normal form

$$\begin{aligned} \dot{\boldsymbol{x}}_1 &= \boldsymbol{x}_2 \\ \dot{\boldsymbol{x}}_2 &= \boldsymbol{f}(\boldsymbol{x}_1, \boldsymbol{x}_2) + \Delta\boldsymbol{f}(\boldsymbol{x}_1, \boldsymbol{x}_2) + \boldsymbol{B}(\boldsymbol{x}_1, \boldsymbol{x}_2)\boldsymbol{u} \end{aligned}, \tag{3.128}$$

these uncertainties are called matched as long as they lie in the image of $\boldsymbol{B}(\boldsymbol{x}_1, \boldsymbol{x}_2)$ i.e. they are present only in the lower subsystem fulfilling the matching condition for uncertainties [94,96,92,112]. As result the proposed controller are capable to overcome the model uncertainty and increment the damping of the structures under study. Here also a methodology is presented to calculate the required parameters for the controller implementation.

3.4.1 Combined Control Law

The procedure for the calculation of the control law is formulated in a general manner. In later subsection is particularized for the respective robot. The model considered for the controller calculation is given by

$$\boldsymbol{M}(\boldsymbol{q})\,\ddot{\boldsymbol{q}} + \boldsymbol{c}(\boldsymbol{q}, \dot{\boldsymbol{q}}) + \boldsymbol{K}\,\boldsymbol{q} + \boldsymbol{D}\,\dot{\boldsymbol{q}} = \boldsymbol{f}\,, \tag{3.129}$$

where $\boldsymbol{M}(\boldsymbol{q}), \boldsymbol{K}, \boldsymbol{D} \in \mathbb{R}^{n\times n}$, $\boldsymbol{q}, \boldsymbol{c}(\boldsymbol{q}, \dot{\boldsymbol{q}}), \boldsymbol{f} \in \mathbb{R}^{n}$. The following change of variables is performed

$$\begin{bmatrix} \boldsymbol{x}_1 \\ \boldsymbol{x}_2 \end{bmatrix} = \begin{bmatrix} q \\ \dot{q} \end{bmatrix}, \tag{3.130}$$

next the model is formulated as

$$\begin{bmatrix} \dot{\boldsymbol{x}}_1 \\ \boldsymbol{M}(\boldsymbol{x}_1)\,\dot{\boldsymbol{x}}_2 \\ \boldsymbol{y} \end{bmatrix} = \begin{bmatrix} \mathbf{0} & \mathbf{I} \\ -\boldsymbol{K} & -\boldsymbol{D} \\ \mathbf{I} & \mathbf{0} \end{bmatrix} \begin{bmatrix} \boldsymbol{x}_1 \\ \boldsymbol{x}_2 \end{bmatrix} - \begin{bmatrix} \mathbf{0} \\ \boldsymbol{c}(\boldsymbol{x}_1, \boldsymbol{x}_2) \\ \mathbf{0} \end{bmatrix} + \begin{bmatrix} \mathbf{0} \\ \boldsymbol{f} \\ \mathbf{0} \end{bmatrix}, \tag{3.131}$$

where $\boldsymbol{f} = \boldsymbol{u}$, this is done in order to match the notation from Lagrange-Euler formalism and the notation of control design. To calculate the controller, it is assumed that the non-linear system is linear for the control input. The controller is a multiple-input multiple-output (MIMO) Lyapunov based controller with a sliding mode component for the rotational joint as well as for the piezoelectric actuators. First, a linear sliding manifold in the error space is considered

$$\boldsymbol{\sigma} = \dot{\boldsymbol{e}} + \boldsymbol{S}\,\boldsymbol{e}\,, \tag{3.132}$$

where the error is defined as

$$\boldsymbol{e} = \boldsymbol{x}_1 - \boldsymbol{x}_{1\mathrm{d}}\,. \tag{3.133}$$

The surface defined is the error space in order to calculate a controller to perform trajectory tracking. The matrix $\boldsymbol{S}$ contains the parameters λ_i that define the rate of convergence of the induced first order system during sliding mode, it is defined

$$\boldsymbol{S} = \mathrm{diag}(\lambda_i)\,. \tag{3.134}$$

In SMC the sliding variable $\boldsymbol{\sigma}$ must reach the value of zero or a very small value inside a small radius hyper cylinder, to be on the sliding surface and afterwards $\dot{\boldsymbol{\sigma}}$ is equal to zero where the system behaves like a reduced order system independent on the uncertainties [94]. In order to take advantage of some properties of the robot model structure the vector of Coriolis and centripetal effects is decomposed in

$$\boldsymbol{c}(\boldsymbol{x}_1, \boldsymbol{x}_2) = \boldsymbol{C}(\boldsymbol{x}_1, \boldsymbol{x}_2)\boldsymbol{x}_2 , \tag{3.135}$$

then each component of the matrix $\boldsymbol{C}(\boldsymbol{x}_1, \boldsymbol{x}_2)$ can be calculated using [16]

$$C_{i,j} = \frac{1}{2}\sum_{k=1}^{n} \frac{\partial M_{i,j}}{\partial x_{1,k}} x_{2,k} + \frac{1}{2}\sum_{k=1}^{n} \left(\left(\frac{\partial M_{i,k}}{\partial x_{1,j}} - \frac{\partial M_{j,k}}{\partial x_{1,i}} \right) x_{2,k} \right) . \tag{3.136}$$

In order to avoid the inversion of $\boldsymbol{M}(\boldsymbol{x}_1)$ the candidate Lyapunov function can be taken as [96]

$$V = \frac{1}{2}\boldsymbol{\sigma}^{\mathrm{T}} \boldsymbol{M}(\boldsymbol{x}_1)\boldsymbol{\sigma} , \tag{3.137}$$

and its time-derivative

$$\dot{V} = \boldsymbol{\sigma}^{\mathrm{T}} \boldsymbol{M}(\boldsymbol{x}_1)\dot{\boldsymbol{\sigma}} + \frac{1}{2}\boldsymbol{\sigma}^{\mathrm{T}} \dot{\boldsymbol{M}}(\boldsymbol{x}_1)\boldsymbol{\sigma} . \tag{3.138}$$

The time-derivative of the sliding manifold is given as

$$\dot{\boldsymbol{\sigma}} = \boldsymbol{S}\,\dot{\boldsymbol{e}} + \ddot{\boldsymbol{e}} . \tag{3.139}$$

The sliding manifold and its time-derivative in terms of the states and set point are

$$\boldsymbol{\sigma} = \dot{\boldsymbol{x}}_1 - \dot{\boldsymbol{x}}_{1\mathrm{d}} + \boldsymbol{S}\left(\boldsymbol{x}_1 - \boldsymbol{x}_{1\mathrm{d}}\right), \tag{3.140}$$

and

$$\dot{\boldsymbol{\sigma}} = \boldsymbol{S}\left(\dot{\boldsymbol{x}}_1 - \dot{\boldsymbol{x}}_{1\mathrm{d}}\right) + \ddot{\boldsymbol{x}}_1 - \ddot{\boldsymbol{x}}_{1\mathrm{d}} = \boldsymbol{S}\left(\dot{\boldsymbol{x}}_1 - \dot{\boldsymbol{x}}_{1\mathrm{d}}\right) + \dot{\boldsymbol{x}}_2 - \ddot{\boldsymbol{x}}_{1\mathrm{d}} . \tag{3.141}$$

Subsequently multiplying $\dot{\boldsymbol{\sigma}}$ by $\boldsymbol{M}(\boldsymbol{x}_1)$

$$\boldsymbol{M}\dot{\boldsymbol{\sigma}} = \boldsymbol{M}\boldsymbol{S}\,\dot{\boldsymbol{x}}_1 - \boldsymbol{M}\dot{\boldsymbol{x}}_{1\mathrm{d}} + \boldsymbol{M}\dot{\boldsymbol{x}}_2 - \boldsymbol{M}\ddot{\boldsymbol{x}}_{1\mathrm{d}} . \tag{3.142}$$

The state and time dependency are not shown for the sake of simplicity in the notation. Now $\boldsymbol{M}\dot{\boldsymbol{x}}_2$ is substituted from the dynamic model of the system

$$\boldsymbol{M}\dot{\boldsymbol{\sigma}} = \boldsymbol{M}\boldsymbol{S}\,\dot{\boldsymbol{x}}_1 - \boldsymbol{M}\dot{\boldsymbol{x}}_{1\mathrm{d}} + \boldsymbol{u} - \boldsymbol{K}\boldsymbol{x}_1 - \boldsymbol{D}\boldsymbol{x}_2 + \boldsymbol{C}\boldsymbol{S}\boldsymbol{x}_1 - \boldsymbol{M}\ddot{\boldsymbol{x}}_{1\mathrm{d}} . \tag{3.143}$$

Then (3.143) is substituted in (3.138)

$$\dot{V} = \boldsymbol{\sigma}^{\mathrm{T}}\left(\boldsymbol{u} - \boldsymbol{K}\boldsymbol{x}_1 - \boldsymbol{D}\boldsymbol{x}_2 - \boldsymbol{C}\boldsymbol{x}_2 + \boldsymbol{M}\boldsymbol{S}\boldsymbol{x}_2 - \boldsymbol{M}\boldsymbol{S}\boldsymbol{x}_{2\mathrm{d}} - \boldsymbol{M}\dot{\boldsymbol{x}}_{2\mathrm{d}}\right) + \frac{1}{2}\boldsymbol{\sigma}^{\mathrm{T}}\dot{\boldsymbol{M}}\boldsymbol{\sigma} . \tag{3.144}$$

From (3.140) an expression for $\boldsymbol{x}_2$ is obtained

$$\boldsymbol{x}_2 = \dot{\boldsymbol{x}}_1 = \dot{\boldsymbol{x}}_{1\mathrm{d}} + \boldsymbol{S}\boldsymbol{x}_{1\mathrm{d}} - \boldsymbol{S}\boldsymbol{x}_1 + \boldsymbol{\sigma} , \tag{3.145}$$

substituting $\boldsymbol{x}_2$ in (3.144)

$$\begin{aligned} \dot{V} = {} & \boldsymbol{\sigma}^{\mathrm{T}}\left(\boldsymbol{u} - \boldsymbol{K}\boldsymbol{x}_1 - \boldsymbol{D}\boldsymbol{x}_2 - \boldsymbol{C}\dot{\boldsymbol{x}}_{1\mathrm{d}} - \boldsymbol{C}\boldsymbol{S}\boldsymbol{x}_{1\mathrm{d}} + \boldsymbol{C}\boldsymbol{S}\boldsymbol{x}_1 + \boldsymbol{M}\boldsymbol{S}\boldsymbol{x}_2 - \boldsymbol{M}\boldsymbol{S}\boldsymbol{x}_{2\mathrm{d}} - \boldsymbol{M}\dot{\boldsymbol{x}}_{2\mathrm{d}}\right)\ldots \\ & -\boldsymbol{\sigma}^{\mathrm{T}}\boldsymbol{C}\boldsymbol{\sigma} + \frac{1}{2}\boldsymbol{\sigma}^{\mathrm{T}}\dot{\boldsymbol{M}}\boldsymbol{\sigma} \end{aligned} . \tag{3.146}$$

Under the assumption of low transversal deformation and according to the robots model properties [16], the matrix $\dot{\boldsymbol{M}} - 2\boldsymbol{C}$ must be skew-symmetric

$$\boldsymbol{\sigma}^{\mathrm{T}}\left(\dot{\boldsymbol{M}}(\boldsymbol{x}_1,\boldsymbol{x}_2)-2\boldsymbol{C}(\boldsymbol{x}_1,\boldsymbol{x}_2)\right)\boldsymbol{\sigma}=0\,, \tag{3.147}$$

then the last term of (3.146) can be eliminated

$$\dot{V}=\boldsymbol{\sigma}^{\mathrm{T}}\left(\boldsymbol{u}-\boldsymbol{K}\boldsymbol{x}_1-\boldsymbol{D}\boldsymbol{x}_2+\boldsymbol{C}\boldsymbol{S}\boldsymbol{x}_1-\boldsymbol{C}\boldsymbol{S}\boldsymbol{x}_{1\mathrm{d}}-\boldsymbol{C}\boldsymbol{x}_{2\mathrm{d}}+\boldsymbol{M}\boldsymbol{S}\boldsymbol{x}_2-\boldsymbol{M}\boldsymbol{S}\boldsymbol{x}_{2\mathrm{d}}-\boldsymbol{M}\dot{\boldsymbol{x}}_{2\mathrm{d}}\right). \tag{3.148}$$

The control law is made up of two parts

$$\boldsymbol{u}=\hat{\boldsymbol{u}}+\boldsymbol{u}_{\mathrm{SM}}\ .$$

In order to ensure the existence of a sliding mode, $\boldsymbol{u}$ is chosen to make $\dot{V}$ negative definite. With this the states trajectories will converge to the sliding surface. The first part of $\boldsymbol{u}$ influences the system as if the model were perfectly known. It is similar to the equivalent control part of SMC theory [92]. This part of the control law is defined by

$$\hat{\boldsymbol{u}}=\hat{\boldsymbol{K}}\boldsymbol{x}_1+\hat{\boldsymbol{D}}\boldsymbol{x}_2+\hat{\boldsymbol{C}}\boldsymbol{S}\left(\boldsymbol{x}_{1\mathrm{d}}-\boldsymbol{x}_1\right)+\hat{\boldsymbol{C}}\boldsymbol{x}_{2\mathrm{d}}+\hat{\boldsymbol{M}}\boldsymbol{S}\left(\boldsymbol{x}_{2\mathrm{d}}-\boldsymbol{x}_2\right)+\hat{\boldsymbol{M}}\dot{\boldsymbol{x}}_{2\mathrm{d}}\,. \tag{3.149}$$

The symbol $\hat{\bullet}$ above the elements indicates that they are estimated values for these parameters i.e. they come from the model. On the other hand, the corrective nonlinear part of the control law is chosen to be a switching function

$$\boldsymbol{u}_{\mathrm{SM}}=\boldsymbol{P}\,\mathrm{sgn}\left(\boldsymbol{\sigma}\right)\qquad\boldsymbol{P}=\mathrm{diag}\left(\rho_i\right). \tag{3.150}$$

Then the time-derivative of the candidate Lyapunov function is given by

$$\dot{V}=\boldsymbol{\sigma}^{\mathrm{T}}\left(\tilde{\boldsymbol{M}}\left(\boldsymbol{S}\left(\boldsymbol{x}_{2\mathrm{d}}-\boldsymbol{x}_2\right)+\dot{\boldsymbol{x}}_{2\mathrm{d}}\right)+\tilde{\boldsymbol{C}}\left(\boldsymbol{S}\left(\boldsymbol{x}_{1\mathrm{d}}-\boldsymbol{x}_1\right)+\boldsymbol{x}_{2\mathrm{d}}\right)+\tilde{\boldsymbol{K}}\boldsymbol{x}_1+\tilde{\boldsymbol{D}}\boldsymbol{x}_2\right)-\sum_{i=1}^{n}\rho_i\left|\sigma_i\right|, \tag{3.151}$$

where $\tilde{\bullet}=\bullet-\hat{\bullet}$, which represents the difference between the real model parameter and the approximated model parameter. The system is stable as long as the nonlinear part of control law fulfils

$$\rho_i\geq\left|\left[\tilde{\boldsymbol{M}}\left(\boldsymbol{S}\left(\boldsymbol{x}_{2\mathrm{d}}-\boldsymbol{x}_2\right)+\dot{\boldsymbol{x}}_{2\mathrm{d}}\right)+\tilde{\boldsymbol{C}}\left(\boldsymbol{S}\left(\boldsymbol{x}_{1\mathrm{d}}-\boldsymbol{x}_1\right)+\boldsymbol{x}_{2\mathrm{d}}\right)+\tilde{\boldsymbol{K}}\boldsymbol{x}_1+\tilde{\boldsymbol{D}}\boldsymbol{x}_2\right]_i\right|+\eta_i\,. \tag{3.152}$$

The minimum value of ρ_i is calculated

$$\rho_{i_{\min}}=\max\left|\left[\tilde{\boldsymbol{M}}\left(\boldsymbol{S}\left(\boldsymbol{x}_{2\mathrm{d}}-\boldsymbol{x}_2\right)+\dot{\boldsymbol{x}}_{2\mathrm{d}}\right)+\tilde{\boldsymbol{C}}\left(\boldsymbol{S}\left(\boldsymbol{x}_{1\mathrm{d}}-\boldsymbol{x}_1\right)+\boldsymbol{x}_{2\mathrm{d}}\right)+\tilde{\boldsymbol{K}}\boldsymbol{x}_1+\tilde{\boldsymbol{D}}\boldsymbol{x}_2\right]_i\right|. \tag{3.153}$$

After the continuous part of the control law has been implemented in the hardware, these values can be estimated by

$$\begin{aligned}\rho_{i_{\min}}\geq\max\Big|&\boldsymbol{M}(\boldsymbol{x}_{1_{\mathrm{exp}}})\left(\boldsymbol{S}\left(\boldsymbol{x}_{2\mathrm{d}}-\boldsymbol{x}_{2_{\mathrm{exp}}}\right)+\dot{\boldsymbol{x}}_{2\mathrm{d}}\right)+\boldsymbol{C}(\boldsymbol{x}_{1_{\mathrm{exp}}},\boldsymbol{x}_{2_{\mathrm{exp}}})\left(\boldsymbol{S}\left(\boldsymbol{x}_{1\mathrm{d}}-\boldsymbol{x}_{1_{\mathrm{exp}}}\right)+\boldsymbol{x}_{2\mathrm{d}}\right)\\&+\boldsymbol{K}\boldsymbol{x}_{1_{\mathrm{exp}}}+\boldsymbol{D}\boldsymbol{x}_{2_{\mathrm{exp}}}-\hat{\boldsymbol{M}}(\boldsymbol{x}_{1_{\mathrm{sim}}})\left(\boldsymbol{S}\left(\boldsymbol{x}_{2\mathrm{d}}-\boldsymbol{x}_{2_{\mathrm{sim}}}\right)+\dot{\boldsymbol{x}}_{2\mathrm{d}}\right)\\&+\hat{\boldsymbol{C}}(\boldsymbol{x}_{1_{\mathrm{sim}}},\boldsymbol{x}_{2_{\mathrm{sim}}})\left(\boldsymbol{S}\left(\boldsymbol{x}_{1\mathrm{d}}-\boldsymbol{x}_{1_{\mathrm{sim}}}\right)+\boldsymbol{x}_{2\mathrm{d}}\right)+\hat{\boldsymbol{K}}\boldsymbol{x}_{1_{\mathrm{sim}}}+\hat{\boldsymbol{D}}\boldsymbol{x}_{2_{\mathrm{sim}}}\Big|_i\end{aligned}, \tag{3.154}$$

where $\boldsymbol{x}_{1_{\mathrm{exp}}}$ and $\boldsymbol{x}_{2_{\mathrm{exp}}}$ come from experimentation without the switching part, $\boldsymbol{x}_{1_{\mathrm{sim}}}$ and $\boldsymbol{x}_{2_{\mathrm{sim}}}$ come from the simulated model under the same test conditions. With this procedure values for ρ_i can be estimated. The system is stable as long as the discontinuous part of control law fulfils

$$\dot{V}\leq-\sum_{i=1}^{n}\rho_i\left|\sigma_i\right|. \tag{3.155}$$

The proposed procedure for the controller calculation is outlined in Fig. 3.9. This can be applied for the controller calculation of the robotic structures of this work. An important remark is that for the controller formulation a simplified model of the robots is used, the simplified model has one flexible DOF per link. The model simplification for controller

calculation is straightforward. Nevertheless for the calculation of the required parameters or boundary values from simulation the 2 DOF per link is used.
As in the previous control approaches, the values of λ_i define the behavior of the system in sliding mode, indeed they are the poles of the reduced dynamics of the system and also have direct influence in the active damping of the structure. This parameter is limited by actuator saturation and more significantly by the frequency of the next not considered mode of vibration.

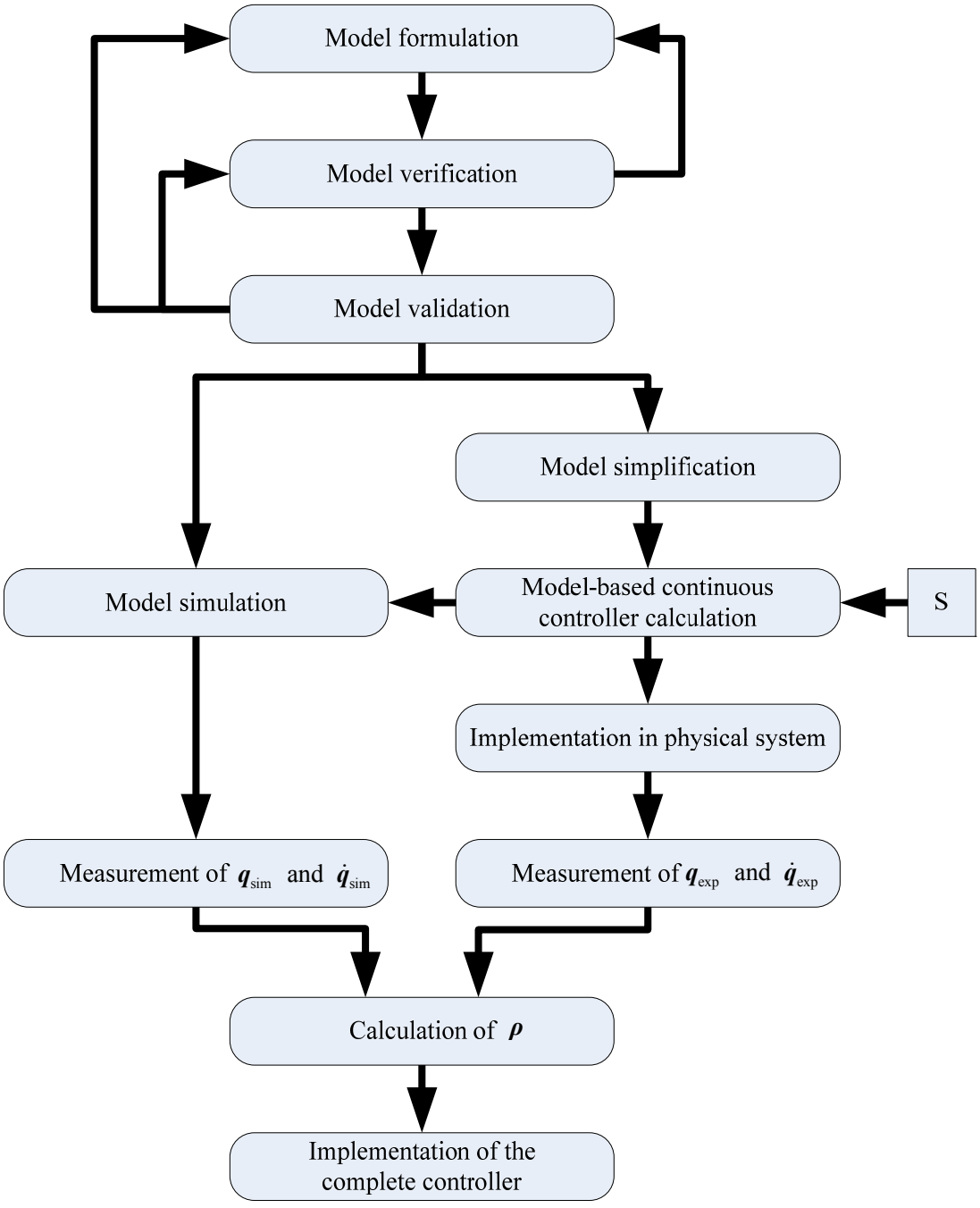

Figure 3.9: Proposed sequence for Lyapunov model-based controller calculation.

3.4.2 Centralized Approach

The control strategy, proposed in the previous section, provides an alternative for the reduction of unwanted vibrations of the studied flexible robotic structures. The

implementation is similar but the most significant difference lies in the number of DOF. The robots are considered as MIMO systems and the controllers as well. The most important point here is that the interaction between the different inputs and the state variables is taken into account.

3.4.2.1 One Flexible-link Robot (MIMO-SMC)

In this case, the robot is provided only with one rotational actuator, a pair of piezo electric actuators, a pair of strain gages, incremental encoder and payload. The procedure for the controller calculation has already been explained. The model used for the controller calculation is

$$\boldsymbol{M}(\boldsymbol{q})\,\ddot{\boldsymbol{q}} + \boldsymbol{c}(\boldsymbol{q},\dot{\boldsymbol{q}}) + \boldsymbol{K}\,\boldsymbol{q} + \boldsymbol{D}\,\dot{\boldsymbol{q}} = \boldsymbol{f}\,, \tag{3.156}$$

where $\boldsymbol{M}(\boldsymbol{q}), \boldsymbol{K}, \boldsymbol{D} \in \mathbb{R}^{n\times n}$, $\boldsymbol{q}, \boldsymbol{c}(\boldsymbol{q},\dot{\boldsymbol{q}}), \boldsymbol{f} \in \mathbb{R}^{n}$ and $n = n_{\mathrm{R}} + n_{\mathrm{F}} = 1+1 = 2$. The change of variables is

$$\boldsymbol{x}_1 = \boldsymbol{q} = \begin{bmatrix} q_1 \\ q_2 \end{bmatrix}, \boldsymbol{x}_2 = \dot{\boldsymbol{q}} = \begin{bmatrix} \dot{q}_1 \\ \dot{q}_2 \end{bmatrix}. \tag{3.157}$$

The model is formulated as

$$\begin{bmatrix} \dot{\boldsymbol{x}}_1 \\ \boldsymbol{M}(\boldsymbol{x}_1)\,\dot{\boldsymbol{x}}_2 \\ \boldsymbol{y} \end{bmatrix} = \begin{bmatrix} \mathbf{0} & \mathbf{I} \\ -\boldsymbol{K} & -\boldsymbol{D} \\ \mathbf{I} & \mathbf{0} \end{bmatrix} \begin{bmatrix} \boldsymbol{x}_1 \\ \boldsymbol{x}_2 \end{bmatrix} + \begin{bmatrix} \mathbf{0} \\ \boldsymbol{c}(\boldsymbol{x}_1,\boldsymbol{x}_2) \\ \mathbf{0} \end{bmatrix} + \begin{bmatrix} \mathbf{0} \\ \boldsymbol{f} \\ \mathbf{0} \end{bmatrix}. \tag{3.158}$$

This model is given in section 2.2.1 and all the matrix and vector functions are given developed there. The input signal is defined as

$$\boldsymbol{u} = \boldsymbol{f} = \boldsymbol{B}_{\mathrm{pi}} \begin{bmatrix} \tau_{\mathrm{m}} - \tau_{\mathrm{fr}} \\ v_{\mathrm{p}} \end{bmatrix} = \begin{bmatrix} 1 & 0 \\ 0 & \bar{c}\left(\phi_1'(x_{\mathrm{a}2}) - \phi_1'(x_{\mathrm{a}1})\right) \end{bmatrix} \begin{bmatrix} \tau_{\mathrm{m}} - \tau_{\mathrm{fr}} \\ v_{\mathrm{p}} \end{bmatrix}. \tag{3.159}$$

The control structure for the implementation is shown in Fig. 3.10.

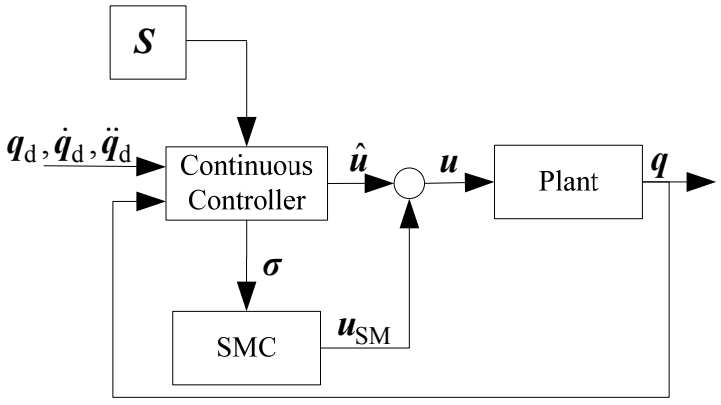

Figure 3.10: Centralized control structure.

3.4.2.2 Two Flexible-link Robot (MIMO-SMC)

This is the most complex controller due to the amount of DOF of the system to be controlled. Here the interaction between inputs and states is considered. In this case the robot is provided with two rotational actuators, two pairs of piezo electric actuators, two pair of strain gages, two incremental encoders and a payload. The procedure for the controller calculation has been already explained. The model used for the controller calculation is

$$\boldsymbol{M}(\boldsymbol{q})\,\ddot{\boldsymbol{q}} + \boldsymbol{c}(\boldsymbol{q},\dot{\boldsymbol{q}}) + \boldsymbol{K}\,\boldsymbol{q} + \boldsymbol{D}\,\dot{\boldsymbol{q}} = \boldsymbol{f}\,, \tag{3.160}$$

where $\boldsymbol{M}(\boldsymbol{q}), \boldsymbol{K}, \boldsymbol{D} \in \mathbb{R}^{n\times n}$, $\boldsymbol{q}, \boldsymbol{c}(\boldsymbol{q}, \dot{\boldsymbol{q}}), \boldsymbol{f} \in \mathbb{R}^{n}$ and $n = n_R + n_{F1} + n_{F2} = 2+1+1 = 4$. The change of variables is

$$\boldsymbol{x}_1 = \boldsymbol{q} = \begin{bmatrix} q_1 \\ q_2 \\ q_3 \\ q_4 \end{bmatrix}, \boldsymbol{x}_2 = \dot{\boldsymbol{q}} = \begin{bmatrix} \dot{q}_1 \\ \dot{q}_2 \\ \dot{q}_3 \\ \dot{q}_4 \end{bmatrix}. \tag{3.161}$$

The model is formulated as

$$\begin{bmatrix} \dot{\boldsymbol{x}}_1 \\ \boldsymbol{M}(\boldsymbol{x}_1)\,\dot{\boldsymbol{x}}_2 \\ \boldsymbol{y} \end{bmatrix} = \begin{bmatrix} \mathbf{0} & \mathbf{I} \\ -\boldsymbol{K} & -\boldsymbol{D} \\ \mathbf{I} & \mathbf{0} \end{bmatrix} \begin{bmatrix} \boldsymbol{x}_1 \\ \boldsymbol{x}_2 \end{bmatrix} + \begin{bmatrix} \mathbf{0} \\ \boldsymbol{c}(\boldsymbol{x}_1, \boldsymbol{x}_2) \\ \mathbf{0} \end{bmatrix} + \begin{bmatrix} \mathbf{0} \\ \boldsymbol{f} \\ \mathbf{0} \end{bmatrix}. \tag{3.162}$$

This model is given in section 2.2.1 and all the matrix and vector functions are given developed there. The input signal is defined as

$$\boldsymbol{u} = \boldsymbol{f} = \boldsymbol{B}_{\mathrm{pi}} \begin{bmatrix} \tau_{\mathrm{m}_1} - \tau_{\mathrm{fr}_1} \\ \tau_{\mathrm{m}_2} - \tau_{\mathrm{fr}_2} \\ v_{\mathrm{p}_1} \\ v_{\mathrm{p}_2} \end{bmatrix}, \tag{3.163}$$

where

$$\boldsymbol{u} = \boldsymbol{f} = \begin{bmatrix} 1 & 0 & 0 & 0 \\ 0 & 1 & 0 & 0 \\ 0 & 0 & \overline{c}_1\left(\phi'_{11}(x_{\mathrm{a}2}) - \phi'_{11}(x_{\mathrm{a}1})\right) & 0 \\ 0 & 0 & 0 & \overline{c}_2\left(\phi'_{11}(x_{\mathrm{a}2}) - \phi'_{11}(x_{\mathrm{a}1})\right) \end{bmatrix} \begin{bmatrix} \tau_{\mathrm{m}_1} - \tau_{\mathrm{fr}_1} \\ \tau_{\mathrm{m}_2} - \tau_{\mathrm{fr}_2} \\ v_{\mathrm{p}_1} \\ v_{\mathrm{p}_2} \end{bmatrix}. \tag{3.164}$$

The control structure for the implementation is shown in Fig. 3.10.

Last but not least important is the fact shown by [113], overestimation of structure stiffness may lead to unstable closed-loop response of the original manipulator system, using a model-based control law. The boundary conditions used for the flexible-link modeling in multilink flexible robotic structures are configuration dependent, in the case of two link robots depend on q_2. The boundary conditions used for the controller calculation were calculated assuming $q_2 = 0$, in this configuration the resonance frequencies have their lowest values avoiding the overestimation of them when the system assumes and configuration where $q_2 \neq 0$.

3.4.3 Partially Decentralized Approach

In order to have less computational complexity the robot is modeled separately for each joint-link group. With this approach the effect of the centrifugal and centripetal force induced by the movement of the second joint is neglected by the controllers. The effectiveness of this approach will be experimentally tested. Here one controller per group is calculated in the same fashion as in section 3.4.2.1.

3.4.3.1 Two Flexible-link Robot (2MIMO-SMC)

In this case, the robot is provided with two rotational actuators, two pairs of piezo electric actuators, two pairs of strain gages, two incremental encoders and a payload. The procedure for the controller calculation has already been explained. This approach has the advantage that

it can easily be extended to additional serial links. The model used for the controller calculation is

$$\boldsymbol{M}_i(\boldsymbol{q}_i)\,\ddot{\boldsymbol{q}}_i + \boldsymbol{c}_i(\boldsymbol{q}_i,\dot{\boldsymbol{q}}_i) + \boldsymbol{K}_i\,\boldsymbol{q}_i + \boldsymbol{D}_i\,\dot{\boldsymbol{q}}_i = \boldsymbol{f}_i \qquad i=1,2, \tag{3.165}$$

where $\boldsymbol{M}_i(\boldsymbol{q}_i), \boldsymbol{K}_i, \boldsymbol{D}_i \in \mathbb{R}^{n_i \times n_i}$, $\boldsymbol{q}_i, \boldsymbol{c}_i(\boldsymbol{q}_i,\dot{\boldsymbol{q}}_i), \boldsymbol{f}_i \in \mathbb{R}^{n_i}$, $n_1 = n_{\mathrm{R}_1} + n_{\mathrm{F}_1} = 1+1 = 2$ and $n_2 = n_{\mathrm{R}_2} + n_{\mathrm{F}_2} = 1+1 = 2$. The change of variables is

$$\boldsymbol{x}_{1_i} = \boldsymbol{q}_i = \begin{bmatrix} q_1 \\ q_2 \end{bmatrix}_i, \boldsymbol{x}_{2_i} = \dot{\boldsymbol{q}}_i = \begin{bmatrix} \dot{q}_1 \\ \dot{q}_2 \end{bmatrix}_i \qquad i=1,2. \tag{3.166}$$

The model is formulated as

$$\begin{bmatrix} \dot{\boldsymbol{x}}_1 \\ \boldsymbol{M}(\boldsymbol{x}_1)\,\dot{\boldsymbol{x}}_2 \\ \boldsymbol{y} \end{bmatrix}_i = \begin{bmatrix} \boldsymbol{0} & \boldsymbol{\mathrm{I}} \\ -\boldsymbol{K} & -\boldsymbol{D} \\ \boldsymbol{\mathrm{I}} & \boldsymbol{0} \end{bmatrix}_i \begin{bmatrix} \boldsymbol{x}_1 \\ \boldsymbol{x}_2 \end{bmatrix}_i + \begin{bmatrix} \boldsymbol{0} \\ \boldsymbol{c}(\boldsymbol{x}_1,\boldsymbol{x}_2) \\ \boldsymbol{0} \end{bmatrix}_i + \begin{bmatrix} \boldsymbol{0} \\ \boldsymbol{f} \\ \boldsymbol{0} \end{bmatrix}_i \qquad i=1,2. \tag{3.167}$$

This model is given in section 2.2.1 and all the matrix and vector functions are given developed there. The input signal is defined as

$$\boldsymbol{u} = \boldsymbol{f} = \boldsymbol{B}_{\mathrm{pi}_i} \begin{bmatrix} \tau_{\mathrm{m}} - \tau_{\mathrm{fr}} \\ v_{\mathrm{p}} \end{bmatrix}_i = \begin{bmatrix} 1 & 0 \\ 0 & \bar{c}\left(\phi_1'(x_{\mathrm{a}2}) - \phi_1'(x_{\mathrm{a}1})\right) \end{bmatrix}_i \begin{bmatrix} \tau_{\mathrm{m}} - \tau_{\mathrm{fr}} \\ v_{\mathrm{p}} \end{bmatrix}_i \qquad i=1,2. \tag{3.168}$$

The control structure for the implementation is shown in Fig. 3.11.

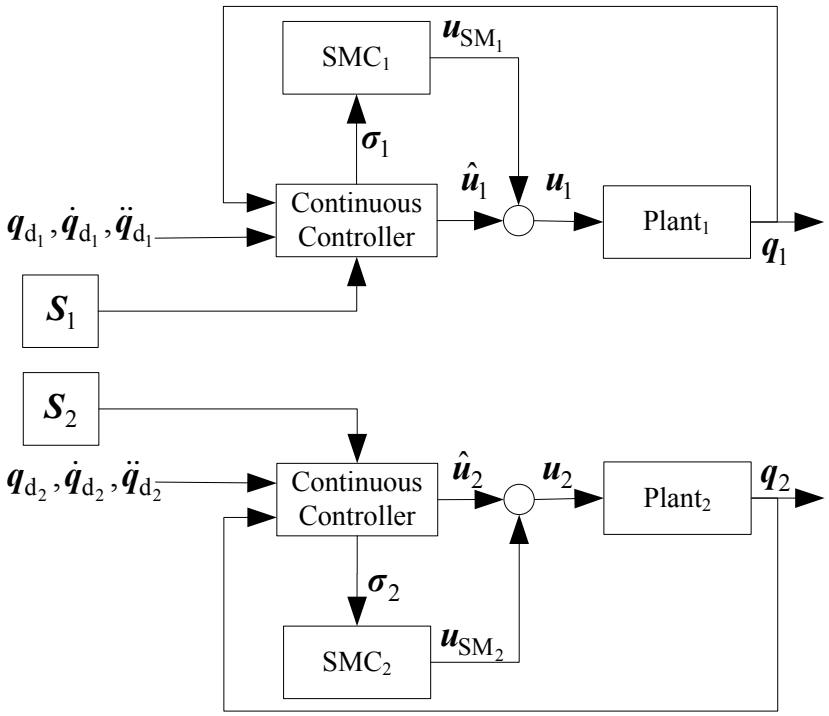

Figure 3.11: Decentralized control structure.

4 Test Bed and Experimental Results

The proposed control strategies were tested and its effectiveness was verified experimentally in a real system. A test bed was developed and constructed to conduct the required experiments.

4.1 Test Bed

The first requirement to fulfill of a structure to study vibration is to stay without movement and to be rigid compared with the elements under study. Normally this kind of test devices a joined to the floor in order to be connected to an enormous inertia. In our case, the test bed was supposed to be movable. Then a massive structure was proposed for this objective. The structure was developed with the feature of versatility. With this, different kinds of flexible structures can be studied.

The base structure is made of structural steel and is capable to provide a suitable platform for the study of vertical or horizontal flexible beams and flexible-link robots with a planar horizontal workspace (see Fig. 4.1). With some changes in the support of the robot, the workspace plane can be set vertical, it was done so for future research.

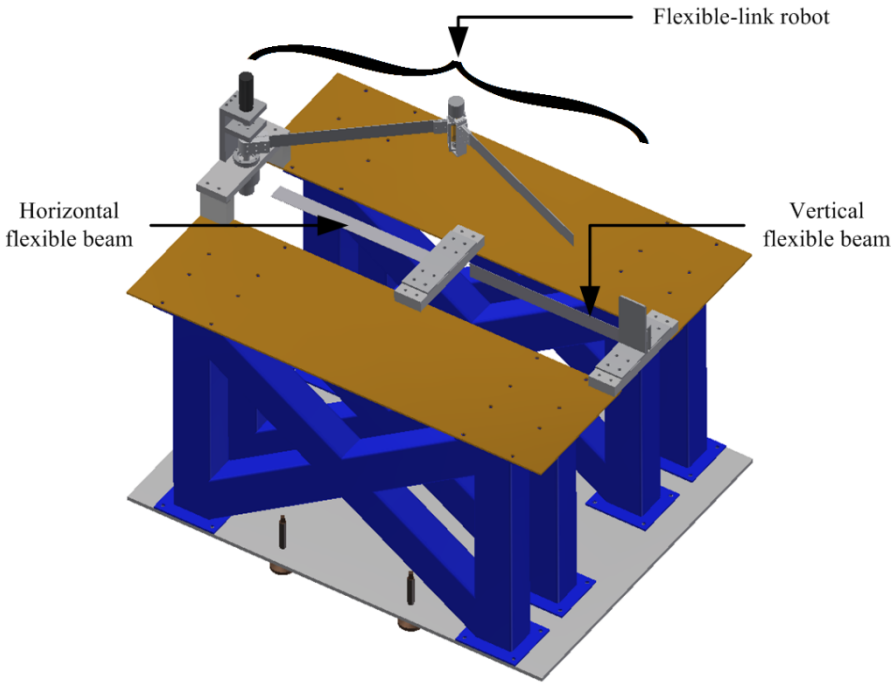

Figure 4.1: Test bed.

The rotational actuators according to the mechanical configuration makes the joint space to be restricted to $-90° \leq q_{R_i} \leq 90°$. This range defines the robot's cartesian workspaces, for the one flexible-link the workspace is a semicircumference with an angle of 180°. On the other hand for the two flexible-link robot subjected to the same joint space the Cartesian workspace can be determined graphically. The first link is located in discrete angular positions inside its range and then for each position the second joint is moved from its minimum value to its maximum value as it is shown in Fig. 4.2. The definitive cartesian workspace considering the dimensions of the links and joints (see Tab. 2.6) is shown in Fig. 4.3. The cartesian workspace

of a robot is defined as the domain defined by all the points that the end effector of the robot can reach with different configurations or as it is stated in [106] are those points in which the inverse kinematics has solution and it is nonsingular.

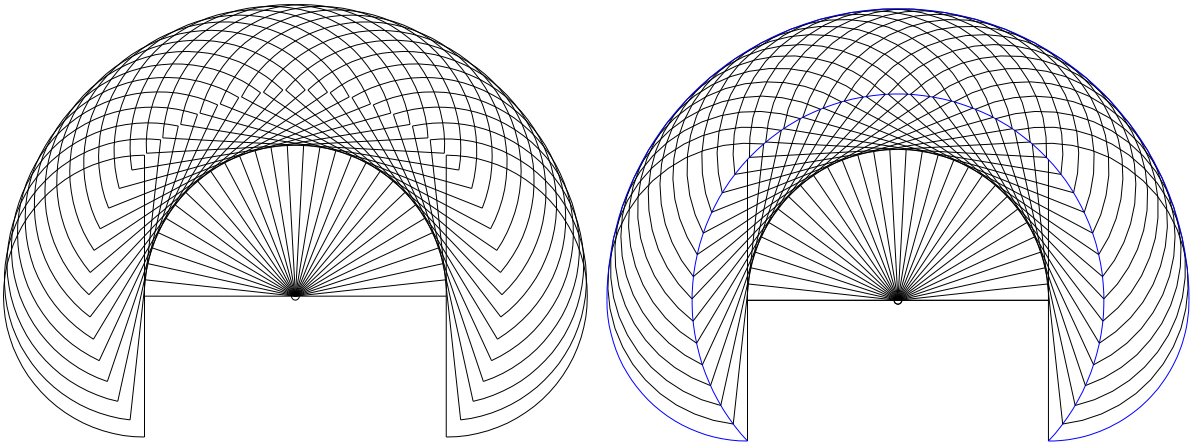

Figure 4.2: Definition of the reachable workspace.

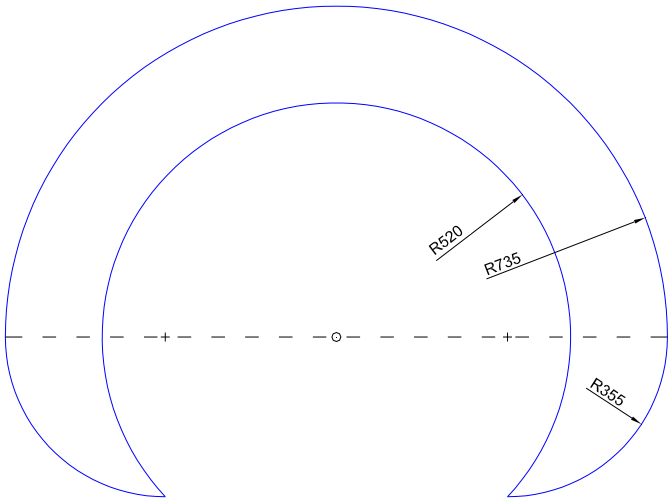

Figure 4.3: Definitive workspace. (Distances are given in mm).

From the control point of view the test bed has different kind of equipment such as sensors, actuators, amplifiers, rapid prototyping card. These elements are shown in Fig. 4.4. The *computer with prototyping card* contains a dSPACE card 1104 for the implementation of the controllers to be used, these controllers are programmed in Matlab-Simulink and directly loaded in the card. *The CP connector panel* is used to distribute all the input and output possibilities of the DS 1104. The *motors unit* contains two Maxon Motors LLC controllers EPOS2 50/5, which can be used as positioning controller PID with feedforward gain or just as amplifiers for the servomotors with a current control loop. Also in this unit are contained two Maxon Motors LLC PI controllers ESCON 36/2 DC, these are used to control the speed of motors used for the generation of harmonics disturbances , if required for the experiment.

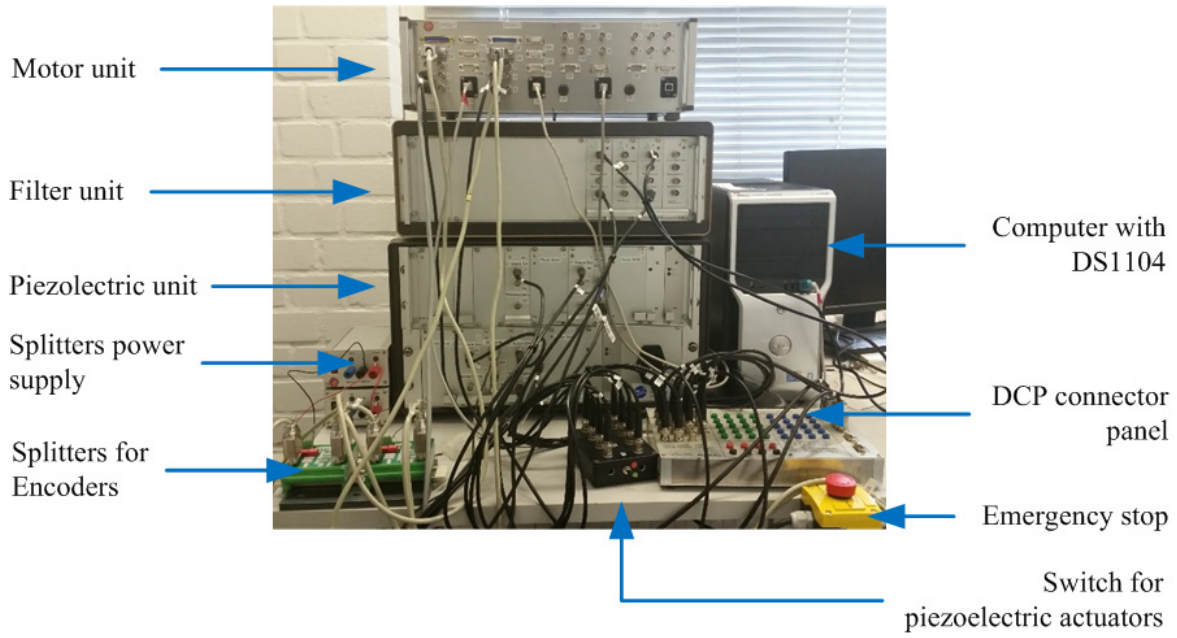

Figure 4.4: Experimental control setup.

The *filter unit* contains anti-aliasing filters for the signal conditioning from the sensors, they are Butterworth filter of eighth order with cut off frequencies of 200 Hz. The *piezoelectric unit* includes four piezoelectric amplifiers PI Instruments PI E413.D2. Four low pass filters for signal conditioning from and to the piezoelectric actuators. *Impulse Splitter for Incremental Encoders* Motrona GV204 are used to divide the signal from each incremental encoder and send it to the motor controllers and to the DS1104. Emergency stop is used for safety reasons in case the system turns into an instable behavior. The *switch for piezoelectric actuators* is used to activate and deactivate the AVC control loop. Also Wheatstone bridges are used for the acquisition of signal from strain gages, the amplifier units are Soemer LAU 63.1, the rest of the bridge was constructed by the electronic workshop of the institute.

The inputs of the system are provided by the actuators, here only two kinds of actuators are used. As rotational actuators servomotors are provided with harmonic drives, for the first joint Harmonic Drive PMA-8A-50-01-E1000ML and for the second joint Harmonic Drive PMA-5A-80-01-E512ML. The patch piezoelectric actuators used for AVC are P 876.A12 DuraAct. The input for the controller is acquired by the sensors. Strain gages HBM 1-LY13-6/350 forming a half bride to obtain temperature compensation are used to measure deformation. Two high resolution incremental encoders GPI RS137S to get accurately the angular position of the joints. One capacitive accelerometer ASC 4411LN at the tip of the flexible structure is used just to verify the effectiveness of the control strategies.

The interaction between the elements of the experimental setup depends on the test to be performed. The different proposed control strategies are implemented and tested in: cantilever beam (Fig. 4.5 and 4.6), one flexible-link robot (Fig. 4.7 and 4.8) and two flexible-link robot (Fig. 4.9 and 4.10) with physical parameters given in Tab. 2.1,2.4 and 2.6, respectively.

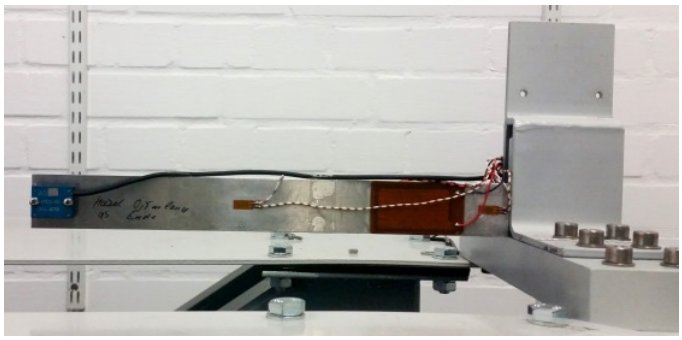

Figure 4.5: Flexible beam setup.

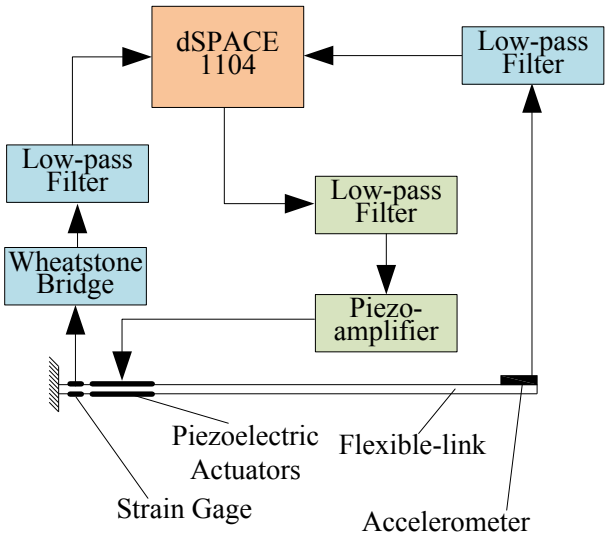

Figure 4.6: Schematic beam setup.

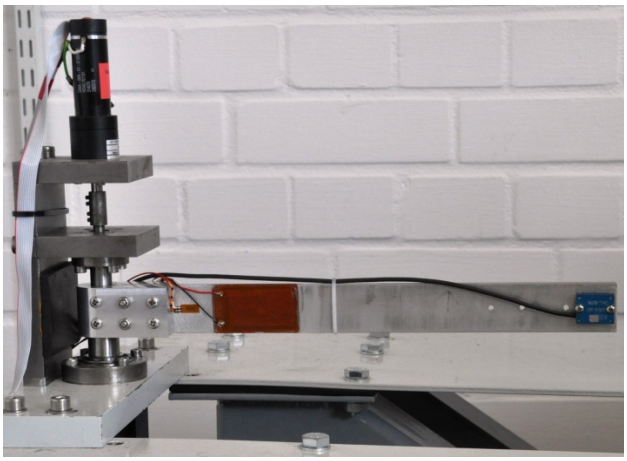

Figure 4.7: One flexible-link robot setup.

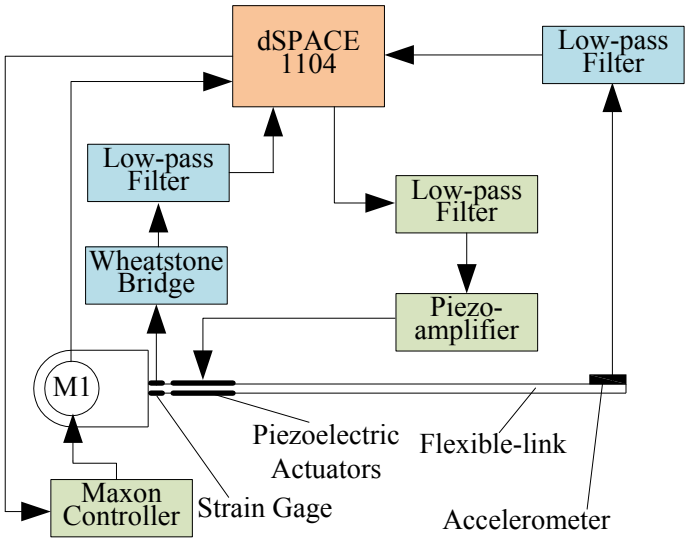

Figure 4.8: Schematic one flexible-link robot setup.

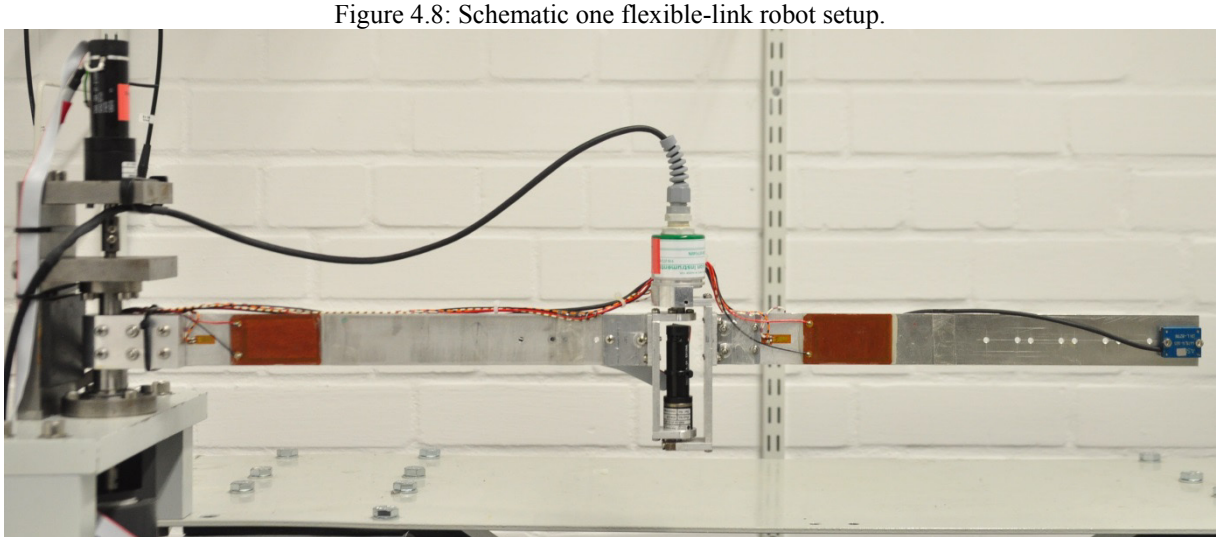

Figure 4.9: Two flexible-link robot setup.

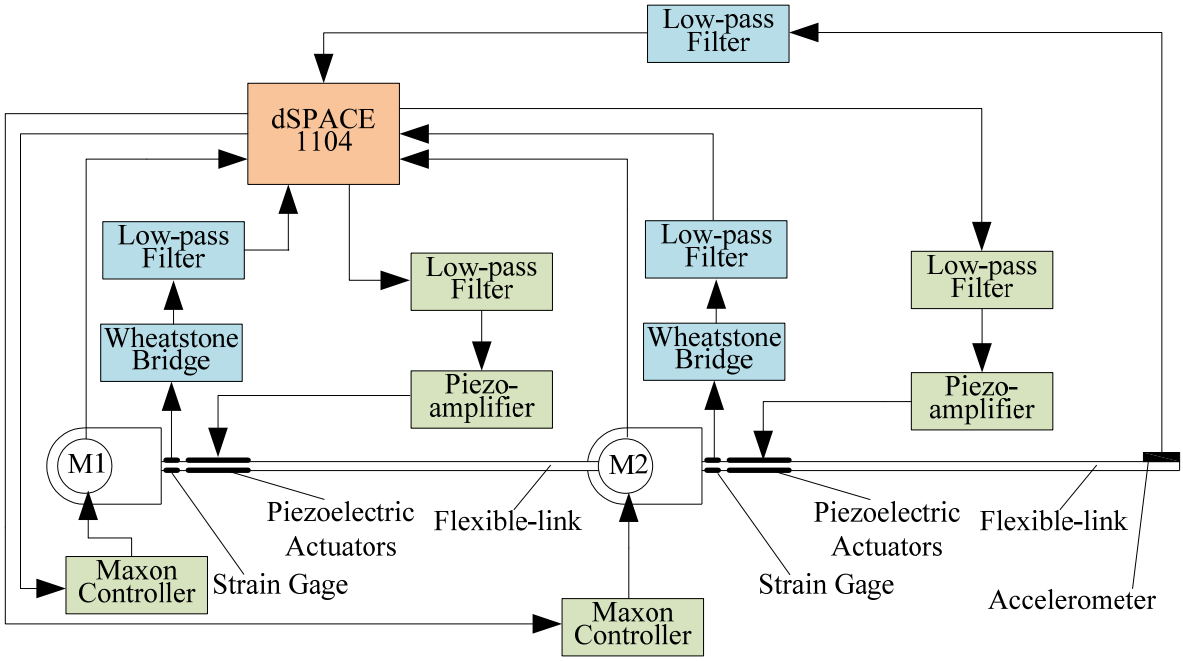

Figure 4.10: Schematic two flexible-link robot setup.

4.2 Experimental Results

Several tests were performed on the flexible structures analyzed in this study. The results are presented using the same order of the control design section. All the implementation was realized in a dSPACE DS1104 control prototyping card. The controllers are implemented using a sampling time of 0.001 s and a continuous solver Runge-Kutta O(4). The proposed controllers include sign functions in their formulation, these are approximated with saturation functions in order to avoid excessive presence of chattering due to the introduced discontinuity. The controllers have been designed to asymptotically force the sliding variable to zero. Therefore, the damping of the structures has been increased. All the robotic structures under study were subjected to acceleration limited joint trajectories, whose parameters are given for each experience. The acceleration and deceleration phases in the two flexible-link robot occur at different times for the two links case in order to have a more demanding situation for the system to be controlled.

4.2.1 Cantilever Beam

Here the controller for the flexible beam (see Fig. 4.5) proposed in section 3.2 is implemented. The controller was designed to increase the structural damping of the beam. For this experience only a pair of sensors located near the clamped end of the beam used. The physical parameters of the beam are given in Tab. 2.1. In Fig. 4.11 and 4.12 are shown the results when the beam is subjected to a transient disturbance. The controller was calculated with $\lambda = 20$.

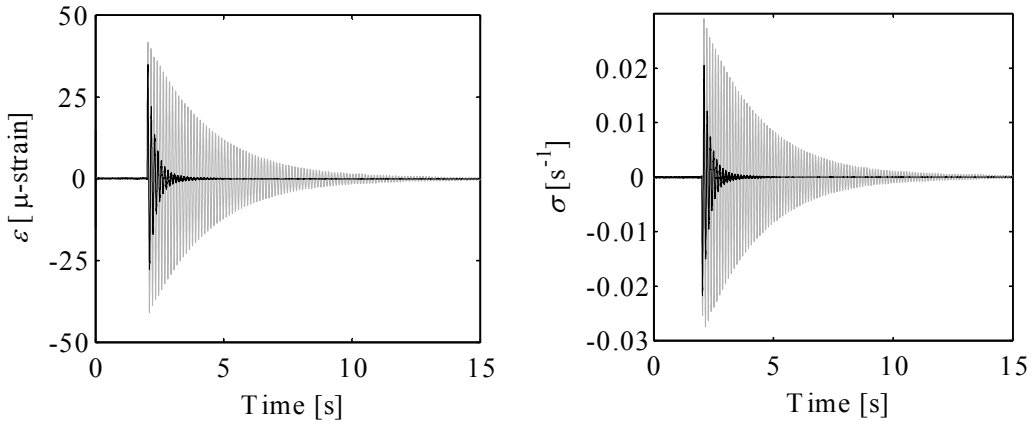

Figure 4.11: Response to a transient disturbance of a flexible beam. Left: deformation, right: sliding flexible variable. Black: Gray: without AVC. Black: with AVC.

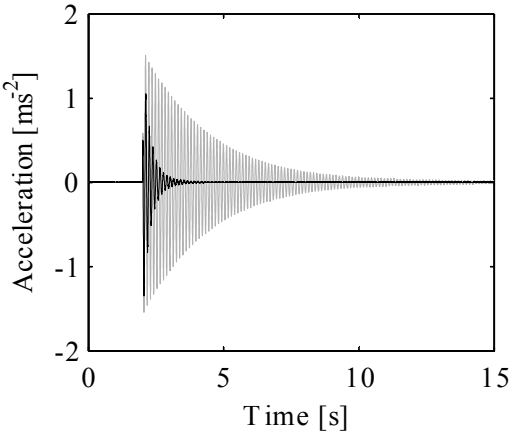

Figure 4.12: Acceleration response to a transient disturbance of a flexible beam.
Gray: without AVC. Black: with AVC.

4.2.2 Dual Loop Approach

This approach is proposed in section 3.3 for both flexible-link robotic structures. The joint are controlled by PID controllers and the vibration of the links is damped out with second order SMC. Therefore, the damping of links has been increased; this can be seen in the transient behavior after reaching the desired position. The AVC controllers were calculated independently for each link.

The one flexible-link robot is subjected to trapezoidal joint trajectory with $\ddot{q}_{1d_{max}} = 4.1\text{rad/s}^2$ and $\dot{q}_{1d_{max}} = 0.8\text{rad/s}$. In Figs. 4.13 and 4.14 are shown the experimental results for the one flexible-link robot for a value of $\lambda = 20\text{m/s}$, $b = 0.75\text{m/s}^3$ $\hat{c} = 1.25\text{m/s}$.

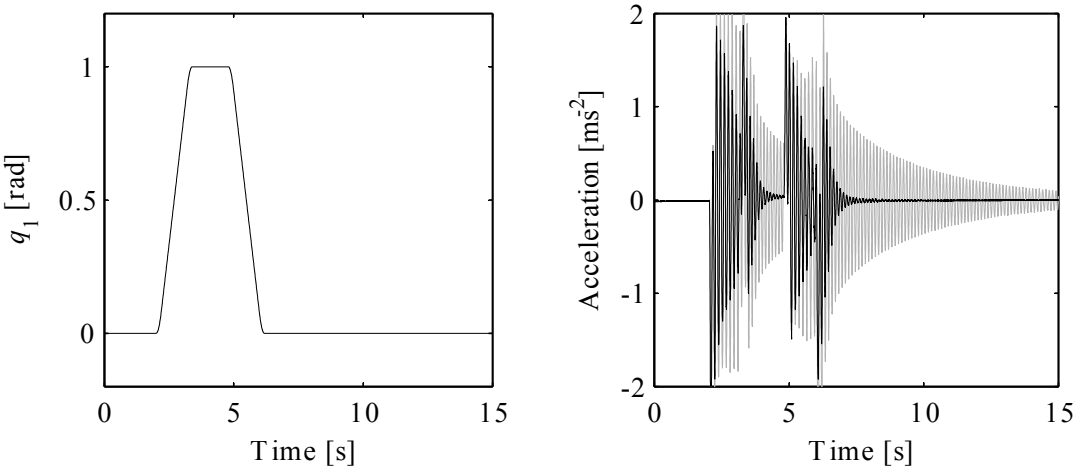

Figure 4.13: Left: joint position, right: acceleration at the tip of the robot.
Gray: without AVC. Black: with AVC.

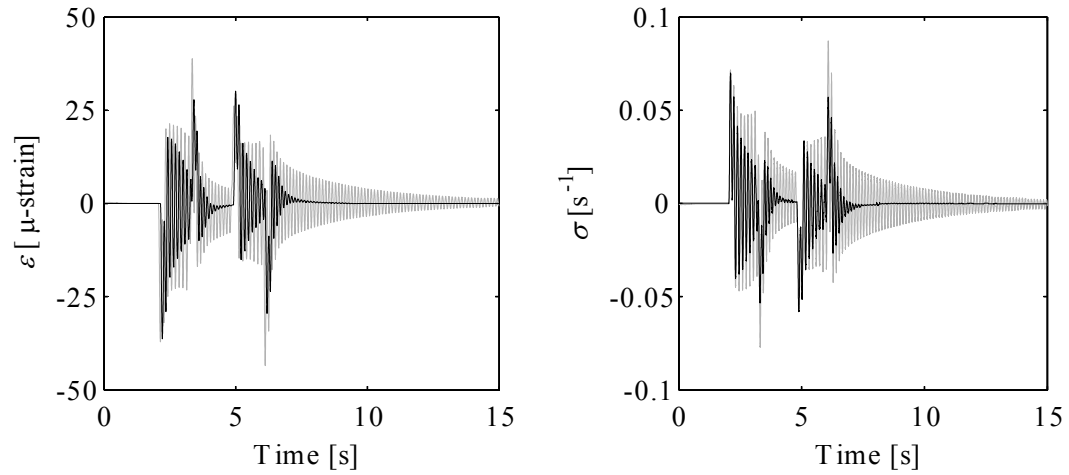

Figure 4.14: Left: deformation, right: sliding variable.
Gray: without AVC. Black: with AVC.

The two flexible-link robot is tested with this approach. Subjected to trajectories for the first joint with $\ddot{q}_{11d_{max}} = 1\text{rad/s}^2$ and $\dot{q}_{11d_{max}} = 0.5\text{rad/s}$, for the second joint with $\ddot{q}_{12d_{max}} = 1.5\text{rad/s}^2$ and $\dot{q}_{12d_{max}} = 0.75\text{rad/s}$. In Figs. 4.15, 4.16 and 4.17 are show the experimental results for the two flexible-link robot for values of $\lambda_1 = 5$, $\lambda_2 = 15$, $b_1 = 40$, $b_2 = 140$, $\hat{c}_1 = 9$ and $\hat{c}_2 = 17$.

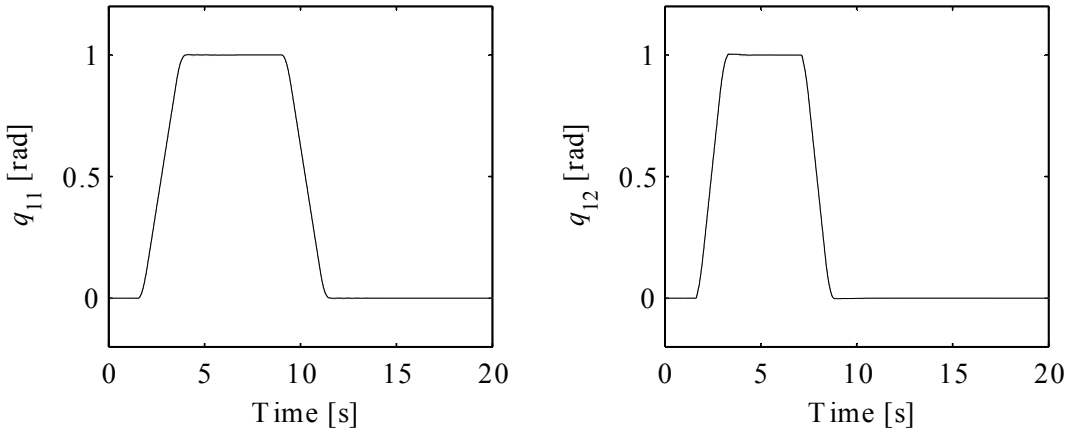

Figure 4.15: Joint position. Left: first joint, right: second joint.
Gray: without AVC. Black: with AVC.

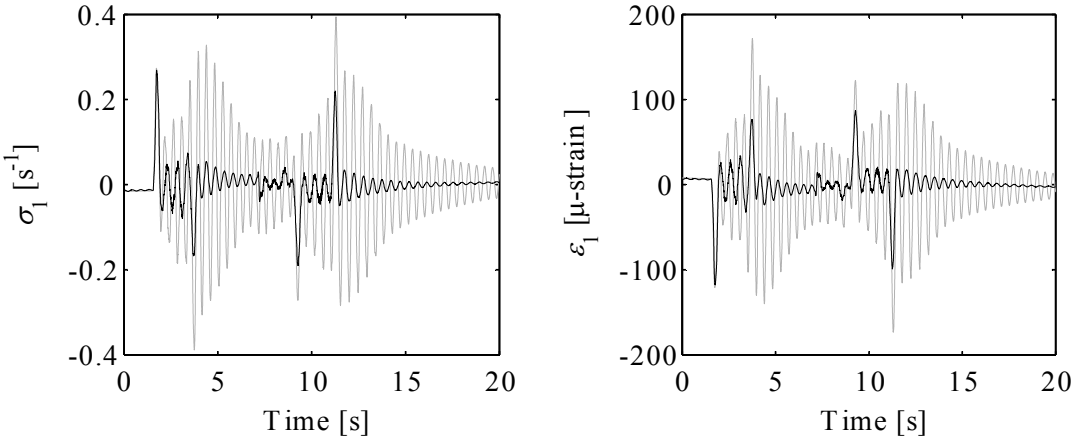

Figure 4.16:First link variables Left: sliding variable, right: deformation.
Gray: without AVC. Black: with AVC.

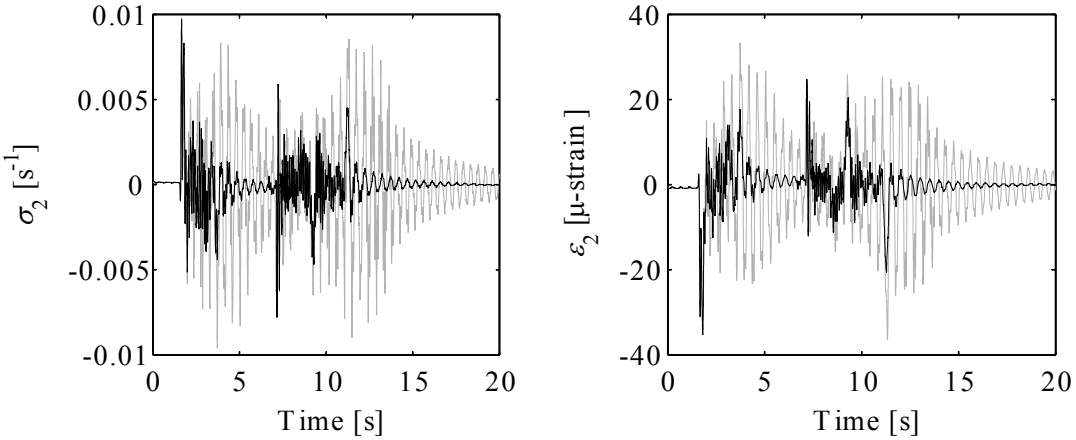

Figure 4.17: Second link variables Left: sliding variable, right: deformation.
Gray: without AVC. Black: with AVC.

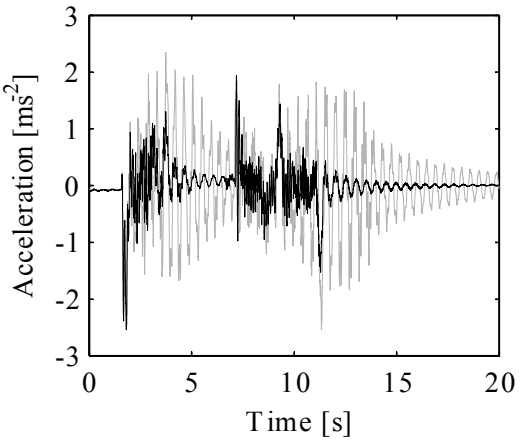

Figure 4.18: Acceleration measured at the tip of the robot.
Gray: without AVC. Black: with AVC.

A good tracking is achieved for both joints and it is improved with the AVC loops. The deformation and sliding variables of the links are shown; from these measurements can be seen that the model used and the control strategy allows not only the improvement of links damping, also to reduce the vibrations during the moving phases as well. The time evolution of the sliding variables is shown, accomplishing the pursued objective, the AVC makes the system to reach faster the sliding surface. Tip acceleration shows the decrease in settling time with the inclusion of the AVC loops

4.2.3 Centralized Approach

This approach is proposed in section 3.4 for both flexible-link robotic structures. Here only one controller was calculated for each robot. The MIMO controller includes the MIMO model in its structure, then it considers the relationship between the rigid and flexible variables.

The one flexible-link robot is subjected to trapezoidal joint trajectory with $\ddot{q}_{1d_{max}} = 4.1 \text{rad/s}^2$ and $\dot{q}_{1d_{max}} = 0.8 \text{rad/s}$. In Figs. 4.19, 4.20 and 4.21 are show the experimental results for the one flexible-link robot for a value of $\lambda_1 = 30$, $\lambda_2 = 25$, $\rho_1 = 0.125$, $\rho_2 = 0.75$.

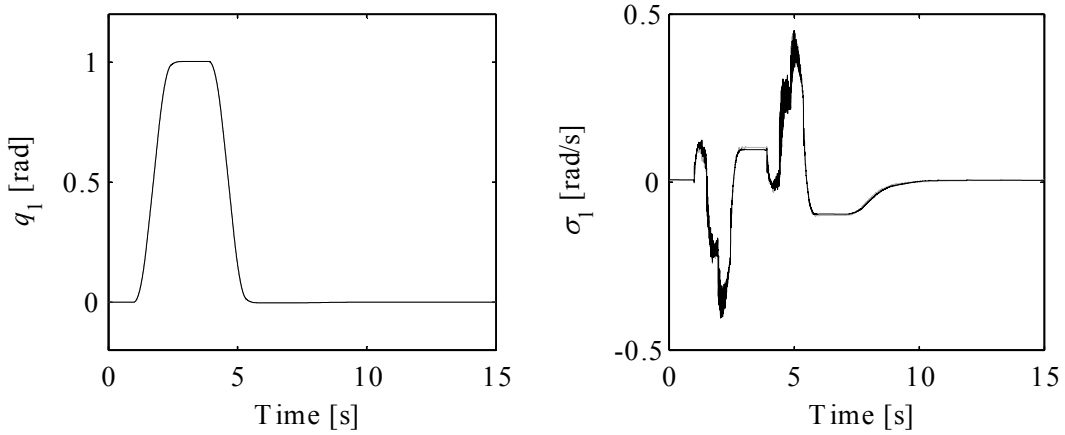

Figure 4.19: Left: joint position, right: joint sliding variable.
Gray: without AVC. Black: with AVC.

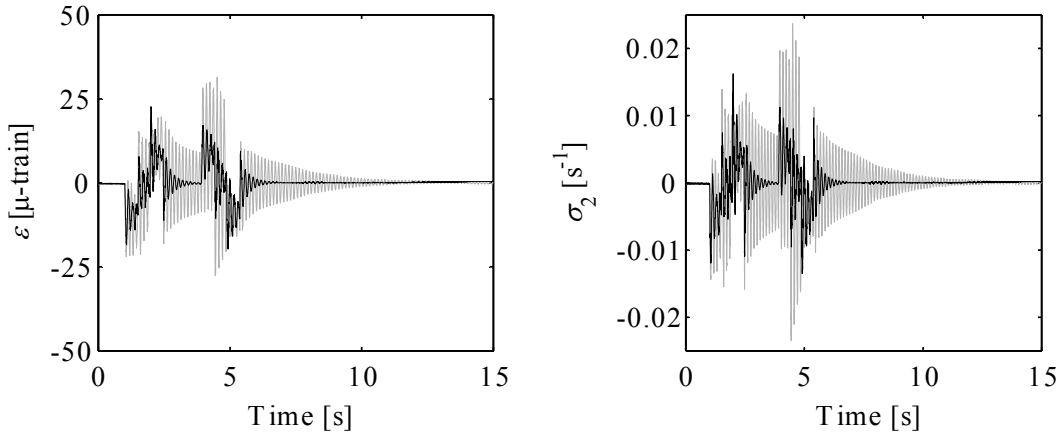

Figure 4.20: Left: deformation, right: flexible sliding variable.
Gray: without AVC. Black: with AVC.

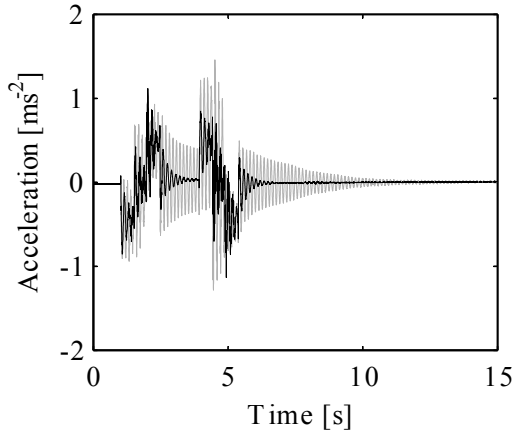

Figure 4.21: Acceleration measured at the tip of the robot.
Gray: without AVC. Black: with AVC.

The joint follows the prescribed trajectory with a small overshoot. Regarding acceleration and deformation, both have a similar behavior, where the damping of the flexible link has been significantly increased, also in the moving stages the vibration is also reduced. It can be seen that then piezoelectric actuators do not have influence on the convergence of the joint sliding variable, this is due to the clamped boundary condition assumed during the modeling process. On the other hand, with the influence of the piezoelectric actuators the sliding mode variable related to the flexible link decays to zero faster.

The two flexible-link robot is also tested with this approach. Subjected to trajectories for the first joint with $\ddot{q}_{1d_{max}} = 1\,\mathrm{rad/s^2}$ and $\dot{q}_{1d_{max}} = 0.5\,\mathrm{rad/s}$, for the second joint with $\ddot{q}_{2d_{max}} = 1.5\,\mathrm{rad/s^2}$ and $\dot{q}_{2d_{max}} = 0.75\,\mathrm{rad/s}$. In Figs. 4.22, 4.23, 4.24, 4.25 and 4.26 are shown the experimental results for the two flexible-link robot for a value of $\lambda_1 = 5$, $\lambda_2 = 7$, $\lambda_3 = 5$, $\lambda_4 = 10$, $\rho_1 = 0.006$, $\rho_2 = 0.003$ $\rho_3 = 0.115$ and $\rho_4 = 0.15$.

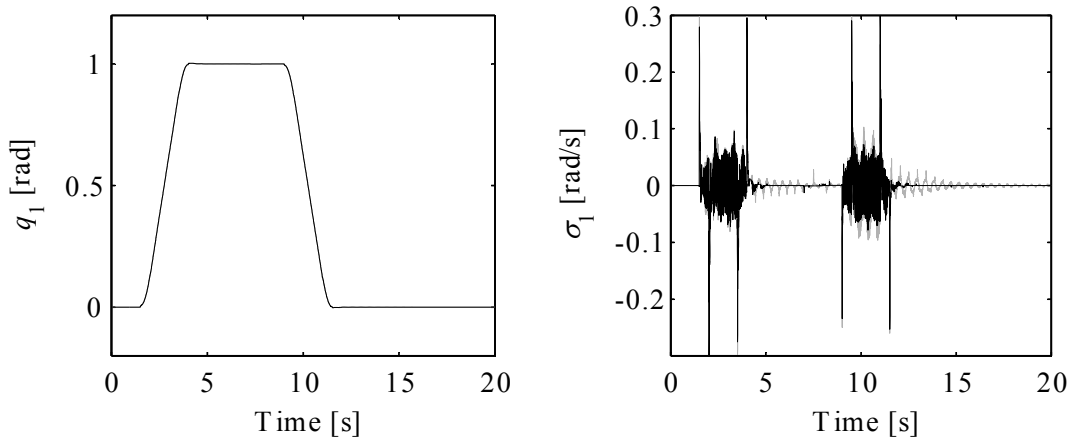

Figure 4.22: First joint. Left: joint position, right: joint sliding variable.
Gray: without AVC. Black: with AVC.

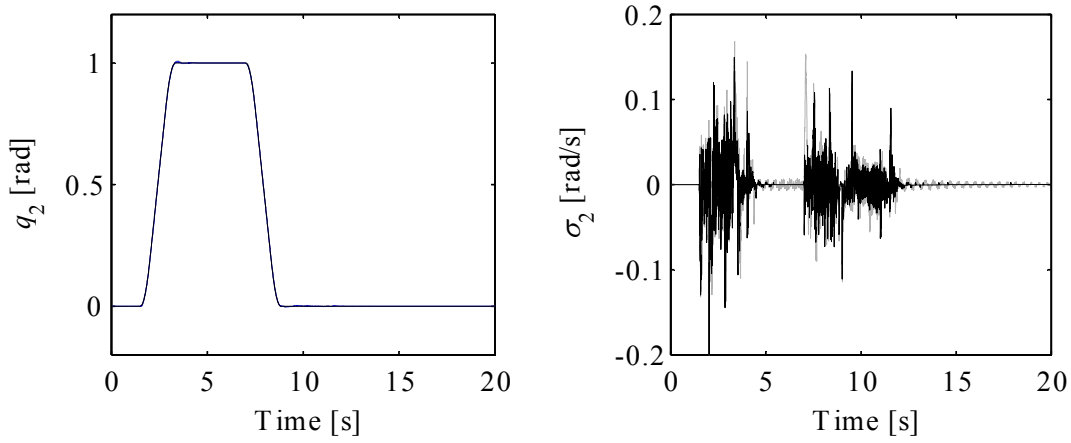

Figure 4.23: Second joint. Left: joint position, right: joint sliding variable.
Gray: without AVC. Black: with AVC.

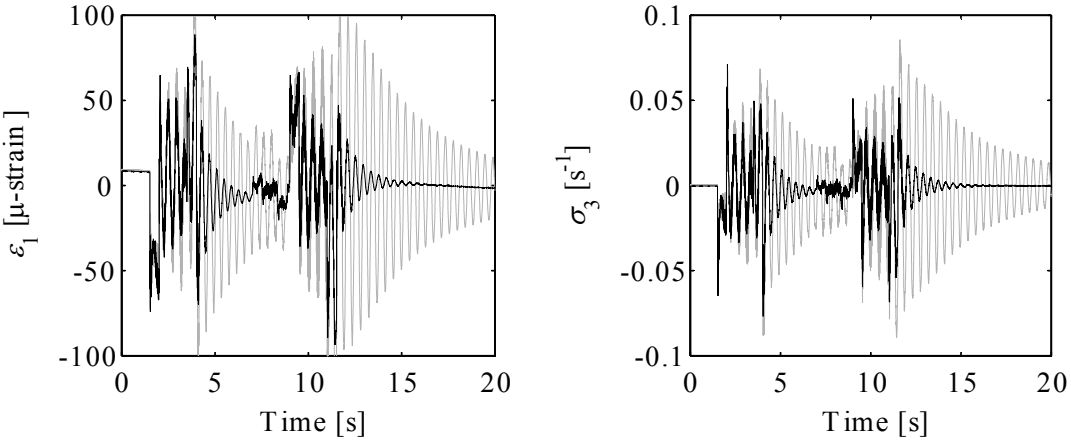

Figure 4.24: First link. Left: deformation, right: flexible sliding variable.
Gray: without AVC. Black: with AVC.

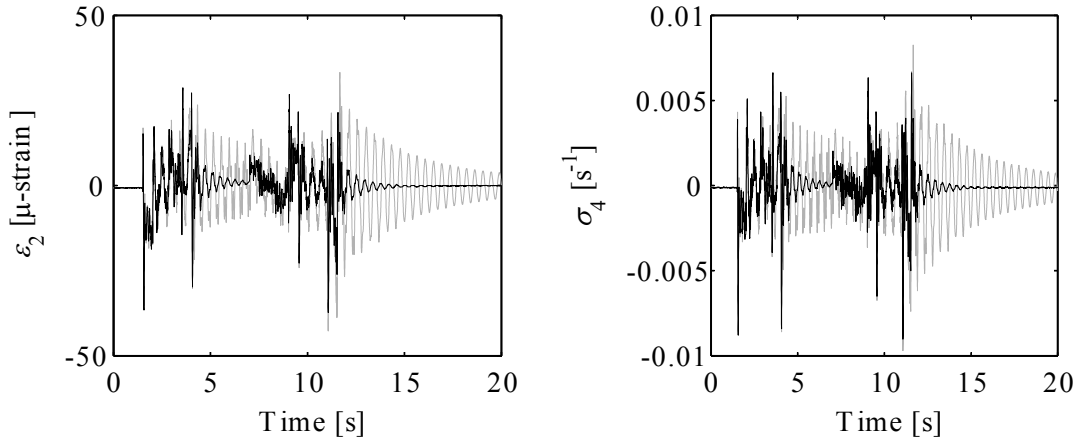

Figure 4.25: Second link. Left: deformation, right: flexible sliding variable.
Gray: without AVC. Black: with AVC.

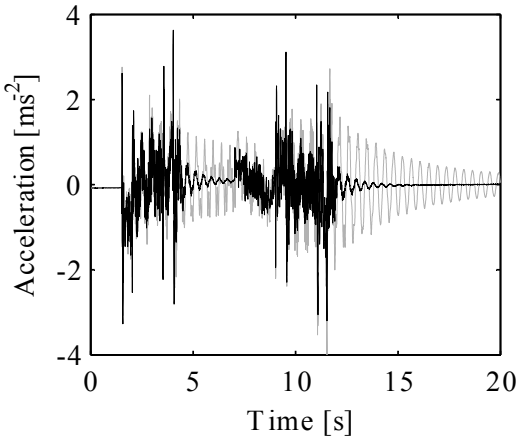

Figure 4.26: Acceleration measured at the tip of the robot.
Gray: without AVC. Black: with AVC.

Here also a good tracking is achieved with a small overshoot which is attenuated with the piezoelectric actuators. The sliding variables related to the joints confirm the influence of the piezoelectric actuators on the improvement of the damping and its influence on joint tracking, this more evident for the first joint as long as the PZTs reduce the structural vibration and it has a direct influence on joint positioning. The deformations of links confirm that control strategy allows not only the improvement of links damping, but also to reduce the vibrations during the moving phases. Furthermore, the links are passive elements and with the piezoelectric AVC complement the sliding surface is reached faster resulting in a shorter settling time. The acceleration measurement at the tip of the robot also confirms the improvement of the damping.

4.2.4 Decentralized Approach

This approach is proposed in section 3.4.3 for the two flexible-link robot. For this experience two MIMO controllers were calculated for each joint flexible link group. This controller does not contain all the dynamics information of the robot because it does not contain coupling terms between the links. But it represents a less complex control structure to increase the damping of the robot compared with the centralized approach.

The two flexible-link robot is tested with this approach. Subjected to trajectories for the first joint with $\ddot{q}_{11\mathrm{d}_{\max}} = 1\,\mathrm{rad/s^2}$ and $\dot{q}_{11\mathrm{d}_{\max}} = 0.5\,\mathrm{rad/s}$, and for the second joint with

$\ddot{q}_{12d_{max}} = 1.5\,\mathrm{rad/s^2}$ and $\dot{q}_{12d_{max}} = 0.75\,\mathrm{rad/s}$. In Figs. 4.27, 4.28, 4.29, 4.30 and 4.31 are shown the experimental results for the two flexible-link robot for a value of $\lambda_{11} = 5$, $\lambda_{12} = 5$, $\rho_{11} = 0.012$, $\rho_{12} = 0.2$, $\lambda_{21} = 7$, $\lambda_{22} = 10$, $\rho_{21} = 0.006$ and $\rho_{22} = 0.15$.

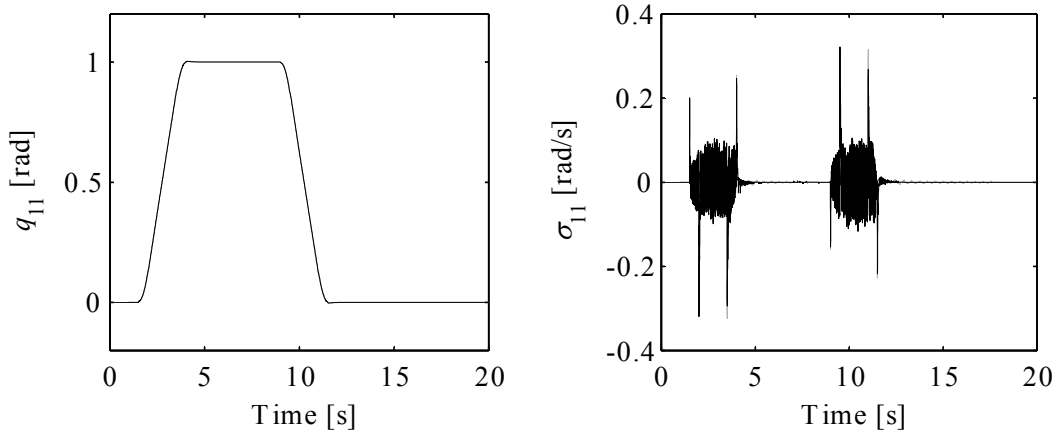

Figure 4.27: First joint. Left: joint position, right: joint sliding variable.
Gray: without AVC. Black: with AVC.

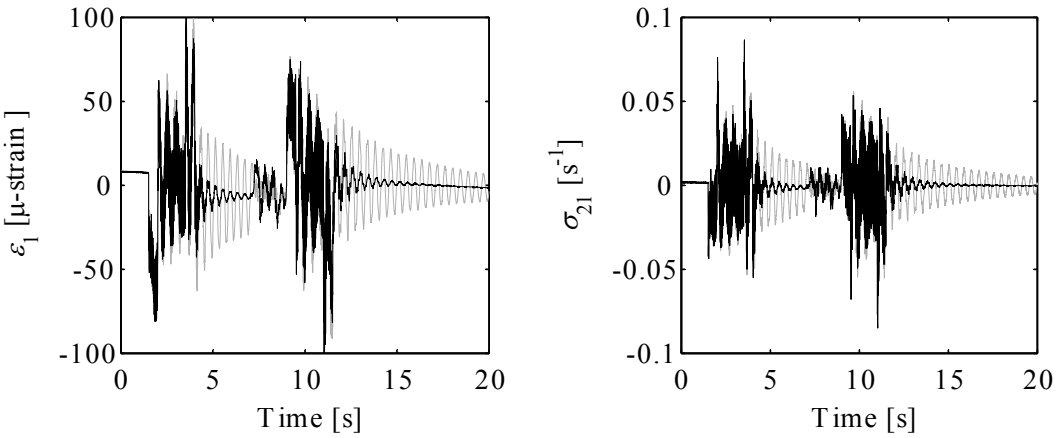

Figure 4.28: First link. Left: deformation, right: flexible sliding variable.
Gray: without AVC. Black: with AVC.

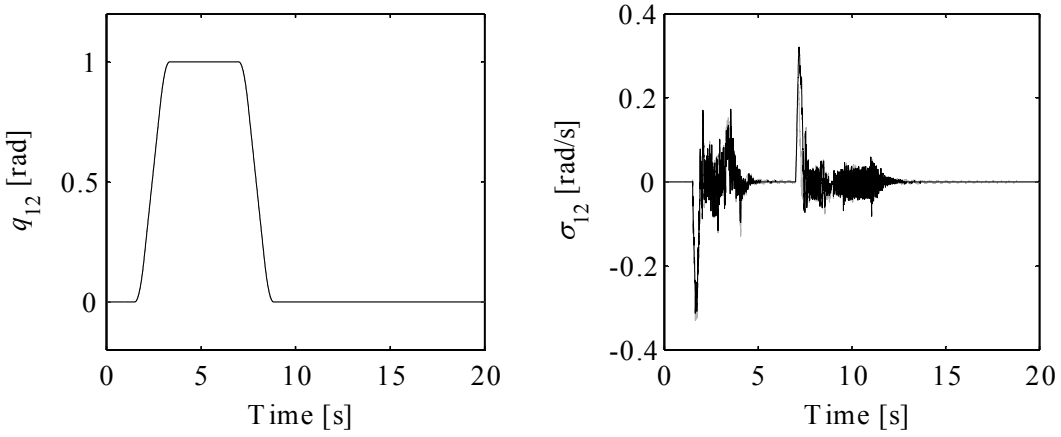

Figure 4.29: Second joint. Left: joint position, right: joint sliding variable.
Gray: without AVC. Black: with AVC.

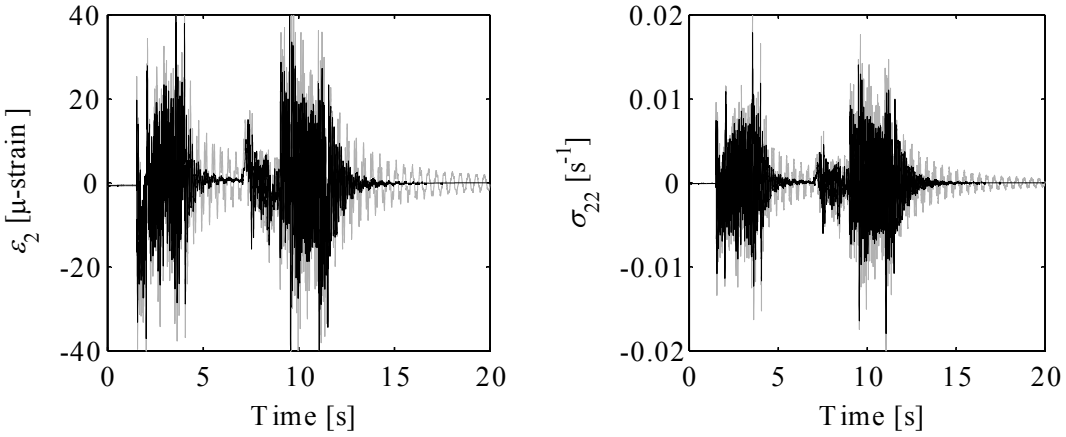

Figure 4.30: Second link. Left: deformation, right: flexible sliding variable.
Gray: without AVC. Black: with AVC.

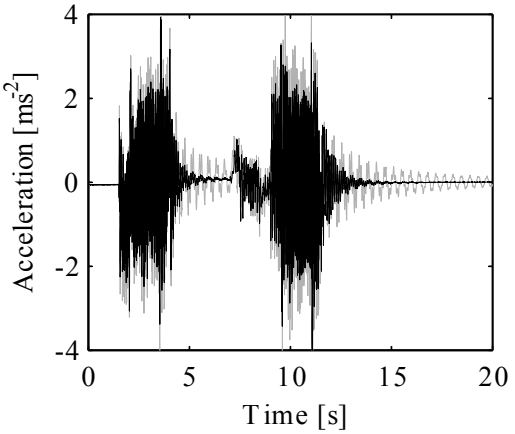

Figure 4.31: Acceleration measured at the tip of the robot.
Gray: without AVC. Black: with AVC.

Here at joint level a good trajectory tracking is achieved for both joints. Again as in the one flexible-link robot the piezoelectric actuators do not have influence on the position of the joints. The deformation of the links is shown, where the vibration of the first link has a considerable influence in the whole structure. The sliding variable fluctuates considerably during the moving phase because the connection between the two links is not considered, but the objective is to decrease the settling time which is accomplished even with this approximation. Nevertheless, the piezoelectric actuators have less influence in the moving phase.

4.3 Discussion of Results

The development of models of flexible-link structures is a demanding and time-consuming task and its complexity increases significantly when the number flexible or rigid DOF is bigger. Hence considerable amount of research can be found for the one flexible-link case, whereas for the two flexible-link case with experimental results the amount is considerably reduced and for the multi flexible-link case only some simulation results can be found. In the model formulation presented in this work two flexible DOF are considered for each link. Indeed for the model-based controllers reduced versions of the complete models are used. It introduces deviations or uncertainties between the model and the real system. The uncertainties are unavoidable, they were treated with robust control strategies, namely SMC (described in chapter 3).

The experimental results show that it is possible to reduce the unwanted vibration in flexible-link structures by means of piezoelectric actuators using AVC techniques with SMC. All the proposed control approaches fulfill their objective of reducing the settling time. Consequently, the formulated models contain the required information about the dynamic of the system. The model used for calculation of the decentralized controller, although it neglects the interaction between the links, is also capable to reduce the unwanted vibrations. Similarly the dual loop controller can reduce the vibration by increasing independently the damping of the links. The flexible-link robots object of this work are subjected to the same conditions under the same joint conditions to compare with each other. In Tab. 4.1. The faster rejection of vibration is obtained in the cantilever beam. The best performance in the flexible-link robots is obtained with the centralized controller; it was expected to be so, as long as the model used for the controller is MIMO. Similarly the dual loop and decentralized controller reduce the vibration but in longer times, nevertheless the controller complexity is much lower.

Table 4.1 Settling time comparison for the proposed control approaches (values in s)

	Dual loop		Centralized		Decentralized	
Structure	Without AVC	With AVC	Without AVC	With AVC	Without AVC	With AVC
Cantilever beam	-	-	11.67	1.61	-	-
One flexible-link robot	18.18	3.73	7.91	1.68	-	-
Two flexible-link robot	13.17	5.58	10.9	3.08	11.76	3.52

Considering the selection between the proposed controllers, for the flexible-link robots for low joint speeds the dual loop is a possible choice due to its lower computational complexity at the expense of performance. On the other hand, if good performance is required the centralized approach must be the choice taking into account the higher calculation capability required for the implementation. This is summarized in Fig. 4.32. Furthermore, if the robot is going to operate at higher speeds than the used in the experiments the centralized approach is recommended, considering the fact that the effect of nonlinearities of the model increases with the operational joint speed.

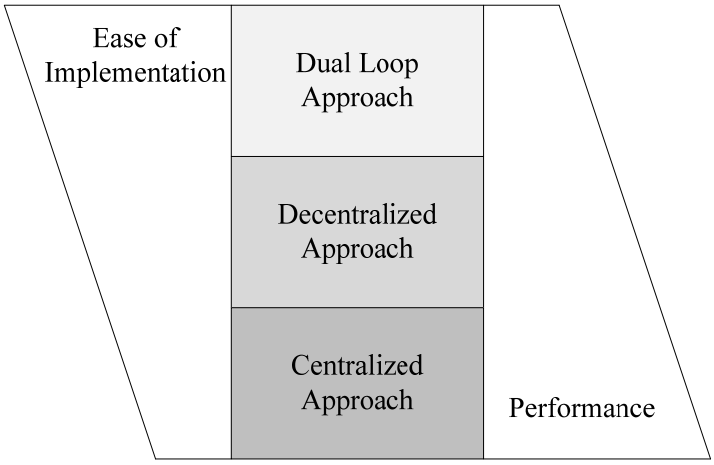

Figure 4.32: Comparison in performance and ease of implementation of the proposed control approaches.

Other aspect to be taken into account is the adjustment of the rate of convergence λ, because this value is primary limited to be a fraction of the first nonmodeled natural frequency. During the control design for the two flexible-link robot, it was assumed that the first nonmodeled dynamics was due to the second mode of flexion. However during the implementation, the controller suffers from unexpected excessive chattering. Then after plotting the spectrograms of the signals acquired from the real system a new component appeared in the scene: a

torsional mode for the first link due to the inertia of the second joint (see Figs. 2.56 and 2.57). Hence this value of frequency defined a lower boundary value for λ.

5 Summary and Conclusions

This work bears with the modeling and control of flexible-link structures using model-based controllers with SMC complement. The models and the systems were used to extract the information required for controllers formulation. Then boundary values of matched uncertainties or the model itself is included in the controller if necessary by the control approach. To the best authors knowledge, it is novel and has not been yet reported in the literature.

Novel kinematic considerations were taken into account in the model formulation, incorporation of clamped offset to consider rigid support of the flexible links, normally the flexible link is assumed to start at the joint rotational axis. Additionally, the distal joint is divided into relative fixed and movil parts, thus different angular positions and velocities as well as inertias can be considered due to the induced gearbox inertia. The models were formulated following the Lagrangian formalism with a recursive kinematic formulation, the discretization of the distributed flexibility was done using AMM. Under the assumption of clamped-free boundary conditions the natural frequencies and modes of deformation were calculated. Then the equations of motion were assembled in a novelty manner, where the terms associated to the distributed mass and flexibility are separated from those related to the rigid and concentrated mass. This provides an environment to monitor the contribution of different model components in the dynamic behavior of the flexible-link robots. Furthermore, the models were evaluated under a novel proposed verification process which took into account the formal properties of robot models. Indeed, the robots model were calculated through two independent ways and subsequently compared in simulations, the evaluation process showed correspondence between the models. Conversely, the models of robots found in the literature are only subjected to debugging processes, but in this work the debugging process is accompanied with additional tests to triangulate and contrast the simulation results. The validation process was performed exciting the structures and their models with a chirp signal through the piezoelectric actuators and bang-bang torque signal through the rotational actuators. The responses were compared and there were some discrepancies for frequencies above 30 Hz. It was due to non modeled nonlinearities that introduce overtones from the chirp signal and prematurely excited higher modes of the structure, specially a torsional mode in the first link. This discrepancy beetwen the model and real system was considered during the control design including a robust complement.

The controllers were calculated from the models. The boundaries of the rates of convergence defined in the sliding surfaces depend on the natural frequencies of the system/model which have a direct influence on the induced damping. So in the dual loop approach the model provides also the boundaries of the uncertainties and nonliniearities then the rate of convergence is defined for implementation. In contrast, the Lyapunov model-based controllers are calculated with predefined rates of convergence then with the model and the physical system the discrepancies are estimated with a novel proposed methodology. The discrepancies due to model errors or uncertainties are atenuated with sliding mode complement. As long as the models of the flexible-link robots are nonlinear, the resulting controllers are also nonlinear. Hence the controllers are capable to increase the damping of the flexible links and for the robots provide good trajectory tracking, thus considerable reduction of settling time. The experimental results demonstrate that the consideration of one flexible DOF for each link provides a model with enough information of the dynamics of the system to reject unwanted vibrations during the moving and settling phases. Also the experimental

results showed that approximating to a linear behavior of the piezoelectric actuators the control objectives can be achieved.

The future work will be focused in the model by the inclusion of: additional flexible DOF, joint flexibility, torsional DOF in the first link and incorporation of an additional rigid first link. There are proposals to improve the performance of the controllers such as development of robust-adaptive or intelligent control strategies to overcome the changes in payload and incorporation of input shaping prefilters to the existing controllers.

Appendix A Influence of Piezoelectric Actuators

A.1 Model of Piezoelectric Actuators

The piezoelectric actuators are bonded at each side of the flexible beam in order to get a bigger moment. Their location along the flexible beam is shown in Fig. A.1.

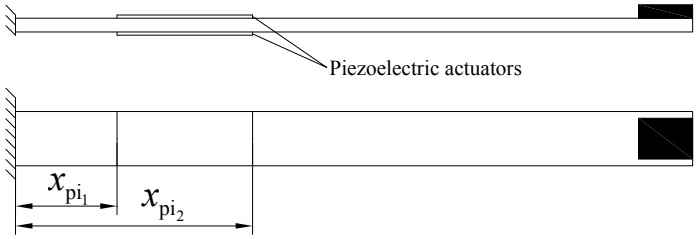

Figure A.1: Transversal section of the beam in the actuator location.

The pairs of piezoelectric actuators are located along the flexible beam according to the principle of maximal modal deformation [114], which is also confirmed by the second derivative of the mode shapes for the links. A linear distribution of the normal stress is assumed. The energy added to the flexible beam by a pair of symmetric located patch piezoelectric actuators is given by

$$W = M_{\mathrm{pi}}(x,t)\frac{\partial^2 w(x,t)}{\partial x^2}. \tag{A.1}$$

The bending moment applied along the piezoelectric actuators on the beam is stated as

$$M_{\mathrm{pi}}(x,t) = \bar{c}v_{\mathrm{pi}}(t)\left(\theta(x-x_{\mathrm{pi}_2}) - \theta(x-x_{\mathrm{pi}_1})\right), \tag{A.2}$$

where $\bar{c}$ is a constant which depends on physical properties of the actuator, $v_{\mathrm{pi}}(t)$ is the voltage applied and $\theta(x)$ is the unit step function. $\bar{c}$ is given by [115]

$$\bar{c} = -\frac{1}{2}d_{31}E_{\mathrm{pi}}b_{\mathrm{pi}}\left(t_{\mathrm{b}} + t_{\mathrm{pi}}\right). \tag{A.3}$$

Using the AMM discretization approach and substituting (A.2) in (A.1)

$$W = M_{\mathrm{pi}}(x,t)\sum_{i=1}^{n}\phi_i''(x)\,q_i(t). \tag{A.4}$$

The evaluation is done in the domain of influence of the piezoelectric actuators

$$W = \int_{x_{\mathrm{pi}_1}}^{x_{\mathrm{pi}_2}} \bar{c}v_{\mathrm{pi}}(t)\sum_{i=1}^{n}\phi_i''(x)\,q_i(t)dx, \tag{A.5}$$

$$W = \left(\bar{c}v_{\mathrm{pi}}(t)\sum_{i=1}^{n}\phi_i'(x)\,q_i(t)\right)\Bigg|_{x_{\mathrm{pi}_1}}^{x_{\mathrm{pi}_2}}. \tag{A.6}$$

In order to adequate the equation form to the model of the robot the following reformulation is performed

$$W = \boldsymbol{M}_{\mathrm{pi}}^{\mathrm{T}}\boldsymbol{q}(t) \tag{A.7}$$

where

$$\boldsymbol{M}_{\mathrm{pi}}^{\mathrm{T}} = \bar{c}\left[\phi_1'(x_{\mathrm{pi}_2}) - \phi_1'(x_{\mathrm{pi}_1}) \quad \phi_2'(x_{\mathrm{pi}_2}) - \phi_2'(x_{\mathrm{pi}_1}) \quad \cdots \quad \phi_n'(x_{\mathrm{pi}_2}) - \phi_n'(x_{\mathrm{pi}_1})\right] v_{\mathrm{pi}}(t) \tag{A.8}$$

$\boldsymbol{M}_{\mathrm{pi}}$ contains the influence of the applied bending moment related to each flexible DOF. For the case of the flexible beam it is associated to the input matrix in the following way

$$\boldsymbol{M}_{\mathrm{pi}} = \boldsymbol{B}_{\mathrm{pi}} v_{\mathrm{pi}}(t)\,. \tag{A.9}$$

In the model of the flexible beam two flexible DOF are considered, then the input matrix in given by

$$\boldsymbol{B}_{\mathrm{pi}} = \left[\bar{c}\left(\phi_1'(x_{\mathrm{pi}_2}) - \phi_1'(x_{\mathrm{pi}_1})\right) \;\; \bar{c}\left(\phi_2'(x_{\mathrm{pi}_2}) - \phi_2'(x_{\mathrm{pi}_1})\right)\right]^{\mathrm{T}}. \tag{A.10}$$

The piezoelectric patch actuators are symmetrically placed to the flexural neutral axis of the links in order to obtain a maximal applied moment, where the control signal to each patch is inverted with respect to the other i.e. when an actuator is subjected to compression its counterpart is subjected to extension (see Fig. A.2).

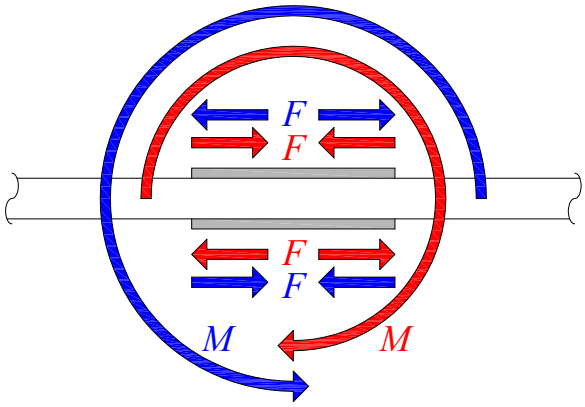

Figure A.2: Moment applied by the piezoelectric actuators.

A.2 Influence of Piezoelectric Actuators in Energy Balance

The inclusion of piezoelectric actuators during the energy formulation introduces some changes in the formulation. But here it will be shown that these effects can be neglected. The physical parameters of the beam are given in Tab. 2.1 and the transversal section of the actuator and beam are shown in Fig. A.3.

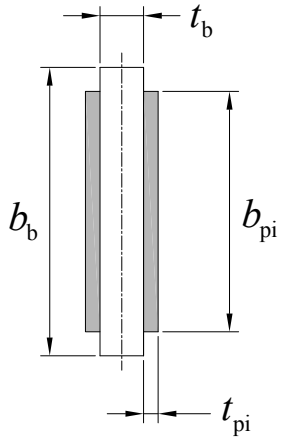

Figure A.3: Transversal section of the beam in the actuator location.

The lateral bending occurs with respect to the vertical symmetry axis. Perfect bonding is assumed between actuator and flexible beam. The second moment of area of the actuators with respect to the bending axis after applying Steiner's theorem is given by

$$I_{\mathrm{pi}} = b_{\mathrm{pi}}\left(\frac{2}{3}t_{\mathrm{pi}}^3 + t_{\mathrm{pi}}^2 t_{\mathrm{b}} + \frac{t_{\mathrm{pi}} t_{\mathrm{b}}^2}{2}\right). \tag{A.11}$$

The orthogonality condition is modified to include the piezoelectric actuators

$$\int_0^l \rho_{\mathrm{l}}\, \phi_i(x)\, \phi_j(x)\, dx + m_{\mathrm{p}}\, \phi_i(l)\, \phi_j(l) + J_{\mathrm{p}}\, \phi_i'(l)\, \phi_j'(l) + \int_{x_{\mathrm{pi_l}}}^{x_{\mathrm{pi2}}} \rho_{\mathrm{pi}}\, \phi_i(x)\, \phi_j(x)\, dx = m_{\mathrm{l}} \delta_{ij}, \tag{A.12}$$

with this modified orthogonality condition and the boundary conditions given in section 2.1.2. Then the mode shapes are calculated, in Fig. A.4 the mode shapes with and without piezoelectric actuators are shown.

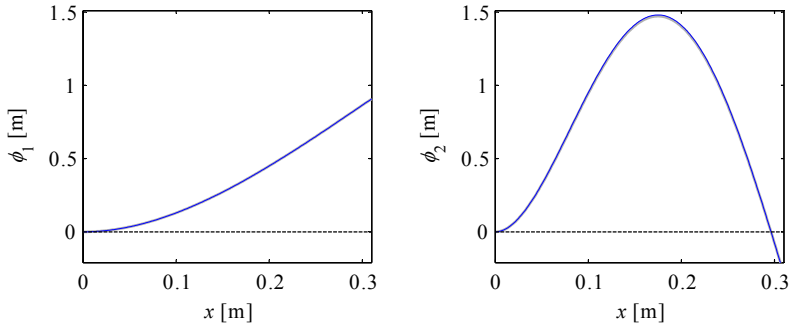

Figure A.4: Comparison of the mode shapes.

The presence of the piezoelectric actuators has very small influence on the mode shapes, the biggest deviation occurs for the second mode in the peak of the curve but it still remain small (see Fig. A.5).

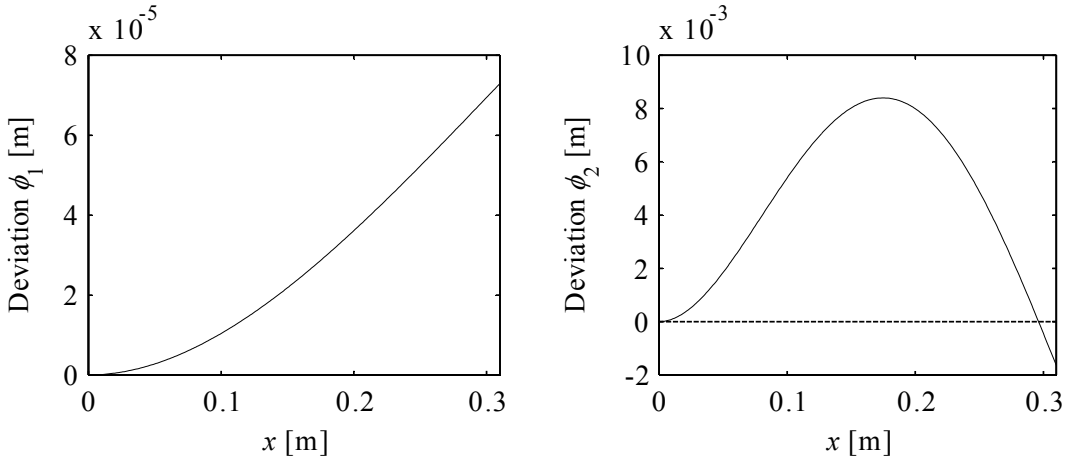

Figure A.5: Deviation of the mode shapes.

The potential energy for the beam needs to include the strain energy stored product of the actuators' deformations, the potential energy can be expressed as

$$U = \frac{1}{2} EI \int_0^l \left(\frac{\partial^2 w(x,t)}{\partial x^2}\right)^2 dx + \frac{1}{2}(EI)_{\mathrm{a}} \int_{x_{\mathrm{pi_l}}}^{x_{\mathrm{pi2}}} \left(\frac{\partial^2 w(x,t)}{\partial x^2}\right)^2 dx. \tag{A.13}$$

Applying the Lagrangian formalism for the potential energy and considering two flexible DOF

$$\frac{\partial U}{\partial q_1}=\left(EI\int_0^l \phi_1''^2(x)dx+\left(EI\right)_{\text{pi}}\int_{x_{\text{pi}_1}}^{x_{\text{pi}_2}}\phi_1''^2(x)dx\right)q_1(t)+\left(EI\int_0^l \phi_1''(x)\phi_2''(x)dx+\left(EI\right)_{\text{pi}}\int_{x_{\text{pi}_1}}^{x_{\text{pi}_2}}\phi_1''(x)\phi_2''(x)dx\right)q_2(t) \tag{A.14}$$

$$\frac{\partial U}{\partial q_2}=\left(EI\int_0^l \phi_1''(x)\phi_2''(x)dx+\left(EI\right)_{\text{pi}}\int_{x_{\text{pi}_1}}^{x_{\text{pi}_2}}\phi_1''(x)\phi_2''(x)dx\right)q_1(t)+\left(EI\int_0^l \phi_2''^2(x)dx+\left(EI\right)_{\text{pi}}\int_{x_{\text{pi}_1}}^{x_{\text{pi}_2}}\phi_2''^2(x)dx\right)q_2(t) \tag{A.15}$$

From these expressions the stiffness of the beam can be formulated

$$k_{1,1}=EI\int_0^l \phi_1''^2(x)dx+\left(EI\right)_{\text{pi}}\int_{x_{\text{pi}_1}}^{x_{\text{pi}_2}}\phi_1''^2(x)dx \tag{A.16}$$

$$k_{1,2}=EI\int_0^l \phi_1''(x)\phi_2''(x)dx+\left(EI\right)_{\text{pi}}\int_{x_{\text{pi}_1}}^{x_{\text{pi}_2}}\phi_1''(x)\phi_2''(x)dx\approx 0 \tag{A.17}$$

$$k_{2,1}=EI\int_0^l \phi_1''(x)\phi_2''(x)dx+\left(EI\right)_{\text{pi}}\int_{x_{\text{pi}_1}}^{x_{\text{pi}_2}}\phi_1''(x)\phi_2''(x)dx\approx 0 \tag{A.18}$$

$$k_{2,2}=EI\int_0^l \phi_2''^2(x)dx+\left(EI\right)_{\text{pi}}\int_{x_{\text{pi}_1}}^{x_{\text{pi}_2}}\phi_2''^2(x)dx \tag{A.19}$$

The values of stiffness matrix without piezoelectric actuators

$$\boldsymbol{K}=\begin{bmatrix}135 & 0\\ 0 & 13229\end{bmatrix} \tag{A.20}$$

and with piezoelectric actuators

$$\boldsymbol{K}=\begin{bmatrix}139 & 0\\ 0 & 13031\end{bmatrix}. \tag{A.21}$$

Considering the small changes introduced in the structure the passive effect of the piezoelectric actuator can be neglected without introducing a significant error. The effect of the mass of the piezoelectric actuators is also neglected because the actuators have a very low weight (0.002 g) compared with the flexible links. Besides their low mass, they are located near the rotation axes of the robot. The pair of the one flexible-link robot or the first link of the two flexible-link robot is located near the first joint then it has low velocity and for the second link the piezoelectric actuators have a bigger velocity but are located near the second joint which has around 100 times the mass of the pair of actuators.

Appendix B Kinematic Relations

Direct kinematic modeling of robots with a work space restricted to a plane can be formulated in terms of displacements (vectors) and rotations (matrices).

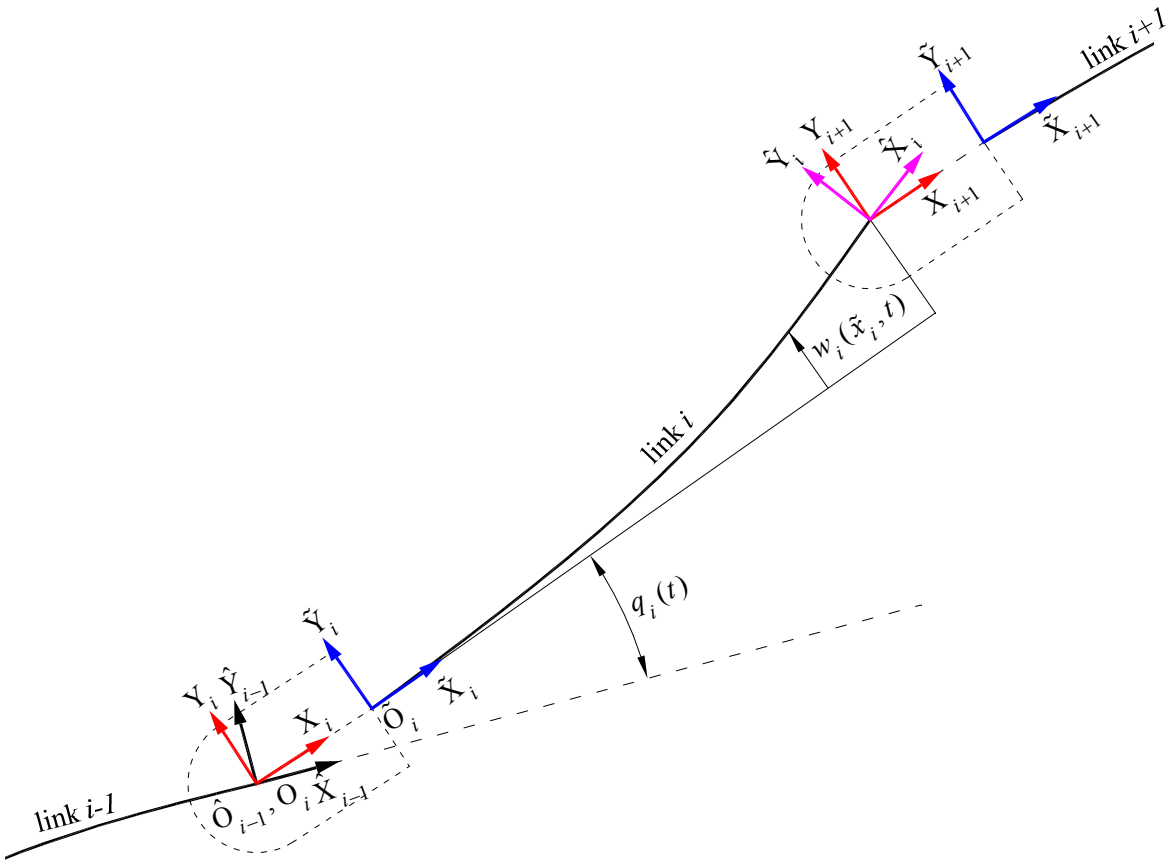

Figure B.1: General frame assignment.

According to Fig. B.2, the absolute position $\boldsymbol{p}_i$ of one point along the flexible link *i* is given by a sum of vectors

$$\boldsymbol{p}_i = \boldsymbol{r}_i + \boldsymbol{W}_i {}^i\boldsymbol{p}_i \ , \tag{B.1}$$

where

$${}^i\boldsymbol{p}_i = {}^i\boldsymbol{r}_{Ci} + {}^i\tilde{\boldsymbol{p}}_i \ , \tag{B.2}$$

$${}^i\boldsymbol{r}_{Ci} = \left[\overline{O_i\tilde{O}_i} \ \ 0\right]^T \ , \tag{B.3}$$

$${}^i\tilde{\boldsymbol{p}}_i = \left[\tilde{x}_i \ \ w_i(\tilde{x}_i, t)\right]^T \ . \tag{B.4}$$

The vector ${}^i\boldsymbol{r}_{Ci}$ is introduced to take into account the rigid displacement added by the clamps. The absolute velocity $\dot{\boldsymbol{p}}_i$ of one point along the flexible link *i* is given by

$$\dot{\boldsymbol{p}}_i = \dot{\boldsymbol{r}}_i + \dot{\boldsymbol{W}}_i {}^i\boldsymbol{p}_i + \boldsymbol{W}_i {}^i\dot{\boldsymbol{p}}_i, \tag{B.5}$$

where

$${}^i\dot{\boldsymbol{p}}_i = {}^i\dot{\tilde{\boldsymbol{p}}}_i = \left[0 \ \ \dot{w}_i(\tilde{x}_i, t)\right]^T . \tag{B.6}$$

Here $\boldsymbol{W}_i$ and $\dot{\boldsymbol{W}}_i$ represent the cumulative transformation and its time-derivative from inertial frame to frame *i*, it will be later explained.

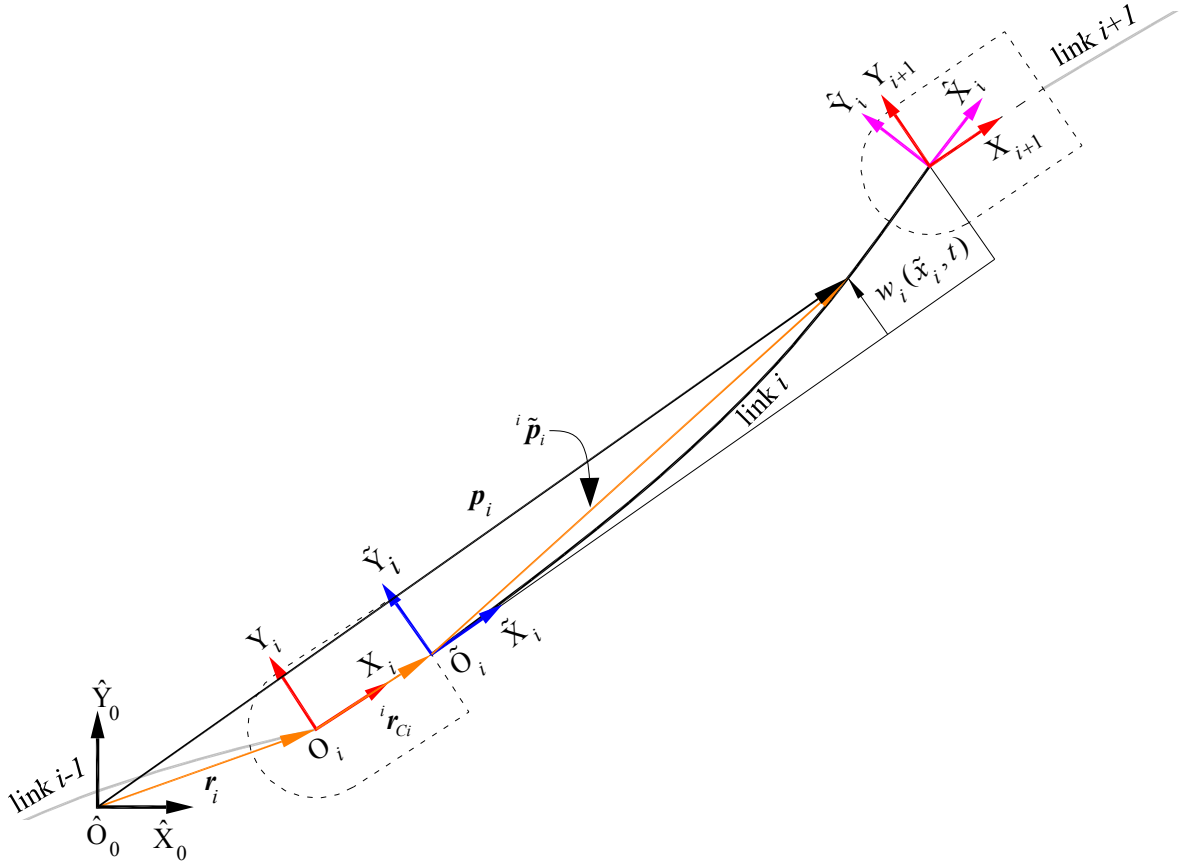

Figure B.2: Definition of absolute position $\boldsymbol{p}_i$ of one point along the link *i*.

In the same manner according to Fig. B.3, the absolute position of end point $\boldsymbol{r}_{i+1}$ and its time derivative $\dot{\boldsymbol{r}}_{i+1}$ of the flexible link *i* are given by

$$\boldsymbol{r}_{i+1} = \boldsymbol{r}_i + \boldsymbol{W}_i\, {}^i\boldsymbol{r}_{i+1}, \tag{B.7}$$

$$\dot{\boldsymbol{r}}_{i+1} = \dot{\boldsymbol{r}}_i + \dot{\boldsymbol{W}}_i\, {}^i\boldsymbol{r}_{i+1} + \boldsymbol{W}_i\, {}^i\dot{\boldsymbol{r}}_{i+1} \tag{B.8}$$

where

$${}^i\boldsymbol{r}_{i+1} = {}^i\boldsymbol{r}_{Ci} + {}^i\tilde{\boldsymbol{r}}_{i+1}, \tag{B.9}$$

$${}^i\tilde{\boldsymbol{r}}_{i+1} = \begin{bmatrix} l_i & w_{ei} \end{bmatrix}^{\mathrm{T}}. \tag{B.10}$$

$${}^i\dot{\boldsymbol{r}}_{i+1} = {}^i\dot{\tilde{\boldsymbol{r}}}_{i+1} = \begin{bmatrix} 0 & \dot{w}_{ei} \end{bmatrix}^{\mathrm{T}}. \tag{B.11}$$

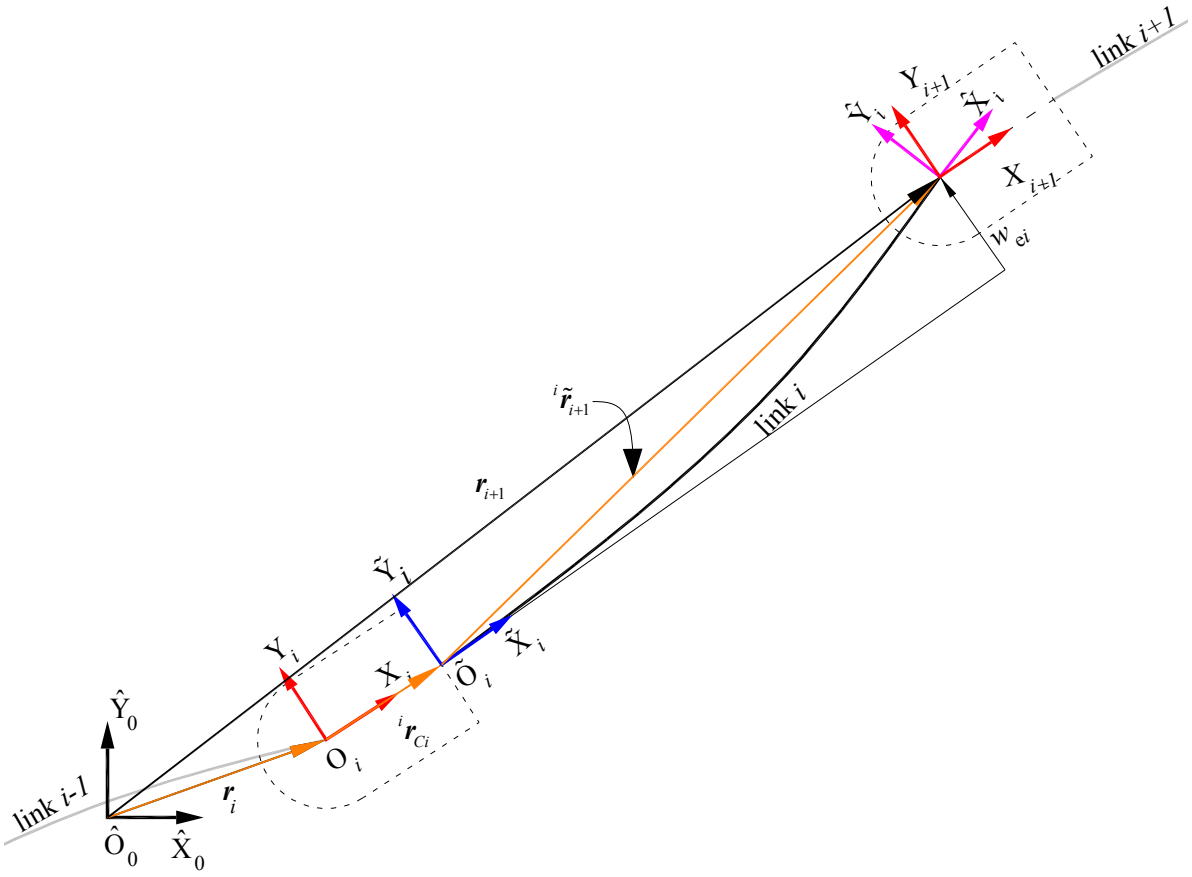

Figure B.3: Definition of absolute position $\boldsymbol{r}_{i+1}$ of one point along the link i.

For the absolute angular position and absolute angular velocity of the distal end of each link a distinction has to be done. According to Fig. B.4, the absolute angular position $\hat{\alpha}_i$ and angular velocity $\dot{\hat{\alpha}}_i$ of frame $\left(\hat{X}_i, \hat{Y}_i\right)$ are given by

$$\hat{\alpha}_i = \sum_{j=1}^{i-1} q_j + \sum_{k=1}^{i-1} w'_{\mathrm{e}\,k} \quad 1 < i < n_{\mathrm{R}} \ , \tag{B.12}$$

$$\dot{\hat{\alpha}}_i = \sum_{j=1}^{i-1} \dot{q}_j + \sum_{k=1}^{i-1} \dot{w}'_{\mathrm{e}\,k} \quad 1 < i < n_{\mathrm{R}} \ . \tag{B.13}$$

The absolute angular position α_i and angular velocity $\dot{\alpha}_i$ of frame $\left(X_{i+1}, Y_{i+1}\right)$ are given by

$$\alpha_i = \sum_{j=1}^{i} q_j + \sum_{k=1}^{i-1} w'_{\mathrm{e}\,k} \quad i \le n_{\mathrm{R}} + 1 \ , \tag{B.14}$$

$$\dot{\alpha}_i = \sum_{j=1}^{i} \dot{q}_j + \sum_{k=1}^{i-1} \dot{w}'_{\mathrm{e}\,k} \quad i \le n_{\mathrm{R}} + 1 \ . \tag{B.15}$$

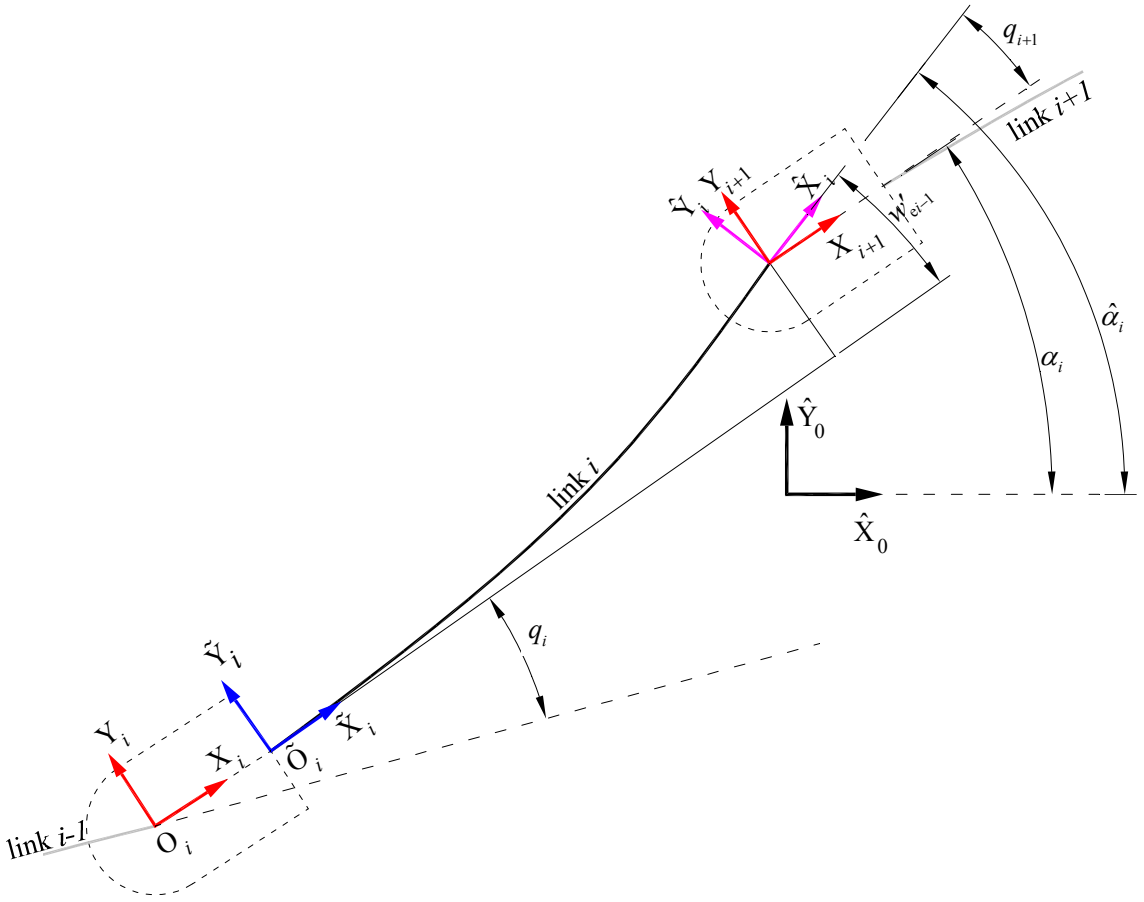

Figure B.4: Definition of absolute rotation α_i of frames at the tip of link *i*.

The cumulative transformation $\boldsymbol{W}_i$ from inertial frame $(\hat{X}_0, \hat{Y}_0)$ can be defined recursively

$$\boldsymbol{W}_i = \boldsymbol{W}_{i-1}\boldsymbol{E}_{i-1}\boldsymbol{A}_i = \hat{\boldsymbol{W}}_{i-1}\boldsymbol{A}_i, \tag{B.16}$$

The change of orientation due to the rotational joint is included in

$$\boldsymbol{A}_i = \begin{bmatrix} \cos(q_i) & -\sin(q_i) \\ \sin(q_i) & \cos(q_i) \end{bmatrix}. \tag{B.17}$$

$\hat{\boldsymbol{W}}_{i-1} = \boldsymbol{W}_{i-1}\boldsymbol{E}_{i-1}$ accounts for the transformation induced by the previous links. Where $\boldsymbol{E}_i$ represent the influence of the elastic deformation of the previous link in the orientation and it is defined as

$$\boldsymbol{E}_i = \begin{bmatrix} 1 & -\left.\dfrac{\partial w_i(\tilde{x}_i,t)}{\partial \tilde{x}_i}\right|_{\tilde{x}_i=l_i} \\ \left.\dfrac{\partial w_i(\tilde{x}_i,t)}{\partial \tilde{x}_i}\right|_{\tilde{x}_i=l_i} & 1 \end{bmatrix} = \begin{bmatrix} 1 & -w'_{e\,i} \\ w'_{e\,i} & 1 \end{bmatrix}. \tag{B.18}$$

The time derivatives $\dot{\boldsymbol{A}}_i$, $\dot{\boldsymbol{E}}_i$ and $\dot{\boldsymbol{W}}_i$ are given by

$$\dot{\boldsymbol{A}}_i = \boldsymbol{S}\boldsymbol{A}_i\dot{q}_i \tag{B.19}$$

$$\boldsymbol{S} = \begin{bmatrix} 0 & -1 \\ 1 & 0 \end{bmatrix} \tag{B.20}$$

$$\dot{\boldsymbol{E}}_i = \boldsymbol{S}\dot{w}'_{ie} \tag{B.21}$$

$$\dot{\boldsymbol{W}}_i = \dot{\hat{\boldsymbol{W}}}_{i-1}\boldsymbol{A}_i + \hat{\boldsymbol{W}}_{i-1}\dot{\boldsymbol{A}}_i \tag{B.22}$$

$$\dot{\hat{\boldsymbol{W}}}_i = \dot{\boldsymbol{W}}_i\boldsymbol{E}_i + \boldsymbol{W}_i\dot{\boldsymbol{E}}_i \tag{B.23}$$

These transformation matrices are orthonormal, from this condition some properties can be used for the deduction of the robot model

$$\boldsymbol{A}_i^{\mathrm{T}}\boldsymbol{A}_i = \boldsymbol{I}\,, \tag{B.24}$$

$$\boldsymbol{E}_i^{\mathrm{T}}\boldsymbol{E}_i = \boldsymbol{I}\,, \tag{B.25}$$

$$\boldsymbol{S}_i^{\mathrm{T}}\boldsymbol{S}_i = \boldsymbol{I}\,, \tag{B.26}$$

$$\boldsymbol{A}_i^{\mathrm{T}}\dot{\boldsymbol{A}}_i = \boldsymbol{S}q_i\,, \tag{B.27}$$

$$\boldsymbol{E}_i^{\mathrm{T}}\dot{\boldsymbol{E}}_i = \left(\boldsymbol{I}w'_{ie} + \boldsymbol{S}\right)\dot{w}'_{ie}\,. \tag{B.28}$$

B.1 Kinematic Relation for One Flexible-link Robot

Here the particularization for the one flexible-link robot is done.

The location of any point along the link and its time derivative

$$\boldsymbol{p}_1 = \boldsymbol{r}_1 + \boldsymbol{W}_1\,{}^1\boldsymbol{p}_1 = \boldsymbol{A}_1\,{}^1\boldsymbol{p}_1\,, \tag{B.29}$$

$$\boldsymbol{r}_1 = \begin{bmatrix}0 & 0\end{bmatrix}^{\mathrm{T}}, \tag{B.30}$$

$${}^1\boldsymbol{p}_1 = {}^1\boldsymbol{r}_{\mathrm{C}} + {}^1\tilde{\boldsymbol{p}}_1\,, \tag{B.31}$$

$${}^1\boldsymbol{r}_{\mathrm{C}} = \begin{bmatrix}\overline{\mathrm{O}_1\tilde{\mathrm{O}}_1} & 0\end{bmatrix}^{\mathrm{T}}, \tag{B.32}$$

$${}^1\tilde{\boldsymbol{p}}_1 = \begin{bmatrix}\tilde{x}_1 & w_1(\tilde{x}_1,t)\end{bmatrix}^{\mathrm{T}}, \tag{B.33}$$

$${}^1\boldsymbol{p}_1 = \begin{bmatrix}\tilde{x}_1 + \overline{\mathrm{O}_1\tilde{\mathrm{O}}_1} & w_1(\tilde{x}_1,t)\end{bmatrix}^{\mathrm{T}}, \tag{B.34}$$

$$\boldsymbol{A}_1 = \begin{bmatrix}\cos(q_1) & -\sin(q_1)\\ \sin(q_1) & \cos(q_1)\end{bmatrix}, \tag{B.35}$$

$$\boldsymbol{p}_1 = \begin{bmatrix}\cos(q_1) & -\sin(q_1)\\ \sin(q_1) & \cos(q_1)\end{bmatrix}\begin{bmatrix}\overline{\mathrm{O}_1\tilde{\mathrm{O}}_1} + \tilde{x}_1\\ w_1(\tilde{x}_1,t)\end{bmatrix}, \tag{B.36}$$

$$\dot{\boldsymbol{p}}_1 = \dot{\boldsymbol{r}}_1 + \dot{\boldsymbol{A}}_1\,{}^1\boldsymbol{p}_1 + \boldsymbol{A}_1\,{}^1\dot{\boldsymbol{p}}_1\,, \tag{B.37}$$

$$\dot{\boldsymbol{r}}_1 = \begin{bmatrix}0 & 0\end{bmatrix}^{\mathrm{T}}, \tag{B.38}$$

$$\dot{\boldsymbol{A}}_1 = \boldsymbol{S}\boldsymbol{A}_1\dot{q}_1\,, \tag{B.39}$$

$${}^1\dot{\boldsymbol{p}}_1 = \begin{bmatrix}0 & \dot{w}_1(\tilde{x}_1,t)\end{bmatrix}^{\mathrm{T}}, \tag{B.40}$$

$$\dot{\boldsymbol{p}}_1 = \boldsymbol{S}\boldsymbol{A}_1\,{}^1\boldsymbol{p}_1\dot{q}_1 + \boldsymbol{A}_1\,{}^1\dot{\boldsymbol{p}}_1\,, \tag{B.41}$$

$$\dot{\boldsymbol{p}}_1 = S\begin{bmatrix}\cos(q_1) & -\sin(q_1)\\ \sin(q_1) & \cos(q_1)\end{bmatrix}\begin{bmatrix}\overline{\mathrm{O}_1\tilde{\mathrm{O}}_1} + \tilde{x}_1\\ w_1(\tilde{x}_1,t)\end{bmatrix}\dot{q}_1 + \begin{bmatrix}\cos(q_1) & -\sin(q_1)\\ \sin(q_1) & \cos(q_1)\end{bmatrix}\begin{bmatrix}0\\ \dot{w}_1(\tilde{x}_1,t)\end{bmatrix}. \tag{B.42}$$

In analog way for $\boldsymbol{r}_2$ and $\dot{\boldsymbol{r}}_2$

$$\boldsymbol{r}_2 = \boldsymbol{r}_1 + \boldsymbol{W}_1\,{}^1\boldsymbol{r}_2\,, \tag{B.43}$$

$$ {}^{1}\boldsymbol{r}_2 = \begin{bmatrix} \overline{\mathrm{O}_1\tilde{\mathrm{O}}_1} + l_1 \\ w_{\mathrm{e}1} \end{bmatrix}, \tag{B.44} $$

$$ \boldsymbol{r}_2 = \begin{bmatrix} \cos(q_1) & -\sin(q_1) \\ \sin(q_1) & \cos(q_1) \end{bmatrix} \begin{bmatrix} \overline{\mathrm{O}_1\tilde{\mathrm{O}}_1} + l_1 \\ w_{\mathrm{e}1} \end{bmatrix}, \tag{B.45} $$

$$ \dot{\boldsymbol{r}}_2 = \dot{\boldsymbol{A}}_1 {}^{1}\boldsymbol{r}_2 + \boldsymbol{A}_1 {}^{1}\dot{\boldsymbol{r}}_2 \ , \tag{B.46} $$

$$ {}^{1}\dot{\boldsymbol{r}}_2 = \begin{bmatrix} 0 & \dot{w}_{\mathrm{e}1} \end{bmatrix}^{\mathrm{T}}, \tag{B.47} $$

$$ \dot{\boldsymbol{r}}_2 = \boldsymbol{S}\boldsymbol{A}_1 {}^{1}\boldsymbol{r}_2 \dot{q}_1 + \boldsymbol{A}_1 {}^{1}\dot{\boldsymbol{r}}_2, \tag{B.48} $$

$$ \dot{\boldsymbol{r}}_2 = S \begin{bmatrix} \cos(q_1) & -\sin(q_1) \\ \sin(q_1) & \cos(q_1) \end{bmatrix} \begin{bmatrix} \overline{\mathrm{O}_i\tilde{\mathrm{O}}_1} + l_1 \\ w_{\mathrm{e}1} \end{bmatrix} + \begin{bmatrix} \cos(q_1) & -\sin(q_1) \\ \sin(q_1) & \cos(q_1) \end{bmatrix} \begin{bmatrix} 0 \\ \dot{w}_{\mathrm{e}1} \end{bmatrix}. \tag{B.49} $$

The required angles and angular velocities

$$ \alpha_1 = q_1 \ , \tag{B.50} $$

$$ \dot{\alpha}_1 = \dot{q}_1 \ , \tag{B.51} $$

$$ \alpha_2 = q_1 + w'_{\mathrm{e}1} \ , \tag{B.52} $$

$$ \dot{\alpha}_2 = \dot{q}_1 + \dot{w}'_{\mathrm{e}1} \, . \tag{B.53} $$

B.2 Kinematic Relation for Two Flexible-link Robot

The kinematic relations are the same from (B.29) to (B.51). For the sake of simplification in equations in this robot model the definition of the involved vectors are given, but it are not substituted in the final expression.

The angles and angular velocities of the tip of the first link

$$ \hat{\alpha}_2 = q_1 + w'_{\mathrm{e}1} \ , \tag{B.54} $$

$$ \dot{\hat{\alpha}}_2 = \dot{q}_1 + \dot{w}'_{\mathrm{e}1}, \tag{B.55} $$

$$ \alpha_2 = q_1 + q_2 + w'_{\mathrm{e}1} \ , \tag{B.56} $$

$$ \dot{\alpha}_2 = \dot{q}_1 + \dot{q}_2 + \dot{w}'_{\mathrm{e}1} \, . \tag{B.57} $$

The location of any point along the second link and its time derivative

$$ \boldsymbol{p}_2 = \boldsymbol{r}_2 + \boldsymbol{W}_2 {}^{2}\boldsymbol{p}_2 = \boldsymbol{W}_1 {}^{1}\boldsymbol{r}_2 + \boldsymbol{W}_2 {}^{2}\boldsymbol{p}_2, \tag{B.58} $$

$$ \boldsymbol{W}_1 = \boldsymbol{A}_1, \tag{B.59} $$

$$ \boldsymbol{W}_2 = \boldsymbol{A}_1 \boldsymbol{E}_1 \boldsymbol{A}_2 = \hat{\boldsymbol{W}}_1 \boldsymbol{A}_2, \tag{B.60} $$

$$ \boldsymbol{A}_2 = \begin{bmatrix} \cos(q_2) & -\sin(q_2) \\ \sin(q_2) & \cos(q_2) \end{bmatrix}, \tag{B.61} $$

$$ \boldsymbol{E}_1 = \begin{bmatrix} 1 & -\left.\dfrac{\partial w_1(\tilde{x}_1, t)}{\partial \tilde{x}_1}\right|_{\tilde{x}_1 = l_1} \\ \left.\dfrac{\partial w_1(\tilde{x}_1, t)}{\partial \tilde{x}_1}\right|_{\tilde{x}_1 = l_1} & 1 \end{bmatrix} = \begin{bmatrix} 1 & -w'_{\mathrm{e}1} \\ w'_{\mathrm{e}1} & 1 \end{bmatrix}, \tag{B.62} $$

$$ {}^{2}\boldsymbol{p}_2 = {}^{2}\boldsymbol{r}_{\mathrm{C}2} + {}^{2}\tilde{\boldsymbol{p}}_2 \ , \tag{B.63} $$

$$ {}^{2}\boldsymbol{r}_{\mathrm{C}2} = \begin{bmatrix} \overline{\mathrm{O}_2\tilde{\mathrm{O}}_2} & 0 \end{bmatrix}^{\mathrm{T}} \ , \tag{B.64} $$

$$ {}^{2}\tilde{\boldsymbol{p}}_2 = \left[\tilde{x}_2 \quad w_2(\tilde{x}_2, t)\right]^{\mathrm{T}} , \tag{B.65} $$

$$ {}^{2}\boldsymbol{p}_2 = \left[\tilde{x}_2 + \overline{\mathrm{O}_2\tilde{\mathrm{O}}_2} \quad w_2(\tilde{x}_2, t)\right]^{\mathrm{T}} , \tag{B.66} $$

$$ \boldsymbol{p}_2 = \boldsymbol{A}_1\left({}^{1}\boldsymbol{r}_2 + \boldsymbol{E}_1\boldsymbol{A}_2\,{}^{2}\boldsymbol{p}_2\right) = \boldsymbol{A}_1\,{}^{1}\boldsymbol{r}_2 + \boldsymbol{A}_1\boldsymbol{E}_1\boldsymbol{A}_2\,{}^{2}\boldsymbol{p}_2 , \tag{B.67} $$

$$ \dot{\boldsymbol{p}}_2 = \dot{\boldsymbol{r}}_2 + \dot{\boldsymbol{W}}_2\,{}^{2}\boldsymbol{p}_2 + \boldsymbol{W}_2\,{}^{2}\dot{\boldsymbol{p}}_2 , \tag{B.68} $$

$$ \dot{\boldsymbol{W}}_2 = \dot{\hat{\boldsymbol{W}}}_1\boldsymbol{A}_2 + \hat{\boldsymbol{W}}_1\dot{\boldsymbol{A}}_2 = \left(\dot{\boldsymbol{W}}_1\boldsymbol{E}_1 + \boldsymbol{W}_1\dot{\boldsymbol{E}}_1\right)\boldsymbol{A}_2 + \boldsymbol{W}_1\boldsymbol{E}_1\dot{\boldsymbol{A}}_2 , \tag{B.69} $$

$$ \dot{\boldsymbol{W}}_2 = \boldsymbol{S}\boldsymbol{A}_1\boldsymbol{E}_1\boldsymbol{A}_2\dot{q}_1 + \boldsymbol{A}_1\dot{\boldsymbol{E}}_1\boldsymbol{A}_2 + \boldsymbol{A}_1\boldsymbol{E}_1\boldsymbol{S}\boldsymbol{A}_2\dot{q}_2 , \tag{B.70} $$

$$ \dot{\boldsymbol{p}}_2 = \begin{array}{l} \boldsymbol{S}\boldsymbol{A}_1\,{}^{1}\boldsymbol{r}_2\dot{q}_1 + \boldsymbol{A}_1\,{}^{1}\dot{\boldsymbol{r}}_2 + \boldsymbol{S}\boldsymbol{A}_1\boldsymbol{E}_1\boldsymbol{A}_2\,{}^{2}\boldsymbol{p}_2\dot{q}_1 + \ldots \\ \ldots + \boldsymbol{A}_1\dot{\boldsymbol{E}}_1\boldsymbol{A}_2\,{}^{2}\boldsymbol{p}_2 + \boldsymbol{A}_1\boldsymbol{E}_1\boldsymbol{S}\boldsymbol{A}_2\,{}^{2}\boldsymbol{p}_2\dot{q}_2 + \boldsymbol{A}_1\boldsymbol{E}_1\boldsymbol{A}_2\,{}^{2}\dot{\boldsymbol{p}}_2 \end{array} . \tag{B.71} $$

In analog way for $\boldsymbol{r}_3$ and $\dot{\boldsymbol{r}}_3$

$$ \boldsymbol{r}_3 = \boldsymbol{r}_2 + \boldsymbol{W}_2\,{}^{2}\boldsymbol{r}_3 = \boldsymbol{W}_1\,{}^{1}\boldsymbol{r}_2 + \boldsymbol{W}_2\,{}^{2}\boldsymbol{r}_3 , \tag{B.72} $$

$$ {}^{2}\boldsymbol{r}_3 = \begin{bmatrix} \overline{\mathrm{O}_2\tilde{\mathrm{O}}_2} + l_2 \\ w_{\mathrm{e}2} \end{bmatrix}, \tag{B.73} $$

$$ \boldsymbol{r}_3 = \boldsymbol{A}_1\left({}^{1}\boldsymbol{r}_2 + \boldsymbol{E}_1\boldsymbol{A}_2\,{}^{2}\boldsymbol{r}_3\right) = \boldsymbol{A}_1\,{}^{1}\boldsymbol{r}_2 + \boldsymbol{A}_1\boldsymbol{E}_1\boldsymbol{A}_2\,{}^{2}\boldsymbol{r}_3 , \tag{B.74} $$

$$ \dot{\boldsymbol{r}}_3 = \dot{\boldsymbol{r}}_2 + \dot{\boldsymbol{W}}_2\,{}^{2}\boldsymbol{r}_3 + \boldsymbol{W}_2\,{}^{2}\dot{\boldsymbol{r}}_3 , \tag{B.75} $$

$$ \dot{\boldsymbol{r}}_3 = \begin{array}{l} \boldsymbol{S}\boldsymbol{A}_1\,{}^{1}\boldsymbol{r}_2\dot{q}_1 + \boldsymbol{A}_1\,{}^{1}\dot{\boldsymbol{r}}_2 + \boldsymbol{S}\boldsymbol{A}_1\boldsymbol{E}_1\boldsymbol{A}_2\,{}^{2}\boldsymbol{r}_3\dot{q}_1 + \cdots \\ \cdots + \boldsymbol{A}_1\dot{\boldsymbol{E}}_1\boldsymbol{A}_2\,{}^{2}\boldsymbol{r}_3 + \boldsymbol{A}_1\boldsymbol{E}_1\boldsymbol{S}\boldsymbol{A}_2\,{}^{2}\boldsymbol{r}_3\dot{q}_2 + \boldsymbol{A}_1\boldsymbol{E}_1\boldsymbol{A}_2\,{}^{2}\dot{\boldsymbol{r}}_3 \end{array} . \tag{B.76} $$

Finally the absolute angular position and absolute angular velocity of the last frame are

$$ \alpha_3 = q_1 + q_2 + w'_{\mathrm{e}1} + w'_{\mathrm{e}2} , \tag{B.77} $$

$$ \dot{\alpha}_3 = \dot{q}_1 + \dot{q}_2 + \dot{w}'_{\mathrm{e}1} + \dot{w}'_{\mathrm{e}2} , \tag{B.78} $$

respectively.

Appendix C Relation between Energy Terms and Kinematic Terms

C.1 Relation between Energy Terms and Kinematic Relations for One Flexible-link Robot

The components coming from the Lagrangian are used to formulate the equation of motion

$$\begin{bmatrix} \dfrac{d}{dt}\dfrac{\partial T_{\mathrm{h}}}{\partial \dot{q}_1}+\dfrac{d}{dt}\dfrac{\partial T_{\mathrm{l}}}{\partial \dot{q}_1}+\dfrac{d}{dt}\dfrac{\partial T_{\mathrm{p}}}{\partial \dot{q}_1} \\ \dfrac{d}{dt}\dfrac{\partial T_{\mathrm{l}}}{\partial \dot{q}_2}+\dfrac{d}{dt}\dfrac{\partial T_{\mathrm{p}}}{\partial \dot{q}_2}-\dfrac{\partial T_{\mathrm{l}}}{\partial q_2}-\dfrac{\partial T_{\mathrm{p}}}{\partial q_2}+\dfrac{\partial U}{\partial q_2} \\ \dfrac{d}{dt}\dfrac{\partial T_{\mathrm{l}}}{\partial \dot{q}_3}+\dfrac{d}{dt}\dfrac{\partial T_{\mathrm{p}}}{\partial \dot{q}_3}-\dfrac{\partial T_{\mathrm{l}}}{\partial q_3}-\dfrac{\partial T_{\mathrm{p}}}{\partial q_3}+\dfrac{\partial U}{\partial q_3} \end{bmatrix}=\begin{bmatrix} f_1 \\ f_2 \\ f_3 \end{bmatrix} \tag{C.1}$$

whose components are related with the physical parameters and kinematic relations in the following form:

$$\frac{d}{dt}\frac{\partial T_{\mathrm{h}}}{\partial \dot{q}_1}=J_{\mathrm{h}}\ddot{q}_1, \tag{C.2}$$

$$\begin{aligned}\frac{d}{dt}\frac{\partial T_{\mathrm{l}}}{\partial \dot{q}_1}=&\ddot{q}_1\rho_l\int_0^{l}{}^{1}\boldsymbol{p}_1(\tilde{x}_1)^{\mathrm{T}}\,{}^{1}\boldsymbol{p}_1(\tilde{x}_1)d\tilde{x}_1+\ddot{q}_2\rho_l\int_0^{l}\tilde{x}_1\phi_1(\tilde{x}_1)d\tilde{x}_1+\ldots \\ &\ddot{q}_3\rho_l\int_0^{l}\tilde{x}_1\phi_2(\tilde{x}_1)d\tilde{x}_1+TL1q1t\_B\end{aligned}, \tag{C.3}$$

$$TL1q1t\_B=\dot{q}_1\rho_l\int_0^{l}{}^{1}\boldsymbol{p}_1(\tilde{x}_1)^{\mathrm{T}}\,{}^{1}\dot{\boldsymbol{p}}_1(\tilde{x}_1)d\tilde{x}_1, \tag{C.4}$$

$$\begin{aligned}\frac{d}{dt}\frac{\partial T_{\mathrm{p}}}{\partial \dot{q}_1}=&\left[m_{\mathrm{p}}\,{}^{1}\boldsymbol{r}_2^{\mathrm{T}}\,{}^{1}\boldsymbol{r}_2+J_{\mathrm{p}}\right]\ddot{q}_1+\left[\left(l+\overline{\mathrm{O}_1\tilde{\mathrm{O}}_1}\right)m_{\mathrm{p}}\phi_{\mathrm{e}1}+J_{\mathrm{p}}\phi'_{\mathrm{e}1}\right]\ddot{q}_2+\ldots \\ &\left[\left(l+\overline{\mathrm{O}_1\tilde{\mathrm{O}}_1}\right)m_{\mathrm{p}}\phi_{\mathrm{e}2}+J_{\mathrm{p}}\phi'_{\mathrm{e}2}\right]\ddot{q}_3+TPq1t\_B\end{aligned}, \tag{C.5}$$

$$TPq1t\_B=2m_{\mathrm{p}}\,{}^{1}\boldsymbol{r}_2^{\mathrm{T}}\,{}^{1}\dot{\boldsymbol{r}}_2\,\dot{q}_1, \tag{C.6}$$

$$\frac{d}{dt}\frac{\partial T_{\mathrm{l}}}{\partial \dot{q}_2}=\ddot{q}_1\rho_l\int_0^{l}\tilde{x}_1\phi_1(\tilde{x}_1)d\tilde{x}_1+\ddot{q}_2\rho_l\int_0^{l}\tilde{x}_1\phi_1(\tilde{x}_1)^2d\tilde{x}_1+\ddot{q}_3\rho_l\int_0^{l}\tilde{x}_1\phi_1(\tilde{x}_1)\phi_2(\tilde{x}_1)d\tilde{x}_1, \tag{C.7}$$

$$\frac{d}{dt}\frac{\partial T_{\mathrm{p}}}{\partial \dot{q}_2}=\left[\left(l+\overline{\mathrm{O}_1\tilde{\mathrm{O}}_1}\right)m_{\mathrm{p}}\phi_{\mathrm{e}1}+J_{\mathrm{p}}\phi'_{\mathrm{e}1}\right]\ddot{q}_1+\left(m_{\mathrm{p}}\phi_{\mathrm{e}1}^2+J_{\mathrm{p}}\phi_{\mathrm{e}1}'^2\right)\ddot{q}_2+\left(m_{\mathrm{p}}\phi_{\mathrm{e}1}\phi_{\mathrm{e}2}+J_{\mathrm{p}}\phi'_{\mathrm{e}1}\phi'_{\mathrm{e}2}\right)\ddot{q}_3, \tag{C.8}$$

$$\frac{\partial T_{\mathrm{l}}}{\partial q_2}=TL1q2\_B=\dot{q}_1^2q_2\rho_l\int_0^{l}\phi_1(\tilde{x}_1)^2d\tilde{x}_1+\dot{q}_1^2q_3\rho_l\int_0^{l}\phi_1(\tilde{x}_1)\phi_2(\tilde{x}_1)d\tilde{x}_1, \tag{C.9}$$

$$\frac{\partial T_{\mathrm{p}}}{\partial q_2}=TPq2\_B=m_{\mathrm{p}}\left(\phi_{\mathrm{e}1}^2q_2+\phi_{\mathrm{e}1}\phi_{\mathrm{e}2}q_3\right)\dot{q}_1^2, \tag{C.10}$$

$$\frac{\partial U}{\partial q_2}=q_2EI\int_0^{l}\phi_1''(\tilde{x}_1)^2d\tilde{x}_1+q_3EI\int_0^{l}\phi_1''(\tilde{x}_1)\phi_2''(\tilde{x}_1)d\tilde{x}_1, \tag{C.11}$$

$$\frac{d}{dt}\frac{\partial T_{\mathrm{l}}}{\partial \dot{q}_3} = \ddot{q}_1\rho_l\int_0^l \tilde{x}_1\phi_2(\tilde{x}_1)d\tilde{x}_1 + \ddot{q}_2\rho_l\int_0^l \tilde{x}_1\phi_1(\tilde{x}_1)\phi_2(\tilde{x}_1)d\tilde{x}_1 + \ddot{q}_3\rho_l\int_0^l \tilde{x}_1\phi_2(\tilde{x}_1)^2 d\tilde{x}_1\,, \tag{C.12}$$

$$\frac{d}{dt}\frac{\partial T_{\mathrm{p}}}{\partial \dot{q}_3} = \left[\left(l+\overline{\mathrm{O}_1\tilde{\mathrm{O}}_1}\right)m_{\mathrm{p}}\phi_{\mathrm{e}2} + J_{\mathrm{p}}\phi'_{\mathrm{e}2}\right]\ddot{q}_1 + \left(m_{\mathrm{p}}\phi_{\mathrm{e}1}\phi_{\mathrm{e}2} + J_{\mathrm{p}}\phi'_{\mathrm{e}1}\phi'_{\mathrm{e}2}\right)\ddot{q}_2 + \left(m_{\mathrm{p}}\phi_{\mathrm{e}2}^2 + J_{\mathrm{p}}\phi'^2_{\mathrm{e}2}\right)\ddot{q}_3\,, \tag{C.13}$$

$$\frac{\partial T_{\mathrm{l}}}{\partial q_3} = TL1q3\_B = \dot{q}_1^2 q_2\rho_l\int_0^l \phi_1(\tilde{x}_1)\phi_2(\tilde{x}_1)d\tilde{x}_1 + \dot{q}_1^2 q_3\rho_l\int_0^l \phi_1(\tilde{x}_1)^2 d\tilde{x}_1\,, \tag{C.14}$$

$$\frac{\partial T_{\mathrm{p}}}{\partial q_3} = TPq3\_B = m_{\mathrm{p}}\left(\phi_{\mathrm{e}1}\phi_{\mathrm{e}2}q_2 + \phi_{\mathrm{e}2}^2 q_3\right)\dot{q}_1^2 \tag{C.15}$$

and

$$\frac{\partial U}{\partial q_3} = q_2 EI\int_0^l \phi_1''(\tilde{x}_1)\phi_2''(\tilde{x}_1)d\tilde{x}_1 + q_3 EI\int_0^l \phi_2''(\tilde{x}_1)^2 d\tilde{x}_1\,. \tag{C.16}$$

Where all the terms ending in "*_B*" are separated and conform the vector of Coriolis and centripetal effects i.e.

$$\boldsymbol{c}(\boldsymbol{q},\dot{\boldsymbol{q}}) = \begin{bmatrix} TL1q1t\_B + TPq1t\_B \\ TL1q2\_B + TPq2\_B \\ TL1q3\_B + TPq3\_B \end{bmatrix}. \tag{C.17}$$

C.2 Relation between Energy Terms and Kinematic Relations for Two Flexible-link Robot

The components coming from the Lagrangian are used to formulate the equation of motion

$$\begin{bmatrix} \frac{d}{dt}\frac{\partial T_{\mathrm{h}_1}}{\partial \dot{q}_1} + \frac{d}{dt}\frac{\partial T_{\mathrm{h}_2}}{\partial \dot{q}_1} + \frac{d}{dt}\frac{\partial T_{\mathrm{l}_1}}{\partial \dot{q}_1} + \frac{d}{dt}\frac{\partial T_{\mathrm{l}_2}}{\partial \dot{q}_1} + \frac{d}{dt}\frac{\partial T_{\mathrm{p}}}{\partial \dot{q}_1} \\ \frac{d}{dt}\frac{\partial T_{\mathrm{h}_2}}{\partial \dot{q}_2} + \frac{d}{dt}\frac{\partial T_{\mathrm{l}_2}}{\partial \dot{q}_2} + \frac{d}{dt}\frac{\partial T_{\mathrm{p}}}{\partial \dot{q}_2} - \frac{\partial T_{\mathrm{l}_2}}{\partial q_2} - \frac{\partial T_{\mathrm{p}}}{\partial q_2} \\ \frac{d}{dt}\frac{\partial T_{\mathrm{h}_2}}{\partial \dot{q}_3} + \frac{d}{dt}\frac{\partial T_{\mathrm{l}_1}}{\partial \dot{q}_3} + \frac{d}{dt}\frac{\partial T_{\mathrm{l}_2}}{\partial \dot{q}_3} + \frac{d}{dt}\frac{\partial T_{\mathrm{p}}}{\partial \dot{q}_3} - \frac{\partial T_{\mathrm{h}_2}}{\partial q_3} - \frac{\partial T_{\mathrm{l}_1}}{\partial q_3} - \frac{\partial T_{\mathrm{l}_2}}{\partial q_3} - \frac{\partial T_{\mathrm{p}}}{\partial q_3} + \frac{\partial U_{\mathrm{l}_1}}{\partial q_3} \\ \frac{d}{dt}\frac{\partial T_{\mathrm{h}_2}}{\partial \dot{q}_4} + \frac{d}{dt}\frac{\partial T_{\mathrm{l}_1}}{\partial \dot{q}_4} + \frac{d}{dt}\frac{\partial T_{\mathrm{l}_2}}{\partial \dot{q}_4} + \frac{d}{dt}\frac{\partial T_{\mathrm{p}}}{\partial \dot{q}_4} - \frac{\partial T_{\mathrm{h}_2}}{\partial q_4} - \frac{\partial T_{\mathrm{l}_1}}{\partial q_4} - \frac{\partial T_{\mathrm{l}_2}}{\partial q_4} - \frac{\partial T_{\mathrm{p}}}{\partial q_4} + \frac{\partial U_{\mathrm{l}_1}}{\partial q_4} \\ \frac{d}{dt}\frac{\partial T_{\mathrm{l}_2}}{\partial \dot{q}_5} + \frac{d}{dt}\frac{\partial T_{\mathrm{p}}}{\partial \dot{q}_5} - \frac{\partial T_{\mathrm{l}_2}}{\partial q_5} - \frac{\partial T_{\mathrm{p}}}{\partial q_5} + \frac{\partial U_{\mathrm{l}_2}}{\partial q_5} \\ \frac{d}{dt}\frac{\partial T_{\mathrm{l}_2}}{\partial \dot{q}_6} + \frac{d}{dt}\frac{\partial T_{\mathrm{p}}}{\partial \dot{q}_6} - \frac{\partial T_{\mathrm{l}_2}}{\partial q_6} - \frac{\partial T_{\mathrm{p}}}{\partial q_6} + \frac{\partial U_{\mathrm{l}_2}}{\partial q_6} \end{bmatrix} = \begin{bmatrix} f_1 \\ f_2 \\ f_3 \\ f_4 \\ f_5 \\ f_6 \end{bmatrix}, \tag{C.18}$$

whose components are related with the physical parameters and kinematic relations in the following form:

$$\frac{d}{dt}\frac{\partial T_{\mathrm{h}_1}}{\partial \dot{q}_1} = J_{\mathrm{h}_1}\ddot{q}_1\,, \tag{C.19}$$

$$\frac{d}{dt}\frac{\partial T_{\mathrm{h}_2}}{\partial \dot{q}_1} = \begin{matrix} Th2q1t\_A1\ddot{q}_1 + Th2q1t\_A2\ddot{q}_2 + Th2q1t\_A3\ddot{q}_3 + \cdots \\ Th2q1t\_A4\ddot{q}_4 + Th2q1t\_B \end{matrix}, \tag{C.20}$$

where

$$Th2q1t\_A1 = \left(J_{\mathrm{h}_2} + m_{\mathrm{h}_2}\,{}^{1}\boldsymbol{r}_2^{\mathrm{T}\,1}\boldsymbol{r}_2\right), \tag{C.21}$$

$$Th2q1t\_A2 = J_{\mathrm{h}_2}, \tag{C.22}$$

$$Th2q1t\_A3 = m_{\mathrm{h}_2}\left(l_1 + \overline{\mathrm{O}_1\tilde{\mathrm{O}}_1}\right)\phi_{\mathrm{e}11} + J_{\mathrm{h}_2}\phi'_{\mathrm{e}11}, \tag{C.23}$$

$$Th2q1t\_A4 = m_{\mathrm{h}_2}\left(l_1 + \overline{\mathrm{O}_1\tilde{\mathrm{O}}_1}\right)\phi_{\mathrm{e}12} + J_{\mathrm{h}_2}\phi'_{\mathrm{e}12}, \tag{C.24}$$

$$Th2q1t\_B = 2m_{\mathrm{h}_2}\,{}^{1}\boldsymbol{r}_2^{\mathrm{T}\,1}\boldsymbol{r}_2\dot{q}_1, \tag{C.25}$$

$$\frac{d}{dt}\frac{\partial T_{\mathrm{l}_1}}{\partial \dot{q}_1} = TL1q1t\_A1\ddot{q}_1 + TL1q1t\_A3\ddot{q}_3 + TL1q1t\_A4\ddot{q}_4 + TL1q1t\_B, \tag{C.26}$$

where

$$TL1q1t\_A1 = \rho_{\mathrm{l}_1}\int_0^{l_1}{}^{1}\boldsymbol{p}_1^{\mathrm{T}\,1}\boldsymbol{p}_1 d\tilde{x}_1, \tag{C.27}$$

$$TL1q1t\_A3 = \rho_{\mathrm{l}_1}\int_0^{l_1}\tilde{x}_1\phi_{11}(\tilde{x}_1)d\tilde{x}_1, \tag{C.28}$$

$$TL1q1t\_A4 = \rho_{\mathrm{l}_1}\int_0^{l_1}\tilde{x}_1\phi_{12}(\tilde{x}_1)d\tilde{x}_1, \tag{C.29}$$

$$TL1q1t\_B = 2\rho_{\mathrm{l}_1}\int_0^{l_1}{}^{1}\boldsymbol{p}_1^{\mathrm{T}\,1}\dot{\boldsymbol{p}}_1 d\tilde{x}_1\dot{q}_1, \tag{C.30}$$

$$\frac{d}{dt}\frac{\partial T_{\mathrm{l}_2}}{\partial \dot{q}_1} = \begin{matrix} TL2q1t\_A1\ddot{q}_1 + TL2q1t\_A2\ddot{q}_2 + TL2q1t\_A3\ddot{q}_3 + \cdots \\ TL2q1t\_A4\ddot{q}_4 + TL2q1t\_A5\ddot{q}_5 + TL2q1t\_A6\ddot{q}_6 + TL2q1t\_B \end{matrix}, \tag{C.31}$$

where

$$TL2q1t\_A1 = \rho_{\mathrm{l}_2}\int_0^{l_2}\left({}^{1}\boldsymbol{r}_2^{\mathrm{T}\,1}\boldsymbol{r}_2 + 2\,{}^{2}\boldsymbol{p}_2^{\mathrm{T}}\boldsymbol{A}_2^{\mathrm{T}}\boldsymbol{E}_1^{\mathrm{T}\,1}\boldsymbol{r}_2 + {}^{2}\boldsymbol{p}_2^{\mathrm{T}\,2}\boldsymbol{p}_2\right)d\tilde{x}_2, \tag{C.32}$$

$$TL2q1t\_A2 = \rho_{\mathrm{l}_2}\int_0^{l_2}\left({}^{2}\boldsymbol{p}_2^{\mathrm{T}}\boldsymbol{A}_2^{\mathrm{T}}\boldsymbol{E}_1^{\mathrm{T}\,1}\boldsymbol{r}_2 + {}^{2}\boldsymbol{p}_2^{\mathrm{T}\,2}\boldsymbol{p}_2\right)d\tilde{x}_2, \tag{C.33}$$

$$TL2q1t\_A3 = \rho_{\mathrm{l}_2}\int_0^{l_2}\left(\left({}^{2}\boldsymbol{p}_2^{\mathrm{T}}\boldsymbol{A}_2^{\mathrm{T}\,1}\boldsymbol{r}_2 + {}^{2}\boldsymbol{p}_2^{\mathrm{T}}\boldsymbol{E}_1\,{}^{2}\boldsymbol{p}_2\right)\phi'_{\mathrm{e}11} + \begin{bmatrix}0 & \phi_{\mathrm{e}11}\end{bmatrix}\left(\boldsymbol{S}\boldsymbol{E}_1\boldsymbol{A}_2\,{}^{2}\boldsymbol{p}_2 + \boldsymbol{S}\,{}^{1}\boldsymbol{r}_2\right)\right)d\tilde{x}_2, \tag{C.34}$$

$$TL2q1t\_A4 = \rho_{\mathrm{l}_2}\int_0^{l_2}\left(\left({}^{2}\boldsymbol{p}_2^{\mathrm{T}}\boldsymbol{A}_2^{\mathrm{T}\,1}\boldsymbol{r}_2 + {}^{2}\boldsymbol{p}_2^{\mathrm{T}}\boldsymbol{E}_1\,{}^{2}\boldsymbol{p}_2\right)\phi'_{\mathrm{e}12} + \begin{bmatrix}0 & \phi_{\mathrm{e}12}\end{bmatrix}\left(\boldsymbol{S}\boldsymbol{E}_1\boldsymbol{A}_2\,{}^{2}\boldsymbol{p}_2 + \boldsymbol{S}\,{}^{1}\boldsymbol{r}_2\right)\right)d\tilde{x}_2, \tag{C.35}$$

$$TL2q1t\_A5 = \rho_{\mathrm{l}_2}\int_0^{l_2}\begin{bmatrix}0 & \phi_{21}(\tilde{x}_2)\end{bmatrix}\left(\boldsymbol{A}_2^{\mathrm{T}}\boldsymbol{E}_1^{\mathrm{T}}\boldsymbol{S}\,{}^{1}\boldsymbol{r}_2 + \boldsymbol{S}\,{}^{2}\boldsymbol{p}_2\right)d\tilde{x}_2, \tag{C.36}$$

$$TL2q1t\_A6 = \rho_{\mathrm{l}_2}\int_0^{l_2}\begin{bmatrix}0 & \phi_{22}(\tilde{x}_2)\end{bmatrix}\left(\boldsymbol{A}_2^{\mathrm{T}}\boldsymbol{E}_1^{\mathrm{T}}\boldsymbol{S}\,{}^{1}\boldsymbol{r}_2 + \boldsymbol{S}\,{}^{2}\boldsymbol{p}_2\right)d\tilde{x}_2, \tag{C.37}$$

$$TL2q1t\_B = \rho_{\mathrm{l}_2}\int_0^{l_2}\left(TL2q1t\_B1 + TL2q1t\_B2 + TL2q1t\_B3\right)d\tilde{x}_2, \tag{C.38}$$

where

$$TL2q1t\_B1 = \begin{matrix} 2\,{}^{1}\boldsymbol{r}_2^{\mathrm{T}\,1}\dot{\boldsymbol{r}}_2\dot{q}_1 + 2\,{}^{2}\dot{\boldsymbol{p}}_2^{\mathrm{T}}\boldsymbol{A}_2^{\mathrm{T}}\boldsymbol{E}_1^{\mathrm{T}\,1}\boldsymbol{r}_2\dot{q}_1 + 2\,{}^{2}\boldsymbol{p}_2^{\mathrm{T}}\boldsymbol{A}_2^{\mathrm{T}}\boldsymbol{E}_1^{\mathrm{T}}\boldsymbol{S}^{\mathrm{T}\,1}\boldsymbol{r}_2\dot{q}_1\dot{q}_2 + \cdots \\ 2\,{}^{2}\boldsymbol{p}_2^{\mathrm{T}}\boldsymbol{A}_2^{\mathrm{T}}\dot{\boldsymbol{E}}_1^{\mathrm{T}\,1}\boldsymbol{r}_2\dot{q}_1 + 2\,{}^{2}\boldsymbol{p}_2^{\mathrm{T}}\boldsymbol{A}_2^{\mathrm{T}}\boldsymbol{E}_1^{\mathrm{T}\,1}\dot{\boldsymbol{r}}_2\dot{q}_1 \end{matrix}, \tag{C.39}$$

$$TL2q1t\_B2 = 2\,{}^{2}\dot{\boldsymbol{p}}_2^{\mathrm{T}}\boldsymbol{A}_2^{\mathrm{T}}\dot{\boldsymbol{E}}_1^{\mathrm{T}}\boldsymbol{S}\,{}^{1}\boldsymbol{r}_2 + 2\,{}^{2}\boldsymbol{p}_2^{\mathrm{T}}\boldsymbol{A}_2^{\mathrm{T}}\dot{\boldsymbol{E}}_1^{\mathrm{T}\,1}\boldsymbol{r}_2\dot{q}_2 + 2\,{}^{2}\dot{\boldsymbol{p}}_2^{\mathrm{T}}\boldsymbol{A}_2^{\mathrm{T}}\boldsymbol{E}_1^{\mathrm{T}\,1}\boldsymbol{r}_2\dot{q}_2 + {}^{2}\boldsymbol{p}_2^{\mathrm{T}}\boldsymbol{A}_2^{\mathrm{T}}\boldsymbol{S}^{\mathrm{T}}\boldsymbol{E}_1^{\mathrm{T}\,1}\boldsymbol{r}_2\dot{q}_2^2, \tag{C.40}$$

$$TL2q1t\_B3 = 2^{2}\boldsymbol{p}_2^{\mathrm{T}}\,{}^{2}\dot{\boldsymbol{p}}_2\dot{q}_1 + {}^{2}\dot{\boldsymbol{p}}_2^{\mathrm{T}}\dot{\boldsymbol{E}}_1^{\mathrm{T}}\boldsymbol{S}\boldsymbol{E}_1\,{}^{2}\boldsymbol{p}_2 + {}^{2}\boldsymbol{p}_2^{\mathrm{T}}\dot{\boldsymbol{E}}_1^{\mathrm{T}}\boldsymbol{S}\boldsymbol{E}_1\,{}^{2}\dot{\boldsymbol{p}}_2 + 2^{2}\boldsymbol{p}_2^{\mathrm{T}}\,{}^{2}\dot{\boldsymbol{p}}_2\dot{q}_2\,, \tag{C.41}$$

$$\frac{d}{dt}\frac{\partial T_{\mathrm{p}}}{\partial \dot{q}_1} = TPq1t\_A1\ddot{q}_1 + TPq1t\_A2\ddot{q}_2 + TPq1t\_A3\ddot{q}_3 + \cdots \\ TPq1t\_A4\ddot{q}_4 + TPq1t\_A5\ddot{q}_5 + TPq1t\_A6\ddot{q}_6 + TPq1t\_B \,, \tag{C.42}$$

where

$$TPq1t\_A1 = m_{\mathrm{p}}\left({}^{1}\boldsymbol{r}_2^{\mathrm{T}}\,{}^{1}\boldsymbol{r}_2 + 2\,{}^{1}\boldsymbol{r}_2^{\mathrm{T}}E_1A_2\,{}^{2}\boldsymbol{r}_3 + {}^{2}\boldsymbol{r}_3^{\mathrm{T}}\,{}^{2}\boldsymbol{r}_3\right) + J_{\mathrm{p}}\,, \tag{C.43}$$

$$TPq1t\_A2 = m_{\mathrm{p}}\left({}^{2}\boldsymbol{r}_3^{\mathrm{T}}\boldsymbol{A}_2^{\mathrm{T}}\boldsymbol{E}_1^{\mathrm{T}}\,{}^{1}\boldsymbol{r}_2 + {}^{2}\boldsymbol{r}_3^{\mathrm{T}}\,{}^{2}\boldsymbol{r}_3\right) + J_{\mathrm{p}}\,, \tag{C.44}$$

$$TPq1t\_A3 = m_{\mathrm{p}}\left[0\ \ \phi_{\mathrm{e}11}\right]\left(\boldsymbol{S}\boldsymbol{E}_1\boldsymbol{A}_2\,{}^{2}\boldsymbol{r}_3 + \boldsymbol{S}\,{}^{1}\boldsymbol{r}_2\right) + m_{\mathrm{p}}\left({}^{2}\boldsymbol{r}_3^{\mathrm{T}}\boldsymbol{A}_2^{\mathrm{T}}\,{}^{1}\boldsymbol{r}_2 + {}^{2}\boldsymbol{r}_3^{\mathrm{T}}\boldsymbol{E}_1\,{}^{2}\boldsymbol{r}_3\right)\phi'_{\mathrm{e}11} + J_{\mathrm{p}}\phi'_{\mathrm{e}11}\,, \tag{C.45}$$

$$TPq1t\_A4 = m_{\mathrm{p}}\left[0\ \ \phi_{\mathrm{e}12}\right]\left(\boldsymbol{S}\boldsymbol{E}_1\boldsymbol{A}_2\,{}^{2}\boldsymbol{r}_3 + \boldsymbol{S}\,{}^{1}\boldsymbol{r}_2\right) + m_{\mathrm{p}}\left({}^{2}\boldsymbol{r}_3^{\mathrm{T}}\boldsymbol{A}_2^{\mathrm{T}}\,{}^{1}\boldsymbol{r}_2 + {}^{2}\boldsymbol{r}_3^{\mathrm{T}}\boldsymbol{E}_1\,{}^{2}\boldsymbol{r}_3\right)\phi'_{\mathrm{e}12} + J_{\mathrm{p}}\phi'_{\mathrm{e}12}\,, \tag{C.46}$$

$$TPq1t\_A5 = m_{\mathrm{p}}\left[0\ \ \phi_{\mathrm{e}21}\right]\left(\boldsymbol{A}_2^{\mathrm{T}}\boldsymbol{E}_1^{\mathrm{T}}\boldsymbol{S}\,{}^{1}\boldsymbol{r}_2 + \boldsymbol{S}\,{}^{2}\boldsymbol{r}_3\right) + J_{\mathrm{p}}\phi'_{\mathrm{e}21}\,, \tag{C.47}$$

$$TPq1t\_A6 = m_{\mathrm{p}}\left[0\ \ \phi_{\mathrm{e}22}\right]\left(\boldsymbol{A}_2^{\mathrm{T}}\boldsymbol{E}_1^{\mathrm{T}}\boldsymbol{S}\,{}^{1}\boldsymbol{r}_2 + \boldsymbol{S}\,{}^{2}\boldsymbol{r}_3\right) + J_{\mathrm{p}}\phi'_{\mathrm{e}22}\,, \tag{C.48}$$

$$TPq1t\_B = m_{\mathrm{p}}\left(TPq1t\_B1 + TPq1t\_B2 + TPq1t\_B3\right), \tag{C.49}$$

where

$$TPq1t\_B1 = 2\,{}^{1}\boldsymbol{r}_2^{\mathrm{T}}\,{}^{1}\dot{\boldsymbol{r}}_2\dot{q}_1 + 2\,{}^{1}\dot{\boldsymbol{r}}_2^{\mathrm{T}}\boldsymbol{E}_1\boldsymbol{A}_2\,{}^{2}\boldsymbol{r}_3\dot{q}_1 + 2\,{}^{1}\boldsymbol{r}_2^{\mathrm{T}}\dot{\boldsymbol{E}}_1\boldsymbol{A}_2\,{}^{2}\boldsymbol{r}_3\dot{q}_1 + \cdots \\ 2\,{}^{1}\boldsymbol{r}_2^{\mathrm{T}}\boldsymbol{E}_1\boldsymbol{S}\boldsymbol{A}_2\,{}^{2}\boldsymbol{r}_3\dot{q}_1\dot{q}_2 + 2\,{}^{1}\boldsymbol{r}_2^{\mathrm{T}}\boldsymbol{E}_1\boldsymbol{A}_2\,{}^{2}\dot{\boldsymbol{r}}_3\dot{q}_1 \,, \tag{C.50}$$

$$TPq1t\_B2 = 2^{2}\boldsymbol{r}_3^{\mathrm{T}}\,{}^{2}\dot{\boldsymbol{r}}_3\dot{q}_1 + 2^{2}\dot{\boldsymbol{r}}_3^{\mathrm{T}}\boldsymbol{A}_2^{\mathrm{T}}\dot{\boldsymbol{E}}_1^{\mathrm{T}}\boldsymbol{S}\,{}^{1}\boldsymbol{r}_2 + 2^{2}\boldsymbol{r}_3^{\mathrm{T}}\boldsymbol{A}_2^{\mathrm{T}}\dot{\boldsymbol{E}}_1^{\mathrm{T}}\,{}^{1}\boldsymbol{r}_2\dot{q}_2 + {}^{2}\dot{\boldsymbol{r}}_3^{\mathrm{T}}\dot{\boldsymbol{E}}_1^{\mathrm{T}}\boldsymbol{S}\boldsymbol{E}_1\,{}^{2}\boldsymbol{r}_3\,, \tag{C.51}$$

$$TPq1t\_B3 = {}^{2}\boldsymbol{r}_3^{\mathrm{T}}\dot{\boldsymbol{E}}_1^{\mathrm{T}}\boldsymbol{S}\boldsymbol{E}_1\,{}^{2}\dot{\boldsymbol{r}}_3 + 2^{2}\dot{\boldsymbol{r}}_3^{\mathrm{T}}\boldsymbol{A}_2^{\mathrm{T}}\boldsymbol{E}_1^{\mathrm{T}}\,{}^{1}\boldsymbol{r}_2\dot{q}_2 + {}^{2}\boldsymbol{r}_3^{\mathrm{T}}\boldsymbol{A}_2^{\mathrm{T}}\boldsymbol{S}^{\mathrm{T}}\boldsymbol{E}_1^{\mathrm{T}}\,{}^{1}\boldsymbol{r}_2\dot{q}_2^{2} + 2^{2}\boldsymbol{r}_3^{\mathrm{T}}\,{}^{2}\dot{\boldsymbol{r}}_3\dot{q}_2\,, \tag{C.52}$$

$$\frac{d}{dt}\frac{\partial T_{\mathrm{h}_2}}{\partial \dot{q}_2} = J_{\mathrm{h}_2}\ddot{q}_1 + J_{h_{2BC}}\ddot{q}_2 + J_{\mathrm{h}_2}\phi'_{\mathrm{e}11}\ddot{q}_3 + J_{\mathrm{h}_2}\phi'_{\mathrm{e}12}\ddot{q}_4\,, \tag{C.53}$$

$$\frac{d}{dt}\frac{\partial T_{\mathrm{l}_2}}{\partial \dot{q}_2} = TL2q2t\_A1\ddot{q}_1 + TL2q2t\_A2\ddot{q}_2 + TL2q2t\_A3\ddot{q}_3 + \cdots \\ TL2q2t\_A4\ddot{q}_4 + TL2q2t\_A5\ddot{q}_5 + TL2q2t\_A6\ddot{q}_6 + TL2q2t\_B \,, \tag{C.54}$$

where

$$TL2q2t\_A1 = \rho_{\mathrm{l}_2}\int_0^{l_2}\left({}^{2}\boldsymbol{p}_2^{\mathrm{T}}\boldsymbol{A}_2^{\mathrm{T}}\boldsymbol{E}_1^{\mathrm{T}}\,{}^{1}\boldsymbol{r}_2 + {}^{2}\boldsymbol{p}_2^{\mathrm{T}}\,{}^{2}\boldsymbol{p}_2\right)d\tilde{x}_2\,, \tag{C.55}$$

$$TL2q2t\_A2 = \rho_{\mathrm{l}_2}\int_0^{l_2}{}^{2}\boldsymbol{p}_2^{\mathrm{T}}\,{}^{2}\boldsymbol{p}_2\,d\tilde{x}_2\,, \tag{C.56}$$

$$TL2q2t\_A3 = \rho_{\mathrm{l}_2}\int_0^{l_2}\left(\left[0\ \ \phi_{\mathrm{e}11}\right]\boldsymbol{E}_1\boldsymbol{S}\boldsymbol{A}_2\,{}^{2}\boldsymbol{p}_2 + {}^{2}\boldsymbol{p}_2^{\mathrm{T}}\boldsymbol{E}_1\,{}^{2}\boldsymbol{p}_2\phi'_{\mathrm{e}11}\right)d\tilde{x}_2\,, \tag{C.57}$$

$$TL2q2t\_A4 = \rho_{\mathrm{l}_2}\int_0^{l_2}\left(\left[0\ \ \phi_{\mathrm{e}12}\right]\boldsymbol{E}_1\boldsymbol{S}\boldsymbol{A}_2\,{}^{2}\boldsymbol{p}_2 + {}^{2}\boldsymbol{p}_2^{\mathrm{T}}\boldsymbol{E}_1\,{}^{2}\boldsymbol{p}_2\phi'_{\mathrm{e}12}\right)d\tilde{x}_2\,, \tag{C.58}$$

$$TL2q2t\_A5 = \rho_{\mathrm{l}_2}\int_0^{l_2}\left[0\ \ \phi_{\mathrm{e}21}\right]\boldsymbol{S}\,{}^{2}\boldsymbol{p}_2 d\tilde{x}_2\,, \tag{C.59}$$

$$TL2q2t\_A6 = \rho_{\mathrm{l}_2}\int_0^{l_2}\left[0\ \ \phi_{\mathrm{e}22}\right]\boldsymbol{S}\,{}^{2}\boldsymbol{p}_2 d\tilde{x}_2\,, \tag{C.60}$$

$$TL2q2t\_B = \rho_{\mathrm{l}_2}\int_0^{l_2}\left(TL2q2t\_B1 + TL2q2t\_B2 + TL2q2t\_B3\right)d\tilde{x}_2\,, \tag{C.61}$$

where

$$TL2q2t\_B1 = {}^{1}\dot{\boldsymbol{r}}_2^{\mathrm{T}}\boldsymbol{E}_1\boldsymbol{A}_2\,{}^{2}\boldsymbol{p}_2\dot{q}_1 + {}^{1}\boldsymbol{r}_2^{\mathrm{T}}\dot{\boldsymbol{E}}_1\boldsymbol{A}_2\,{}^{2}\boldsymbol{p}_2\dot{q}_1 + {}^{1}\boldsymbol{r}_2^{\mathrm{T}}\boldsymbol{E}_1\boldsymbol{S}\boldsymbol{A}_2\,{}^{2}\boldsymbol{p}_2\dot{q}_1\dot{q}_2 + {}^{1}\boldsymbol{r}_2^{\mathrm{T}}\boldsymbol{E}_1\boldsymbol{A}_2\,{}^{2}\dot{\boldsymbol{p}}_2\dot{q}_1\,, \tag{C.62}$$

$$TL2q2t\_B2 = {}^{1}\dot{\boldsymbol{r}}_2^{\mathrm{T}}\dot{\boldsymbol{E}}_1\boldsymbol{S}\boldsymbol{A}_2\,{}^{2}\boldsymbol{p}_2 - {}^{1}\dot{\boldsymbol{r}}_2^{\mathrm{T}}\boldsymbol{E}_1\boldsymbol{A}_2\,{}^{2}\boldsymbol{p}_2\dot{q}_2 + {}^{1}\dot{\boldsymbol{r}}_2^{\mathrm{T}}\boldsymbol{E}_1\boldsymbol{S}\boldsymbol{A}_2\,{}^{2}\dot{\boldsymbol{p}}_2 + 2^{2}\boldsymbol{p}_2^{\mathrm{T}}\,{}^{2}\dot{\boldsymbol{p}}_2\dot{q}_1\,, \tag{C.63}$$

$$TL2q2t\_B3 = {}^{2}\dot{\boldsymbol{p}}_2^{\mathrm{T}}\dot{\boldsymbol{E}}_1^{\mathrm{T}}\boldsymbol{E}_1\boldsymbol{S}\,{}^{2}\boldsymbol{p}_2 + {}^{2}\boldsymbol{p}_2^{\mathrm{T}}\dot{\boldsymbol{E}}_1^{\mathrm{T}}\boldsymbol{E}_1\boldsymbol{S}\,{}^{2}\dot{\boldsymbol{p}}_2 + 2\,{}^{2}\boldsymbol{p}_2^{\mathrm{T}}\,{}^{2}\dot{\boldsymbol{p}}_2\dot{q}_2, \tag{C.64}$$

$$\frac{d}{dt}\frac{\partial T_{\mathrm{p}}}{\partial \dot{q}_2} = TPq2t\_A1\ddot{q}_1 + TPq2t\_A2\ddot{q}_2 + TPq2t\_A3\ddot{q}_3 + \cdots \\ TPq2t\_A4\ddot{q}_4 + TPq2t\_A5\ddot{q}_5 + TPq2t\_A6\ddot{q}_6 + TPq2t\_B, \tag{C.65}$$

where

$$TPq2t\_A1 = m_{\mathrm{p}}\left({}^{2}\boldsymbol{r}_3^{\mathrm{T}}\boldsymbol{A}_2^{\mathrm{T}}\boldsymbol{E}_1^{\mathrm{T}}\,{}^{1}\boldsymbol{r}_2 + {}^{2}\boldsymbol{r}_3^{\mathrm{T}}\,{}^{2}\boldsymbol{r}_3\right) + J_{\mathrm{p}}, \tag{C.66}$$

$$TPq2t\_A2 = m_{\mathrm{p}}\,{}^{2}\boldsymbol{r}_3^{\mathrm{T}}\,{}^{2}\boldsymbol{r}_3 + J_{\mathrm{p}}, \tag{C.67}$$

$$TPq2t\_A3 = m_{\mathrm{p}}\left(\begin{bmatrix}0 & \phi_{\mathrm{e}11}\end{bmatrix}\boldsymbol{E}_1\boldsymbol{S}\boldsymbol{A}_2\,{}^{2}\boldsymbol{r}_3 + {}^{2}\boldsymbol{r}_3^{\mathrm{T}}\boldsymbol{E}_1\,{}^{2}\boldsymbol{r}_3\phi'_{\mathrm{e}11}\right) + J_{\mathrm{p}}\phi'_{\mathrm{e}11}, \tag{C.68}$$

$$TPq2t\_A4 = m_{\mathrm{p}}\left(\begin{bmatrix}0 & \phi_{\mathrm{e}12}\end{bmatrix}\boldsymbol{E}_1\boldsymbol{S}\boldsymbol{A}_2\,{}^{2}\boldsymbol{r}_3 + {}^{2}\boldsymbol{r}_3^{\mathrm{T}}\boldsymbol{E}_1\,{}^{2}\boldsymbol{r}_3\phi'_{\mathrm{e}12}\right) + J_{\mathrm{p}}\phi'_{\mathrm{e}12}, \tag{C.69}$$

$$TPq2t\_A5 = m_p\begin{bmatrix}0 & \phi_{\mathrm{e}21}\end{bmatrix}\boldsymbol{S}\,{}^{2}\boldsymbol{r}_3 + J_{\mathrm{p}}\phi'_{\mathrm{e}21}, \tag{C.70}$$

$$TPq2t\_A6 = m_p\begin{bmatrix}0 & \phi_{\mathrm{e}22}\end{bmatrix}\boldsymbol{S}\,{}^{2}\boldsymbol{r}_3 + J_{\mathrm{p}}\phi'_{\mathrm{e}22}, \tag{C.71}$$

$$TPq2t\_B = m_{\mathrm{p}}\left(TPq2t\_B1 + TPq2t\_B2 + TPq2t\_B3\right), \tag{C.72}$$

where

$$TPq2t\_B1 = {}^{1}\dot{\boldsymbol{r}}_2^{\mathrm{T}}\boldsymbol{E}_1\boldsymbol{A}_2\,{}^{2}\boldsymbol{r}_3\dot{q}_1 + {}^{1}\boldsymbol{r}_2^{\mathrm{T}}\dot{\boldsymbol{E}}_1\boldsymbol{A}_2\,{}^{2}\boldsymbol{r}_3\dot{q}_1 + {}^{1}\boldsymbol{r}_2^{\mathrm{T}}\boldsymbol{E}_1\boldsymbol{S}\boldsymbol{A}_2\,{}^{2}\boldsymbol{r}_3\dot{q}_1\dot{q}_2 + {}^{1}\boldsymbol{r}_2^{\mathrm{T}}\boldsymbol{E}_1\boldsymbol{A}_2\,{}^{2}\dot{\boldsymbol{r}}_3\dot{q}_1, \tag{C.73}$$

$$TPq2t\_B2 = {}^{1}\dot{\boldsymbol{r}}_2^{\mathrm{T}}\dot{\boldsymbol{E}}_1\boldsymbol{S}\boldsymbol{A}_2\,{}^{2}\boldsymbol{r}_3 - {}^{1}\dot{\boldsymbol{r}}_2^{\mathrm{T}}\boldsymbol{E}_1\boldsymbol{A}_2\,{}^{2}\boldsymbol{r}_3\dot{q}_2 + {}^{1}\dot{\boldsymbol{r}}_2^{\mathrm{T}}\boldsymbol{E}_1\boldsymbol{S}\boldsymbol{A}_2\,{}^{2}\dot{\boldsymbol{r}}_3 + 2\,{}^{2}\boldsymbol{r}_3^{\mathrm{T}}\,{}^{2}\dot{\boldsymbol{r}}_3\dot{q}_1, \tag{C.74}$$

$$TPq2t\_B3 = {}^{2}\dot{\boldsymbol{r}}_3^{\mathrm{T}}\dot{\boldsymbol{E}}_1^{\mathrm{T}}\boldsymbol{E}_1\boldsymbol{S}\,{}^{2}\boldsymbol{r}_3 + {}^{2}\boldsymbol{r}_3^{\mathrm{T}}\dot{\boldsymbol{E}}_1^{\mathrm{T}}\boldsymbol{E}_1\boldsymbol{S}\,{}^{2}\dot{\boldsymbol{r}}_3 + 2\,{}^{2}\boldsymbol{r}_3^{\mathrm{T}}\,{}^{2}\dot{\boldsymbol{r}}_3\dot{q}_2, \tag{C.75}$$

$$\frac{\partial T_{\mathrm{l}_2}}{\partial q_2} = \rho_{\mathrm{l}_2}\int_0^{l_2}\left(TL2q2\_C1 + TL2q2\_C2\right)d\tilde{x}_2, \tag{C.76},$$

where

$$TL2q2\_C1 = -{}^{1}\boldsymbol{r}_2^{\mathrm{T}}\boldsymbol{S}^{\mathrm{T}}\boldsymbol{E}_1\boldsymbol{A}_2\,{}^{2}\boldsymbol{p}_2\dot{q}_1^2 - {}^{1}\dot{\boldsymbol{r}}_2^{\mathrm{T}}\boldsymbol{E}_1\boldsymbol{A}_2\,{}^{2}\boldsymbol{p}_2\dot{q}_1 + {}^{1}\boldsymbol{r}_2^{\mathrm{T}}\dot{\boldsymbol{E}}_1\boldsymbol{A}_2\,{}^{2}\boldsymbol{p}_2\dot{q}_1 + {}^{1}\dot{\boldsymbol{r}}_2^{\mathrm{T}}\dot{\boldsymbol{E}}_1\boldsymbol{S}\boldsymbol{A}_2\,{}^{2}\boldsymbol{p}_2, \tag{C.77}$$

$$TL2q2\_C2 = -{}^{1}\boldsymbol{r}_2^{\mathrm{T}}\boldsymbol{S}^{\mathrm{T}}\boldsymbol{E}_1\boldsymbol{A}_2\,{}^{2}\boldsymbol{p}_2\dot{q}_1\dot{q}_2 - {}^{1}\dot{\boldsymbol{r}}_2^{\mathrm{T}}\boldsymbol{E}_1\boldsymbol{A}_2\,{}^{2}\boldsymbol{p}_2\dot{q}_2 + {}^{1}\boldsymbol{r}_2^{\mathrm{T}}\boldsymbol{E}_1\boldsymbol{A}_2\,{}^{2}\dot{\boldsymbol{p}}_2\dot{q}_1 + {}^{1}\dot{\boldsymbol{r}}_2^{\mathrm{T}}\boldsymbol{E}_1\boldsymbol{S}\boldsymbol{A}_2\,{}^{2}\dot{\boldsymbol{p}}_2, \tag{C.78}$$

$$\frac{\partial T_{\mathrm{p}}}{\partial q_2} = m_{\mathrm{p}}\left(TPq2\_C1 + TPq2\_C2\right), \tag{C.79}$$

where

$$TPq2\_C1 = -{}^{1}\boldsymbol{r}_2^{\mathrm{T}}\boldsymbol{S}^{\mathrm{T}}\boldsymbol{E}_1\boldsymbol{A}_2\,{}^{2}\boldsymbol{r}_3\dot{q}_1^2 - {}^{1}\dot{\boldsymbol{r}}_2^{\mathrm{T}}\boldsymbol{E}_1\boldsymbol{A}_2\,{}^{2}\boldsymbol{r}_3\dot{q}_1 + {}^{1}\boldsymbol{r}_2^{\mathrm{T}}\dot{\boldsymbol{E}}_1\boldsymbol{A}_2\,{}^{2}\boldsymbol{r}_3\dot{q}_1 + {}^{1}\dot{\boldsymbol{r}}_2^{\mathrm{T}}\dot{\boldsymbol{E}}_1\boldsymbol{S}\boldsymbol{A}_2\,{}^{2}\boldsymbol{r}_3, \tag{C.80}$$

$$TPq2\_C2 = -{}^{1}\boldsymbol{r}_2^{\mathrm{T}}\boldsymbol{S}^{\mathrm{T}}\boldsymbol{E}_1\boldsymbol{A}_2\,{}^{2}\boldsymbol{r}_3\dot{q}_1\dot{q}_2 - {}^{1}\dot{\boldsymbol{r}}_2^{\mathrm{T}}\boldsymbol{E}_1\boldsymbol{A}_2\,{}^{2}\boldsymbol{r}_3\dot{q}_2 + {}^{1}\boldsymbol{r}_2^{\mathrm{T}}\boldsymbol{E}_1\boldsymbol{A}_2\,{}^{2}\dot{\boldsymbol{r}}_3\dot{q}_1 + {}^{1}\dot{\boldsymbol{r}}_2^{\mathrm{T}}\boldsymbol{E}_1\boldsymbol{S}\boldsymbol{A}_2\,{}^{2}\dot{\boldsymbol{r}}_3, \tag{C.81}$$

$$\frac{d}{dt}\frac{\partial T_{\mathrm{h}_2}}{\partial \dot{q}_3} = Th2q3t\_A1\ddot{q}_1 + Th2q3t\_A2\ddot{q}_2 + Th2q3t\_A3\ddot{q}_3 + Th2q3t\_A4\ddot{q}_4, \tag{C.82}$$

where

$$Th2q3t\_A1 = m_{\mathrm{h}_2}\left(l_1 + \overline{\mathrm{O}_1\tilde{\mathrm{O}}_1}\right)\phi_{\mathrm{e}11} + J_{\mathrm{h}_2}\phi'_{\mathrm{e}11}, \tag{C.83}$$

$$Th2q3t\_A2 = J_{\mathrm{h}_2}\phi'_{\mathrm{e}11}, \tag{C.84}$$

$$Th2q3t\_A3 = m_{\mathrm{h}_2}\phi_{\mathrm{e}11}^2 + J_{\mathrm{h}_2}\phi'^2_{\mathrm{e}11}, \tag{C.85}$$

$$Th2q3t\_A4 = m_{\mathrm{h}_2}\phi_{\mathrm{e}11}\phi_{\mathrm{e}12} + J_{\mathrm{h}_2}\phi'_{\mathrm{e}11}\phi'_{\mathrm{e}12}, \tag{C.86}$$

$$\frac{d}{dt}\frac{\partial T_{\mathrm{l}_1}}{\partial \dot{q}_3} = \rho_{\mathrm{l}_1}\int_0^{l_1}\tilde{x}_1\phi_{11}(\tilde{x}_1)d\tilde{x}_1\ddot{q}_1 + \rho_{\mathrm{l}_1}\int_0^{l_1}\phi_{11}(\tilde{x}_1)^2 d\tilde{x}_1\ddot{q}_3 + \rho_{\mathrm{l}_1}\int_0^{l_1}\phi_{11}(\tilde{x}_1)\phi_{12}(\tilde{x}_1)d\tilde{x}_1\ddot{q}_4, \tag{C.87}$$

$$\frac{d}{dt}\frac{\partial T_{\mathrm{l}_2}}{\partial \dot{q}_3} = TL2q3t\_A1\ddot{q}_1 + TL2q3t\_A2\ddot{q}_2 + TL2q3t\_A3\ddot{q}_3 + \cdots \\ TL2q3t\_A4\ddot{q}_4 + TL2q3t\_A5\ddot{q}_5 + TL2q3t\_A6\ddot{q}_6 + TL2q3t\_B \quad , \tag{C.88}$$

where

$$TL2q3t\_A1 = \rho_{\mathrm{l}_2}\int_0^{l_2}\left(\left({}^2\boldsymbol{p}_2^{\mathrm{T}}\boldsymbol{A}_2^{\mathrm{T}}{}^1\boldsymbol{r}_2 + {}^2\boldsymbol{p}_2^{\mathrm{T}}\boldsymbol{E}_1{}^2\boldsymbol{p}_2\right)\phi'_{\mathrm{e}11} + \begin{bmatrix}0 & \phi_{\mathrm{e}11}\end{bmatrix}\left(\boldsymbol{S}\boldsymbol{E}_1\boldsymbol{A}_2{}^2\boldsymbol{p}_2 + \boldsymbol{S}{}^1\boldsymbol{r}_2\right)\right)d\tilde{x}_2 , \tag{C.89}$$

$$TL2q3t\_A2 = \rho_{\mathrm{l}_2}\int_0^{l_2}\left(\begin{bmatrix}0 & \phi_{\mathrm{e}11}\end{bmatrix}\boldsymbol{E}_1\boldsymbol{S}\boldsymbol{A}_2{}^2\boldsymbol{p}_2 + {}^2\boldsymbol{p}_2^{\mathrm{T}}\boldsymbol{E}_1{}^2\boldsymbol{p}_2\phi'_{\mathrm{e}11}\right)d\tilde{x}_2 , \tag{C.90}$$

$$TL2q3t\_A3 = \rho_{\mathrm{l}_2}\int_0^{l_2}\left(\phi_{\mathrm{e}11}^2 + {}^2\boldsymbol{p}_2^{\mathrm{T}}\boldsymbol{A}_2^{\mathrm{T}}\boldsymbol{S}^{\mathrm{T}}\begin{bmatrix}0 & \phi_{\mathrm{e}11}\end{bmatrix}^{\mathrm{T}}\phi'_{\mathrm{e}11}\right)d\tilde{x}_2 + \\ \rho_{\mathrm{l}_2}\int_0^{l_2}\left(\begin{bmatrix}0 & \phi_{\mathrm{e}11}\end{bmatrix}\boldsymbol{S}\boldsymbol{A}_2{}^2\boldsymbol{p}_2\phi'_{\mathrm{e}11} + {}^2\boldsymbol{p}_2^{\mathrm{T}}{}^2\boldsymbol{p}_2\phi'^2_{\mathrm{e}11}\right)d\tilde{x}_2 \quad , \tag{C.91}$$

$$TL2q3t\_A4 = \rho_{\mathrm{l}_2}\int_0^{l_2}\left(\phi_{\mathrm{e}11}\phi_{\mathrm{e}12} + {}^2\boldsymbol{p}_2^{\mathrm{T}}\boldsymbol{A}_2^{\mathrm{T}}\boldsymbol{S}^{\mathrm{T}}\begin{bmatrix}0 & \phi_{\mathrm{e}11}\end{bmatrix}^{\mathrm{T}}\phi'_{\mathrm{e}12}\right)d\tilde{x}_2 + \cdots \\ \rho_{\mathrm{l}_2}\int_0^{l_2}\left(\begin{bmatrix}0 & \phi_{\mathrm{e}12}\end{bmatrix}\boldsymbol{S}\boldsymbol{A}_2{}^2\boldsymbol{p}_2\phi'_{\mathrm{e}11} + {}^2\boldsymbol{p}_2^{\mathrm{T}}{}^2\boldsymbol{p}_2\phi'_{\mathrm{e}11}\phi'_{\mathrm{e}12}\right)d\tilde{x}_2 \quad , \tag{C.92}$$

$$TL2q3t\_A5 = \rho_{\mathrm{l}_2}\int_0^{l_2}\left(\begin{bmatrix}0 & \phi_{21}(\tilde{x}_2)\end{bmatrix}\boldsymbol{A}_2^{\mathrm{T}}\boldsymbol{E}_1^{\mathrm{T}}\begin{bmatrix}0 & \phi_{\mathrm{e}11}\end{bmatrix}^{\mathrm{T}} + \begin{bmatrix}0 & \phi_{21}(\tilde{x}_2)\end{bmatrix}\boldsymbol{E}_1^{\mathrm{T}}\boldsymbol{S}{}^2\boldsymbol{p}_2\phi'_{\mathrm{e}11}\right)d\tilde{x}_2 , \tag{C.93}$$

$$TL2q3t\_A6 = \rho_{\mathrm{l}_2}\int_0^{l_2}\left(\begin{bmatrix}0 & \phi_{22}(\tilde{x}_2)\end{bmatrix}\boldsymbol{A}_2^{\mathrm{T}}\boldsymbol{E}_1^{\mathrm{T}}\begin{bmatrix}0 & \phi_{\mathrm{e}11}\end{bmatrix}^{\mathrm{T}} + \begin{bmatrix}0 & \phi_{22}(\tilde{x}_2)\end{bmatrix}\boldsymbol{E}_1^{\mathrm{T}}\boldsymbol{S}{}^2\boldsymbol{p}_2\phi'_{\mathrm{e}11}\right)d\tilde{x}_2 , \tag{C.94}$$

$$TL2q3t\_B = \rho_{\mathrm{l}_2}\int_0^{l_2}\left(TL2q3t\_B1 + TL2q3t\_B2 + TL2q3t\_B3\right)d\tilde{x}_2 + \cdots \\ \rho_{\mathrm{l}_2}\int_0^{l_2}\left(TL2q3t\_B4 + TL2q3t\_B5\right)d\tilde{x}_2 \quad , \tag{C.95}$$

where

$$TL2q3t\_B1 = {}^2\dot{\boldsymbol{p}}_2^{\mathrm{T}}\boldsymbol{A}_2^{\mathrm{T}}\boldsymbol{E}_1^{\mathrm{T}}\boldsymbol{S}^{\mathrm{T}}\begin{bmatrix}0 & \phi_{\mathrm{e}11}\end{bmatrix}^{\mathrm{T}}\dot{q}_2 - {}^2\boldsymbol{p}_2^{\mathrm{T}}\boldsymbol{A}_2^{\mathrm{T}}\boldsymbol{E}_1^{\mathrm{T}}\begin{bmatrix}0 & \phi_{\mathrm{e}11}\end{bmatrix}^{\mathrm{T}}\dot{q}_1\dot{q}_2 + \cdots \\ {}^2\boldsymbol{p}_2^{\mathrm{T}}\boldsymbol{A}_2^{\mathrm{T}}\dot{\boldsymbol{E}}_1^{\mathrm{T}}\boldsymbol{S}^{\mathrm{T}}\begin{bmatrix}0 & \phi_{\mathrm{e}11}\end{bmatrix}^{\mathrm{T}}\dot{q}_1 + 2{}^2\dot{\boldsymbol{p}}_2^{\mathrm{T}}\boldsymbol{A}_2^{\mathrm{T}}\boldsymbol{E}_1^{\mathrm{T}}\begin{bmatrix}0 & \phi_{\mathrm{e}11}\end{bmatrix}^{\mathrm{T}} \quad , \tag{C.96}$$

$$TL2q3t\_B2 = 2{}^2\boldsymbol{p}_2^{\mathrm{T}}\boldsymbol{A}_2^{\mathrm{T}}\boldsymbol{S}^{\mathrm{T}}\dot{\boldsymbol{E}}_1^{\mathrm{T}}\begin{bmatrix}0 & \phi_{\mathrm{e}11}\end{bmatrix}^{\mathrm{T}}\dot{q}_2 + 2{}^2\dot{\boldsymbol{p}}_2^{\mathrm{T}}\boldsymbol{A}_2^{\mathrm{T}}\boldsymbol{S}^{\mathrm{T}}\boldsymbol{E}_1^{\mathrm{T}}\begin{bmatrix}0 & \phi_{\mathrm{e}11}\end{bmatrix}^{\mathrm{T}}\dot{q}_2 + \cdots \\ -{}^2\boldsymbol{p}_2^{\mathrm{T}}\boldsymbol{A}_2^{\mathrm{T}}\boldsymbol{E}_1^{\mathrm{T}}\begin{bmatrix}0 & \phi_{\mathrm{e}11}\end{bmatrix}^{\mathrm{T}}\dot{q}_2^2 + {}^1\dot{\boldsymbol{r}}_2^{\mathrm{T}}\boldsymbol{A}_2{}^2\boldsymbol{p}_2\phi'_{\mathrm{e}11}\dot{q}_1 \quad , \tag{C.97}$$

$$TL2q3t\_B3 = {}^1\boldsymbol{r}_2^{\mathrm{T}}\boldsymbol{S}\boldsymbol{A}_2{}^2\boldsymbol{p}_2\phi'_{\mathrm{e}11}\dot{q}_1\dot{q}_2 + {}^1\boldsymbol{r}_2^{\mathrm{T}}\boldsymbol{A}_2{}^2\dot{\boldsymbol{p}}_2\phi'_{\mathrm{e}11}\dot{q}_1 - {}^1\dot{\boldsymbol{r}}_2^{\mathrm{T}}\boldsymbol{A}_2{}^2\boldsymbol{p}_2\phi'_{\mathrm{e}11}\dot{q}_2 + {}^1\dot{\boldsymbol{r}}_2^{\mathrm{T}}\boldsymbol{S}\boldsymbol{A}_2{}^2\dot{\boldsymbol{p}}_2\phi'_{\mathrm{e}11} , \tag{C.98}$$

$$TL2q3t\_B4 = {}^2\dot{\boldsymbol{p}}_2^{\mathrm{T}}\boldsymbol{E}_1^{\mathrm{T}}{}^2\boldsymbol{p}_2\phi'_{\mathrm{e}11}\dot{q}_1 + {}^2\boldsymbol{p}_2^{\mathrm{T}}\boldsymbol{E}_1^{\mathrm{T}}{}^2\dot{\boldsymbol{p}}_2\phi'_{\mathrm{e}11}\dot{q}_1 + {}^2\dot{\boldsymbol{p}}_2^{\mathrm{T}}\dot{\boldsymbol{E}}_1^{\mathrm{T}}\boldsymbol{S}{}^2\boldsymbol{p}_2\phi'_{\mathrm{e}11} + {}^2\boldsymbol{p}_2^{\mathrm{T}}\dot{\boldsymbol{E}}_1^{\mathrm{T}}\boldsymbol{S}{}^2\dot{\boldsymbol{p}}_2\phi'_{\mathrm{e}11} , \tag{C.99}$$

$$TL2q3t\_B5 = {}^2\dot{\boldsymbol{p}}_2^{\mathrm{T}}\boldsymbol{E}_1^{\mathrm{T}}{}^2\boldsymbol{p}_2\phi'_{\mathrm{e}11}\dot{q}_2 + {}^2\boldsymbol{p}_2^{\mathrm{T}}\boldsymbol{E}_1^{\mathrm{T}}{}^2\dot{\boldsymbol{p}}_2\phi'_{\mathrm{e}11}\dot{q}_2 + {}^2\dot{\boldsymbol{p}}_2^{\mathrm{T}}\dot{\boldsymbol{E}}_1^{\mathrm{T}}\boldsymbol{S}{}^2\boldsymbol{p}_2\phi'_{\mathrm{e}11} + {}^2\dot{\boldsymbol{p}}_2^{\mathrm{T}}\boldsymbol{E}_1^{\mathrm{T}}\boldsymbol{S}{}^2\dot{\boldsymbol{p}}_2\phi'_{\mathrm{e}11} , \tag{C.100}$$

$$\frac{d}{dt}\frac{\partial T_{\mathrm{p}}}{\partial \dot{q}_3} = TPq3t\_A1\ddot{q}_1 + TPq3t\_A2\ddot{q}_2 + TPq3t\_A3\ddot{q}_3 + \cdots \\ TPq3t\_A4\ddot{q}_4 + TPq3t\_A5\ddot{q}_5 + TPq3t\_A6\ddot{q}_6 + TPq3t\_B \quad , \tag{C.101}$$

where

$$TPq3t\_A1 = m_{\mathrm{p}}\begin{bmatrix}0 & \phi_{\mathrm{e}11}\end{bmatrix}\left(\boldsymbol{S}\boldsymbol{E}_1\boldsymbol{A}_2{}^2\boldsymbol{r}_3 + \boldsymbol{S}{}^1\boldsymbol{r}_2\right) + m_{\mathrm{p}}\left({}^2\boldsymbol{r}_3^{\mathrm{T}}\boldsymbol{A}_2^{\mathrm{T}}{}^1\boldsymbol{r}_2 + {}^2\boldsymbol{r}_3^{\mathrm{T}}\boldsymbol{E}_1{}^2\boldsymbol{r}_3\right)\phi'_{\mathrm{e}11} + J_{\mathrm{p}}\phi'_{\mathrm{e}11} , \tag{C.102}$$

$$TPq3t\_A2 = m_{\mathrm{p}}\left(\begin{bmatrix}0 & \phi_{\mathrm{e}11}\end{bmatrix}\boldsymbol{E}_1\boldsymbol{S}\boldsymbol{A}_2{}^2\boldsymbol{r}_3 + {}^2\boldsymbol{r}_3^{\mathrm{T}}\boldsymbol{E}_1{}^2\boldsymbol{r}_3\phi'_{\mathrm{e}11}\right) + J_{\mathrm{p}}\phi'_{\mathrm{e}11} , \tag{C.103}$$

$$TPq3t\_A3 = m_{\mathrm{p}}\left(\phi_{\mathrm{e}11}^2 + {}^2\boldsymbol{r}_3^{\mathrm{T}}\boldsymbol{A}_2^{\mathrm{T}}\boldsymbol{S}^{\mathrm{T}}\begin{bmatrix}0 & \phi_{\mathrm{e}11}\end{bmatrix}^{\mathrm{T}}\phi'_{\mathrm{e}11}\right) + \cdots \\ J_{\mathrm{p}}\phi'^2_{\mathrm{e}11} + m_{\mathrm{p}}\left(\begin{bmatrix}0 & \phi_{\mathrm{e}11}\end{bmatrix}\boldsymbol{S}\boldsymbol{A}_2{}^2\boldsymbol{r}_3\phi'_{\mathrm{e}11} + {}^2\boldsymbol{r}_3^{\mathrm{T}}{}^2\boldsymbol{r}_3\phi'^2_{\mathrm{e}11}\right) \quad , \tag{C.104}$$

$$TPq3t\_A4 = m_{\mathrm{p}}\left(\phi_{\mathrm{e}11}\phi_{\mathrm{e}12} + {}^{2}\boldsymbol{r}_{3}^{\mathrm{T}}\boldsymbol{A}_{2}^{\mathrm{T}}\boldsymbol{S}^{\mathrm{T}}\begin{bmatrix}0 & \phi_{\mathrm{e}11}\end{bmatrix}^{\mathrm{T}}\phi'_{\mathrm{e}12}\right)+\cdots$$
$$J_{\mathrm{p}}\phi'_{\mathrm{e}11}\phi'_{\mathrm{e}12} + m_{\mathrm{p}}\left(\begin{bmatrix}0 & \phi_{\mathrm{e}12}\end{bmatrix}\boldsymbol{S}\boldsymbol{A}_{2}\,{}^{2}\boldsymbol{r}_{3}\phi'_{\mathrm{e}11} + {}^{2}\boldsymbol{r}_{3}^{\mathrm{T}}\,{}^{2}\boldsymbol{r}_{3}\phi'_{\mathrm{e}11}\phi'_{\mathrm{e}12}\right), \tag{C.105}$$

$$TPq3t\_A5 = m_{\mathrm{p}}\left(\begin{bmatrix}0 & \phi_{\mathrm{e}21}\end{bmatrix}\boldsymbol{A}_{2}^{\mathrm{T}}\boldsymbol{E}_{1}^{\mathrm{T}}\begin{bmatrix}0 & \phi_{\mathrm{e}11}\end{bmatrix}^{\mathrm{T}} + \begin{bmatrix}0 & \phi_{\mathrm{e}21}\end{bmatrix}\boldsymbol{E}_{1}^{\mathrm{T}}\boldsymbol{S}\,{}^{2}\boldsymbol{r}_{3}\phi'_{\mathrm{e}11}\right) + J_{\mathrm{p}}\phi'_{\mathrm{e}11}\phi'_{\mathrm{e}21}, \tag{C.106}$$

$$TPq3t\_A6 = m_{\mathrm{p}}\left(\begin{bmatrix}0 & \phi_{\mathrm{e}22}\end{bmatrix}\boldsymbol{A}_{2}^{\mathrm{T}}\boldsymbol{E}_{1}^{\mathrm{T}}\begin{bmatrix}0 & \phi_{\mathrm{e}11}\end{bmatrix}^{\mathrm{T}} + \begin{bmatrix}0 & \phi_{\mathrm{e}22}\end{bmatrix}\boldsymbol{E}_{1}^{\mathrm{T}}\boldsymbol{S}\,{}^{2}\boldsymbol{r}_{3}\phi'_{\mathrm{e}11}\right) + J_{\mathrm{p}}\phi'_{\mathrm{e}11}\phi'_{\mathrm{e}22}, \tag{C.107}$$

$$TPq3t\_B = m_{\mathrm{p}}\left(TPq3t\_B1 + TPq3t\_B2 + TPq3t\_B3\right)+\cdots$$
$$m_{\mathrm{p}}\left(TPq3t\_B4 + TPq3t\_B5\right), \tag{C.108}$$

where

$$TPq3t\_B1 = {}^{2}\dot{\boldsymbol{r}}_{3}^{\mathrm{T}}\boldsymbol{A}_{2}^{\mathrm{T}}\boldsymbol{E}_{1}^{\mathrm{T}}\boldsymbol{S}^{\mathrm{T}}\begin{bmatrix}0 & \phi_{\mathrm{e}11}\end{bmatrix}^{\mathrm{T}}\dot{q}_{2} - {}^{2}\boldsymbol{r}_{3}^{\mathrm{T}}\boldsymbol{A}_{2}^{\mathrm{T}}\boldsymbol{E}_{1}^{\mathrm{T}}\begin{bmatrix}0 & \phi_{\mathrm{e}11}\end{bmatrix}^{\mathrm{T}}\dot{q}_{1}\dot{q}_{2}+\cdots$$
$${}^{2}\boldsymbol{r}_{3}^{\mathrm{T}}\boldsymbol{A}_{2}^{\mathrm{T}}\dot{\boldsymbol{E}}_{1}^{\mathrm{T}}\boldsymbol{S}^{\mathrm{T}}\begin{bmatrix}0 & \phi_{\mathrm{e}11}\end{bmatrix}^{\mathrm{T}}\dot{q}_{1} + 2\,{}^{2}\dot{\boldsymbol{r}}_{3}^{\mathrm{T}}\boldsymbol{A}_{2}^{\mathrm{T}}\dot{\boldsymbol{E}}_{1}^{\mathrm{T}}\begin{bmatrix}0 & \phi_{\mathrm{e}11}\end{bmatrix}^{\mathrm{T}}, \tag{C.109}$$

$$TPq3t\_B2 = 2\,{}^{2}\boldsymbol{r}_{3}^{\mathrm{T}}\boldsymbol{A}_{2}^{\mathrm{T}}\boldsymbol{S}^{\mathrm{T}}\dot{\boldsymbol{E}}_{1}^{\mathrm{T}}\begin{bmatrix}0 & \phi_{\mathrm{e}11}\end{bmatrix}^{\mathrm{T}}\dot{q}_{2} + 2\,{}^{2}\dot{\boldsymbol{r}}_{3}^{\mathrm{T}}\boldsymbol{A}_{2}^{\mathrm{T}}\boldsymbol{S}^{\mathrm{T}}\boldsymbol{E}_{1}^{\mathrm{T}}\begin{bmatrix}0 & \phi_{\mathrm{e}11}\end{bmatrix}^{\mathrm{T}}\dot{q}_{2}+\cdots$$
$$-\,{}^{2}\boldsymbol{r}_{3}^{\mathrm{T}}\boldsymbol{A}_{2}^{\mathrm{T}}\boldsymbol{E}_{1}^{\mathrm{T}}\begin{bmatrix}0 & \phi_{\mathrm{e}11}\end{bmatrix}^{\mathrm{T}}\dot{q}_{2}^{2} + {}^{1}\dot{\boldsymbol{r}}_{2}^{\mathrm{T}}\boldsymbol{A}_{2}\,{}^{2}\boldsymbol{r}_{3}\phi'_{\mathrm{e}11}\dot{q}_{1}, \tag{C.110}$$

$$TPq3t\_B3 = {}^{1}\boldsymbol{r}_{2}^{\mathrm{T}}\boldsymbol{S}\boldsymbol{A}_{2}\,{}^{2}\boldsymbol{r}_{3}\phi'_{\mathrm{e}11}\dot{q}_{1}\dot{q}_{2} + {}^{1}\boldsymbol{r}_{2}^{\mathrm{T}}\boldsymbol{A}_{2}\,{}^{2}\dot{\boldsymbol{r}}_{3}\phi'_{\mathrm{e}11}\dot{q}_{1} - {}^{1}\dot{\boldsymbol{r}}_{2}^{\mathrm{T}}\boldsymbol{A}_{2}\,{}^{2}\boldsymbol{r}_{3}\phi'_{\mathrm{e}11}\dot{q}_{2} + {}^{1}\dot{\boldsymbol{r}}_{2}^{\mathrm{T}}\boldsymbol{S}\boldsymbol{A}_{2}\,{}^{2}\dot{\boldsymbol{r}}_{3}\phi'_{\mathrm{e}11}, \tag{C.111}$$

$$TPq3t\_B4 = {}^{2}\dot{\boldsymbol{r}}_{3}^{\mathrm{T}}\boldsymbol{E}_{1}^{\mathrm{T}}\,{}^{2}\boldsymbol{r}_{3}\phi'_{\mathrm{e}11}\dot{q}_{1} + {}^{2}\boldsymbol{r}_{3}^{\mathrm{T}}\boldsymbol{E}_{1}^{\mathrm{T}}\,{}^{2}\dot{\boldsymbol{r}}_{3}\phi'_{\mathrm{e}11}\dot{q}_{1} + {}^{2}\dot{\boldsymbol{r}}_{3}^{\mathrm{T}}\dot{\boldsymbol{E}}_{1}^{\mathrm{T}}\boldsymbol{S}\,{}^{2}\boldsymbol{r}_{3}\phi'_{\mathrm{e}11} + {}^{2}\boldsymbol{r}_{3}^{\mathrm{T}}\dot{\boldsymbol{E}}_{1}^{\mathrm{T}}\boldsymbol{S}\,{}^{2}\dot{\boldsymbol{r}}_{3}\phi'_{\mathrm{e}11}, \tag{C.112}$$

$$TPq3t\_B5 = {}^{2}\dot{\boldsymbol{r}}_{3}^{\mathrm{T}}\boldsymbol{E}_{1}^{\mathrm{T}}\,{}^{2}\boldsymbol{r}_{3}\phi'_{\mathrm{e}11}\dot{q}_{2} + {}^{2}\boldsymbol{r}_{3}^{\mathrm{T}}\boldsymbol{E}_{1}^{\mathrm{T}}\,{}^{2}\dot{\boldsymbol{r}}_{3}\phi'_{\mathrm{e}11}\dot{q}_{2} + {}^{2}\dot{\boldsymbol{r}}_{3}^{\mathrm{T}}\dot{\boldsymbol{E}}_{1}^{\mathrm{T}}\boldsymbol{S}\,{}^{2}\boldsymbol{r}_{3}\phi'_{\mathrm{e}11} + {}^{2}\dot{\boldsymbol{r}}_{3}^{\mathrm{T}}\boldsymbol{E}_{1}^{\mathrm{T}}\boldsymbol{S}\,{}^{2}\dot{\boldsymbol{r}}_{3}\phi'_{\mathrm{e}11}, \tag{C.113}$$

$$\frac{\partial T_{\mathrm{h}_2}}{\partial q_3} = m_{\mathrm{h}_2}\,{}^{1}\boldsymbol{r}_{2}^{\mathrm{T}}\begin{bmatrix}0 & \phi_{\mathrm{e}11}\end{bmatrix}^{\mathrm{T}}\dot{q}_{1}^{2}, \tag{C.114}$$

$$\frac{\partial T_{\mathrm{l}_1}}{\partial q_3} = \rho_{\mathrm{l}_1}\int_{0}^{l_1}{}^{1}\boldsymbol{p}_{1}^{\mathrm{T}}\begin{bmatrix}0 & \phi_{1}(\tilde{x}_{1})\end{bmatrix}^{\mathrm{T}}d\tilde{x}_{1}\dot{q}_{1}^{2}, \tag{C.115}$$

$$\frac{\partial T_{\mathrm{l}_2}}{\partial q_3} = \rho_{\mathrm{l}_2}\int_{0}^{l_2}\left(TL2q3\_C1 + TL2q3\_C2 + TL2q3\_C3\right)d\tilde{x}_{2}+\cdots$$
$$\rho_{\mathrm{l}_2}\int_{0}^{l_2}\left(TL2q3\_C4 + TL2q3\_C5\right)d\tilde{x}_{2}, \tag{C.116}$$

where

$$TL2q3\_C1 = {}^{1}\boldsymbol{r}_{2}^{\mathrm{T}}\begin{bmatrix}0 & \phi_{\mathrm{e}11}\end{bmatrix}^{\mathrm{T}}\dot{q}_{1}^{2} + {}^{2}\boldsymbol{p}_{2}^{\mathrm{T}}\boldsymbol{A}_{2}^{\mathrm{T}}\boldsymbol{E}_{1}^{\mathrm{T}}\begin{bmatrix}0 & \phi_{\mathrm{e}11}\end{bmatrix}^{\mathrm{T}}\dot{q}_{1}^{2}+\cdots$$
$${}^{2}\boldsymbol{p}_{2}^{\mathrm{T}}\boldsymbol{A}_{2}^{\mathrm{T}}\dot{\boldsymbol{E}}_{1}^{\mathrm{T}}\boldsymbol{S}\begin{bmatrix}0 & \phi_{\mathrm{e}11}\end{bmatrix}^{\mathrm{T}}\dot{q}_{1} + {}^{2}\boldsymbol{p}_{2}^{\mathrm{T}}\boldsymbol{A}_{2}^{\mathrm{T}}\boldsymbol{E}_{1}^{\mathrm{T}}\begin{bmatrix}0 & \phi_{\mathrm{e}11}\end{bmatrix}^{\mathrm{T}}\dot{q}_{1}\dot{q}_{2}, \tag{C.117}$$

$$TL2q3\_C2 = {}^{2}\dot{\boldsymbol{p}}_{2}^{\mathrm{T}}\boldsymbol{A}_{2}^{\mathrm{T}}\boldsymbol{E}_{1}^{\mathrm{T}}\boldsymbol{S}\begin{bmatrix}0 & \phi_{\mathrm{e}11}\end{bmatrix}^{\mathrm{T}}\dot{q}_{1} - {}^{1}\boldsymbol{r}_{2}^{\mathrm{T}}\boldsymbol{S}^{\mathrm{T}}\boldsymbol{A}_{2}\,{}^{2}\boldsymbol{p}_{2}\phi'_{\mathrm{e}11}\dot{q}_{1}^{2}+\cdots$$
$$-\,{}^{1}\dot{\boldsymbol{r}}_{2}^{\mathrm{T}}\boldsymbol{A}_{2}\,{}^{2}\boldsymbol{p}_{2}\phi'_{\mathrm{e}11}\dot{q}_{1} - {}^{2}\boldsymbol{p}_{2}^{\mathrm{T}}\boldsymbol{E}_{1}^{\mathrm{T}}\boldsymbol{S}^{\mathrm{T}}\,{}^{2}\boldsymbol{p}_{2}\phi'_{\mathrm{e}11}\dot{q}_{1}^{2}, \tag{C.118}$$

$$TL2q3\_C3 = -2\,{}^{2}\boldsymbol{p}_{2}^{\mathrm{T}}\boldsymbol{S}^{\mathrm{T}}\boldsymbol{E}_{1}^{\mathrm{T}}\,{}^{2}\boldsymbol{p}_{2}\phi'_{\mathrm{e}11}\dot{q}_{1}\dot{q}_{2} - {}^{1}\boldsymbol{r}_{2}^{\mathrm{T}}\boldsymbol{S}^{\mathrm{T}}\boldsymbol{A}_{2}\,{}^{2}\boldsymbol{p}_{2}\phi'_{\mathrm{e}11}\dot{q}_{1}\dot{q}_{2}+\cdots$$
$$-\,{}^{1}\dot{\boldsymbol{r}}_{2}^{\mathrm{T}}\boldsymbol{A}_{2}\,{}^{2}\boldsymbol{p}_{2}\phi'_{\mathrm{e}11}\dot{q}_{2} - \boldsymbol{p}_{2}^{\mathrm{T}}\boldsymbol{S}^{\mathrm{T}}\boldsymbol{E}_{1}^{\mathrm{T}}\,{}^{2}\boldsymbol{p}_{2}\phi'_{\mathrm{e}11}\dot{q}_{2}^{2}, \tag{C.119}$$

$$TL2q3\_C4 = -{}^{2}\dot{\boldsymbol{p}}_{2}^{\mathrm{T}}\boldsymbol{E}_{1}^{\mathrm{T}}\,{}^{2}\boldsymbol{p}_{2}\phi'_{\mathrm{e}11}\dot{q}_{2} + {}^{1}\boldsymbol{r}_{2}^{\mathrm{T}}\boldsymbol{A}_{2}\,{}^{2}\dot{\boldsymbol{p}}_{2}\phi'_{\mathrm{e}11}\dot{q}_{1}+\cdots$$
$${}^{1}\dot{\boldsymbol{r}}_{2}^{\mathrm{T}}\boldsymbol{S}\boldsymbol{A}_{2}\,{}^{2}\dot{\boldsymbol{p}}_{2}\phi'_{\mathrm{e}11} + {}^{2}\boldsymbol{p}_{2}^{\mathrm{T}}\dot{\boldsymbol{E}}_{1}^{\mathrm{T}}\boldsymbol{S}\,{}^{2}\dot{\boldsymbol{p}}_{2}\phi'_{\mathrm{e}11}, \tag{C.120}$$

$$TL2q3\_C5 = {}^{2}\boldsymbol{p}_{2}^{\mathrm{T}}\boldsymbol{E}_{1}^{\mathrm{T}}\,{}^{2}\dot{\boldsymbol{p}}_{2}\phi'_{\mathrm{e}11}\dot{q}_{2} + {}^{2}\dot{\boldsymbol{p}}_{2}^{\mathrm{T}}\boldsymbol{E}_{1}^{\mathrm{T}}\boldsymbol{S}\,{}^{2}\dot{\boldsymbol{p}}_{2}\phi'_{\mathrm{e}11}+\cdots$$
$$-\,{}^{2}\dot{\boldsymbol{p}}_{2}^{\mathrm{T}}\boldsymbol{E}_{1}^{\mathrm{T}}\,{}^{2}\boldsymbol{p}_{2}\phi'_{\mathrm{e}11}\dot{q}_{1} + {}^{2}\boldsymbol{p}_{2}^{\mathrm{T}}\boldsymbol{E}_{1}^{\mathrm{T}}\,{}^{2}\dot{\boldsymbol{p}}_{2}\phi'_{\mathrm{e}11}\dot{q}_{1}, \tag{C.121}$$

$$\frac{\partial T_{\mathrm{p}}}{\partial q_3} = \begin{array}{l} m_{\mathrm{p}}\left(TPq3\_C1 + TPq3\_C2\right) + \cdots \\ m_{\mathrm{p}}\left(TPq3\_C3 + TPq3\_C4\right) \end{array}, \tag{C.122}$$

where

$$TPq3\_C1 = \begin{array}{l} {}^{1}\boldsymbol{r}_2^{\mathrm{T}}\left[0 \;\; \phi_{\mathrm{e}11}\right]^{\mathrm{T}} \dot{q}_1^2 + {}^{2}\boldsymbol{r}_3^{\mathrm{T}}\boldsymbol{A}_2^{\mathrm{T}}\boldsymbol{E}_1^{\mathrm{T}}\left[0 \;\; \phi_{\mathrm{e}11}\right]^{\mathrm{T}} \dot{q}_1^2 + \cdots \\ {}^{2}\boldsymbol{r}_3^{\mathrm{T}}\boldsymbol{A}_2^{\mathrm{T}}\dot{\boldsymbol{E}}_1^{\mathrm{T}}\boldsymbol{S}\left[0 \;\; \phi_{\mathrm{e}11}\right]^{\mathrm{T}} \dot{q}_1 + {}^{2}\boldsymbol{r}_3^{\mathrm{T}}\boldsymbol{A}_2^{\mathrm{T}}\boldsymbol{E}_1^{\mathrm{T}}\left[0 \;\; \phi_{\mathrm{e}11}\right]^{\mathrm{T}} \dot{q}_1\dot{q}_2 \end{array}, \tag{C.123}$$

$$TPq3\_C2 = \begin{array}{l} +{}^{2}\dot{\boldsymbol{r}}_3^{\mathrm{T}}\boldsymbol{A}_2^{\mathrm{T}}\boldsymbol{E}_1^{\mathrm{T}}\boldsymbol{S}\left[0 \;\; \phi_{\mathrm{e}11}\right]^{\mathrm{T}} \dot{q}_1 - {}^{1}\boldsymbol{r}_2^{\mathrm{T}}\boldsymbol{S}^{\mathrm{T}}\boldsymbol{A}_2\,{}^{2}\boldsymbol{r}_3\phi'_{\mathrm{e}11}\left(\dot{q}_1+\dot{q}_2\right)\dot{q}_1 + \cdots \\ -{}^{1}\dot{\boldsymbol{r}}_2^{\mathrm{T}}\boldsymbol{A}_2\,{}^{2}\boldsymbol{r}_3\phi'_{\mathrm{e}11}\left(\dot{q}_1+\dot{q}_2\right) - {}^{2}\boldsymbol{r}_3^{\mathrm{T}}\boldsymbol{E}_1^{\mathrm{T}}\boldsymbol{S}^{\mathrm{T}}\,{}^{2}\boldsymbol{r}_3\phi'_{\mathrm{e}11}\left(\dot{q}_1+\dot{q}_2\right)\dot{q}_1 \end{array}, \tag{C.124}$$

$$TPq3\_C3 = \begin{array}{l} -{}^{2}\boldsymbol{r}_3^{\mathrm{T}}\boldsymbol{S}^{\mathrm{T}}\boldsymbol{E}_1^{\mathrm{T}}\,{}^{2}\boldsymbol{r}_3\phi'_{\mathrm{e}11}\left(\dot{q}_1+\dot{q}_2\right)\dot{q}_2 - {}^{2}\dot{\boldsymbol{r}}_3^{\mathrm{T}}\boldsymbol{E}_1^{\mathrm{T}}\,{}^{2}\boldsymbol{r}_3\phi'_{\mathrm{e}11}\left(\dot{q}_1+\dot{q}_2\right) + \cdots \\ {}^{1}\boldsymbol{r}_2^{\mathrm{T}}\boldsymbol{A}_2\,{}^{2}\dot{\boldsymbol{r}}_3\phi'_{\mathrm{e}11}\dot{q}_1 + {}^{1}\dot{\boldsymbol{r}}_2^{\mathrm{T}}\boldsymbol{S}\boldsymbol{A}_2\,{}^{2}\dot{\boldsymbol{r}}_3\phi'_{\mathrm{e}11} \end{array}, \tag{C.125}$$

$$TPq3\_C4 = \begin{array}{l} {}^{2}\boldsymbol{r}_3^{\mathrm{T}}\boldsymbol{E}_1^{\mathrm{T}}\,{}^{2}\dot{\boldsymbol{r}}_3\phi'_{\mathrm{e}11}\dot{q}_1 + {}^{2}\boldsymbol{r}_3^{\mathrm{T}}\dot{\boldsymbol{E}}_1^{\mathrm{T}}\boldsymbol{S}^{2}\dot{\boldsymbol{r}}_3\phi'_{\mathrm{e}11} + \cdots \\ +{}^{2}\boldsymbol{r}_3^{\mathrm{T}}\boldsymbol{E}_1^{\mathrm{T}}\,{}^{2}\dot{\boldsymbol{r}}_3\phi'_{\mathrm{e}11}\dot{q}_2 + {}^{2}\dot{\boldsymbol{r}}_3^{\mathrm{T}}\boldsymbol{E}_1^{\mathrm{T}}\boldsymbol{S}^{2}\dot{\boldsymbol{r}}_3\phi'_{\mathrm{e}11} \end{array}, \tag{C.126}$$

$$\frac{\partial U_{\mathrm{l}_1}}{\partial q_3} = \left(EI\right)_1 \int_0^{l_1}\left(\phi_{11}(\tilde{x}_1)\sum_{i=1}^{2}\phi_{1i}(\tilde{x}_1)q_{i+2}\right)d\tilde{x}_1, \tag{C.127}$$

$$\frac{d}{dt}\frac{\partial T_{\mathrm{h}_2}}{\partial \dot{q}_4} = Th2q4t\_A1\ddot{q}_1 + Th2q4t\_A2\ddot{q}_2 + Th2q4t\_A3\ddot{q}_3 + Th2q4t\_A4\ddot{q}_4, \tag{C.128}$$

where

$$Th2q4t\_A1 = m_{\mathrm{h}_2}\left(l_1 + \overline{\mathrm{O}_1\tilde{\mathrm{O}}_1}\right)\phi_{\mathrm{e}12} + J_{\mathrm{h}_2}\phi'_{\mathrm{e}12}, \tag{C.129}$$

$$Th2q4t\_A2 = m_{\mathrm{h}_2}\left(l_1 + \overline{\mathrm{O}_1\tilde{\mathrm{O}}_1}\right)\phi_{\mathrm{e}12} + J_{\mathrm{h}_2}\phi'_{\mathrm{e}12}, \tag{C.130}$$

$$Th2q4t\_A3 = m_{\mathrm{h}_2}\phi_{\mathrm{e}11}\phi_{\mathrm{e}12} + J_{\mathrm{h}_2}\phi'_{\mathrm{e}11}\phi'_{\mathrm{e}12}, \tag{C.131}$$

$$Th2q4t\_A = m_{\mathrm{h}_2}\phi_{\mathrm{e}12}^2 + J_{\mathrm{h}_2}\phi'^2_{\mathrm{e}12}, \tag{C.132}$$

$$\frac{d}{dt}\frac{\partial T_{\mathrm{l}_1}}{\partial \dot{q}_4} = \rho_{\mathrm{l}_1}\int_0^{l_1}\tilde{x}_1\phi_{12}(\tilde{x}_1)d\tilde{x}_1 + \rho_{\mathrm{l}_1}\int_0^{l_1}\phi_{11}(\tilde{x}_1)\phi_{12}(\tilde{x}_1)d\tilde{x}_1 + \rho_{\mathrm{l}_1}\int_0^{l_1}\phi_{12}(\tilde{x}_1)^2 d\tilde{x}_1, \tag{C.133}$$

$$\frac{d}{dt}\frac{\partial T_{\mathrm{l}_2}}{\partial \dot{q}_4} = \begin{array}{l} TL2q4t\_A1\ddot{q}_1 + TL2q4t\_A2\ddot{q}_2 + TL2q4t\_A3\ddot{q}_3 + \cdots \\ TL2q4t\_A4\ddot{q}_4 + TL2q4t\_A5\ddot{q}_5 + TL2q4t\_A6\ddot{q}_6 + TL2q4t\_B \end{array}, \tag{C.134}$$

where

$$TL2q4t\_A1 = \rho_{\mathrm{l}_2}\int_0^{l_2}\left(\left({}^{2}\boldsymbol{p}_2^{\mathrm{T}}\boldsymbol{A}_2^{\mathrm{T}}\,{}^{1}\boldsymbol{r}_2 + {}^{2}\boldsymbol{p}_2^{\mathrm{T}}\boldsymbol{E}_1\,{}^{2}\boldsymbol{p}_2\right)\phi'_{\mathrm{e}12} + \left[0 \;\; \phi_{\mathrm{e}12}\right]\left(\boldsymbol{S}\boldsymbol{E}_1\boldsymbol{A}_2\,{}^{2}\boldsymbol{p}_2 + \boldsymbol{S}\,{}^{1}\boldsymbol{r}_2\right)\right)d\tilde{x}_2, \tag{C.135}$$

$$TL2q4t\_A2 = \rho_{\mathrm{l}_2}\int_0^{l_2}\left(\left[0 \;\; \phi_{\mathrm{e}12}\right]\boldsymbol{E}_1\boldsymbol{S}\boldsymbol{A}_2\,{}^{2}\boldsymbol{p}_2 + {}^{2}\boldsymbol{p}_2^{\mathrm{T}}\boldsymbol{E}_1\,{}^{2}\boldsymbol{p}_2\phi'_{\mathrm{e}12}\right)d\tilde{x}_2, \tag{C.136}$$

$$TL2q4t\_A3 = \begin{array}{l} \rho_{\mathrm{l}_2}\int_0^{l_2}\left(\phi_{\mathrm{e}11}\phi_{\mathrm{e}12} + {}^{2}\boldsymbol{p}_2^{\mathrm{T}}\boldsymbol{A}_2^{\mathrm{T}}\boldsymbol{S}^{\mathrm{T}}\left[0 \;\; \phi_{\mathrm{e}11}\right]^{\mathrm{T}}\phi'_{\mathrm{e}12}\right)d\tilde{x}_2 + \cdots \\ \rho_{\mathrm{l}_2}\int_0^{l_2}\left(\left[0 \;\; \phi_{\mathrm{e}12}\right]\boldsymbol{S}\boldsymbol{A}_2\,{}^{2}\boldsymbol{p}_2\phi'_{\mathrm{e}11} + {}^{2}\boldsymbol{p}_2^{\mathrm{T}}\,{}^{2}\boldsymbol{p}_2\phi'_{\mathrm{e}11}\phi'_{\mathrm{e}12}\right)d\tilde{x}_2 \end{array}, \tag{C.137}$$

$$TL2q4t\_A4 = \begin{array}{l} \rho_{\mathrm{l}_2}\int_0^{l_2}\left(\phi_{\mathrm{e}12}^2 + {}^{2}\boldsymbol{p}_2^{\mathrm{T}}\boldsymbol{A}_2^{\mathrm{T}}\boldsymbol{S}^{\mathrm{T}}\left[0 \;\; \phi_{\mathrm{e}12}\right]^{\mathrm{T}}\phi'_{\mathrm{e}12} + \left[0 \;\; \phi_{\mathrm{e}12}\right]\boldsymbol{S}\boldsymbol{A}_2\,{}^{2}\boldsymbol{p}_2\phi'_{\mathrm{e}12}\right)d\tilde{x}_2 + \cdots \\ \rho_{\mathrm{l}_2}\int_0^{l_2}\left({}^{2}\boldsymbol{p}_2^{\mathrm{T}}\,{}^{2}\boldsymbol{p}_2\phi'^2_{\mathrm{e}12}\right)d\tilde{x}_2 \end{array}, \tag{C.138}$$

$$TL2q4t\_A5 = \rho_{l_2}\int_0^{l_2}\left(\left[0\ \ \phi_{21}(\tilde{x}_2)\right]\boldsymbol{A}_2^{\mathrm{T}}\boldsymbol{E}_1^{\mathrm{T}}\left[0\ \ \phi_{e12}\right]^{\mathrm{T}} + \left[0\ \ \phi_{21}(\tilde{x}_2)\right]\boldsymbol{E}_1^{\mathrm{T}}\boldsymbol{S}^{2}\boldsymbol{p}_2\phi'_{e12}\right)d\tilde{x}_2\,, \tag{C.139}$$

$$TL2q4t\_A6 = \rho_{l_2}\int_0^{l_2}\left(\left[0\ \ \phi_{22}(\tilde{x}_2)\right]\boldsymbol{A}_2^{\mathrm{T}}\boldsymbol{E}_1^{\mathrm{T}}\left[0\ \ \phi_{e12}\right]^{\mathrm{T}} + \left[0\ \ \phi_{22}(\tilde{x}_2)\right]\boldsymbol{E}_1^{\mathrm{T}}\boldsymbol{S}^{2}\boldsymbol{p}_2\phi'_{e12}\right)d\tilde{x}_2\,, \tag{C.140}$$

$$\begin{aligned} TL2q4t\_B \;=\; & \rho_{l_2}\int_0^{l_2}\left(TL2q4t\_B1 + TL2q4t\_B2 + TL2q4t\_B3\right)d\tilde{x}_2 + \cdots \\ & \rho_{l_2}\int_0^{l_2}\left(TL2q4t\_B4 + TL2q4t\_B5\right)d\tilde{x}_2 \end{aligned}\,, \tag{C.141}$$

where

$$\begin{aligned} TL2q4t\_B1 \;=\; & {}^{2}\dot{\boldsymbol{p}}_2^{\mathrm{T}}\boldsymbol{A}_2^{\mathrm{T}}\boldsymbol{E}_1^{\mathrm{T}}\boldsymbol{S}^{\mathrm{T}}\left[0\ \ \phi_{e12}\right]^{\mathrm{T}}\dot{q}_2 - {}^{2}\boldsymbol{p}_2^{\mathrm{T}}\boldsymbol{A}_2^{\mathrm{T}}\boldsymbol{E}_1^{\mathrm{T}}\left[0\ \ \phi_{e12}\right]^{\mathrm{T}}\dot{q}_1\dot{q}_2 + \cdots \\ & {}^{2}\boldsymbol{p}_2^{\mathrm{T}}\boldsymbol{A}_2^{\mathrm{T}}\dot{\boldsymbol{E}}_1^{\mathrm{T}}\boldsymbol{S}^{\mathrm{T}}\left[0\ \ \phi_{e12}\right]^{\mathrm{T}}\dot{q}_1 + 2\,{}^{2}\dot{\boldsymbol{p}}_2^{\mathrm{T}}\boldsymbol{A}_2^{\mathrm{T}}\dot{\boldsymbol{E}}_1^{\mathrm{T}}\left[0\ \ \phi_{e12}\right]^{\mathrm{T}} \end{aligned}\,, \tag{C.142}$$

$$\begin{aligned} TL2q4t\_B2 \;=\; & 2\,{}^{2}\boldsymbol{p}_2^{\mathrm{T}}\boldsymbol{A}_2^{\mathrm{T}}\boldsymbol{S}^{\mathrm{T}}\dot{\boldsymbol{E}}_1^{\mathrm{T}}\left[0\ \ \phi_{e12}\right]^{\mathrm{T}}\dot{q}_2 + 2\,{}^{2}\dot{\boldsymbol{p}}_2^{\mathrm{T}}\boldsymbol{A}_2^{\mathrm{T}}\boldsymbol{S}^{\mathrm{T}}\boldsymbol{E}_1^{\mathrm{T}}\left[0\ \ \phi_{e12}\right]^{\mathrm{T}}\dot{q}_2 + \cdots \\ & - {}^{2}\boldsymbol{p}_2^{\mathrm{T}}\boldsymbol{A}_2^{\mathrm{T}}\boldsymbol{E}_1^{\mathrm{T}}\left[0\ \ \phi_{e12}\right]^{\mathrm{T}}\dot{q}_2^{2} + {}^{1}\dot{\boldsymbol{r}}_2^{\mathrm{T}}\boldsymbol{A}_2\,{}^{2}\boldsymbol{p}_2\phi'_{e12}\dot{q}_1 \end{aligned}\,, \tag{C.143}$$

$$TL2q4t\_B3 = {}^{1}\boldsymbol{r}_2^{\mathrm{T}}\boldsymbol{S}\boldsymbol{A}_2\,{}^{2}\boldsymbol{p}_2\phi'_{e12}\dot{q}_1\dot{q}_2 + {}^{1}\boldsymbol{r}_2^{\mathrm{T}}\boldsymbol{A}_2\,{}^{2}\dot{\boldsymbol{p}}_2\phi'_{e12}\dot{q}_1 - {}^{1}\dot{\boldsymbol{r}}_2^{\mathrm{T}}\boldsymbol{A}_2\,{}^{2}\boldsymbol{p}_2\phi'_{e12}\dot{q}_2 + {}^{1}\dot{\boldsymbol{r}}_2^{\mathrm{T}}\boldsymbol{S}\boldsymbol{A}_2\,{}^{2}\dot{\boldsymbol{p}}_2\phi'_{e12}\,, \tag{C.144}$$

$$TL2q4t\_B4 = {}^{2}\dot{\boldsymbol{p}}_2^{\mathrm{T}}\boldsymbol{E}_1^{\mathrm{T}}\,{}^{2}\boldsymbol{p}_2\phi'_{e12}\dot{q}_1 + {}^{2}\boldsymbol{p}_2^{\mathrm{T}}\boldsymbol{E}_1^{\mathrm{T}}\,{}^{2}\dot{\boldsymbol{p}}_2\phi'_{e12}\dot{q}_1 + {}^{2}\dot{\boldsymbol{p}}_2^{\mathrm{T}}\dot{\boldsymbol{E}}_1^{\mathrm{T}}\boldsymbol{S}^{2}\boldsymbol{p}_2\phi'_{e12} + {}^{2}\boldsymbol{p}_2^{\mathrm{T}}\dot{\boldsymbol{E}}_1^{\mathrm{T}}\boldsymbol{S}^{2}\dot{\boldsymbol{p}}_2\phi'_{e12}\,, \tag{C.145}$$

$$TL2q3t\_B5 = {}^{2}\dot{\boldsymbol{p}}_2^{\mathrm{T}}\boldsymbol{E}_1^{\mathrm{T}}\,{}^{2}\boldsymbol{p}_2\phi'_{e12}\dot{q}_2 + {}^{2}\boldsymbol{p}_2^{\mathrm{T}}\boldsymbol{E}_1^{\mathrm{T}}\,{}^{2}\dot{\boldsymbol{p}}_2\phi'_{e12}\dot{q}_2 + {}^{2}\dot{\boldsymbol{p}}_2^{\mathrm{T}}\dot{\boldsymbol{E}}_1^{\mathrm{T}}\boldsymbol{S}^{2}\boldsymbol{p}_2\phi'_{e12} + {}^{2}\dot{\boldsymbol{p}}_2^{\mathrm{T}}\boldsymbol{E}_1^{\mathrm{T}}\boldsymbol{S}^{2}\dot{\boldsymbol{p}}_2\phi'_{e12}\,, \tag{C.146}$$

$$\begin{aligned} \frac{d}{dt}\frac{\partial T_{\mathrm{p}}}{\partial\dot{q}_4} \;=\; & TPq4t\_A1\ddot{q}_1 + TPq4t\_A2\ddot{q}_2 + TPq4t\_A3\ddot{q}_3 + \cdots \\ & TPq4t\_A4\ddot{q}_4 + TPq4t\_A5\ddot{q}_5 + TPq4t\_A6\ddot{q}_6 + TPq4t\_B \end{aligned} \tag{C.147}$$

where

$$TPq4t\_A1 = m_{\mathrm{p}}\left[0\ \ \phi_{e12}\right]\left(\boldsymbol{S}\boldsymbol{E}_1\boldsymbol{A}_2\,{}^{2}\boldsymbol{r}_3 + \boldsymbol{S}\,{}^{1}\boldsymbol{r}_2\right) + m_{\mathrm{p}}\left({}^{2}\boldsymbol{r}_3^{\mathrm{T}}\boldsymbol{A}_2^{\mathrm{T}}\,{}^{1}\boldsymbol{r}_2 + {}^{2}\boldsymbol{r}_3^{\mathrm{T}}\boldsymbol{E}_1\,{}^{2}\boldsymbol{r}_3\right)\phi'_{e12} + J_{\mathrm{p}}\phi'_{e12}\,, \tag{C.148}$$

$$TPq4t\_A2 = m_{\mathrm{p}}\left(\left[0\ \ \phi_{e12}\right]\boldsymbol{E}_1\boldsymbol{S}\boldsymbol{A}_2\,{}^{2}\boldsymbol{r}_3 + {}^{2}\boldsymbol{r}_3^{\mathrm{T}}\boldsymbol{E}_1\,{}^{2}\boldsymbol{r}_3\phi'_{e12}\right) + J_{\mathrm{p}}\phi'_{e12}\,, \tag{C.149}$$

$$\begin{aligned} TPq4t\_A3 \;=\; & m_{\mathrm{p}}\left(\phi_{e11}\phi_{e12} + {}^{2}\boldsymbol{r}_3^{\mathrm{T}}\boldsymbol{A}_2^{\mathrm{T}}\boldsymbol{S}^{\mathrm{T}}\left[0\ \ \phi_{e11}\right]^{\mathrm{T}}\phi'_{e12}\right) + \cdots \\ & J_{\mathrm{p}}\phi'_{e11}\phi'_{e12} + m_{\mathrm{p}}\left(\left[0\ \ \phi_{e12}\right]\boldsymbol{S}\boldsymbol{A}_2\,{}^{2}\boldsymbol{r}_3\phi'_{e11} + {}^{2}\boldsymbol{r}_3^{\mathrm{T}}\,{}^{2}\boldsymbol{r}_3\phi'_{e11}\phi'_{e12}\right) \end{aligned}\,, \tag{C.150}$$

$$\begin{aligned} TPq4t\_A4 \;=\; & m_{\mathrm{p}}\left(\phi_{e12}^{2} + {}^{2}\boldsymbol{r}_3^{\mathrm{T}}\boldsymbol{A}_2^{\mathrm{T}}\boldsymbol{S}^{\mathrm{T}}\left[0\ \ \phi_{e12}\right]^{\mathrm{T}}\phi'_{e12}\right) + \cdots \\ & J_{\mathrm{p}}\phi'^{2}_{e12} + m_{\mathrm{p}}\left(\left[0\ \ \phi_{e12}\right]\boldsymbol{S}\boldsymbol{A}_2\,{}^{2}\boldsymbol{r}_3\phi'_{e12} + {}^{2}\boldsymbol{r}_3^{\mathrm{T}}\,{}^{2}\boldsymbol{r}_3\phi'^{2}_{e12}\right) \end{aligned}\,, \tag{C.151}$$

$$\begin{aligned} TPq4t\_A5 \;=\; & m_{\mathrm{p}}\left(\left[0\ \ \phi_{e21}\right]\boldsymbol{A}_2^{\mathrm{T}}\boldsymbol{E}_1^{\mathrm{T}}\left[0\ \ \phi_{e12}\right]^{\mathrm{T}}\right) + J_{\mathrm{p}}\phi'_{e12}\phi'_{e21} + \cdots \\ & m_{\mathrm{p}}\left(\left[0\ \ \phi_{e21}\right]\boldsymbol{E}_1^{\mathrm{T}}\boldsymbol{S}^{2}\boldsymbol{r}_3\phi'_{e12}\right) \end{aligned}\,, \tag{C.152}$$

$$\begin{aligned} TPq4t\_A6 \;=\; & m_{\mathrm{p}}\left(\left[0\ \ \phi_{e22}\right]\boldsymbol{A}_2^{\mathrm{T}}\boldsymbol{E}_1^{\mathrm{T}}\left[0\ \ \phi_{e12}\right]^{\mathrm{T}}\right) + J_{\mathrm{p}}\phi'_{e12}\phi'_{e22} + \cdots \\ & m_{\mathrm{p}}\left(\left[0\ \ \phi_{e22}\right]\boldsymbol{E}_1^{\mathrm{T}}\boldsymbol{S}^{2}\boldsymbol{r}_3\phi'_{e12}\right) \end{aligned}\,, \tag{C.153}$$

$$\begin{aligned} TPq4t\_B \;=\; & m_{\mathrm{p}}\left(TPq4t\_B1 + TPq4t\_B2 + TPq4t\_B3\right) + \cdots \\ & m_{\mathrm{p}}\left(TPq4t\_B4 + TPq4t\_B5\right) \end{aligned}\,, \tag{C.154}$$

where

$$\begin{aligned} TPq4t\_B1 \;=\; & {}^{2}\dot{\boldsymbol{r}}_3^{\mathrm{T}}\boldsymbol{A}_2^{\mathrm{T}}\boldsymbol{E}_1^{\mathrm{T}}\boldsymbol{S}^{\mathrm{T}}\left[0\ \ \phi_{e12}\right]^{\mathrm{T}}\dot{q}_2 - {}^{2}\boldsymbol{r}_3^{\mathrm{T}}\boldsymbol{A}_2^{\mathrm{T}}\boldsymbol{E}_1^{\mathrm{T}}\left[0\ \ \phi_{e12}\right]^{\mathrm{T}}\dot{q}_1\dot{q}_2 + \cdots \\ & {}^{2}\boldsymbol{r}_3^{\mathrm{T}}\boldsymbol{A}_2^{\mathrm{T}}\dot{\boldsymbol{E}}_1^{\mathrm{T}}\boldsymbol{S}^{\mathrm{T}}\left[0\ \ \phi_{e12}\right]^{\mathrm{T}}\dot{q}_1 + 2\,{}^{2}\dot{\boldsymbol{r}}_3^{\mathrm{T}}\boldsymbol{A}_2^{\mathrm{T}}\dot{\boldsymbol{E}}_1^{\mathrm{T}}\left[0\ \ \phi_{e12}\right]^{\mathrm{T}} \end{aligned}\,, \tag{C.155}$$

$$TPq4t\_B2 = 2\,{}^{2}\boldsymbol{r}_3^{\mathrm{T}}\boldsymbol{A}_2^{\mathrm{T}}\boldsymbol{S}^{\mathrm{T}}\dot{\boldsymbol{E}}_1^{\mathrm{T}}\begin{bmatrix}0 & \phi_{\mathrm{e}12}\end{bmatrix}^{\mathrm{T}}\dot{q}_2 + 2\,{}^{2}\dot{\boldsymbol{r}}_3^{\mathrm{T}}\boldsymbol{A}_2^{\mathrm{T}}\boldsymbol{S}^{\mathrm{T}}\boldsymbol{E}_1^{\mathrm{T}}\begin{bmatrix}0 & \phi_{\mathrm{e}12}\end{bmatrix}^{\mathrm{T}}\dot{q}_2 + \cdots - {}^{2}\boldsymbol{r}_3^{\mathrm{T}}\boldsymbol{A}_2^{\mathrm{T}}\boldsymbol{E}_1^{\mathrm{T}}\begin{bmatrix}0 & \phi_{\mathrm{e}12}\end{bmatrix}^{\mathrm{T}}\dot{q}_2^2 + {}^{1}\dot{\boldsymbol{r}}_2^{\mathrm{T}}\boldsymbol{A}_2\,{}^{2}\boldsymbol{r}_3\phi'_{\mathrm{e}12}\dot{q}_1, \tag{C.156}$$

$$TPq4t\_B3 = {}^{1}\boldsymbol{r}_2^{\mathrm{T}}\boldsymbol{S}\boldsymbol{A}_2\,{}^{2}\boldsymbol{r}_3\phi'_{\mathrm{e}12}\dot{q}_1\dot{q}_2 + {}^{1}\boldsymbol{r}_2^{\mathrm{T}}\boldsymbol{A}_2\,{}^{2}\dot{\boldsymbol{r}}_3\phi'_{\mathrm{e}12}\dot{q}_1 - {}^{1}\dot{\boldsymbol{r}}_2^{\mathrm{T}}\boldsymbol{A}_2\,{}^{2}\boldsymbol{r}_3\phi'_{\mathrm{e}12}\dot{q}_2 + {}^{1}\dot{\boldsymbol{r}}_2^{\mathrm{T}}\boldsymbol{S}\boldsymbol{A}_2\,{}^{2}\dot{\boldsymbol{r}}_3\phi'_{\mathrm{e}12}, \tag{C.157}$$

$$TPq4t\_B4 = {}^{2}\dot{\boldsymbol{r}}_3^{\mathrm{T}}\boldsymbol{E}_1^{\mathrm{T}}\,{}^{2}\boldsymbol{r}_3\phi'_{\mathrm{e}12}\dot{q}_1 + {}^{2}\boldsymbol{r}_3^{\mathrm{T}}\dot{\boldsymbol{E}}_1^{\mathrm{T}}\,{}^{2}\boldsymbol{r}_3\phi'_{\mathrm{e}12}\dot{q}_1 + {}^{2}\dot{\boldsymbol{r}}_3^{\mathrm{T}}\dot{\boldsymbol{E}}_1^{\mathrm{T}}\boldsymbol{S}\,{}^{2}\boldsymbol{r}_3\phi'_{\mathrm{e}12} + {}^{2}\boldsymbol{r}_3^{\mathrm{T}}\dot{\boldsymbol{E}}_1^{\mathrm{T}}\boldsymbol{S}\,{}^{2}\dot{\boldsymbol{r}}_3\phi'_{\mathrm{e}12}, \tag{C.158}$$

$$TPq4t\_B5 = {}^{2}\dot{\boldsymbol{r}}_3^{\mathrm{T}}\boldsymbol{E}_1^{\mathrm{T}}\,{}^{2}\boldsymbol{r}_3\phi'_{\mathrm{e}12}\dot{q}_2 + {}^{2}\boldsymbol{r}_3^{\mathrm{T}}\boldsymbol{E}_1^{\mathrm{T}}\,{}^{2}\dot{\boldsymbol{r}}_3\phi'_{\mathrm{e}12}\dot{q}_2 + {}^{2}\dot{\boldsymbol{r}}_3^{\mathrm{T}}\dot{\boldsymbol{E}}_1^{\mathrm{T}}\boldsymbol{S}\,{}^{2}\boldsymbol{r}_3\phi'_{\mathrm{e}12} + {}^{2}\dot{\boldsymbol{r}}_3^{\mathrm{T}}\boldsymbol{E}_1^{\mathrm{T}}\boldsymbol{S}\,{}^{2}\dot{\boldsymbol{r}}_3\phi'_{\mathrm{e}12}, \tag{C.159}$$

$$\frac{\partial T_{\mathrm{h}_2}}{\partial q_4} = m_{\mathrm{h}_2}\,{}^{1}\boldsymbol{r}_2^{\mathrm{T}}\begin{bmatrix}0 & \phi_{\mathrm{e}12}\end{bmatrix}^{\mathrm{T}}\dot{q}_1^2, \tag{C.160}$$

$$\frac{\partial T_{\mathrm{l}_1}}{\partial q_4} = \rho_{\mathrm{l}_1}\int_0^{l_1}{}^{1}\boldsymbol{p}_1^{\mathrm{T}}\begin{bmatrix}0 & \phi_{12}(\tilde{x}_1)\end{bmatrix}^{\mathrm{T}}d\tilde{x}_1\dot{q}_1^2, \tag{C.161}$$

$$\frac{\partial T_{\mathrm{l}_2}}{\partial q_4} = \rho_{\mathrm{l}_2}\int_0^{l_2}\left(TL2q4\_C1 + TL2q4\_C2 + TL2q4\_C3\right)d\tilde{x}_2 + \cdots \rho_{\mathrm{l}_2}\int_0^{l_2}\left(TL2q4\_C4 + TL2q4\_C5\right)d\tilde{x}_2, \tag{C.162}$$

where

$$TL2q4\_C1 = {}^{1}\boldsymbol{r}_2^{\mathrm{T}}\begin{bmatrix}0 & \phi_{\mathrm{e}12}\end{bmatrix}^{\mathrm{T}}\dot{q}_1^2 + {}^{2}\boldsymbol{p}_2^{\mathrm{T}}\boldsymbol{A}_2^{\mathrm{T}}\boldsymbol{E}_1^{\mathrm{T}}\begin{bmatrix}0 & \phi_{\mathrm{e}12}\end{bmatrix}^{\mathrm{T}}\dot{q}_1^2 + \cdots {}^{2}\boldsymbol{p}_2^{\mathrm{T}}\boldsymbol{A}_2^{\mathrm{T}}\dot{\boldsymbol{E}}_1^{\mathrm{T}}\boldsymbol{S}\begin{bmatrix}0 & \phi_{\mathrm{e}12}\end{bmatrix}^{\mathrm{T}}\dot{q}_1 + {}^{2}\boldsymbol{p}_2^{\mathrm{T}}\boldsymbol{A}_2^{\mathrm{T}}\boldsymbol{E}_1^{\mathrm{T}}\begin{bmatrix}0 & \phi_{\mathrm{e}12}\end{bmatrix}^{\mathrm{T}}\dot{q}_1\dot{q}_2, \tag{C.163}$$

$$TL2q4\_C2 = {}^{2}\dot{\boldsymbol{p}}_2^{\mathrm{T}}\boldsymbol{A}_2^{\mathrm{T}}\boldsymbol{E}_1^{\mathrm{T}}\boldsymbol{S}\begin{bmatrix}0 & \phi_{\mathrm{e}12}\end{bmatrix}^{\mathrm{T}}\dot{q}_1 - {}^{1}\boldsymbol{r}_2^{\mathrm{T}}\boldsymbol{S}^{\mathrm{T}}\boldsymbol{A}_2\,{}^{2}\boldsymbol{p}_2\phi'_{\mathrm{e}12}\dot{q}_1^2 + \cdots - {}^{1}\dot{\boldsymbol{r}}_2^{\mathrm{T}}\boldsymbol{A}_2\,{}^{2}\boldsymbol{p}_2\phi'_{\mathrm{e}12}\dot{q}_1 - {}^{2}\boldsymbol{p}_2^{\mathrm{T}}\boldsymbol{E}_1^{\mathrm{T}}\boldsymbol{S}^{\mathrm{T}}\,{}^{2}\boldsymbol{p}_2\phi'_{\mathrm{e}12}\dot{q}_1^2, \tag{C.164}$$

$$TL2q4\_C3 = -2\,{}^{2}\boldsymbol{p}_2^{\mathrm{T}}\boldsymbol{S}^{\mathrm{T}}\boldsymbol{E}_1^{\mathrm{T}}\,{}^{2}\boldsymbol{p}_2\phi'_{\mathrm{e}12}\dot{q}_1\dot{q}_2 - {}^{1}\boldsymbol{r}_2^{\mathrm{T}}\boldsymbol{S}^{\mathrm{T}}\boldsymbol{A}_2\,{}^{2}\boldsymbol{p}_2\phi'_{\mathrm{e}12}\dot{q}_1\dot{q}_2 + \cdots - {}^{1}\dot{\boldsymbol{r}}_2^{\mathrm{T}}\boldsymbol{A}_2\,{}^{2}\boldsymbol{p}_2\phi'_{\mathrm{e}12}\dot{q}_2 - \boldsymbol{p}_2^{\mathrm{T}}\boldsymbol{S}^{\mathrm{T}}\boldsymbol{E}_1^{\mathrm{T}}\,{}^{2}\boldsymbol{p}_2\phi'_{\mathrm{e}12}\dot{q}_2^2, \tag{C.165}$$

$$TL2q4\_C4 = -{}^{2}\dot{\boldsymbol{p}}_2^{\mathrm{T}}\boldsymbol{E}_1^{\mathrm{T}}\,{}^{2}\boldsymbol{p}_2\phi'_{\mathrm{e}12}\dot{q}_2 + {}^{1}\boldsymbol{r}_2^{\mathrm{T}}\boldsymbol{A}_2\,{}^{2}\dot{\boldsymbol{p}}_2\phi'_{\mathrm{e}12}\dot{q}_1 + \cdots {}^{1}\dot{\boldsymbol{r}}_2^{\mathrm{T}}\boldsymbol{S}\boldsymbol{A}_2\,{}^{2}\dot{\boldsymbol{p}}_2\phi'_{\mathrm{e}12} + {}^{2}\boldsymbol{p}_2^{\mathrm{T}}\dot{\boldsymbol{E}}_1^{\mathrm{T}}\boldsymbol{S}\,{}^{2}\dot{\boldsymbol{p}}_2\phi'_{\mathrm{e}12}, \tag{C.166}$$

$$TL2q4\_C5 = {}^{2}\boldsymbol{p}_2^{\mathrm{T}}\boldsymbol{E}_1^{\mathrm{T}}\,{}^{2}\dot{\boldsymbol{p}}_2\phi'_{\mathrm{e}12}\dot{q}_2 + {}^{2}\dot{\boldsymbol{p}}_2^{\mathrm{T}}\boldsymbol{E}_1^{\mathrm{T}}\boldsymbol{S}\,{}^{2}\dot{\boldsymbol{p}}_2\phi'_{\mathrm{e}12} + \cdots - {}^{2}\dot{\boldsymbol{p}}_2^{\mathrm{T}}\boldsymbol{E}_1^{\mathrm{T}}\,{}^{2}\boldsymbol{p}_2\phi'_{\mathrm{e}12}\dot{q}_1 + {}^{2}\boldsymbol{p}_2^{\mathrm{T}}\boldsymbol{E}_1^{\mathrm{T}}\,{}^{2}\dot{\boldsymbol{p}}_2\phi'_{\mathrm{e}12}\dot{q}_1, \tag{C.167}$$

$$\frac{\partial T_{\mathrm{p}}}{\partial q_4} = m_{\mathrm{p}}\left(TPq4\_C1 + TPq4\_C2 + TPq4\_C3 + TPq4\_C4\right), \tag{C.168}$$

where

$$TPq4\_C1 = {}^{1}\boldsymbol{r}_2^{\mathrm{T}}\begin{bmatrix}0 & \phi_{\mathrm{e}12}\end{bmatrix}^{\mathrm{T}}\dot{q}_1^2 + {}^{2}\boldsymbol{r}_3^{\mathrm{T}}\boldsymbol{A}_2^{\mathrm{T}}\boldsymbol{E}_1^{\mathrm{T}}\begin{bmatrix}0 & \phi_{\mathrm{e}12}\end{bmatrix}^{\mathrm{T}}\dot{q}_1^2 + \cdots {}^{2}\boldsymbol{r}_3^{\mathrm{T}}\boldsymbol{A}_2^{\mathrm{T}}\dot{\boldsymbol{E}}_1^{\mathrm{T}}\boldsymbol{S}\begin{bmatrix}0 & \phi_{\mathrm{e}12}\end{bmatrix}^{\mathrm{T}}\dot{q}_1 + {}^{2}\boldsymbol{r}_3^{\mathrm{T}}\boldsymbol{A}_2^{\mathrm{T}}\boldsymbol{E}_1^{\mathrm{T}}\begin{bmatrix}0 & \phi_{\mathrm{e}12}\end{bmatrix}^{\mathrm{T}}\dot{q}_1\dot{q}_2, \tag{C.169}$$

$$TPq4\_C2 = +{}^{2}\dot{\boldsymbol{r}}_3^{\mathrm{T}}\boldsymbol{A}_2^{\mathrm{T}}\boldsymbol{E}_1^{\mathrm{T}}\boldsymbol{S}\begin{bmatrix}0 & \phi_{\mathrm{e}12}\end{bmatrix}^{\mathrm{T}}\dot{q}_1 - {}^{1}\boldsymbol{r}_2^{\mathrm{T}}\boldsymbol{S}^{\mathrm{T}}\boldsymbol{A}_2\,{}^{2}\boldsymbol{r}_3\phi'_{\mathrm{e}12}\left(\dot{q}_1+\dot{q}_2\right)\dot{q}_1 + \cdots - {}^{1}\dot{\boldsymbol{r}}_2^{\mathrm{T}}\boldsymbol{A}_2\,{}^{2}\boldsymbol{r}_3\phi'_{\mathrm{e}12}\left(\dot{q}_1+\dot{q}_2\right) - {}^{2}\boldsymbol{r}_3^{\mathrm{T}}\boldsymbol{E}_1^{\mathrm{T}}\boldsymbol{S}^{\mathrm{T}}\,{}^{2}\boldsymbol{r}_3\phi'_{\mathrm{e}12}\left(\dot{q}_1+\dot{q}_2\right)\dot{q}_1, \tag{C.170}$$

$$TPq4\_C3 = -{}^{2}\boldsymbol{r}_3^{\mathrm{T}}\boldsymbol{S}^{\mathrm{T}}\boldsymbol{E}_1^{\mathrm{T}}\,{}^{2}\boldsymbol{r}_3\phi'_{\mathrm{e}12}\left(\dot{q}_1+\dot{q}_2\right)\dot{q}_2 - {}^{2}\dot{\boldsymbol{r}}_3^{\mathrm{T}}\boldsymbol{E}_1^{\mathrm{T}}\,{}^{2}\boldsymbol{r}_3\phi'_{\mathrm{e}12}\left(\dot{q}_1+\dot{q}_2\right) + \cdots {}^{1}\boldsymbol{r}_2^{\mathrm{T}}\boldsymbol{A}_2\,{}^{2}\dot{\boldsymbol{r}}_3\phi'_{\mathrm{e}12}\dot{q}_1 + {}^{1}\dot{\boldsymbol{r}}_2^{\mathrm{T}}\boldsymbol{S}\boldsymbol{A}_2\,{}^{2}\dot{\boldsymbol{r}}_3\phi'_{\mathrm{e}12}, \tag{C.171}$$

$$TPq4\_C4 = {}^{2}\boldsymbol{r}_3^{\mathrm{T}}\boldsymbol{E}_1^{\mathrm{T}}\,{}^{2}\dot{\boldsymbol{r}}_3\phi'_{\mathrm{e}12}\dot{q}_1 + {}^{2}\boldsymbol{r}_3^{\mathrm{T}}\dot{\boldsymbol{E}}_1^{\mathrm{T}}\boldsymbol{S}\,{}^{2}\dot{\boldsymbol{r}}_3\phi'_{\mathrm{e}12} + \cdots {}^{2}\boldsymbol{r}_3^{\mathrm{T}}\boldsymbol{E}_1^{\mathrm{T}}\,{}^{2}\dot{\boldsymbol{r}}_3\phi'_{\mathrm{e}12}\dot{q}_2 + {}^{2}\dot{\boldsymbol{r}}_3^{\mathrm{T}}\boldsymbol{E}_1^{\mathrm{T}}\boldsymbol{S}\,{}^{2}\dot{\boldsymbol{r}}_3\phi'_{\mathrm{e}12}, \tag{C.172}$$

$$\frac{\partial U_{\mathrm{l}_1}}{\partial q_4} = \left(EI\right)_1 \int_0^{l_1} \left(\phi_{12}(\tilde{x}_1) \sum_{i=1}^{2} \phi_{1i}(\tilde{x}_1) q_{i+2} \right) d\tilde{x}_1 ,$$

$$\begin{aligned} \frac{d}{dt}\frac{\partial T_{\mathrm{l}_2}}{\partial \dot{q}_5} \;=\; & TL2q5t\_A1\ddot{q}_1 + TL2q5t\_A2\ddot{q}_2 + TL2q5t\_A3\ddot{q}_3 + \cdots \\ & TL2q5t\_A4\ddot{q}_4 + TL2q5t\_A5\ddot{q}_5 + TL2q5t\_A6\ddot{q}_6 + TL2q5t\_B \end{aligned} , \tag{C.173}$$

where

$$TL2q5t\_A1 = \rho_{\mathrm{l}_2} \int_0^{l_2} \begin{bmatrix} 0 & \phi_{21}(\tilde{x}_2) \end{bmatrix} \left(\boldsymbol{A}_2^{\mathrm{T}} \boldsymbol{E}_1^{\mathrm{T}} \boldsymbol{S}^{1} \boldsymbol{r}_2 + \boldsymbol{S}^{2} \boldsymbol{p}_2 \right) d\tilde{x}_2 , \tag{C.174}$$

$$TL2q5t\_A2 = \rho_{\mathrm{l}_2} \int_0^{l_2} \begin{bmatrix} 0 & \phi_{\mathrm{e}21} \end{bmatrix} \boldsymbol{S}^{2} \boldsymbol{p}_2 d\tilde{x}_2 , \tag{C.175}$$

$$TL2q5t\_A3 = \rho_{\mathrm{l}_2} \int_0^{l_2} \left(\begin{bmatrix} 0 & \phi_{21}(\tilde{x}_2) \end{bmatrix} \boldsymbol{A}_2^{\mathrm{T}} \boldsymbol{E}_1^{\mathrm{T}} \begin{bmatrix} 0 & \phi_{\mathrm{e}11} \end{bmatrix}^{\mathrm{T}} + \begin{bmatrix} 0 & \phi_{21}(\tilde{x}_2) \end{bmatrix} \boldsymbol{E}_1^{\mathrm{T}} \boldsymbol{S}^{2} \boldsymbol{p}_2 \phi'_{\mathrm{e}11} \right) d\tilde{x}_2 , \tag{C.176}$$

$$TL2q5t\_A4 = \rho_{\mathrm{l}_2} \int_0^{l_2} \left(\begin{bmatrix} 0 & \phi_{21}(\tilde{x}_2) \end{bmatrix} \boldsymbol{A}_2^{\mathrm{T}} \boldsymbol{E}_1^{\mathrm{T}} \begin{bmatrix} 0 & \phi_{\mathrm{e}12} \end{bmatrix}^{\mathrm{T}} + \begin{bmatrix} 0 & \phi_{21}(\tilde{x}_2) \end{bmatrix} \boldsymbol{E}_1^{\mathrm{T}} \boldsymbol{S}^{2} \boldsymbol{p}_2 \phi'_{\mathrm{e}12} \right) d\tilde{x}_2 , \tag{C.177}$$

$$TL2q5t\_A5 = \rho_{\mathrm{l}_2} \int_0^{l_2} \phi_{21}(\tilde{x}_2)^2 d\tilde{x}_2 , \tag{C.178}$$

$$TL2q5t\_A6 = \rho_{\mathrm{l}_2} \int_0^{l_2} \phi_{21}(\tilde{x}_2) \phi_{22}(\tilde{x}_2) d\tilde{x}_2 , \tag{C.179}$$

$$TL2q5t\_B = \rho_{\mathrm{l}_2} \int_0^{l_2} \left(TL2q5t\_B1 + TL2q5t\_B2 \right) d\tilde{x}_2 , \tag{C.180}$$

where

$$\begin{aligned} TL2q5t\_B1 \;=\; & {}^{1}\dot{\boldsymbol{r}}_2^{\mathrm{T}} \boldsymbol{S}^{\mathrm{T}} \boldsymbol{E}_1 \boldsymbol{A}_2 \begin{bmatrix} 0 & \phi_{21}(\tilde{x}_2) \end{bmatrix}^{\mathrm{T}} \dot{q}_1 + {}^{1}\boldsymbol{r}_2^{\mathrm{T}} \boldsymbol{S}^{\mathrm{T}} \dot{\boldsymbol{E}}_1 \boldsymbol{A}_2 \begin{bmatrix} 0 & \phi_{21}(\tilde{x}_2) \end{bmatrix}^{\mathrm{T}} \dot{q}_1 + \cdots \\ & {}^{1}\boldsymbol{r}_2^{\mathrm{T}} \boldsymbol{E}_1 \boldsymbol{A}_2 \begin{bmatrix} 0 & \phi_{21}(\tilde{x}_2) \end{bmatrix}^{\mathrm{T}} \dot{q}_1 \dot{q}_2 + {}^{1}\dot{\boldsymbol{r}}_2^{\mathrm{T}} \dot{\boldsymbol{E}}_1 \boldsymbol{A}_2 \begin{bmatrix} 0 & \phi_{21}(\tilde{x}_2) \end{bmatrix}^{\mathrm{T}} \end{aligned} , \tag{C.181}$$

$$\begin{aligned} TL2q5t\_B2 \;=\; & {}^{1}\dot{\boldsymbol{r}}_2^{\mathrm{T}} \boldsymbol{E}_1 \boldsymbol{S} \boldsymbol{A}_2 \begin{bmatrix} 0 & \phi_{21}(\tilde{x}_2) \end{bmatrix}^{\mathrm{T}} \dot{q}_2 + {}^{2}\dot{\boldsymbol{p}}_2^{\mathrm{T}} \dot{\boldsymbol{E}}_1^{\mathrm{T}} \boldsymbol{E}_1^{\mathrm{T}} \begin{bmatrix} 0 & \phi_{21}(\tilde{x}_2) \end{bmatrix}^{\mathrm{T}} + \cdots \\ & {}^{2}\boldsymbol{p}_2^{\mathrm{T}} \dot{\boldsymbol{E}}_1^{\mathrm{T}} \dot{\boldsymbol{E}}_1^{\mathrm{T}} \begin{bmatrix} 0 & \phi_{21}(\tilde{x}_2) \end{bmatrix}^{\mathrm{T}} \end{aligned} , \tag{C.182}$$

$$\begin{aligned} \frac{d}{dt}\frac{\partial T_{\mathrm{p}}}{\partial \dot{q}_5} \;=\; & TPq5t\_A1\ddot{q}_1 + TPq5t\_A2\ddot{q}_2 + TPq5t\_A3\ddot{q}_3 + \cdots \\ & TPq5t\_A4\ddot{q}_4 + TPq5t\_A5\ddot{q}_5 + TPq5t\_A6\ddot{q}_6 + TPq5t\_B \end{aligned} , \tag{C.183}$$

$$TPq5t\_A1 = m_{\mathrm{p}} \begin{bmatrix} 0 & \phi_{\mathrm{e}21} \end{bmatrix} \left(\boldsymbol{A}_2^{\mathrm{T}} \boldsymbol{E}_1^{\mathrm{T}} \boldsymbol{S}^{1} \boldsymbol{r}_2 + \boldsymbol{S}^{2} \boldsymbol{r}_3 \right) + J_{\mathrm{p}} \phi'_{\mathrm{e}21} , \tag{C.184}$$

$$TPq5t\_A2 = m_p \begin{bmatrix} 0 & \phi_{\mathrm{e}21} \end{bmatrix} \boldsymbol{S}^{2} \boldsymbol{r}_3 + J_{\mathrm{p}} \phi'_{\mathrm{e}21} , \tag{C.185}$$

$$TPq5t\_A3 = m_{\mathrm{p}} \left(\begin{bmatrix} 0 & \phi_{\mathrm{e}21} \end{bmatrix} \boldsymbol{A}_2^{\mathrm{T}} \boldsymbol{E}_1^{\mathrm{T}} \begin{bmatrix} 0 & \phi_{\mathrm{e}11} \end{bmatrix}^{\mathrm{T}} + \begin{bmatrix} 0 & \phi_{\mathrm{e}21} \end{bmatrix} \boldsymbol{E}_1^{\mathrm{T}} \boldsymbol{S}^{2} \boldsymbol{r}_3 \phi'_{\mathrm{e}11} \right) + J_{\mathrm{p}} \phi'_{\mathrm{e}11} \phi'_{\mathrm{e}21} , \tag{C.186}$$

$$\begin{aligned} TPq5t\_A4 \;=\; & m_{\mathrm{p}} \left(\begin{bmatrix} 0 & \phi_{\mathrm{e}21} \end{bmatrix} \boldsymbol{A}_2^{\mathrm{T}} \boldsymbol{E}_1^{\mathrm{T}} \begin{bmatrix} 0 & \phi_{\mathrm{e}12} \end{bmatrix}^{\mathrm{T}} \right) + J_{\mathrm{p}} \phi'_{\mathrm{e}12} \phi'_{\mathrm{e}21} + \cdots \\ & m_{\mathrm{p}} \left(\begin{bmatrix} 0 & \phi_{\mathrm{e}21} \end{bmatrix} \boldsymbol{E}_1^{\mathrm{T}} \boldsymbol{S}^{2} \boldsymbol{r}_3 \phi'_{\mathrm{e}12} \right) \end{aligned} , \tag{C.187}$$

$$TPq5t\_A5 = m_{\mathrm{p}} \phi_{\mathrm{e}21}^2 + J_{\mathrm{p}} \phi'^2_{\mathrm{e}21} , \tag{C.188}$$

$$TPq5t\_A6 = m_{\mathrm{p}} \phi_{\mathrm{e}21} \phi_{\mathrm{e}22} + J_{\mathrm{p}} \phi'_{\mathrm{e}21} \phi'_{\mathrm{e}22} , \tag{C.189}$$

$$TPq5t\_B = m_{\mathrm{p}} \left(TPq5t\_B1 + TPq5t\_B2 \right) , \tag{C.190}$$

where

$$TPq5t\_B1 = {}^1\dot{\boldsymbol{r}}_2^{\mathrm{T}}\boldsymbol{S}^{\mathrm{T}}\boldsymbol{E}_1\boldsymbol{A}_2\begin{bmatrix}0 & \phi_{\mathrm{e}21}\end{bmatrix}^{\mathrm{T}}\dot{q}_1 + {}^1\boldsymbol{r}_2^{\mathrm{T}}\boldsymbol{S}^{\mathrm{T}}\dot{\boldsymbol{E}}_1\boldsymbol{A}_2\begin{bmatrix}0 & \phi_{\mathrm{e}21}\end{bmatrix}^{\mathrm{T}}\dot{q}_1 + \cdots$$
$$ {}^1\boldsymbol{r}_2^{\mathrm{T}}\boldsymbol{E}_1\boldsymbol{A}_2\begin{bmatrix}0 & \phi_{\mathrm{e}21}\end{bmatrix}^{\mathrm{T}}\dot{q}_1\dot{q}_2 + {}^1\dot{\boldsymbol{r}}_2^{\mathrm{T}}\dot{\boldsymbol{E}}_1\boldsymbol{A}_2\begin{bmatrix}0 & \phi_{\mathrm{e}21}\end{bmatrix}^{\mathrm{T}}, \tag{C.191}$$

$$TPq5t\_B2 = {}^1\dot{\boldsymbol{r}}_2^{\mathrm{T}}\boldsymbol{E}_1\boldsymbol{S}\boldsymbol{A}_2\begin{bmatrix}0 & \phi_{\mathrm{e}21}\end{bmatrix}^{\mathrm{T}}\dot{q}_2 + {}^2\dot{\boldsymbol{r}}_3^{\mathrm{T}}\dot{\boldsymbol{E}}_1^{\mathrm{T}}\boldsymbol{E}_1^{\mathrm{T}}\begin{bmatrix}0 & \phi_{\mathrm{e}21}\end{bmatrix}^{\mathrm{T}} + \cdots$$
$$ {}^2\boldsymbol{r}_3^{\mathrm{T}}\dot{\boldsymbol{E}}_1^{\mathrm{T}}\dot{\boldsymbol{E}}_1^{\mathrm{T}}\begin{bmatrix}0 & \phi_{\mathrm{e}21}\end{bmatrix}^{\mathrm{T}}, \tag{C.192}$$

$$\frac{\partial T_{\mathrm{l}_2}}{\partial q_5} = \rho_{\mathrm{l}_2}\int_0^{l_2}\left(TL2q5\_C1 + TL2q5\_C2 + TL2q5\_C3 + TL2q5\_C4\right)d\tilde{x}_2, \tag{C.193}$$

where

$$TL2q5\_C1 = {}^1\boldsymbol{r}_2^{\mathrm{T}}\boldsymbol{E}_1\boldsymbol{A}_2\begin{bmatrix}0 & \phi_{21}(\tilde{x}_2)\end{bmatrix}^{\mathrm{T}}\dot{q}_1^2 + {}^1\dot{\boldsymbol{r}}_2^{\mathrm{T}}\boldsymbol{S}\boldsymbol{E}_1\boldsymbol{A}_2\begin{bmatrix}0 & \phi_{21}(\tilde{x}_2)\end{bmatrix}^{\mathrm{T}}\dot{q}_1 + \cdots$$
$$ {}^2\boldsymbol{p}_2^{\mathrm{T}}\begin{bmatrix}0 & \phi_{21}(\tilde{x}_2)\end{bmatrix}^{\mathrm{T}}\dot{q}_1^2 + {}^2\boldsymbol{p}_2^{\mathrm{T}}\dot{\boldsymbol{E}}_1^{\mathrm{T}}\boldsymbol{S}\boldsymbol{E}_1\begin{bmatrix}0 & \phi_{21}(\tilde{x}_2)\end{bmatrix}^{\mathrm{T}}\dot{q}_1, \tag{C.194}$$

$$TL2q5\_C2 = 2\,{}^2\boldsymbol{p}_2^{\mathrm{T}}\begin{bmatrix}0 & \phi_{21}(\tilde{x}_2)\end{bmatrix}^{\mathrm{T}}\dot{q}_1\dot{q}_2 + {}^1\boldsymbol{r}_2^{\mathrm{T}}\boldsymbol{S}^{\mathrm{T}}\dot{\boldsymbol{E}}_1\boldsymbol{A}_2\begin{bmatrix}0 & \phi_{21}(\tilde{x}_2)\end{bmatrix}^{\mathrm{T}}\dot{q}_1 + \cdots$$
$$ {}^1\dot{\boldsymbol{r}}_2^{\mathrm{T}}\dot{\boldsymbol{E}}_1\boldsymbol{A}_2\begin{bmatrix}0 & \phi_{21}(\tilde{x}_2)\end{bmatrix}^{\mathrm{T}} + {}^2\boldsymbol{p}_2^{\mathrm{T}}\boldsymbol{E}_1^{\mathrm{T}}\boldsymbol{S}^{\mathrm{T}}\dot{\boldsymbol{E}}_1\begin{bmatrix}0 & \phi_{21}(\tilde{x}_2)\end{bmatrix}^{\mathrm{T}}\dot{q}_1, \tag{C.195}$$

$$TL2q5\_C3 = {}^2\boldsymbol{p}_2^{\mathrm{T}}\dot{\boldsymbol{E}}_1^{\mathrm{T}}\dot{\boldsymbol{E}}_1\begin{bmatrix}0 & \phi_{21}(\tilde{x}_2)\end{bmatrix}^{\mathrm{T}} + {}^2\boldsymbol{p}_2^{\mathrm{T}}\boldsymbol{S}^{\mathrm{T}}\boldsymbol{E}_1^{\mathrm{T}}\dot{\boldsymbol{E}}_1\begin{bmatrix}0 & \phi_{21}(\tilde{x}_2)\end{bmatrix}^{\mathrm{T}}\dot{q}_2 + \cdots$$
$$ {}^2\dot{\boldsymbol{p}}_2^{\mathrm{T}}\boldsymbol{E}_1^{\mathrm{T}}\dot{\boldsymbol{E}}_1\begin{bmatrix}0 & \phi_{21}(\tilde{x}_2)\end{bmatrix}^{\mathrm{T}} + {}^1\boldsymbol{r}_2^{\mathrm{T}}\boldsymbol{E}_1\boldsymbol{A}_2\begin{bmatrix}0 & \phi_{21}(\tilde{x}_2)\end{bmatrix}^{\mathrm{T}}\dot{q}_1\dot{q}_2, \tag{C.196}$$

$$TL2q5\_C4 = {}^1\dot{\boldsymbol{r}}_2^{\mathrm{T}}\boldsymbol{E}_1\boldsymbol{S}\boldsymbol{A}_2\begin{bmatrix}0 & \phi_{21}(\tilde{x}_2)\end{bmatrix}^{\mathrm{T}}\dot{q}_2 + {}^2\boldsymbol{p}_2^{\mathrm{T}}\dot{\boldsymbol{E}}_1^{\mathrm{T}}\boldsymbol{E}_1\boldsymbol{S}\begin{bmatrix}0 & \phi_{21}(\tilde{x}_2)\end{bmatrix}^{\mathrm{T}}\dot{q}_2 + \cdots$$
$$ {}^2\boldsymbol{p}_2^{\mathrm{T}}\begin{bmatrix}0 & \phi_{21}(\tilde{x}_2)\end{bmatrix}^{\mathrm{T}}\dot{q}_2^2, \tag{C.197}$$

$$\frac{\partial T_{\mathrm{p}}}{\partial q_5} = m_{\mathrm{p}}\left(TPq5\_C1 + TPq5\_C2 + TPq5\_C3 + TPq5\_C4\right), \tag{C.198}$$

where

$$TPq5\_C1 = {}^1\boldsymbol{r}_2^{\mathrm{T}}\boldsymbol{E}_1\boldsymbol{A}_2\begin{bmatrix}0 & \phi_{\mathrm{e}21}\end{bmatrix}^{\mathrm{T}}\dot{q}_1^2 + {}^1\dot{\boldsymbol{r}}_2^{\mathrm{T}}\boldsymbol{S}\boldsymbol{E}_1\boldsymbol{A}_2\begin{bmatrix}0 & \phi_{\mathrm{e}21}\end{bmatrix}^{\mathrm{T}}\dot{q}_1 + \cdots$$
$$ {}^2\boldsymbol{r}_3^{\mathrm{T}}\begin{bmatrix}0 & \phi_{\mathrm{e}21}\end{bmatrix}^{\mathrm{T}}\dot{q}_1^2 + {}^2\boldsymbol{r}_3^{\mathrm{T}}\dot{\boldsymbol{E}}_1^{\mathrm{T}}\boldsymbol{S}\boldsymbol{E}_1\begin{bmatrix}0 & \phi_{\mathrm{e}21}\end{bmatrix}^{\mathrm{T}}\dot{q}_1, \tag{C.199}$$

$$TPq5\_C2 = 2\,{}^2\boldsymbol{r}_3^{\mathrm{T}}\begin{bmatrix}0 & \phi_{\mathrm{e}21}\end{bmatrix}^{\mathrm{T}}\dot{q}_1\dot{q}_2 + {}^1\boldsymbol{r}_2^{\mathrm{T}}\boldsymbol{S}^{\mathrm{T}}\dot{\boldsymbol{E}}_1\boldsymbol{A}_2\begin{bmatrix}0 & \phi_{\mathrm{e}21}\end{bmatrix}^{\mathrm{T}}\dot{q}_1 + \cdots$$
$$ {}^1\dot{\boldsymbol{r}}_2^{\mathrm{T}}\dot{\boldsymbol{E}}_1\boldsymbol{A}_2\begin{bmatrix}0 & \phi_{\mathrm{e}21}\end{bmatrix}^{\mathrm{T}} + {}^2\boldsymbol{r}_3^{\mathrm{T}}\boldsymbol{E}_1^{\mathrm{T}}\boldsymbol{S}^{\mathrm{T}}\dot{\boldsymbol{E}}_1\begin{bmatrix}0 & \phi_{\mathrm{e}21}\end{bmatrix}^{\mathrm{T}}\dot{q}_1, \tag{C.200}$$

$$TPq5\_C3 = {}^2\boldsymbol{r}_3^{\mathrm{T}}\dot{\boldsymbol{E}}_1^{\mathrm{T}}\dot{\boldsymbol{E}}_1\begin{bmatrix}0 & \phi_{\mathrm{e}21}\end{bmatrix}^{\mathrm{T}} + {}^2\boldsymbol{r}_3^{\mathrm{T}}\boldsymbol{S}^{\mathrm{T}}\boldsymbol{E}_1^{\mathrm{T}}\dot{\boldsymbol{E}}_1\begin{bmatrix}0 & \phi_{\mathrm{e}21}\end{bmatrix}^{\mathrm{T}}\dot{q}_2 + \cdots$$
$$ {}^2\dot{\boldsymbol{r}}_3^{\mathrm{T}}\boldsymbol{E}_1^{\mathrm{T}}\dot{\boldsymbol{E}}_1\begin{bmatrix}0 & \phi_{\mathrm{e}21}\end{bmatrix}^{\mathrm{T}} + {}^1\boldsymbol{r}_2^{\mathrm{T}}\boldsymbol{E}_1\boldsymbol{A}_2\begin{bmatrix}0 & \phi_{\mathrm{e}21}\end{bmatrix}^{\mathrm{T}}\dot{q}_1\dot{q}_2, \tag{C.201}$$

$$TPq5\_C4 = {}^1\dot{\boldsymbol{r}}_2^{\mathrm{T}}\boldsymbol{E}_1\boldsymbol{S}\boldsymbol{A}_2\begin{bmatrix}0 & \phi_{\mathrm{e}21}\end{bmatrix}^{\mathrm{T}}\dot{q}_2 + {}^2\boldsymbol{r}_3^{\mathrm{T}}\dot{\boldsymbol{E}}_1^{\mathrm{T}}\boldsymbol{E}_1\boldsymbol{S}\begin{bmatrix}0 & \phi_{\mathrm{e}21}\end{bmatrix}^{\mathrm{T}}\dot{q}_2 + \cdots$$
$$ {}^2\boldsymbol{r}_3^{\mathrm{T}}\begin{bmatrix}0 & \phi_{\mathrm{e}21}\end{bmatrix}^{\mathrm{T}}\dot{q}_2^2, \tag{C.202}$$

$$\frac{\partial U_{\mathrm{l}_2}}{\partial q_5} = \left(EI\right)_2\int_0^{l_2}\left(\phi_{21}(\tilde{x}_2)\sum_{i=3}^{4}\phi_{2\,i-2}(\tilde{x}_2)q_{i+2}\right)d\tilde{x}_2, \tag{C.203}$$

$$\frac{d}{dt}\frac{\partial T_{\mathrm{l}_2}}{\partial \dot{q}_6} = TL2q6t\_A1\ddot{q}_1 + TL2q6t\_A2\ddot{q}_2 + TL2q6t\_A3\ddot{q}_3 + \cdots$$
$$ TL2q6t\_A4\ddot{q}_4 + TL2q6t\_A5\ddot{q}_5 + TL2q6t\_A6\ddot{q}_6 + TL2q6t\_B, \tag{C.204}$$

where

$$TL2q6t\_A1 = \rho_{\mathrm{l}_2}\int_0^{l_2}\begin{bmatrix}0 & \phi_{22}(\tilde{x}_2)\end{bmatrix}\left(\boldsymbol{A}_2^{\mathrm{T}}\boldsymbol{E}_1^{\mathrm{T}}\boldsymbol{S}\,{}^1\boldsymbol{r}_2 + \boldsymbol{S}\,{}^2\boldsymbol{p}_2\right)d\tilde{x}_2, \tag{C.205}$$

$$TL2q6t\_A2 = \rho_{l_2}\int_0^{l_2}\begin{bmatrix}0 & \phi_{e22}\end{bmatrix}\boldsymbol{S}^2\boldsymbol{p}_2 d\tilde{x}_2\,, \tag{C.206}$$

$$TL2q6t\_A3 = \rho_{l_2}\int_0^{l_2}\left(\begin{bmatrix}0 & \phi_{22}(\tilde{x}_2)\end{bmatrix}\boldsymbol{A}_2^{\mathrm{T}}\boldsymbol{E}_1^{\mathrm{T}}\begin{bmatrix}0 & \phi_{e11}\end{bmatrix}^{\mathrm{T}} + \begin{bmatrix}0 & \phi_{22}(\tilde{x}_2)\end{bmatrix}\boldsymbol{E}_1^{\mathrm{T}}\boldsymbol{S}^2\boldsymbol{p}_2\phi'_{e11}\right)d\tilde{x}_2\,, \tag{C.207}$$

$$TL2q6t\_A4 = \rho_{l_2}\int_0^{l_2}\left(\begin{bmatrix}0 & \phi_{22}(\tilde{x}_2)\end{bmatrix}\boldsymbol{A}_2^{\mathrm{T}}\boldsymbol{E}_1^{\mathrm{T}}\begin{bmatrix}0 & \phi_{e12}\end{bmatrix}^{\mathrm{T}} + \begin{bmatrix}0 & \phi_{22}(\tilde{x}_2)\end{bmatrix}\boldsymbol{E}_1^{\mathrm{T}}\boldsymbol{S}^2\boldsymbol{p}_2\phi'_{e12}\right)d\tilde{x}_2\,, \tag{C.208}$$

$$TL2q6t\_A5 = \rho_{l_2}\int_0^{l_2}\phi_{21}(\tilde{x}_2)\phi_{22}(\tilde{x}_2)d\tilde{x}_2\,, \tag{C.209}$$

$$TL2q6t\_A6 = \rho_{l_2}\int_0^{l_2}\phi_{22}(\tilde{x}_2)^2 d\tilde{x}_2 + m_p\phi_{e22}^2 + J_p\phi'^2_{e22}\,, \tag{C.210}$$

$$TL2q6t\_B = \rho_{l_2}\int_0^{l_2}\left(TL2q6t\_B1 + TL2q6t\_B2\right)d\tilde{x}_2\,, \tag{C.211}$$

where

$$\begin{aligned} TL2q6t\_B1 \;=\; & {}^1\dot{\boldsymbol{r}}_2^{\mathrm{T}}\boldsymbol{S}^{\mathrm{T}}\boldsymbol{E}_1\boldsymbol{A}_2\begin{bmatrix}0 & \phi_{22}(\tilde{x}_2)\end{bmatrix}^{\mathrm{T}}\dot{q}_1 + {}^1\boldsymbol{r}_2^{\mathrm{T}}\boldsymbol{S}^{\mathrm{T}}\dot{\boldsymbol{E}}_1\boldsymbol{A}_2\begin{bmatrix}0 & \phi_{22}(\tilde{x}_2)\end{bmatrix}^{\mathrm{T}}\dot{q}_1 + \cdots \\ & {}^1\boldsymbol{r}_2^{\mathrm{T}}\boldsymbol{E}_1\boldsymbol{A}_2\begin{bmatrix}0 & \phi_{22}(\tilde{x}_2)\end{bmatrix}^{\mathrm{T}}\dot{q}_1\dot{q}_2 + {}^1\dot{\boldsymbol{r}}_2^{\mathrm{T}}\dot{\boldsymbol{E}}_1\boldsymbol{A}_2\begin{bmatrix}0 & \phi_{22}(\tilde{x}_2)\end{bmatrix}^{\mathrm{T}} \end{aligned}, \tag{C.212}$$

$$\begin{aligned} TL2q6t\_B2 \;=\; & {}^1\dot{\boldsymbol{r}}_2^{\mathrm{T}}\boldsymbol{E}_1\boldsymbol{S}\boldsymbol{A}_2\begin{bmatrix}0 & \phi_{22}(\tilde{x}_2)\end{bmatrix}^{\mathrm{T}}\dot{q}_2 + {}^2\dot{\boldsymbol{p}}_2^{\mathrm{T}}\dot{\boldsymbol{E}}_1^{\mathrm{T}}\boldsymbol{E}_1^{\mathrm{T}}\begin{bmatrix}0 & \phi_{22}(\tilde{x}_2)\end{bmatrix}^{\mathrm{T}} + \cdots \\ & {}^2\boldsymbol{p}_2^{\mathrm{T}}\dot{\boldsymbol{E}}_1^{\mathrm{T}}\dot{\boldsymbol{E}}_1^{\mathrm{T}}\begin{bmatrix}0 & \phi_{22}(\tilde{x}_2)\end{bmatrix}^{\mathrm{T}} \end{aligned}, \tag{C.213}$$

$$\begin{aligned} \frac{d}{dt}\frac{\partial T_p}{\partial\dot{q}_6} \;=\; & TPq6t\_A1\ddot{q}_1 + TPq6t\_A2\ddot{q}_2 + TPq6t\_A3\ddot{q}_3 + \cdots \\ & TPq6t\_A4\ddot{q}_4 + TPq6t\_A5\ddot{q}_5 + TPq6t\_A6\ddot{q}_6 + TPq6t\_B \end{aligned}, \tag{C.214}$$

where

$$TPq6t\_A1 = m_p\begin{bmatrix}0 & \phi_{e22}\end{bmatrix}\left(\boldsymbol{A}_2^{\mathrm{T}}\boldsymbol{E}_1^{\mathrm{T}}\boldsymbol{S}^1\boldsymbol{r}_2 + \boldsymbol{S}^2\boldsymbol{r}_3\right) + J_p\phi'_{e22}\,, \tag{C.215}$$

$$TPq6t\_A2 = m_p\begin{bmatrix}0 & \phi_{e22}\end{bmatrix}\boldsymbol{S}^2\boldsymbol{r}_3 + J_p\phi'_{e22}\,, \tag{C.216}$$

$$TPq6t\_A3 = m_p\left(\begin{bmatrix}0 & \phi_{e22}\end{bmatrix}\boldsymbol{A}_2^{\mathrm{T}}\boldsymbol{E}_1^{\mathrm{T}}\begin{bmatrix}0 & \phi_{e11}\end{bmatrix}^{\mathrm{T}} + \begin{bmatrix}0 & \phi_{e22}\end{bmatrix}\boldsymbol{E}_1^{\mathrm{T}}\boldsymbol{S}^2\boldsymbol{r}_3\phi'_{e11}\right) + J_p\phi'_{e11}\phi'_{e22}\,, \tag{C.217}$$

$$\begin{aligned} TPq6t\_A4 \;=\; & m_p\left(\begin{bmatrix}0 & \phi_{e22}\end{bmatrix}\boldsymbol{A}_2^{\mathrm{T}}\boldsymbol{E}_1^{\mathrm{T}}\begin{bmatrix}0 & \phi_{e12}\end{bmatrix}^{\mathrm{T}}\right) + J_p\phi'_{e12}\phi'_{e22} + \cdots \\ & m_p\left(\begin{bmatrix}0 & \phi_{e22}\end{bmatrix}\boldsymbol{E}_1^{\mathrm{T}}\boldsymbol{S}^2\boldsymbol{r}_3\phi'_{e12}\right) \end{aligned}, \tag{C.218}$$

$$TPq6t\_A5 = m_p\phi_{e21}\phi_{e22} + J_p\phi'_{e21}\phi'_{e22}\,, \tag{C.219}$$

$$TPq6t\_A6 = \rho_{l_2}\int_0^{l_2}\phi_{22}(\tilde{x}_2)^2 d\tilde{x}_2 + m_p\phi_{e22}^2 + J_p\phi'^2_{e22}\,, \tag{C.220}$$

$$TPq6t\_B = m_p\left(TPq6t\_B1 + TPq6t\_B2\right), \tag{C.221}$$

where

$$\begin{aligned} TPq6t\_B1 \;=\; & {}^1\dot{\boldsymbol{r}}_2^{\mathrm{T}}\boldsymbol{S}^{\mathrm{T}}\boldsymbol{E}_1\boldsymbol{A}_2\begin{bmatrix}0 & \phi_{e22}\end{bmatrix}^{\mathrm{T}}\dot{q}_1 + {}^1\boldsymbol{r}_2^{\mathrm{T}}\boldsymbol{S}^{\mathrm{T}}\dot{\boldsymbol{E}}_1\boldsymbol{A}_2\begin{bmatrix}0 & \phi_{e22}\end{bmatrix}^{\mathrm{T}}\dot{q}_1 + \cdots \\ & {}^1\boldsymbol{r}_2^{\mathrm{T}}\boldsymbol{E}_1\boldsymbol{A}_2\begin{bmatrix}0 & \phi_{e22}\end{bmatrix}^{\mathrm{T}}\dot{q}_1\dot{q}_2 + {}^1\dot{\boldsymbol{r}}_2^{\mathrm{T}}\dot{\boldsymbol{E}}_1\boldsymbol{A}_2\begin{bmatrix}0 & \phi_{e22}\end{bmatrix}^{\mathrm{T}} \end{aligned}, \tag{C.222}$$

$$\begin{aligned} TPq6t\_B2 \;=\; & {}^1\dot{\boldsymbol{r}}_2^{\mathrm{T}}\boldsymbol{E}_1\boldsymbol{S}\boldsymbol{A}_2\begin{bmatrix}0 & \phi_{e22}\end{bmatrix}^{\mathrm{T}}\dot{q}_2 + {}^2\dot{\boldsymbol{r}}_3^{\mathrm{T}}\dot{\boldsymbol{E}}_1^{\mathrm{T}}\boldsymbol{E}_1^{\mathrm{T}}\begin{bmatrix}0 & \phi_{e22}\end{bmatrix}^{\mathrm{T}} + \cdots \\ & {}^2\boldsymbol{r}_3^{\mathrm{T}}\dot{\boldsymbol{E}}_1^{\mathrm{T}}\dot{\boldsymbol{E}}_1^{\mathrm{T}}\begin{bmatrix}0 & \phi_{e22}\end{bmatrix}^{\mathrm{T}} \end{aligned}, \tag{C.223}$$

$$\frac{\partial T_{l_2}}{\partial q_6} = \rho_{l_2}\int_0^{l_2}\left(TL2q6\_C1 + TL2q6\_C2 + TL2q6\_C3 + TL2q6\_C4\right)d\tilde{x}_2\,, \tag{C.224}$$

where

$$TL2q6\_C1 = {}^{1}\boldsymbol{r}_2^{\mathrm{T}}\boldsymbol{E}_1\boldsymbol{A}_2\left[0\ \ \phi_{22}(\tilde{x}_2)\right]^{\mathrm{T}}\dot{q}_1^2 + {}^{1}\dot{\boldsymbol{r}}_2^{\mathrm{T}}\boldsymbol{S}\boldsymbol{E}_1\boldsymbol{A}_2\left[0\ \ \phi_{22}(\tilde{x}_2)\right]^{\mathrm{T}}\dot{q}_1 + \cdots$$
$$ {}^{2}\boldsymbol{p}_2^{\mathrm{T}}\left[0\ \ \phi_{22}(\tilde{x}_2)\right]^{\mathrm{T}}\dot{q}_1^2 + {}^{2}\boldsymbol{p}_2^{\mathrm{T}}\dot{\boldsymbol{E}}_1^{\mathrm{T}}\boldsymbol{S}\boldsymbol{E}_1\left[0\ \ \phi_{22}(\tilde{x}_2)\right]^{\mathrm{T}}\dot{q}_1 \quad , \tag{C.225}$$

$$TL2q6\_C2 = 2\,{}^{2}\boldsymbol{p}_2^{\mathrm{T}}\left[0\ \ \phi_{22}(\tilde{x}_2)\right]^{\mathrm{T}}\dot{q}_1\dot{q}_2 + {}^{1}\boldsymbol{r}_2^{\mathrm{T}}\boldsymbol{S}^{\mathrm{T}}\dot{\boldsymbol{E}}_1\boldsymbol{A}_2\left[0\ \ \phi_{22}(\tilde{x}_2)\right]^{\mathrm{T}}\dot{q}_1 + \cdots$$
$$ {}^{1}\dot{\boldsymbol{r}}_2^{\mathrm{T}}\dot{\boldsymbol{E}}_1\boldsymbol{A}_2\left[0\ \ \phi_{22}(\tilde{x}_2)\right]^{\mathrm{T}} + {}^{2}\boldsymbol{p}_2^{\mathrm{T}}\boldsymbol{E}_1^{\mathrm{T}}\boldsymbol{S}^{\mathrm{T}}\dot{\boldsymbol{E}}_1\left[0\ \ \phi_{22}(\tilde{x}_2)\right]^{\mathrm{T}}\dot{q}_1 \quad , \tag{C.226}$$

$$TL2q6\_C3 = {}^{2}\boldsymbol{p}_2^{\mathrm{T}}\dot{\boldsymbol{E}}_1^{\mathrm{T}}\dot{\boldsymbol{E}}_1\left[0\ \ \phi_{22}(\tilde{x}_2)\right]^{\mathrm{T}} + {}^{2}\boldsymbol{p}_2^{\mathrm{T}}\boldsymbol{S}^{\mathrm{T}}\boldsymbol{E}_1^{\mathrm{T}}\dot{\boldsymbol{E}}_1\left[0\ \ \phi_{22}(\tilde{x}_2)\right]^{\mathrm{T}}\dot{q}_2 + \cdots$$
$$ {}^{2}\dot{\boldsymbol{p}}_2^{\mathrm{T}}\boldsymbol{E}_1^{\mathrm{T}}\dot{\boldsymbol{E}}_1\left[0\ \ \phi_{22}(\tilde{x}_2)\right]^{\mathrm{T}} + {}^{1}\boldsymbol{r}_2^{\mathrm{T}}\boldsymbol{E}_1\boldsymbol{A}_2\left[0\ \ \phi_{22}(\tilde{x}_2)\right]^{\mathrm{T}}\dot{q}_1\dot{q}_2 \quad , \tag{C.227}$$

$$TL2q6\_C4 = {}^{1}\dot{\boldsymbol{r}}_2^{\mathrm{T}}\boldsymbol{E}_1\boldsymbol{S}\boldsymbol{A}_2\left[0\ \ \phi_{22}(\tilde{x}_2)\right]^{\mathrm{T}}\dot{q}_2 + {}^{2}\boldsymbol{p}_2^{\mathrm{T}}\dot{\boldsymbol{E}}_1^{\mathrm{T}}\boldsymbol{E}_1\boldsymbol{S}\left[0\ \ \phi_{22}(\tilde{x}_2)\right]^{\mathrm{T}}\dot{q}_2 + \cdots$$
$$ {}^{2}\boldsymbol{p}_2^{\mathrm{T}}\left[0\ \ \phi_{22}(\tilde{x}_2)\right]^{\mathrm{T}}\dot{q}_2^2 \quad , \tag{C.228}$$

$$\frac{\partial T_{\mathrm{p}}}{\partial q_6} = m_{\mathrm{p}}\left(TPq6\_C1 + TPq6\_C2 + TPq6\_C3 + TPq6\_C4\right), \tag{C.229}$$

where

$$TPq6\_C1 = {}^{1}\boldsymbol{r}_2^{\mathrm{T}}\boldsymbol{E}_1\boldsymbol{A}_2\left[0\ \ \phi_{\mathrm{e}22}\right]^{\mathrm{T}}\dot{q}_1^2 + {}^{1}\dot{\boldsymbol{r}}_2^{\mathrm{T}}\boldsymbol{S}\boldsymbol{E}_1\boldsymbol{A}_2\left[0\ \ \phi_{\mathrm{e}22}\right]^{\mathrm{T}}\dot{q}_1 + \cdots$$
$$ {}^{2}\boldsymbol{r}_3^{\mathrm{T}}\left[0\ \ \phi_{\mathrm{e}22}\right]^{\mathrm{T}}\dot{q}_1^2 + {}^{2}\boldsymbol{r}_3^{\mathrm{T}}\dot{\boldsymbol{E}}_1^{\mathrm{T}}\boldsymbol{S}\boldsymbol{E}_1\left[0\ \ \phi_{\mathrm{e}22}\right]^{\mathrm{T}}\dot{q}_1 \quad , \tag{C.230}$$

$$TPq6\_C2 = 2\,{}^{2}\boldsymbol{r}_3^{\mathrm{T}}\left[0\ \ \phi_{\mathrm{e}22}\right]^{\mathrm{T}}\dot{q}_1\dot{q}_2 + {}^{1}\boldsymbol{r}_2^{\mathrm{T}}\boldsymbol{S}^{\mathrm{T}}\dot{\boldsymbol{E}}_1\boldsymbol{A}_2\left[0\ \ \phi_{\mathrm{e}22}\right]^{\mathrm{T}}\dot{q}_1 + \cdots$$
$$ {}^{1}\dot{\boldsymbol{r}}_2^{\mathrm{T}}\dot{\boldsymbol{E}}_1\boldsymbol{A}_2\left[0\ \ \phi_{\mathrm{e}22}\right]^{\mathrm{T}} + {}^{2}\boldsymbol{r}_3^{\mathrm{T}}\boldsymbol{E}_1^{\mathrm{T}}\boldsymbol{S}^{\mathrm{T}}\dot{\boldsymbol{E}}_1\left[0\ \ \phi_{\mathrm{e}22}\right]^{\mathrm{T}}\dot{q}_1 \quad , \tag{C.231}$$

$$TPq6\_C3 = {}^{2}\boldsymbol{r}_3^{\mathrm{T}}\dot{\boldsymbol{E}}_1^{\mathrm{T}}\dot{\boldsymbol{E}}_1\left[0\ \ \phi_{\mathrm{e}22}\right]^{\mathrm{T}} + {}^{2}\boldsymbol{r}_3^{\mathrm{T}}\boldsymbol{S}^{\mathrm{T}}\boldsymbol{E}_1^{\mathrm{T}}\dot{\boldsymbol{E}}_1\left[0\ \ \phi_{\mathrm{e}22}\right]^{\mathrm{T}}\dot{q}_2 + \cdots$$
$$ {}^{2}\dot{\boldsymbol{r}}_3^{\mathrm{T}}\boldsymbol{E}_1^{\mathrm{T}}\dot{\boldsymbol{E}}_1\left[0\ \ \phi_{\mathrm{e}22}\right]^{\mathrm{T}} + {}^{1}\boldsymbol{r}_2^{\mathrm{T}}\boldsymbol{E}_1\boldsymbol{A}_2\left[0\ \ \phi_{\mathrm{e}22}\right]^{\mathrm{T}}\dot{q}_1\dot{q}_2 \quad , \tag{C.232}$$

$$TPq6\_C4 = {}^{1}\dot{\boldsymbol{r}}_2^{\mathrm{T}}\boldsymbol{E}_1\boldsymbol{S}\boldsymbol{A}_2\left[0\ \ \phi_{\mathrm{e}22}\right]^{\mathrm{T}}\dot{q}_2 + {}^{2}\boldsymbol{r}_3^{\mathrm{T}}\dot{\boldsymbol{E}}_1^{\mathrm{T}}\boldsymbol{E}_1\boldsymbol{S}\left[0\ \ \phi_{\mathrm{e}22}\right]^{\mathrm{T}}\dot{q}_2 + \cdots$$
$$ {}^{2}\boldsymbol{r}_3^{\mathrm{T}}\left[0\ \ \phi_{\mathrm{e}22}\right]^{\mathrm{T}}\dot{q}_2^2 \quad , \tag{C.233}$$

$$\frac{\partial U_{\mathrm{l}_2}}{\partial q_6} = \left(EI\right)_2\int_0^{l_2}\left(\phi_{22}(\tilde{x}_2)\sum_{i=3}^{4}\phi_{2i}(\tilde{x}_2)q_{i+2}\right)d\tilde{x}_2\ , \tag{C.234}$$

Where all the terms ending in "_*B*" and "_*C*" are separated and conform the vector of Coriolis and centripetal effects

$$\boldsymbol{c}(\boldsymbol{q},\dot{\boldsymbol{q}}) = \begin{bmatrix} Th2q1t\_B + TL1q1t\_B + TL2q1t\_B + TPq1t\_B \\ TL2q2t\_B + TPq2t\_B - TL2q2\_C - TPq2\_C \\ TL2q3t\_B + TPq3t\_B - Th2q3\_C - TL1q3\_C - TL2q3\_C - TPq3\_C \\ TL2q4t\_B + TPq4t\_B - Th2q4\_C - TL1q4\_C - TL2q4\_C - TPq4\_C \\ TL2q5t\_B + TPq5t\_B - TL2q5\_C - TPq5\_C \\ TL2q6t\_B + TPq6t\_B - TL2q6\_C - TPq6\_C \end{bmatrix} \tag{C.235}$$

Appendix D Experimental Determination of Joint Friction Complement

Joint friction has an important Influence in the position control. Here the relation between friction torque and joint velocity is experimentally determined. The friction torque is determined independtly for each joint. The equation of motion for each joint is given by

$$\tau_{\mathrm{m}} - \tau_{\mathrm{fr}} = J_{\mathrm{h}} \ddot{q}_{\mathrm{R}} \,. \tag{D.1}$$

The motors are subjected to rotations with constant rotational speed therefore $\tau_{\mathrm{m}} = \tau_{\mathrm{fr}}$. In each experience the rotational speed of the motor is increased, subsequently the torque through the motor current out is obtained. In Figs. D.1 and D.2 the obtained torque profiles according to the joint rotational are shown. These disconotinuities are incorporated in the controllers approximating them as $\tau_{\mathrm{fr1}} = 0.2604 \tanh(\hat{\beta}\dot{q}_2)\,[\mathrm{Nm}]$ and $\tau_{\mathrm{fr2}} = 0.0517 \tanh(\hat{\beta}\dot{q}_2)\,[\mathrm{Nm}]$ with $\hat{\beta} = 30$.

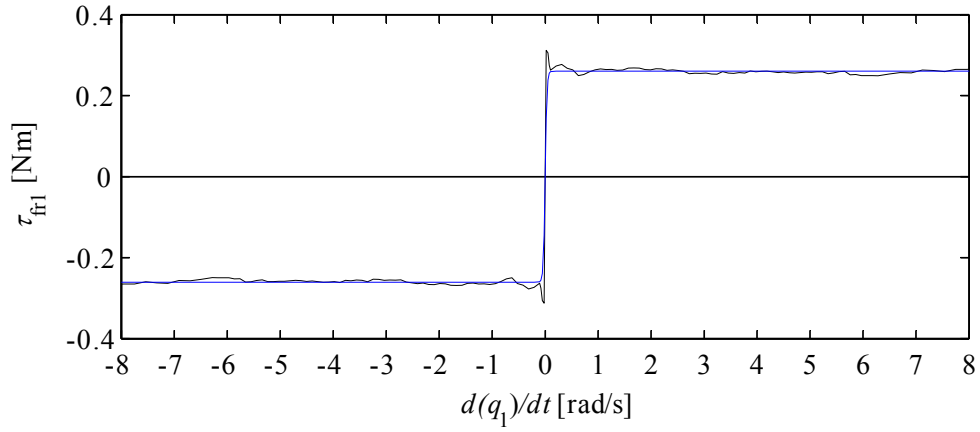

Figure D.1: Friction torque profile for the first joint.
Black: experimental, blue: approximation.

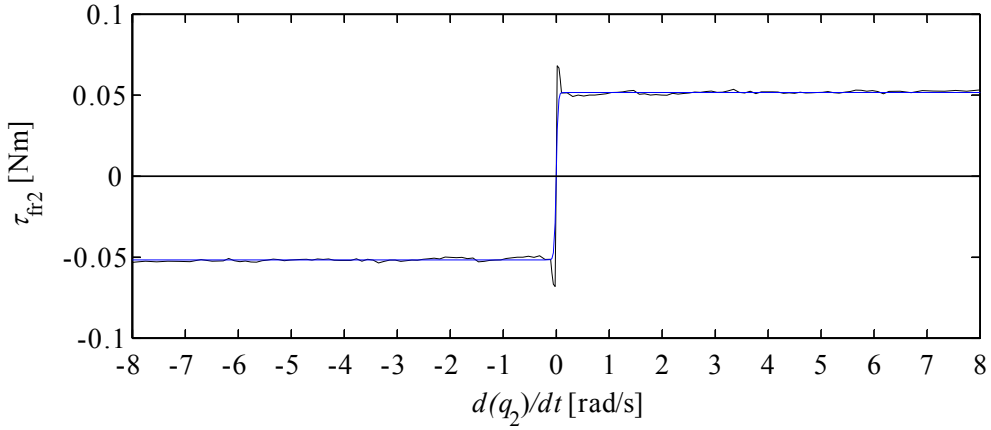

Figure D.2: Friction torque profile for the second joint.
Black: experimental, blue: approximation.

References

[1] S. Dwivedy and P. Eberhard,, "Dynamic analysis of flexible manipulators, a literature review," *Journal of Mechanism and Machine Theory*, vol. 41, no. 7, pp. 749-77, July 2006.

[2] L. Meirovitch, *Elements of vibration analysis*. New York: McGraw-Hill, 1967.

[3] W. Book, "Recursive Lagrangian dynamics of flexible manipulator arms," *The International Journal of Robotics Research*, vol. 3, no. 3, pp. 87-100, Sept. 1984.

[4] G. Hastings and W. Book, "A Linear Dynamic Model for Flexible Robotic Manipulators," *IEEE Control Systems Magazine*, vol. 7, no. 1, pp. 61-64, Feb. 1987.

[5] D. Wang and M. Vidyasagar, "Transfer functions for a single flexible link," in *Proc. of the 1989 IEEE International Conference on Robotics and Automation*, Scottsdale, May 1989, pp. 14-19.

[6] A. De Luca and B. Siciliano, "Closed-form dynamic model of planar multilink lightweight robots," *IEEE Transactions on Systems, Man, and Cybernetics*, vol. 21, no. 4, pp. 826-38, July 1991.

[7] W. Book, "Controlled motion in an elastic world," *Journal of Dynamic Systems Measurement and Control*, vol. 115, no. 2B, pp. 262-91, June 1993.

[8] C. Li and T. Sankar, "Closed-form dynamic model of planar multilink lightweight robots," *IEEE Transactions on Systems, Man, and Cybernetics*, vol. 23, no. 1, pp. 77-95, Feb. 1993.

[9] F. Duarte, P. Ballesteros and C. Bohn, "Modeling and sliding mode control of a single-link flexible robot to reduce the transient response," in *Proc. of the 20th International Conference on Methods and Models in Automation and Robotics (MMAR 2015)*, Miedzyzdroje, Poland, Aug. 2015, pp. 235-40.

[10] F. Duarte, F. Ullah and C. Bohn, "Modeling and dual loop sliding mode control of a two-flexible-link robot to reduce the transient response," to be published in *Proc. of the 24th Mediterranean Conference on Control and Automation (MED2016)*, Athens, Greece, June 2016.

[11] H. Asada, Z. Ma and H. Tokumaru, "Modeling and computation for trajectory control," *ASME J. Dynamic Sys. Meas. Control*, vol. 112, no. 2, pp. 177-85, June 1990.

[12] A. De Luca and B. Siciliano, "Inversion-based nonlinear control of robot arms with flexible links," *Journal of Guidance, Control, and Dynamics*, vol. 16, no. 6, pp. 1169-76, Nov. 1993.

[13] F. Bellezza, L. Lanari and G. Ulivi, "Exact modeling of the flexible slewing link," in *Proc. of the 1990 IEEE International Conference on Robotics and Automation*, Cincinnati, May 1990, pp. 734-39.

[14] E. Barbieri and U. Özgüner, "Unconstrained and constrained mode expansions for a flexible slewing link," in *Proc. of the American Control Conference*, Atlanta, June 1988, pp. 83-88.

[15] J. Gong, S. Ge and T. Lee, "Model-free controllers of a single-link smart material robot," in *Proc. of the American Control Conference*, Philadelphia, June 1998, pp. 3065-69.

[16] C. Canudas, B. Siciliano and G. Bastin, *Theory of robot control*. London: Springer, 1996.

[17] T. Fukuda and A. Arakawa, "Modeling and control characteristics for a two-degrees-of-freedom coupling system of flexible robotic arms," *JSME international journal*, vol. 30, no. 267, pp. 1458-64, Sep. 1987.

[18] S. Cetinkunt and W. Book, "Performance limitations of joint variable-feedback controllers due to manipulator structural flexibility," *IEEE Transactions on Robotics and Automation*, vol. 6, no. 2, pp. 219-31, Apr. 1990.

[19] F. Duarte, P. Ballesteros and C. Bohn, "H_∞ and state-feedback controllers for vibration suppression in a single-link flexible robot," in *Proc. of the 2013 IEEE/ASME International Conference on Advanced Intelligent Mechatronics*, Wollongong, Australia, July 2013, pp. 1719-24.

[20] F. Duarte, P. Ballesteros and C. Bohn, "Rejection of a harmonic and transient disturbance in a single-link flexible robot provided with piezoelectric actuators," in *Proc. of the 2014 IEEE International Conference on Control Applications (CCA)*, Antibes, Oct. 2014, pp. 1735-40.

[21] M. Benosman and G. Vey, "Control of flexible manipulators: a survey," *Robotica*, vol. 22, no. 5, pp. 533-45, Oct. 2004.

[22] B. Jonker, "A finite element dynamic analysis of flexible manipulators," *The International Journal of Robotics Research*, vol. 9, no. 4, pp. 59-74, Aug. 1990.

[23] P. Usoro, R. Nadira and S. Mahil, "A finite element/lagrange approach to modeling lightweight flexible manipulators," *ASME J. Dynamic Sys. Meas. Control*, vol. 108, no. 3, pp. 198-205, Sep. 1986.

[24] G. Naganathan and A. Soni, "Coupling effects of kinematics and flexibility in manipulators," *The International Journal of Robotics Research*, vol. 6, no. 1, pp. 75-84, Mar. 1987.

[25] P. Chedmail, Y. Aoustin and C. Chevallereau, "Modelling and control of flexible robots," *International Journal for Numerical Methods in Engineering*, vol. 32, no. 8, pp. 1595-619, Dec. 1991.

[26] M. Tokhi and Z. Mohamed, "Finite element approach to dynamic modelling of a flexible robot manipulator: performance evaluation and computational requirements," *International Journal for Communications in Numerical Methods in Engineering*, vol. 15, no. 9, pp. 669-78, Sep. 1999.

[27] M. Tokhi, A. Azad and H. Poerwanto, "SCEFMAS: an environment for dynamic characterisation and control of flexible robot manipulators," *International Journal of Engineering Education*, vol. 15, no. 3, pp. 213-26, 1999.

[28] M. Korayem, M. Haghpanahi, H. Rahimi and A. Nikoobin, "Finite element method and optimal control theory for path planning of elastic manipulators," in *New Advanced in Intelligent Decision Technology*, vol. 199, K. G. Phillips-Wren, Ed., Berlin: Springer, 2009, pp. 117-26.

[29] M. Nazemizadeh, H. Nohooji, "An analysis of the finite element method applied on dynamic motion and maximum payload planning of flexible manipulators," *International Transactions of FAMENA*, vol. 39, no. 4, pp. 15-22, Sep. 2015.

[30] A. Muhammad, S. Okamoto and J. Lee, “Active-force control on vibration of a flexible single-link manipulator using a piezoelectric actuator,” in *Transactions on Engineering Technologies*, G. Yang, S. Ao, X. Huang and O. Castillo, Eds., Netherlands, Springer, 2015, pp. 1-15.

[31] X. Wang and J. Mills, “FEM dynamic model for active vibration control of flexible linkages and its application to a planar parallel manipulator,” *Applied Acoustics*, vol. 66, no. 10, pp. 1151-61, Oct. 2015.

[32] G. Piras, W. Cleghorn and J. Mills, “Dynamic finite-element analysis of a planar high-speed, high-precision parallel manipulator with flexible links,” *Mechanism and Machine Theory*, vol. 40, no. 7, pp. 849-62, July 2005.

[33] E. Carrera and M. Serna, “Inverse dynamics of flexible robots,” *Mathematics and Computers in Simulation*, vol. 41, no. 5, pp. 485-508, Aug. 1996.

[34] H. Karagülle, L. Malgaca, M. Dirilmis, M. Akdag and S. Yavuz, “Vibration control of a two-link flexible manipulator,” *Journal of Vibration and Control*, Sep. 2015. DOI: 10.1177/1077546315607694.

[35] D. Fresonke, E. Hernandez and D. Tesar, "Deflection prediction for serial manipulators," in *Proc. of 1988 IEEE International Conference on Robotics and Automation,* Philadelphia, Apr. 1988, pp. 482-87.

[36] S. Tosunoglu, S. Lin and D. Tesar, “Accessibility and controllability of flexible robotic manipulators,” in *Proc. of the American Control Conference*, San Diego, May 1990, pp. 704-11.

[37] V. Feliu, K. Rattan and H. Brown, “Modeling and control of single-link flexible arms with lumped masses,” *Journal of Dynamic Systems, Measurement and Control*, vol. 114, no. 1, pp. 59-69, Mar. 1992.

[38] A. Tzes and S. Yurkovich, “An adaptive input shaping control scheme for vibration suppression in slewing flexible structures,” *IEEE Transactions on Control Systems Technology*, vol. 1, no. 2, pp. 114-21, June 1993.

[39] K. Zuo, V. Drapeau and D. Wang, “Closed loop shaped-input strategies for flexible robots,” *The International Journal of Robotics Research*, vol. 14, no. 5, pp. 510-29, Oct. 1995.

[40] W. Bernzen, “Active vibration control of flexible robots using virtual spring-damper systems,” *Journal of Intelligent and Robotic Systems*, vol. 24, no. 1, pp. 69-88, Jan. 1999.

[41] A. De Luca, "Feedforward/feedback laws for the control of flexible robots," in *Proc. of the 2000 IEEE International Conference on Robotics and Automation,* San Francisco, California, Apr. 2000, pp. 233-40.

[42] S. Tsoa, T. Yangb, W. Xuc and Z. Sunb, “Vibration control for a flexible-link robot arm with deflection feedback,” *International Journal of Non-Linear Mechanics*, vol. 38, no. 1, pp. 51-62, Jan. 2003.

[43] B. Siciliano and W. Book, “A singular perturbation approach to control of lightweight flexible manipulators,” *The International Journal of Robotics Research*, vol. 7, no. 4, pp. 79-90, Aug. 1988.

[44] V. Etxebarria, A. Sanz and I. Lizarraga, "Combining sliding-mode and optimal methods for experiments on controlling a single-link flexible arm," in *Proc. of the World Automation Congress,* Seville, June 2004, pp. 75-80.

[45] V. Etxebarria, A. Sanz and I. Lizarraga, "Control of a lightweight flexible robotic arm using sliding modes," *International Journal of Advanced Robotic System*, vol. 2, no. 2, pp. 103-10, June 2005.

[46] M. Kermani, M. Moallem and R. Patel, "Study of system parameters and control design for a flexible manipulator using piezoelectric transducers," *Smart Materials and Structures*, vol. 14, no. 4, pp. 843-49, July 2005.

[47] Q. Hu and G. Ma, "Variable structure control and active vibration suppression of flexible spacecraft during attitude maneuver," *Aerospace Science and Technology*, vol. 9, no. 4, pp. 307-17, June 2005.

[48] R. Fareh, M. Saad and M. Saad, "Adaptive control for a single flexible link manipulator using sliding mode technique," in *Proc. of the 2009 6th International Multi-Conference on Systems, Signals and Devices,* Djerba, Tunisia, Mar. 2009, pp. 1-6.

[49] T. Mansour, A. Konno and M. Uchiyama, "Vibration based control for flexible link manipulator," in *Robot Manipulators New Achievements*, A. Lazinica and H. Kawai, Eds. InTech, 2010, DOI: 10.5772/9337. Available from: http://www.intechopen.com/books/robot-manipulators-new-achievements/vibration-based-control-for-flexible-link-manipulator [Accesed: Feb. 10, 2015].

[50] A. Shawky, D. Zydek, Y. Elhalwagy and A. Ordys, "Modeling and nonlinear control of a flexible-link manipulator," *Applied Mathematical Modelling*, vol. 37, no. 23, pp. 9591-602, Dec. 2013.

[51] J. Peza-Solís, G. Silva-Navarro and N. Castro-Linares, "Trajectory tracking control in a single flexible-link robot using finite differences and sliding modes," *Journal of Applied Research and Technology*, vol. 13, no. 1, pp. 70-78, Feb. 2015.

[52] F. Khorrami and J. Rastegar, "Simultaneous structure and control design for a flexible pointing system actuated by active materials," in *Proc. of the 34th Conference on Decision and Control*, New Orleans, Los Angeles, Dec. 1995*,* pp. 4374-79.

[53] G. Zhu, T. Lee and S. Ge, "Tip tracking control of a single-link flexible robot: a backstepping approach," *Dynamics and Control*, vol. 7, no. 4, pp. 341-60, Oct. 1997.

[54] D. Sun and J. Mills, "Study on piezoelectric actuators in control of a single-link flexible manipulator," in *Proc. of the 1999 IEEE International Conference on Robotics and Automation,* Detroit, May 1999, pp. 849-54.

[55] D. Sun and J. Mills, J. Shan and S. Tso, "A PZT actuator control of a single-link flexible manipulator based on linear velocity feedback and actuator placement," *Mechatronics*, vol. 14, no. 4, pp. 381-401, May 2004.

[56] K. Hillsley and S. Yurkovich, "Vibration control of a two-link flexible robot arm," in *Proc. of the 1991 IEEE International Conference on Robotics and Automation,* Sacramento, Apr. 1991, pp. 212-16.

[57] K. Hillsley and S. Yurkovich, "Vibration control of a two-link flexible robot arm," *Dynamics and Control*, vol. 3, no. 3, pp. 261-80, July 1993.

[58] F. Khorrami, S. Jain and A. Tzes, "Experiments on rigid body based controllers with input preshaping for a two-link flexible manipulator," *IEEE Transactions on Robotics and Automation*, vol. 10, no. 1, pp. 55-65, Feb. 1994.

[59] F. Khorrami, S. Jain and A. Tzes, "Experimental results on adaptive nonlinear control and input preshaping for multi-link flexible manipulators," *Automatica*, vol. 31, no. 1, pp. 83-97, Jan. 1995.

[60] J. Cheong and S. Lee, "Linear PID composite controller and its tuning for flexible link robots," *Journal of Vibration and Control*, vol. 14, no. 3, pp. 291-318, Mar. 2008.

[61] Y. Li, G. Liu; T. Hong and K. Liu, "Robust control of a two-link flexible manipulator with neural networks based quasi-static deflection compensation," in *Proc. of the 2003 American Control Conference,* Denver, June 2003, pp. 5258-63.

[62] R. Mahamood and J. Pedro, "Hybrid PD/PID controller design for two-link flexible manipulators," in *Proc. of the 2011 8th Asian Control Conference,* Kaohsiung, Taiwan, May 2011, pp. 1358-63.

[63] R. Mahamood and J. Pedro, "Hybrid PD/PID controller design for two-link flexible manipulators," in *Proc. of the World Congress on Engineering and Computer Science,* San Francisco, California, Oct. 2011, pp. 966-71.

[64] G. Parker, D. Segalman, R. Robinett and D. Inman, "Decentralized sliding mode control for flexible link robots," *Journal of Intelligent and Robotic Systems*, vol. 17, no. 1, pp. 61-79, Sep. 1996.

[65] F. Khorrami, I. Zeinoun and E. Tome, "Experimental results on active control of flexible-link manipulators with embedded piezoceramics," in *Proc. of the 1993 IEEE International Conference on Robotics and Automation,* Atlanta, Georgia, May 1993, pp. 222-27.

[66] D. Schoenwald and Ü. Özgüner, "Control of flexible manipulators via singular perturbations and distributed vibration damping," *Dynamics and Control*, vol. 6, no. 1, pp. 5-32, Jan. 1996.

[67] S. Ge, T. Lee and Z. Wang, "Model-free regulation of multi-link smart materials robots," in *Proc. of the 2001 IEEE International Conference on Robotics and Automation,* Seoul, Korea, May 2001, pp. 3871-76.

[68] T. Zebin and M. Alam, "Modeling and control of a two-link flexible manipulator using fuzzy logic and genetic optimization techniques," *Journal of Computers*, vol. 7, no. 3, pp. 578-85, Mar. 2012.

[69] A. Maouche and M. Attari, "Adaptive cerebellar model articulation controller–nonlinear control system for flexible link manipulator," *Journal of Vibration and Control*, vol. 19, no. 14, pp. 2109-23, Oct. 2013.

[70] B. Yuan, W. Book and J. Hagins, "Control of a multi-link flexible manipulator with a decentralized approach," *in Proc. of the 1990 IFAC World Congress,* Tallin, Estonia, Aug. 1990, pp. 255-60.

[71] F. Khorrami, "A two-stage controller for vibration suppression of flexible-link manipulators," in *Proc. of the 29th IEEE Conference on Decision and Control,* Honolulu, Dec. 1990, pp. 2560-65.

[72] A. De Luca, S. Panzieri and G. Ulivi, "Stable inversion control for flexible link manipulators," in *Proc. of the IEEE International Conference on Robotics and Automation,* Leuven, May. 1998, pp. 799-805.

[73] H. Yin, Y. Hoshino and T. Emaru, "Hybrid sliding mode control with optimization for flexible manipulator under fast motion," in *Proc. of the IEEE International Conference on Robotics and Automation,* Shanghai, May. 2011, pp. 458-63.

[74] H. Yin, Y. Kobayashi, J. Xu and F. Huang, "Theoretical and experimental investigation on decomposed dynamic control for a flexible manipulator based on nonlinearity," *Journal of Vibration and Control*, vol. 20, no. 11, pp. 1718-26, Aug. 2014.

[75] M. Sayahkarajy, Z. Mohamed and A. Faudzi, "Review of modelling and control of flexible-link manipulators," *Journal of Systems and Control Engineering*, Apr. 2016. DOI: 10.1177/0959651816642099.

[76] S. Schlesinger, R. Crosbie, R. Gagné, G. Innis, C. Lalwani, "Terminology for model credibility," *SCS Technical Committee on Model Credibility*, vol. 32, no. 3, pp. 103-104, Mar. 1979.

[77] P. Hagedorn and A. Gupta. *Vibrations and waves in continuous mechanical systems*. West Sussex: Wiley, 2007.

[78] R. Blevins, *Formulas for natural frequency and mode shape.* New York: Van Nostrand Reinhold, 1979.

[79] P. Hagedorn, *Technische Mechanik Bd. 3*. Frankfurt am Main: Harry Deutsch, 2007.

[80] O. Zirn, "*Machine tool analysis modelling, simulation and control of machine tool manipulators*," Habilitation Thesis, Department of Mechanical and Process Engineering, ETH Zürich, 2008.

[81] P. Hagedorn and D. Hochlenert, *Mechanical Vibrations: Vibrations of Linear Discrete Systems* (*in german:Technische Schwingungslehre: Schwingungen linearer diskreter mechanischer Systeme*). Frankfurt am Main: Harry Deutsch, 2012.

[82] B. Thacker, S. Doebling, F. Hemez, M. Anderson, J. Pepin and E. Rodriguez, "*Concepts of model verification and validation*," Los Alamos National Laboratory, New Mexico. LA-14167-MS, Oct. 2004

[83] R. Cannon and E. Schmitz, "Initial experiments on the end-point control of a flexible one-link robot," *The International Journal of Robotics Research*, vol. 3, no. 3, pp. 62-75, Sept. 1984.

[84] H. Kanoh and G. Lee, "Vibration control of one-link flexible arm," in *Proc. of the 24th Conference on Decision and Control*, Fort Lauderdale, Dec 1985, pp. 1772-77.

[85] X. Qi and G. Chen, "Mathematical modeling of kinematics and dynamics of certain single Flexible-link robot arm," in *Proc. of the 1st Conference on Control Applications*, Dayton, United States, Sept. 1992, pp. 288-93.

[86] S. Yurkovich, A. Tzes and K. Hillsley "Controlling coupled flexible links rotating in the horizontal plane," in *Proc. of the 9th American Control Conference*, San Diego, May 1990, pp. 362-67.

[87] F. Duarte, P. Ballesteros, X. Shu and C. Bohn, "An LPV discrete-time controller for the rejection of harmonic time-varying disturbances in a lightweight flexible structure," in *Proc. of the American Control Conference*, Washington DC, June 2013, pp. 4092-97.

[88] J. Oh, S. Park, J. Hong and J. Shin, “Active vibration control of flexible cantilever beam using piezo actuator and filtered-X LMS algorithm,” *KSME International Journal*, vol. 12, no. 6, pp. 665-71, July 1998.

[89] V. Feliu, K. Rattan and B. Brown, “Control of flexible arms with friction at the joints,” *IEEE Transactions on Robotics and Automation*, vol. 9, no. 4, pp. 467-75, Aug. 1993.

[90] M. Moallem, “Control and design of flexible-link Manipulators,” Ph.D. dissertation, Department of EIectrical and Computer Engineering, Concordia University Montreal, 1996.

[91] H. Bolandi and S. Esmaeilzadeh, “Analytical modelling and nonlinear strain feedback control of a flexible robot ARM,” *Automatic Control and Computer Sciences*, vol. 42, no. 5, pp. 236-48, Aug. 1993.

[92] Y. Shtessel, C. Edwards, L. Fridman and A. Levant, *Sliding mode control and observation*. Basel: Birkhäuser, 2013.

[93] J. Denavit and R. Hartenberg, "A kinematic notation for lower-pair mechanisms based on matrices," *Transactions ASME Journal of Applied Mechanics,* vol. 77, no. 23, pp. 215-21, 1955.

[94] R. De Carlo, S. Zak; G. Matthews, "Variable structure control of nonlinear multivariable systems: a tutorial," *Proceedings of the IEEE*, vol. 76, no. 3, pp. 212-32, Mar. 1988.

[95] V. Utkin, *Sliding modes in control optimization*. Berlin: Springer, 1992.

[96] J. Slotine and W. Li, *Applied nonlinear control*. New Jersey: Prentice-Hall, 1991.

[97] V. Utkin, J. Guldner and J. Shi, *Sliding modes in control in electromechanical systems*. Boca Ratón: CRC Press, 1999.

[98] A. Filippov, "Differential equations with discontinuous right hand sides," *American Mathematical Society Translations,* vol. 42, no. 2, pp. 199-231, Juni 1964.

[99] J. Hung, W. Gao and J. Hung, “Variable structure control: a survey,” *IEEE Transactions on Industrial Electronics*, vol. 40, no. 1, pp. 2-22, Feb. 1993.

[100] W. Perruquetti and J. Barbot, *Sliding mode control in engineering*. Nueva York: Marcel Decker, 2002.

[101] A. Lukyanov and V. Utkin, “Methods of reducing equations for dynamic systems to a regular form,” *Automation and Remote Control*, vol. 42, no. 4, pp. 413-20, 1981.

[102] W. Perruquetti, P. Borne and J. Richard, "A generalized regular form for sliding mode stabilization of MIMO systems," in *Proc. of the 36th Conference on Decision and Control,* San Diego, Dec. 1997, pp. 957-64.

[103] W. Perruquetti, J. Richard and P. Borne, "A generalized regular form for multivariable sliding mode control," *Mathematical Problems in Engineering*, vol. 7, no. 1, pp. 15-27, 2001.

[104] H. Sira-Ramirez, “Variable structure control of non-linear systems,” *International Journal of Systems Science*, vol. 18, no. 9, pp. 1673-89, Sept. 1987.

[105] K Young, V. Utkin and Ü. Özgüner, “A control engineer’s guide to sliding mode control,” *IEEE Transactions Control Systems Technology*, vol. 7, no. 3, pp. 328-42, May 1999.

[106] J. Craig, *Introduction to Robotics: Mechanics & Control*. Reading: Addison Wesley, 1989.

[107] EPOS2 Positioning Controllers, Application Notes Collection, Maxon Motor, edition Feb. 2012.

[108] N. Smirnov, V. Sabanin, and A. Repin, "Sensitivity and robust tuning of PID controllers with real differentiation," *Thermal Engineering*, vol. 54, no. 10, pp. 777-85, Oct. 2007.

[109] L. Moreno, S. Garrido and C. Balaguer, *Modeling, analysis and control od dynamical systems* (*in Spanish: Modelado, análisis y control de sistemas dinámicos*). Barcelona: Ariel, 2003.

[110] Y. Li, K. Ang and G. Chong, "PID control system analysis and design," *IEEE Transactions Control Systems Magazine*, vol. 26, no. 1, pp. 32-41, Feb. 2006.

[111] S. Spurgeon, "Sliding mode control: a tutorial," in *Proc. of the European Control Conference,* Strasbourg, France, June 2014, pp. 2272-77.

[112] H. Khalil, *Nonlinear systems*. Upper Saddle River: Prentice Hall, 2002.

[113] R. Theodore and A. Ghosal, "Comparison of the assumed modes and finite element models for flexible multilink manipulators," *The International Journal of Robotic Research*, vol. 14, no. 2, pp. 91-111, Apr. 1995.

[114] V. Gupta, M. Sharma and N. Thakur, "Optimization criteria for optimal placement of piezoelectric sensors and actuators on a smart structure: a technical review," *Journal of Intelligent Material Systems and Structures*, vol. 21, no. 12, pp. 1227-43, Aug. 2010

[115] N. Jalili, F. Hong and S. Ge, "Adaptive non model-based piezoelectric control of flexible beams with translational base," in *Proc. of the 2002 American Control Conference,* Anchorage, May 2002, pp. 3802-807.